MARINE GEOPHYSICAL INVESTIGATIONS OVER A PART OF THE EASTERN ARABIAN SEA, NORTHWESTERN INDIAN OCEAN

Thesis submitted

to

Goa University

for the award of degree of

DOCTOR OF PHILOSOPHY

in

Marine Science

by

Anil Kumar Chaubey

National Institute of Oceanography,

Dona Paula - 403 004, Goa, India.

August 1998

TO

MY PARENTS

STATEMENT

As required under the University ordinance 0.19.8 (vi), I state that the present thesis entitled "**MARINE GEOPHYSICAL INVESTIGATIONS OVER A PART OF THE EASTERN ARABIAN SEA, NORTHWESTERN INDIAN OCEAN",** is my original contribution and the same has not been submitted on any previous occasion. To the best of my knowledge, the present study is the first comprehensive work of its kind from the area mentioned.

The literature related to the problem investigated has been cited. Due acknowledgements have been made wherever facilities and suggestions have been availed of.

AKchaubey

ANIL KUMAR CHAUBEY

CERTIFICATE

This is to certify that the thesis entitled '**MARINE GEOPHYSICAL INVESTIGATIONS OVER A PART OF THE EASTERN ARABIAN SEA, NORTHWESTERN INDIAN OCEAN**', submitted by **Mr. Anil Kumar Chaubey** for the award of the degree of Doctor of Philosophy in Marine Science is based on his original studies carried out by him under my supervision. The thesis or any part thereof has not been previously submitted for any other degree or diploma in any universities or institutions.

Place : Dona Paula

Date : 31 August 1998

(Dr. D. Gopala Rao)

Research Guide
Scientist E-II
Geological Oceanography Division
National Institute of Oceanography
Dona Paula - 403 004, Goa

CONTENTS

CHAPTER 3 - ACQUISITION, PROCESSING AND PRESENTATION MARINE GEOPHYSICAL DATA

CHAPTER 4 - IDENTIFICATION OF SEAFLOOR SPREADING MAGNETIC ANOMALIES

PREFACE

In the field of marine sciences India has demonstrated spectacular achievements during the last three decades. With the establishment of the National Institute of Oceanography, Goa, a National Laboratory under Council of Scientific and Industrial Research, New Delhi in 1966, the marine geological and geophysical exploration program was initiated. However, the program was intensified from 1983-84 under the specific project of Geological and Geophysical Surveys of the Continental Margins of India. The author has been an active participant of this program. Under this program a large amount of marine geophysical data from the western continental margin of India and adjoining region were collected from time to time onboard various research vessels.

Earlier geological and geophysical studies carried out in the Arabian Sea have revealed major structural features and a general framework of the evolutionary history of ocean basins and adjoining continental margins. Based on results of these studies, the Eastern Arabian Sea is broadly divided into two crustal provinces; the Eastern Arabian Basin (EAB) and Western Arabian Basin (WAB). The WAB consists of oceanic crust created during symmetric seafloor spreading along the Carlsberg Ridge. Although, the WAB was formed during a period of rapid seafloor spreading and depicts distinct magnetic anomaly lineations, the limited number of magnetic profiles available have led to various speculative magnetic anomaly identifications in the area, resulting in an ill elucidative tectonic framework. Further, the recent studies have indicated that most part of the Eastern Arabian Sea has been evolved due to complex processes of seafloor spreading possibly due to influence of the then Reunion hotspot activities. An understanding of the complex processes will have important consequences on the evolution of the western margin of India, both

geodynamically and thermally, and in illustrating the tectonic framework of the area.

The present investigations are carried out based on analyses of bathymetry, gravity, magnetic and multi-channel seismic reflection data collected in the WAB and adjoining continental margin of India. About 22,400 line kilometers (lkm) of magnetic and bathymetry, 2400 lkm of gravity and 720 lkm of multichannel seismic reflection data have been collected and analyzed inconjunction with published geophysical data to identify seafloor spreading magnetic anomalies and to derive a model for the evolution of the WAB from the Early Tertiary to Present and crustal structure across the western continental margin of India. The results and implications of the tectonics in the evolution of the western continental margin of India are the main contents of the thesis and they are summarized in the nine chapters as follow:

Chapter 1 presents an account of the earlier geophysical investigations in the Indian Ocean with a special emphasis on the Arabian Sea. The chapter also presents the outstanding problems of the Eastern Arabian Sea, study area and objectives of the present study.

In **Chapter 2** the geologic and tectonic setting of the study area and adjoining onshore region are described. Evolutionary history of the Arabian Sea as revealed by marine geophysical investigations with special emphasis on the study area is given inlight of seafloor spreading and plate tectonics.

Chapter 3 contains a brief description of acquisition of marine geophysical data and details of the equipment used for the present studies. The explanations for choosing the orientations and closely spaced layout of profiles in oceanic region and southwestern continental margin are given. The tracks in the WAB are approximately parallel to the seafloor spreading direction and therefore, orthogonal to the oceanic crust magnetic anomalies.

While, on southwestern continental margin of India, they are approximately orthogonal to the margin. Various techniques used for processing and reducing the data are also briefly described.

Chapter 4 outlines the concept of seafloor spreading, and briefly reviews the geomagnetic polarity time scale and correlation and identification of marine magnetic anomalies in detail. The method for computing synthetic magnetic profiles and their comparison with observed profiles for anomaly identification are described. A detailed account of the magnetic anomalies which are identified in the WAB and across the Carlsberg Ridge are described. The Early Tertiary magnetic anomalies 28N through 18N in the WAB and anomalies 11N through 1N across the Carlsberg Ridge are identified. The magnetic lineations are mostly E-W in the WAB and N50°W across the Carlsberg Ridge.

In **Chapter 5** the interpretation of the mapped magnetic lineations are presented. These magnetic lineations exhibit offsets at several places, but do not support the earlier proposed fracture zones considered as orthogonal to the general trend of magnetic lineations to explain these offsets. Instead, the present study indicates the presence of oblique offsets which are inferred to be the diagnostic feature of the propagating ridges. The concept of propagating ridge hypothesis and its various models proposed by earlier workers have been summarized. Finally a schematic model has been proposed depicting paleo-propagation to explain the observed magnetic fabric of the study area. A spreading ridge-hotspot interaction mechanism is suggested to explain the accretionary process of the oceanic crust in this region.

Chapter 6 deals with admittance analysis of gravity and bathymetry data, and two-dimensional modeling of gravity data over the Laccadive Ridge to provide constraints on mode of compensation, nature and origin of the ridge.

The chapter also presents methodology of admittance analysis and two-dimensional free-air gravity modeling. Based on crustal structure and density distribution inferred from the admittance and two-dimensional gravity studies, it is suggested that i) local isostatic compensation by the Airy mechanism is an appropriate model of compensation of the topography of the Laccadive Ridge, and ii) the ridge is a continental fragment.

Chapter 7 presents analysis and interpretation of a regional multichannel seismic reflection data across the western continental margin of India to understand depositional patterns of sediments, and nature and structure of the crust of the margin. The analysis of seismic data have revealed six seismic sequences (H1-H6) overlying the basement representing Paleocene to Late Eocene, Late Eocene to Late Oligocene, Late Oligocene to Middle Miocene, Middle Miocene to Middle Pliocene, Middle Pliocene to Late Pleistocene and Late Pleistocene age. The development of these seismic sequences has been attributed mainly due to the Indian and Eurasian plate collision, eustatic sealevel changes and Himalayan Orogeny. The seismic section of continental shelf and slope region shows three distinct shelf edges; Late Oligocene, Middle Miocene and Present. The Late Oligocene to Middle Miocene sediment deposition of shelf and slope region inferred from the present studies corresponds to an aggradational phase. Whereas, the Middle Miocene to Recent sedimentation is dominated by progradation. The results of the study are presented to explain the nature of ocean-continent transition.

Chapter 8 deals with the history of evolution of oceanic crust of the Eastern Arabian Sea since the Early Tertiary and its implications on the evolution of the western continental margin of India. Schematic reconstruction models depicting evolution of the Arabian Sea at Chron 34 (~84 Ma), Chron 29R (~65 Ma), Chron 28N (~63 Ma), Chron 18N (~39 Ma) and Chron 11N (~30 Ma) have been proposed.

Chapter 9 synthesizes the summary and main conclusions of the present study.

This chapter is followed by references in alphabetical order of the literature cited in the text and Appendix.

ACKNOWLEDGMENTS

It gives me great pleasure to acknowledge the help and advice received during the course of this work. I am especially indebted to my research guide, **Dr. D. Gopala Rao**, Scientist, National Institute of Oceanography (NIO), Goa for his invaluable advice and encouragement. His patience, fruitful discussions and helpful criticisms along the way enabled me to complete this thesis. I place on record the thought provoking and lively discussions with **Shri G.C. Bhattacharya**, Scientist, during this work. I am also grateful to him for introducing me to the topic of ridge-propagation. I take this opportunity to thank **Dr. Rajiv Nigam,** Scientist, for his constant encouragement and help at various stages of the study. These three people have been an inspiration to me.

I express my sincere thanks to **Dr. E. Desa**, Director, NIO, and Head of the Geological Oceanography Division, NIO for permission, facilities and encouragement extended to carry out this work.

I am very much obliged to **Prof. U.M.X. Sangodkar**, Dean, Faculty of Life Sciences and Environment, and **Prof. G.N. Nayak**, Head, Department of Marine Sciences and Marine Biotechnology, Goa University for their help and cooperation on various occasions.

I express my gratitude to my colleagues in the Marine Geophysics Group, NIO. I owe many thanks to **Shri K. Srinivas** for many hours of discussions, advice, criticisms and help during various stages of this work. I am thankful to **Dr. K.S. Krishna** for generously providing me with many hours of his time for critically going through the manuscript which led to an overall improvement of the thesis. This work would not have been completed without the support and inputs from my colleagues, specially **Shri T . Ramprasad,**

Shri G.P.S. Murty, Dr. M.V. Ramana and Dr. K.A. Kamesh Raju. The help of **Shri L.V. Subba Raju, Dr. V. Subrahmanyam, Dr. K.V.L.N.S. Sarma** and **Mrs. Maria Desa** was always available to me.

I profusely thank **Dr. C. Subrahmanyam** and **Dr. B. Ashalatha,** Scientists of National Geophysical Research Institute, Hyderabad for having thoughtful discussions and help during the admittance analysis of gravity data.

I would like to express my sense of gratitude to **Dr. N.H. Hashimi**, Scientist, Geological Oceanography Division, NIO for generously devoting his valuable time for critically editing the manuscript. The valuable help and advice of **Shri M.C. Pathak**, Senior Technical Officer, NIO is highly acknowledged for preparation of the maps.

Most of data used in this study was collected onboard R/V Sagar Kanya belonging to **Department of Ocean Development (DOD),** Government of India.

I record my thanks to the colleagues in the Instrumentation, Marine Survey and Mechanical Engineering groups of the Geological Oceanography Division, NIO for their technical support during the data acquisition. I am also thankful to **Shri S.R. Bhat**, Scientist-in-Charge and his staff in the Publication and Reprography Division, particularly **Shri Md. Wahidullah, Shri Ravindranath Uchil, Shri Satish B. Chitari, Shri Sheikh Ali Karim, Shri Umesh Sirsat. Shri M.P. Tapaswi** and his colleagues of library are thanked for their kind gestures.

The invaluable help rendered by the staff of Computer Center specially **Shri T. Suresh,** Scientist, **Shri A.A.A. Menezes,** Scientist, **Shri K. Ramdasan**,

STA and **Shri D. Mathews**, STA during the processing of multichannel seismic reflection data is highly acknowledged.

My younger brother **Shri Subodh Kumar Chaturvedi**, SRF, Geological Oceanography Division, NIO became an asset during the writing stage of this thesis; I owe to him. Last but not the least I express thanks to my wife **Gyanti** and my two young sons **Anup** and **Manish** for their patience and support which was a continuous source of inspiration to continue this work which extended many days till late in the night.

CHAPTER 1

CHAPTER 1

GENERAL BACKGROUND

1.1 INTRODUCTION

The theory of plate tectonics has provided major clues in understanding the earth's structure and its evolution since late sixties. In this framework, studies of the seafloor spreading magnetic anomalies have provided valuable information of the ages of the oceanfloor and explain lithospheric plate motions and evolutionary history of the ocean basins and margins. The geological and geophysical studies carried out in the Indian Ocean have revealed several major structural features and ages of part of the ocean basins which led to conceptualize the evolutionary history of deep sea basins and adjoining continental margins. The discoveries of offshore oil fields of the continental margins and various types of mineral resources of the nearshore to deep sea regions have necessitated better understanding of the ongoing geological and tectonic processes, and evolutionary history of the regions. However, some parts of the Indian Ocean are yet to be studied systematically to have a complete idea of evolution of the Indian Ocean. The eastern Arabian Sea is one among them. Although the eastern Arabian Sea was formed during a period of rapid seafloor spreading and depicts distinct magnetic anomaly lineations, speculation is prevailing in magnetic anomaly identifications because of limited number of magnetic profiles. Hence, the present tectonic framework in the eastern Arabian Sea is an ill elucidative. Further, the recent studies have indicated that most part of the Arabian Sea has been evolved because of complex processes of seafloor spreading and possibly due to the influence of the Reunion and Comores hotspot activities. A better insight into these complex processes will have important consequences on the evolution of the western margin of India, both geodynamically and thermally, and in illustrating the tectonic framework of the area.

In this introductory chapter, a review of the investigations in the Indian Ocean in general and the eastern Arabian Sea in particular are presented. Furthermore, the chapter also presents the outstanding problems of the eastern Arabian Sea, alongwith description of study area and objectives of the present investigations.

1.2 THE INDIAN OCEAN

The Indian Ocean is the smallest in areal extent (~20% of the world ocean i.e. 73.6×10^6 Sq. km) and youngest among the three major oceans of the world (Figure 1.1). It is bounded to the north by Iran, Pakistan, India and Bangladesh; to the west by Arabia, and Africa; to the east by Australia, the Sunda Islands of Indonesia and the Malayan peninsula, Myanmar (Burma) and Thailand; and to the south by Antarctic continent. In the southwest, the Indian Ocean opens into the Atlantic Ocean near the southern tip of South Africa. Eastwards, it opens into the Pacific Ocean through straits and marginal seas, such as the Sunda straits, the Timor and Java Seas, and the great Australian Bight. It is unique among other oceans of the world with the presence of i) several submarine plateaus, aseismic ridges and hotspots, and ii) the only subduction zone in the northeast implying that majority of the oceanic crust formed during its evolution is still present.

The first integrated scientific study of the Indian Ocean was initiated during the International Geophysical Year (1957-58), however a few other oceanographic expeditions viz., Dana (1928-30), Snellius (1929-30), Mabahiss (1933-34), Challenger (1949-50), Albatross (1950-52) and Ob (1955-57) were made earlier. The data acquired during the expeditions have been analyzed by Wiseman and Seymour-Sewell (1937) and Fairbridge (1948, 1955). Moreover, the first major effort for systematic geological and geophysical investigations of the Indian Ocean came during the International Indian Ocean Expedition (IIOE) between 1959 and 1965. Several international organizations have participated in this program. The investigations carried out during the IIOE period have contributed significantly for the understanding of some of the geologic structures and systematic planning of further geophysical investigations in the ocean. The IIOE was

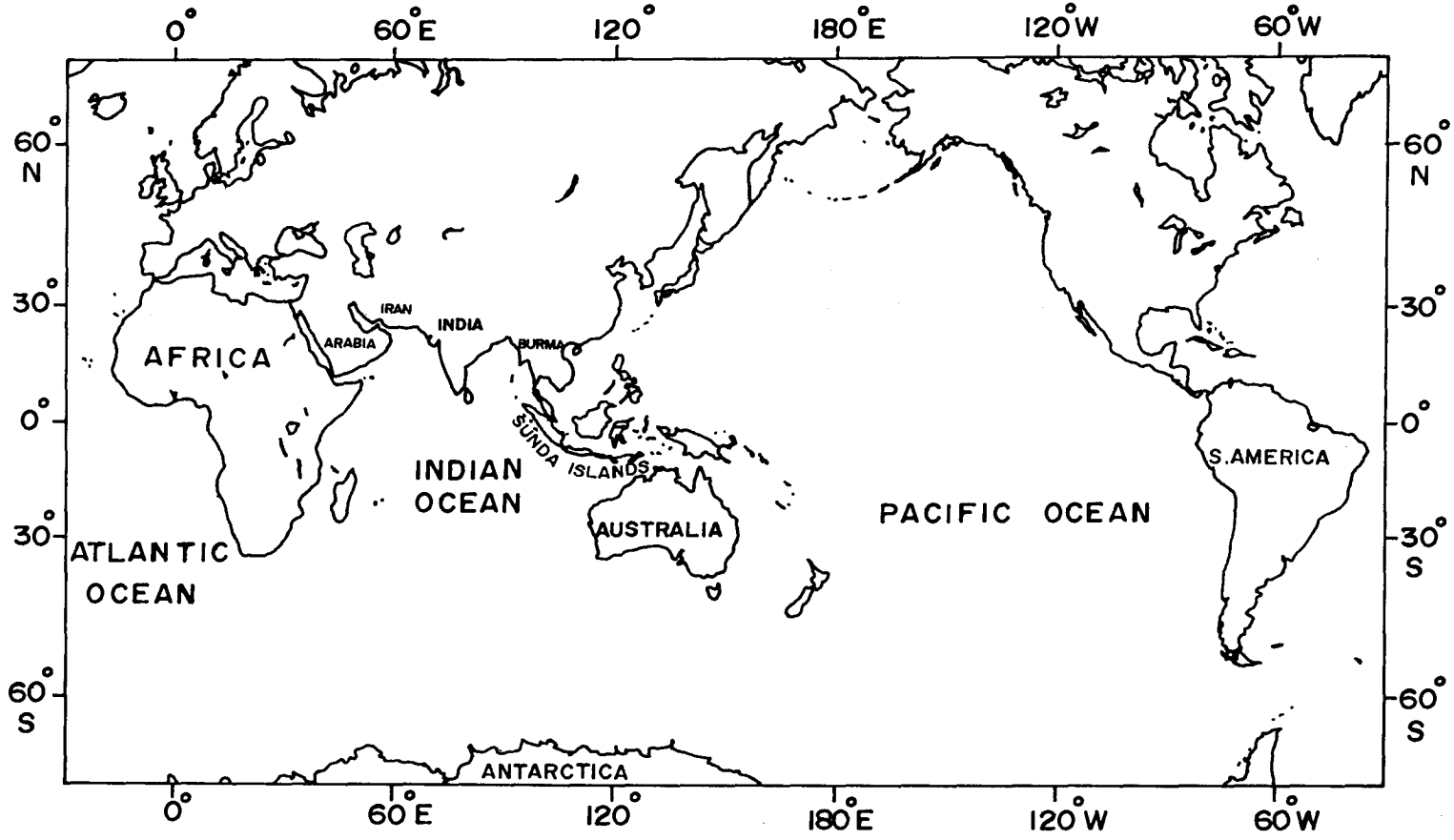

Figure 1.1 The three major oceans of the Earth.

the first major international exercise of its kind which ushered the rate and interests to conduct the oceanographic research. Since then, the level of cooperation among the scientists from many countries has also increased considerably and national oceanographic programs are no longer conducted in the relative isolation. As a result vast amount of data were collected and analyzed which contributed to a large extent in mapping of the physiographic features (Heezen and Tharp, 1965; Udintsev, 1965; Kanaev, 1967). These studies have revealed that the Indian Ocean floor is characterized by seismically active mid-ocean ridge system which mark the boundaries separating the major plates. The northern branch of this ridge system includes east-west trending Sheba Ridge, the northwest-southeast trending Carlsberg Ridge between the Owen Fracture Zone and the equator. The N-S trending Central Indian Ridge (CIR) connects the southern end of the Carlsberg Ridge near the equator to the Rodriguez Triple Junction (RTJ) near 25.5^0S, 70^0E. At the RTJ, the Central Indian Ridge joins the two other branches i.e. the Southwest Indian Ridge (SWIR) and Southeast Indian Ridge (SEIR). The NE-SW trending SWIR runs from the RTJ to the Bouvet Triple Junction in the south Atlantic Ocean, whereas NW-SE trending SEIR connects the RTJ with the Macquarie Triple Junction in the southwest Pacific Ocean (Figure 1.2). Apart from active mid-ocean ridge system, the Indian Ocean floor is also characterized by abundance of large shallow areas scattered all over the ocean variously termed, according to their overall morphology, as banks, plateaus, aseismic ridges, seamount chains or rises. Many of these features trend in a north-south direction and together with the active ridges and surrounding continents, demarcate the Indian Ocean into the number of ocean basins.

The second phase of investigations in the Indian Ocean commenced after the IIOE wherein several major programs including the Deep Sea Drilling Project (DSDP) and Ocean Drilling Program (ODP) were initiated. In the initial phase of DSDP during 1971-1973, Indian Ocean crust has been drilled by 'D/V Glomar Challenger' during its six legs of drilling. The emphasis of the study of the drilled samples and underway geophysical data was to confirm some aspects of plate tectonic theory, especially the

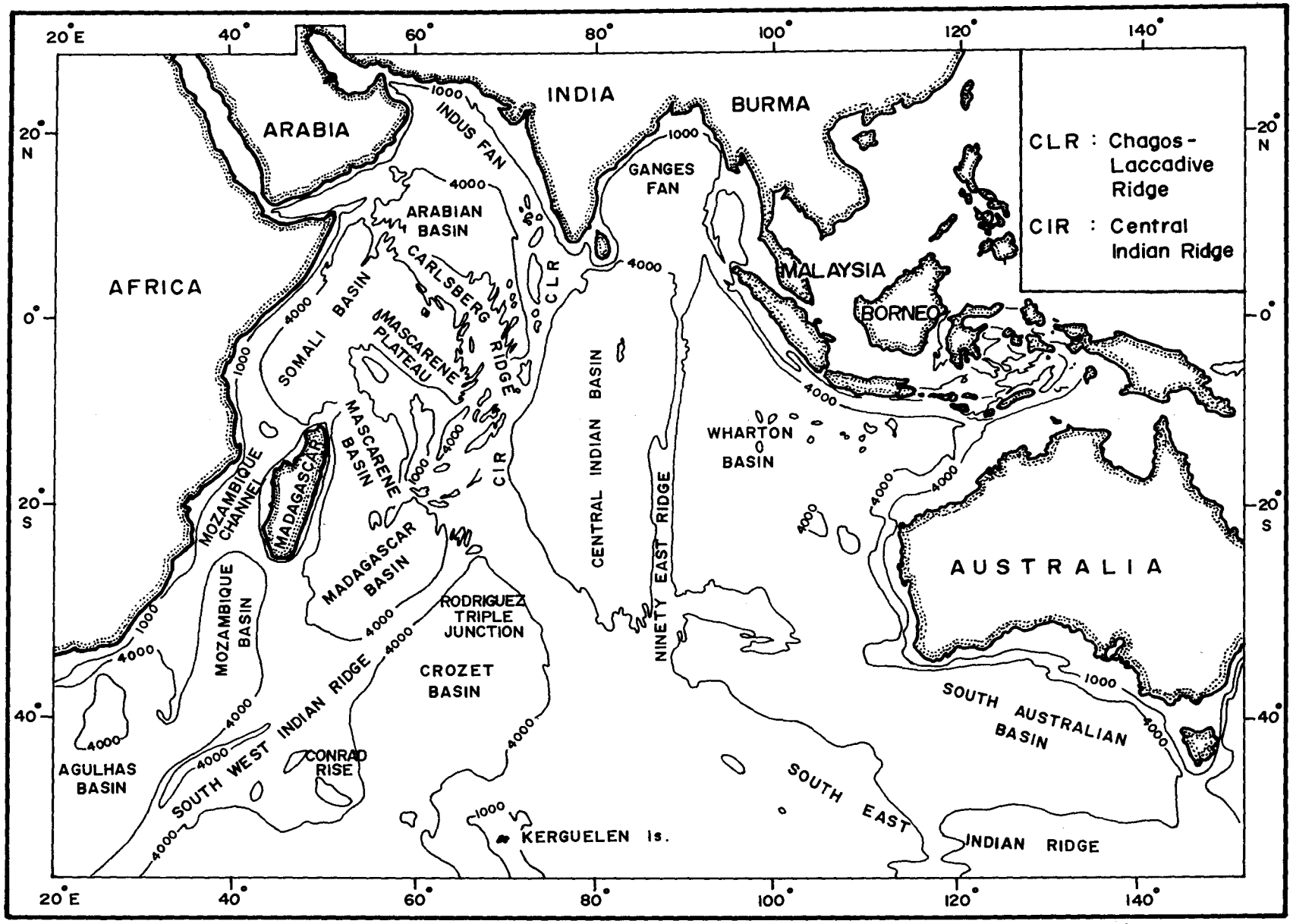

Figure 1.2 Physiographic features of the Indian Ocean (after Laughton et al., 1970a). Major bathymetric features are shown by 1000 and 4000 m depth contours.

breakup of Gondwanaland and formation of the Indian Ocean. Each leg objectives and area of operations are listed in Table 1.1 and the scientific achievements were summarized in several volumes edited by Heirtzler et al. (1977), von der Borch (1978) and Nairn and Stehli (1982). During 1987-1988, further drilling of the oceanic crust was carried out onboard "Joides Resolution" vessel in nine legs and core samples together with underway geophysical data were collected. The objectives and the sites of drilling are described in Table 1.2. The detailed reports of the drilling results are given in the Initial Reports of each leg. The scientific results of the drilling investigations are synthesized and presented in the volumes of each leg. Later, Duncan et al. (1992) have also summarized the results from the nine-legs (115-123) scientific drilling in the Indian Ocean. The results of the studies have revealed that the Indian Ocean is not only unique among other major oceans of the world, but also contains many geological features of global interest. Prominent among them are vast flood basalt provinces (Karoo, Deccan and Rajmahal) and submarine plateaus (Mascarene, Kerguelen-Heard, Broken Ridge) with associated hotspot trails (Chagos-Laccadive Ridge, Ninetyeast Ridge); intraplate deformation in the central Indian Ocean, two of the world's largest deep-sea fans (Indus and Ganges); passive continental margins with rifting ages ranging from Jurassic to Neogene; and zones of active plate collision and tectonics along the Himalayan mountain belt and the Indonesian arc-trench system (Figure 1.3). Many of these features are responsible for the present day configuration of the northwest Indian Ocean. A brief sequence of evolutionary history of the ocean is presented in Chapter 2.

1.3 ARABIAN SEA

The Arabian Sea lies in the northwestern Indian Ocean and occupies an area of nearly 7,50,000 km^2 which is about one-tenth of the area of the Indian Ocean. It is bounded to the west by the Arabia Peninsula and Africa, to the north by Iran and Pakistan, and to the east by India and the Chagos-Laccadive Ridge. Towards south, it extends up to the Mascarene Plateau where it is opened to the northwestern Indian Ocean (Figure 1.4). The earliest geophysical work was carried out in the Arabian Sea

Table 1.1 Details of the Deep Sea Drilling Project (DSDP) in the Indian Ocean (compiled from DSDP reports).

Leg	Drill Sites	Location	Objectives
22	211-218	Wharton Basin and Ninetyeast Ridge	• Tectonics of the Ninetyeast Ridge • Seafloor spreading history of the Wharton and Central Indian Ocean Basin
23a	219-224	Arabian Sea	• Dating of oceanic crust • Nature and origin of the Laccadive Ridge and Owen Fracture Zone • Geologic history of the SE Arabian Sea and the Indus Fan
23b	225-230	Red Sea	• Origin and extent of the heavy metal-rich deposits • Geologic history of the Red Sea
24	231-238	Gulf of Aden, Somali Basin, Mascarene Plateau, CIR and C-L-R	• Geologic history of Gulf of Aden and Somali Basin • Tectonic setting of the Mascarene plateau, CIR and C-L-R
25	239-249	Western and southwest Indian Ocean	• Age and mode of formation of western Somali basin • Stratigraphic column in the Mozambique channel • Nature of basement of Madagascar and Mozambique Ridges
26	250-258	Southern Indian Ocean	• Geologic and tectonic history of the SWIR, southern Ninetyeast Ridge, Broken Ridge, and southern Wharton Basin
27	259-263	Australian continental margin and the Timor Trough in eastern Indian Ocean	• Evolution of the Cuvier Abyssal plain • Sedimentation and tectonic history of the Argo Abyssal plain

Table 1.2 Details of the Ocean Drilling Program (ODP) in the Indian Ocean (compiled from ODP reports)

Leg	Drill Sites	Location	Objectives
115	705-716	Mascarene Plateau, Chagos-Laccadive Ridge	• Hotspot Life Cycle (Reunion) • Plate motion reference frames • Neogene carbonate production/dissolution.
116	717-719	Outermost Bengal Fan	• Intraplate deformation • Uplift history of the Himalayas
117	720-731	Owen Ridge, Oman continental margin, Indus Fan	• History of monsoons • Uplift of the Himalayas • Tectonism of the Owen Ridge
118	732-735	Atlantis II Fracture Zone	• Physical and chemical structure of the lower crust
119	736-746	Kerguelen Plateau, Prydz Bay	• Origin and subsidence history of the Kerguelen Plateau • Glacial history of the east Antarctica.
120	747-751	Kerguelen Plateau	• Origin and tectonics of the Kerguelen Plateau
121	752-758	Broken Ridge, Ninetyeast Ridge	• Lithospheric response to rifting • Hotspot life cycle (Kerguelen)
122	759-764	Northwest Australian margin	• Passive continental rift to drift mechanisms • Triassic-Cretaceous sea level history • Tethyan stratigraphy
123	765-766	Argo abyssal plain, NW Australian margin	• Tethyan stratigraphy • Oldest Indian Ocean crust • Geothermal reference site.
176	735B	Atlantis Bank, Southwest Indian Ridge	• Nature of geologic processes at slow spreading ridges
179	1105-1106	Southwest Indian Ridge and Ninetyeast Ridge	• Origin of gabbroic rocks • Preparation of an oceanfloor geophysical observatory

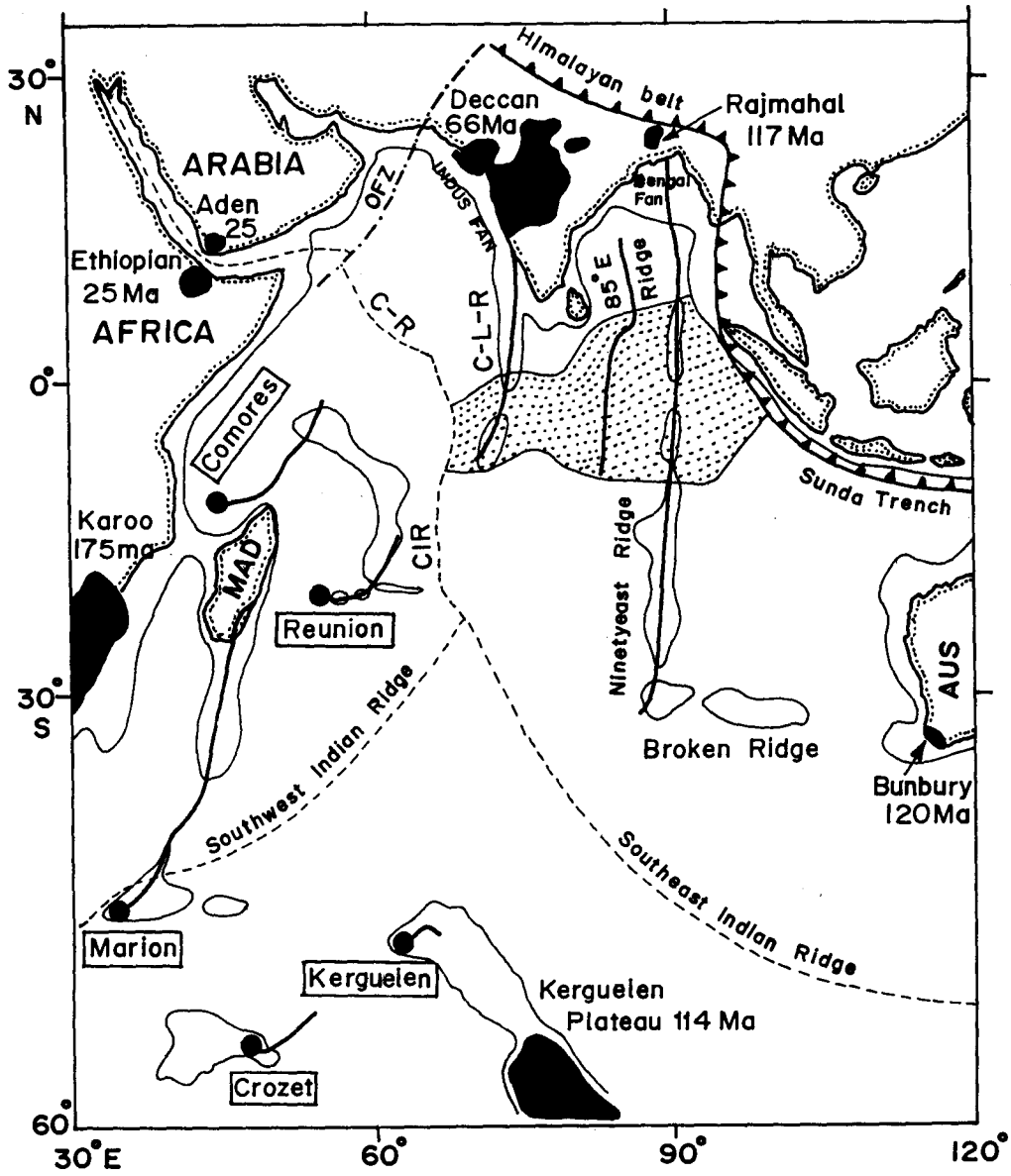

Figure 1.3 Major geological features and hotspot tracks of global interest in the Indian Ocean (compiled from Duncan and Richards, 1991; Muller et al., 1993). Large solid areas are locations of distribution of flood basalt provinces. Solid circles are locations of present day hotspots. Dotted area in the Central Indian Ocean represents intraplate deformation zone.

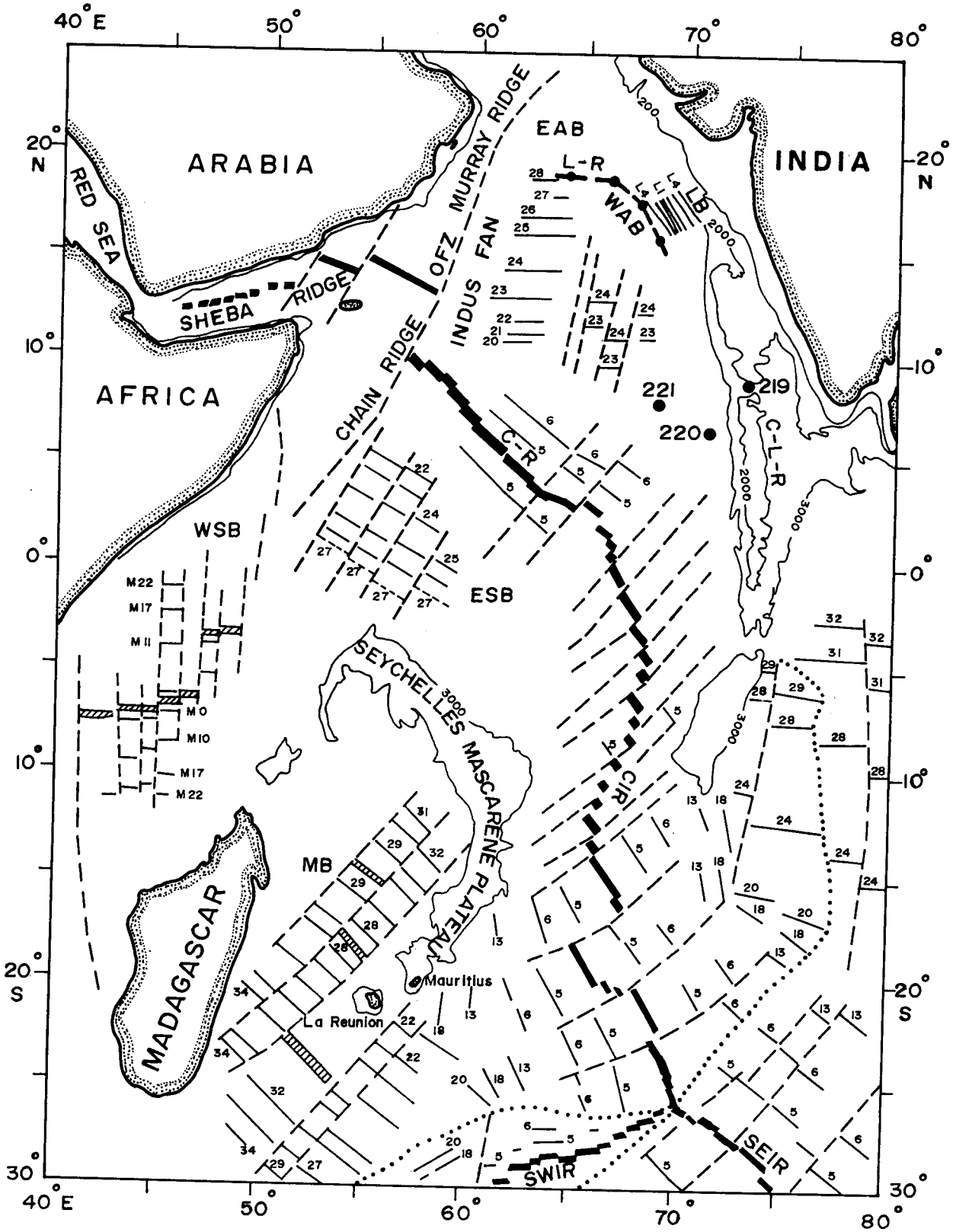

Figure 1.4 Generalized tectonic map of the Arabian Sea, showing magnetic lineations (solid lines), fracture zones (dashed lines) and main structural features (compiled from Naini and Talwani, 1982; Patriat and Segoufin, 1988; Miles and Roest, 1993; Bhattacharya et al., 1994a,b). C-L-R=Chagos-Laccadive Ridge; C-R=Carlsberg Ridge; L-R=Axis of Laxmi Ridge; OFZ=Owen Fracture Zone; WAB=Western Arabian Basin; LB=Laxmi Basin; ESB=Eastern Somali Basin; WSB=Western Somali Basin; MB=Madagascar Basin; L1-L4=Laxmi Basin magnetic lineations; Locations of DSDP Sites are shown with solid circles. Bathymetric contours are in meters. Dotted lines represent the Indian Ocean Triple Junction traces.

during 1959-66 under the International Indian Ocean Expedition followed by the Deep Sea Drilling Project investigations in 1972-74. The next important program in the Arabian Sea was the Ocean Drilling Program during 1987-89. Apart from these studies several countries mainly U.S.A., U.K., France, Russia and India have conducted several geophysical investigations in different parts of the Arabian Sea. The investigations revealed the existence of several plate boundaries in the Arabian Sea. The Macron coast marks the convergent boundary between Indian and Eurasian plates. The Carlsberg Ridge and Owen Fracture Zone form boundaries between Somalian and Indian plates, and Arabian and Indian plates respectively (Figure 1.2). Besides, several major physiographic features were mapped that include the active Carlsberg Ridge, Owen Fracture Zone, Indus Fan, aseismic Laxmi, Chagos-Laccadive and Prathap Ridges. These features divide the Arabian Sea into number of deep basins. Prominent among them are the Arabian Basin, Mascarene Basin, Eastern Somali Basin, and Western Somali Basin (Figure 1.4), which have been formed due to seafloor spreading at still active and extinct spreading centers (McKenzie and Sclater, 1971; Whitmarsh 1974; Norton and Sclater, 1979; Naini and Talwani, 1982; Schlich, 1982; Miles and Roest, 1993). The Arabian Basin, where the study area is located, is bounded to the west by the Owen Fracture Zone and to the northwest by the Murray Ridge. It merges to the north into the Indus Cone (Schlich, 1982). The basin is further divided into number of sub-basins such as Western Arabian Basin, Eastern Arabian Basin, Laxmi Basin etc. A general description of the major physiographic features of the Arabian Basin and the adjoining region is given in the following sections.

1.3.1 INDUS FAN

The Indus Fan, 1,650 km long and 960 km wide, is the second largest deep-sea fan in the world. It extends from the continental shelf of Pakistan in the north to the flanks of the spreading Carlsberg Ridge in the south. Laterally, the sedimentary body of the fan is bounded by the aseismic Chagos-Laccadive Ridge to the east and the Owen Fracture Zone and Murray Ridges to the west. The fan is divided into several basins of

relatively thick sedimentary fill (Naini and Kolla, 1982). The fan sediments and basement have been drilled during the DSDP Leg 23 (Sites 220-223) and ODP Leg 117 (Site 720) investigations. The drilling results led to a greater understanding of the origin and depositional mechanisms of sediments in the fan (Jipa and Kidd, 1974; Whitmarsh et al., 1974; Prell et al., 1989). The studies of the morphology (Coumes and Kolla, 1984; Kolla and Coumes, 1984, 1985, 1987; Droz and Bellaiche, 1987; Ayub, 1992), sediment thickness and nature of acoustic basement (Neprochnov, 1961; Narain et al., 1968; Closs et al., 1969; Ewing et al., 1969; Rao, 1970; Harbison and Bassinger, 1973; Naini and Talwani, 1977, 1982; Naini and Kolla, 1982) of the Indus Fan shed light on the turbidite channels geometry, migration and levies of sediments, maximum sediment thickness (~11 km) at the proximity of the Indus mouth and the underlying oceanic to shear rifted continental crust. Based on analysis of the ancient sediments from DSDP Sites 220 to 223, Weser (1974) concluded that the Indus Fan sedimentation in the Arabian Sea has started in the Middle or Late Oligocene time.

1.3.2 OWEN FRACTURE ZONE

The Owen Fracture Zone, one of the largest fracture zone of the ocean floor, was first identified by Matthews (1966). It trends NE-SW and extends for over 2700 km southwestwards from the coast of Karachi in Pakistan to the middle of the Somali Basin (Kalyayev et al., 1983). It demarcates the transform boundary between the Indian and Arabian plates. Partly, it acts as a right lateral transform fault between the Sheba and Carlsberg Ridges. Physiographically, this fracture zone is represented by northeast trending ridges. The most conspicuous among them are the Chain Ridge in the southwest and the Murray Ridge in the northeast (Figure 1.4).

1.3.3 CARLSBERG RIDGE

The John Murray Expedition (1933-1934) sponsored by the Carlsberg Foundation discovered a mid-ocean ridge in the Arabian Sea which now bears the name Carlsberg Ridge. Based on results of the expedition, Wiseman and Seymour-Sewell

(1937) have interpreted that the Carlsberg Ridge can be traced from the Arabian Sea, through the Gulf of Aden to the Ethiopian rift system. The Carlsberg Ridge runs northwest-southeast between the Owen Fracture Zone and the equator across the middle of the Arabian Sea (Figure 1.3). It continues as the Sheba Ridge beyond the Owen Fracture Zone into the Gulf of Aden (Matthews, 1963, 1966). The Sheba Ridge and the Carlsberg Ridge are offset right laterally by about 300 km along the Owen Fracture Zone (Figure 1.4). The geophysical investigations (Matthews et al., 1965; Cann and Vine, 1966; Vine, 1966; Le Pichon and Heirtzler, 1968; Fisher et al., 1968; McKenzie and Sclater, 1971; Kalyayev et al., 1983; Ramana et al., 1993) over the Carlsberg Ridge have indicated that the ridge, with its rough topography, shows the typical morphology of a slow-spreading ridge. Besides the Owen Fracture Zone, the central part of the ridge is offset by small transform faults, whereas the southern end of the ridge is offset by major transform faults. Further, magnetic anomalies 3 and 5 are mapped on either sides of the ridge. On its western flank, Tisseau (In Schlich, 1982) has identified anomalies 6 and 7. Based on magnetic anomaly pattern Le Pichon and Heirtzler (1968) has estimated a half spreading rate of 1.5 cm/yr, while McKenzie and Sclater (1971) have estimated 1.2-1.3 cm/yr.

1.3.4 CHAGOS-LACCADIVE RIDGE

The Chagos-Laccadive Ridge (C-L-R), a prominent linear aseismic ridge (Heezen and Tharp, 1965), extends almost north-south between 14° N and 9° S and is ~2500 km long and ~200 km wide (Figure 1.4). The ridge is a topographic feature and is slightly arcuate with convex side facing the east. A considerable length of the crest of the ridge is composed of shoals, banks, coral reefs and atolls at depth less than 1500 m and broadly, these shoal areas are grouped as the Laccadive, Maldive and Chagos Islands. The ridge consists of several irregular blocks separated by relatively deep east-west trending channels. The northern part of the ridge is parallel to the western continental shelf of India. The eastern flank of the ridge between 8° and 10° S, is bounded by a steep depression called the Chagos Trench.

The free-air gravity anomalies over the ridge are generally negative. However they are relatively positive (~25 mGal) when compared with the free-air gravity anomalies of the surrounding regions (Kahle and Talwani, 1973, Naini and Talwani, 1982). The southern part of the ridge is associated with the anomalies close to zero with positive values at some places. Magnetic anomalies over the ridge do not show any definite pattern (McKenzie and Sclater, 1971; Naini and Talwani, 1982). Some parts of the ridge are associated with high amplitude magnetic anomaly suggesting volcanic origin.

The origin of the ridge is attributed to various processes such as transform faulting, microcontinent tectonics and a hotspot trace. Francis and Shor (1966), based on seismic refraction measurements, suggested that the ridge is a continuous volcanic feature. They further suggested that between the Maldive and Chagos groups the lavas poured out at oceanic depths, whereas between the Maldive and Laccadive groups, the lavas solidified near the sea surface. Narain et al. (1968), based on seismic refraction results of Francis and Shor (1966), have opined that the ridge in its northern part forms a transition between oceanic crust to the west and continental crust to the east.

Fisher et al. (1971) and McKenzie and Sclater (1971) have suggested that the C-L-R was build up over an old transform fault during the Cretaceous to the Eocene period while India moved northward. Dietz and Holden (1970), Morgan (1972) and Whitmarsh (1974) have suggested mantle hotspot origin of the C-L-R. Avraham and Bunce (1977), based on geophysical evidence, have suggested that the C-L-R is composed of structural elements of multiple origin. They suggested that the ridge consists in part of several north-south fracture zones and in parts of volcanic features formed either by leaky transform faults or by the passage of Indian plate over a hotspot. Further, they suggested that the Maldive Island segment consists of micro-continents that rifted away from India probably before the Paleocene. Detrick et al. (1977) have suggested that the ridge subsided ~2000 m at a rate of normal oceanic crust.

The results of DSDP and ODP suggest that the Deccan Trap volcanic province

of the Indian peninsula and the C-L-R was formed by volcanic build up during the northward motion of Indian plate over the Reunion hotspot (Shipboard Scientific Party, 1988; Richards et al., 1989; Duncan, 1990). However, there is a considerable debate about the nature and origin of the Laccadive Ridge, the northern extension of the C-L-R which parallels the west coast of India. Naini and Talwani (1982), based on crustal structure of the ridge, have interpreted continental nature of the Laccadive Ridge. The crest of the ridge is associated with a graben like feature (Gopala Rao et al., 1987). The magnetic anomalies are less prominent over the eastern half of the Laccadive Ridge compared to the western half where high amplitude anomalies are present. The lack of appreciable magnetic anomalies over the ridge led Gopala Rao et al. (1987) to suggest continental origin for the Laccadive Ridge. It is characterized by a generally raised acoustic basement mantled by transparent sediments. The acoustic basement is governed at places by steep scarps and volcanic intrusives reflected by large amplitude magnetic anomalies.

1.3.5 LAXMI RIDGE

An isolated submarine structure extending northwest-southeast between 15° and 18°N in water depths between 2600 and 3000 m was first reported by Naini and Talwani (1977) and named as the Laxmi Ridge (Naini, 1980). The ridge is overlain by about 500 m thick sediments with P-wave velocities ranging from 1.7 to 3.9 km/s. Naini and Talwani (1982) have interpreted that the ridge is made up of three crustal layers of 1.74, 4.65 and ~11.0 km thick with P-wave velocities of 5.3, 6.2 and 7.15 km/s, respectively. The ridge is associated with low (<-25 mGal) free-air gravity anomaly and lacks correlatable magnetic signatures. Based on crustal structure and low gravity anomalies of the ridge, Naini and Talwani (1982) have suggested continental origin of the Laxmi Ridge. Pandey et al. (1995), based on two-dimensional gravity modeling, have interpreted 11 km thick normal oceanic crust of the ridge with a possible emplacement of an anomalous subcrustal low-density layer between 11 and 19 km depth.

1.3.6 PRATHAP RIDGE

The presence of small structural highs off the western continental shelf of India has been first reported by Harbison and Bassinger (1973). Later basement ridges with steep flanks near the shelf edge between Goa and Mangalore coast were identified by Ramaswamy and Rao (1980). They postulated that some of them are part of continuous basement ridges parallel to the coast. Naini (1980) mapped these structural highs under the continental rise off the southwest coast of India between 8° and 17°N. This structural high varies in width from 50 to 100 km and extends for about 1100 km in a northwest-southeast direction parallel to the western continental shelf edge of India on the east and to the Laccadive Ridge on the west (Figure 1.5). This feature was named by Naini (1980) as the Prathap Ridge. The ridge is mostly buried below the Tertiary sediments and at places occurs as single and multiple peaks along its length. Therefore, it is termed as ridge complex. The ridge is characterized by well developed free-air gravity and magnetic anomalies over the exposed segments of the ridge (Gopala Rao et al., 1987; Subrahmanyam et al., 1989; Krishna et al., 1992). Naini (1980) and Subrahmanyam (1992) have suggested that the ridge might have originated during the initial phase of rifting along the western margin of India and represent a continental sliver, intermingled with dykes and volcanics. Whereas, Krishna et al. (1992) have suggested that the ridge might have formed due to Reunion hotspot activity.

1.3.7 WESTERN ARABIAN BASIN

The Western Arabian Basin (WAB), a part of the Arabian Basin, is bounded to the west by the Owen Fracture Zone which demarcates the transform boundary between the Indian and Arabian plates. The uneven topography of the NW-SE trending active Carlsberg Ridge, which separates the Indian and African plates, forms the southern boundary. Whereas most of the northern and eastern limit of the basin is bounded by the aseismic Laxmi and Laccadive Ridges (Figure 1.5). The basin is covered by Indus Fan sediments which determines the submarine topography. The water depth in this area varies from 3400 m in the north to about 4400 m in the south and relatively smooth and

sediment covered seafloor in general dips southward. The sediment in this basin is of variable thickness and ranges between 1.3 and 4.2 km with velocity variation from 1.7 to 3.8 km/s (Naini, 1980). The crust underlying the sediment display velocities between 5.0 and 7.0 km/s. The basin is underlain by oceanic crust and exhibits well-developed early Tertiary seafloor spreading type magnetic anomalies (McKenzie and Sclater, 1971; Norton and Sclater, 1979; Miles and Roest, 1993).

1.3.8 EASTERN ARABIAN BASIN

The Eastern Arabian Basin (EAB) is located between the Laxmi and Laccadive Ridges and the western continental slope of India. The water depths in the basin range from ~1.4 to 3.6 km. The gross crustal structure of the basin as revealed by seismic refraction results indicates that about 2.4 km of sediment overlies a 11.0 km thick crust (Naini, 1980; Naini and Talwani; 1982). The magnetic anomalies in the basin trend nearly northwest-southeast and are approximately parallel to the present day shelf edge of western India. The basin is characterized by low-amplitude (~20 mGal) short-wavelength (~60 km) free-air gravity low superimposed on a long-wavelength (~350 km) gravity high (Naini, 1980). These observations have led Naini (1980) to believe that the EAB was evolved by taphrogenic process and the crust could be either continental, transitional or oceanic in nature. However, based on thicker crust than normal oceanic crust, and lack of seafloor spreading-type magnetic anomalies, the crust under the EAB was inferred as transitional type and suggested its formation during the initial phase of rifting (Naini, 1980; Naini and Talwani, 1982).

Bhattacharya et al. (1994a) have carried out a detailed geophysical study in the Laxmi Basin. They have defined Laxmi Basin as part of the EAB that is bounded in the west, south and east by the Laxmi Ridge, the northern extremity of the Chagos-Laccadive Ridge and the continental shelf of India respectively. They have reported, for the first time, well correlatable NNW-trending magnetic anomalies in this basin. The magnetic lineations are symmetric about a central negative magnetic anomaly and the axis of symmetry coincides with a characteristic short-wavelength free-air gravity low.

The magnetic lineations are contiguous and parallel to the adjacent segment of the Laxmi Ridge in the west and the continental shelf edge in the east. Based on these observations they opined that the Laxmi Basin magnetic lineations represent a two-limbed seafloor spreading sequence of anomalies 28 through 33 interval of the geomagnetic polarity reversal time scale. Based on these results, they have concluded that the Laxmi Basin is underlain by an oceanic crust. In an other study of multibeam swath bathymetric investigations, Bhattacharya et al. (1994b) have reported NNW-trending linear seamount chain along the axial part of the Laxmi Basin. The chain consists of three major edifices, Raman and Panikkar seamounts and Wadia guyot. The origin of these seamounts is attributed by them due to anomalous volcanism resulting from the interaction of the Reunion hotspot with the extinct spreading center. Geophysical study carried out by Malod et al. (1997) has revealed continuation of the Laxmi Basin magnetic lineations proposed by Bhattacharya et al. (1994a) in a portion of the EAB (northwest of the Laxmi Basin). Their study also suggested presence of oceanic crust in that area. However, they proposed that spreading initiated at Chron 29R synchronous with Deccan Trap eruption and continued till Chron 29 at a relatively high spreading rate (about 5.0 cm/yr full spreading rate).

1.4 OUTSTANDING PROBLEMS

The seafloor spreading history of the Arabian Sea was studied by several workers (McKenzie and Sclater, 1971; Whitmarsh, 1974; Norton and Sclater, 1979; Naini and Talwani, 1982; Schlich, 1982; Miles and Roest, 1993; Mercuriev et al., 1995). These studies revealed that the Western Arabian Basin and its conjugate the Eastern Somali Basin (bounded by the Carlsberg Ridge, the Seychelles Bank and Chain Ridge) are generated by seafloor spreading along the Carlsberg Ridge in two distinct phases. The early phase of spreading commenced during the Early Paleocene when the spreading center between Madagascar and India jumped northward and formed the Carlsberg Ridge separating Seychelles from India. The first phase of spreading ceased or became very slow some time after formation of anomaly 23. This waning phase of

spreading possibly corresponds to the time of the progressive collision of India with Eurasia and major reorganization of spreading geometry in the Indian Ocean (McKenzie and Sclater, 1971; Norton and Sclater, 1979; Schlich, 1982). The spreading during the second phase resumed in a NE-SW direction and is still active in the same direction. Anomaly 5, which is identified conclusively, is the oldest anomaly of this phase, though anomalies 6 and 7 were also reported to have been identified by Tisseau (In Schlich, 1982). However, the timing of the end of the first phase and beginning of the second phase of spreading in the Arabian Sea are yet to be established.

Although the Western Arabian Basin was formed during a period of rapid seafloor spreading and contains distinct magnetic anomaly lineations, the limited number of magnetic profiles available have produced various speculative magnetic anomaly identifications. Consequent tectonic interpretation, particularly adjacent to the continental margin, has been generalized (McKenzie and Sclater, 1971; Norton and Sclater, 1979; Schlich; 1982; Naini and Talwani, 1982; Masson, 1984; Miles and Roest, 1993). The identification of the oldest seafloor spreading anomaly in the Western Arabian Basin is not established conclusively. Anomaly 28 is identified as the oldest magnetic anomaly by McKenzie and Sclater (1971) and Naini and Talwani (1982). On the other hand, in the conjugate Eastern Somali Basin, the oldest identifiable anomaly 29 was considered by McKenzie and Sclater (1971). While Schlich (1982) considered it as anomaly 27. Further, mapping of the seafloor spreading magnetic lineations over large parts of the Western Arabian Basin remained incomplete either due to the presence of many unidentified magnetic lineations or due to absence of any mappable lineations. Several major fracture zones have been identified but poorly constrained.

Although the anomaly lineations in the Western Arabian Basin generally trend east-west, according to some interpretations the early seafloor spreading lineations did not parallel this direction. Masson (1984) proposed an earlier northwest trending spreading phase prior to anomaly 28. While Norton and Sclater (1979) inferred some southeast migration of spreading. Both interpretations have attempted to accommodate

the angular disparity between east-west oceanic magnetic lineations in the Western Arabian Basin and more northwest-southeast trends of the continental shelf of western India and the Laccadive Ridge. However, their relationship to the kinematics of margin formation is not established. As has been mentioned that the Chagos-Laccadive Ridge was formed by volcanic build-up as the Indian Plate migrated over the former position of the Reunion hotspot (Duncan, 1981; Morgan 1981; White and McKenzie, 1989; Ashalatha et al., 1991). However, the geophysical studies carried out so far have not permitted an unequivocal conclusion regarding the nature and origin of the Laccadive Ridge, the northern part of the C-L-R which is parallel to the western Indian margin. Further the location of the ocean-continent boundary and the nature of the marginal structures are not well understood.

1.5 STUDY AREA AND OBJECTIVES OF PRESENT INVESTIGATIONS

The present studies are carried out using bathymetry, gravity, magnetic and multichannel seismic reflection data in a part of the eastern Arabian Sea. The geographical location of the study area is given in the following section.

1.5.1 STUDY AREA

The study area is located in the eastern Arabian Sea and covers the Western Arabian Basin, Laccadive Ridge and southwestern continental margin of India. Geographically, the study area is bounded to the west by the Owen Fracture Zone, to the south by the active Carlsberg Ridge, to the north by the Laxmi Ridge, and to the east by the west coast of India (Figure 1.5).

1.5.2 OBJECTIVES

The present marine geophysical investigations are aimed to decipher crustal structure and provide better constraints to understand the evolution of the study area in particular and eastern Arabian Sea in general. For this purpose, well oriented and closely

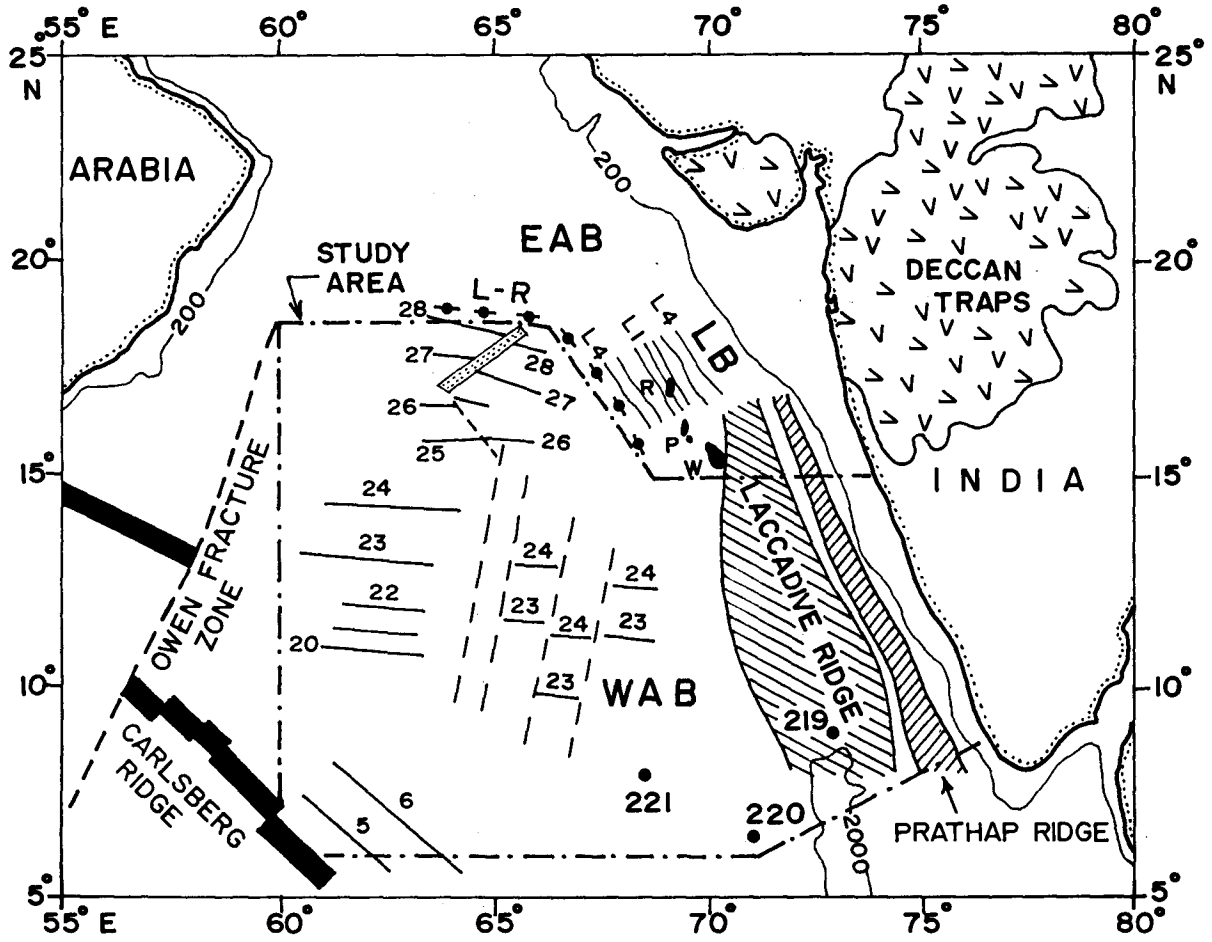

Figure 1.5 Generalized map of the study area (dashed dotted block), showing magnetic lineations (solid lines), fracture zones (dashed lines) and main structural features (compiled from Naini and Talwani, 1982; Bhattacharya et al. 1994a, b; Miles and Roest, 1993). R=Raman Seamount; P=Panikkar Seamount; W=Wadia Guyot; L1–L4 represent magnetic lineations in the Laxmi Basin; LB=Laxmi Basin; L-R=Axis of Laxmi Ridge; EAB=Eastern Arabian Basin; WAB=Western Arabian Basin.

spaced profiles of bathymetry and magnetic data are used to study the linear magnetic anomaly pattern of the Western Arabian Basin. Bathymetry and gravity data are used to study the nature and origin of the Laccadive Ridge. A regional multichannel seismic reflection profile across the central western continental margin of India was analyzed to identify the ocean-continent boundary/transition and to understand sedimentation history, crustal structure and tectonics of the margin. The specific objectives of the investigations are aimed to:

- Identify linear magnetic anomalies and, thereby, establish their trend in the Western Arabian Basin.
- Identify offset pattern of the magnetic lineations of the Western Arabian Basin for delineation of paleo-propagating spreading ridges.
- Study the dynamic characteristics of the paleo-propagators and its interaction with the Reunion hotspot.
- Identify linear magnetic anomalies along two regional profiles extending from the WAB to the Carlsberg Ridge and to establish the timing of the end of the first phase and beginning of the second phase of spreading in the region.
- Provide a reasonable constraints for the nature and origin of the Laccadive Ridge.
- Identify ocean-continent boundary/transition and understand the sedimentation history and crustal structure.
- Understand the evolution of the eastern Arabian Sea and its implication to the development of western continental margin of India.

CHAPTER 2

CHAPTER 2

GEOLOGIC AND TECTONIC FRAMEWORK

2.1 INTRODUCTION

Evolution of the western continental margin of India is closely related to the tectonic history of the Indian subcontinent; its break up during continental rifting, northward movement and finally collision with the Eurasian plate. It is worthwhile to collate the available information on geology, crustal structure and tectonics of the study area with that of the adjoining onshore region to arrive at meaningful interpretation of the geophysical anomalies observed in the study area. The directional trends defined by structural grain on the adjoining onshore area are important because they controlled, to a large extent, the subsequent pattern of the continental fragmentation and rifting that gave rise to the present tectonic configuration of western continental margin of India. This information would facilitate to a better interpretation of the geophysical anomalies observed in the study area and in turn provide a better understanding of the evolution of the margin in time and space. In the following sections, regional geologic and tectonic settings of the study area and adjoining onshore region are described.

2.2 REGIONAL GEOLOGY AND TECTONIC SETTINGS OF ONSHORE REGION

The major portion of the Indian peninsula is a shield and is an ancient fragment of the Gondwanaland. It consists of Archaean gneisses and schists and metamorphosed sedimentary rocks. The rest of the peninsula is covered by the Deccan and Rajmahal Traps (Krishnan, 1968). The onshore region adjoining the study area is the Dharwar craton (also known as Karnataka craton) located approximately between latitudes 8^0 to 17^0 N and longitudes 73^0 to 80^0 E (Figure 2.1). The craton is covered by the Deccan Traps to the north and is bounded by Godavari valley to the northeast, Eastern Ghats to

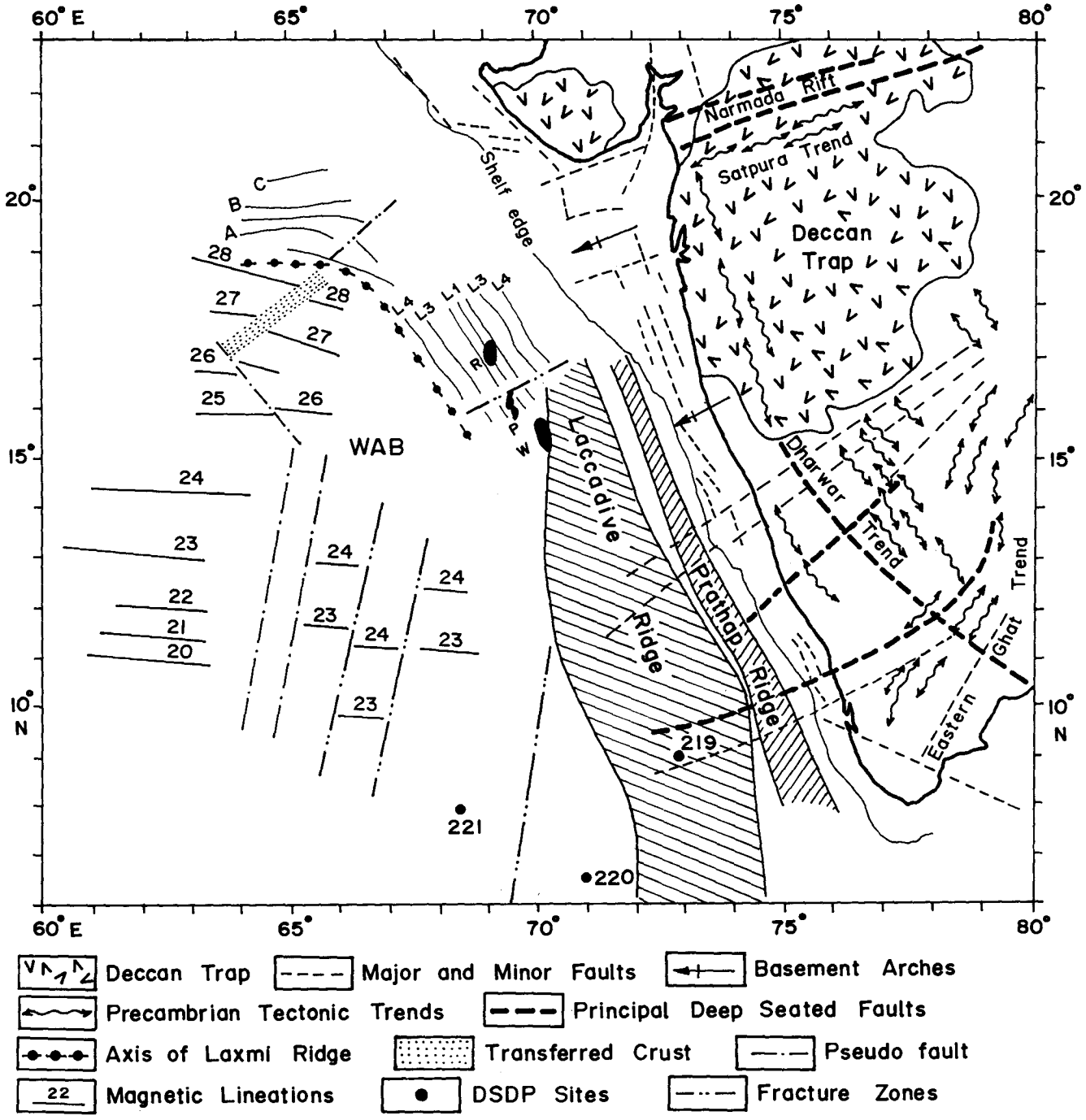

Figure 2.1 Major structural and tectonic trends of the study area and adjoining western Indian subcontinent (compiled from Bhattacharya and Subrahmanyam, 1986; Kolla and Coumes, 1990 and references therein).

the east and south, and the Arabian Sea to the west (Verma, 1991). Major morphological feature of the area is the Western Ghats parallel to the coast and the geology includes the Dharwar schist belts, Closepet granites, Peninsular gneisses, sediments of Cuddapah basin as well as several granitic bodies and charnockites (Verma, 1991). The basement grains of Dharwar craton trend NW-SE to NNW-SSE and is the dominant Precambrian structural and tectonic trend in the western peninsular India (Krishnan, 1968). This trend is parallel to the west coast of India and extends from southern India to the north into the Kutch area, although buried in the north for large distance by the Deccan Traps (Das and Ray, 1976). Apart from the Dharwar trend, the NE-SW Aravalli trend and ENE-WSW Satpura trend along the Narmada-Son lineament in the north, and NE-SW Eastern Ghat trend in the south are the other dominant structural fabric of the western India (Figure 2.1). These major tectonic trends controlled the structural styles of several intracratonic and pericratonic sedimentary basins such as the Kutch, Cambay and Narmada (Raju, 1979; Biswas, 1987).

The Deccan Traps are one of the largest known continental flood basalt (CFB) provinces on earth and is due to a prominent tectonic event that has affected the western and central India. They consist of subaerially erupted successive basaltic flows in the western and central India and their estimated maximum thickness is ~2.0 km. It covers an area of more than $5*10^5$ km^2, almost one-sixth of the total surface area of the Indian Peninsula, with an estimated volume of about $1.5*10^6$ km^3 (Courtillot et al., 1986; Shipboard Scientific Party, 1988; Verma, 1991). The origin, timing and duration of this CFB event has been the subject of considerable debate (Alvarez et al., 1980; Baksi, 1988, 1994; Courtillot et al., 1988; Duncan and Pyle, 1988; Rampino and Stothers, 1988; Negi et al., 1992; Basu et al., 1993). A large thermal anomaly, generated by a deep mantle plume (Reunion hotspot) during continental breakup is commonly postulated to explain the Deccan flood basalt event (Morgan, 1972, 1981; Courtillot et al., 1986; White and McKenzie, 1989; Duncan, 1990; Baksi and Farrar, 1991; Basu et al., 1993). The time of Deccan Traps eruptions are reported to be within 62-72 Ma (Acton and Gordon, 1989); 65-68 Ma (Vandamme et al, 1991), 65-69 Ma (Courtillot et al., 1988) and 64-67 Ma, with peak volcanism at ~65 Ma (Bhattacharji et al., 1996).

However, Courtillot et al. (1986) have suggested that the total duration of Deccan Traps volcanism might not have exceeded the short time span (<1 Ma) around chron 29R (~ 65 Ma).

2.3 REGIONAL GEOLOGY AND STRUCTURAL TRENDS OF THE STUDY AREA

The western continental margin of India, a passive margin , is characterized by i) a wide continental shelf having NW-SE trend, ii) a remarkably straight edge limited by ~200 m isobath, iii) a narrow continental slope bounded between 200 and 2000 m isobath and iv) deep sedimentary basins (Figure 2.2). The shelf is ~300 km wide in Kutch-Saurashtra area and gradually narrows down southward to ~50 km in Kerala offshore area. Complementary to this, the continental slope is narrow in the north but widens towards south (Biswas, 1982, 1987, 1988). The shelf area is comprised of mainly four shelf sub-basins, namely Kutch, Saurashtra, Bombay and Konkan-Kerala offshore basins. The Konkan-Kerala basin is located on the shelf between Vengurla in the north to Cape Comorin in the south.

The prominent structural features of the study area are i) the Konkan-Kerala basin characterized by the horst-graben structures on the shelf, ii) the shelf-margin basin, iii) the Prathap Ridge which divides the shelf margin basin longitudinally into two parts, iv) the Laccadive Ridge, and v) the WAB (Figure 2.1). Earlier studies (Eremenko, 1968; Eremenko and Datta, 1968; Bhattacharya and Subrahmanyam, 1986; Ramana, 1986; Subrahmanyam, 1992) have suggested extension of onshore lineaments over a considerable distance into the offshore region. They include the faults and basements arches of the shelf and are mainly parallel to the Dharwar (NW-SE to NNW-SSE) and Eastern Ghat (NE-SW) trends (Anonymous, 1968). Biswas (1987) has pointed out that the horst-graben structures, basement arches and fault patterns of the shelf areas are formed due to rifting and movements along the ancient Precambrian structural trends. Kolla and Coumes (1990), based on compilation of the basement, faults and structural trends of the western continental margin of India, have inferred that the trends are

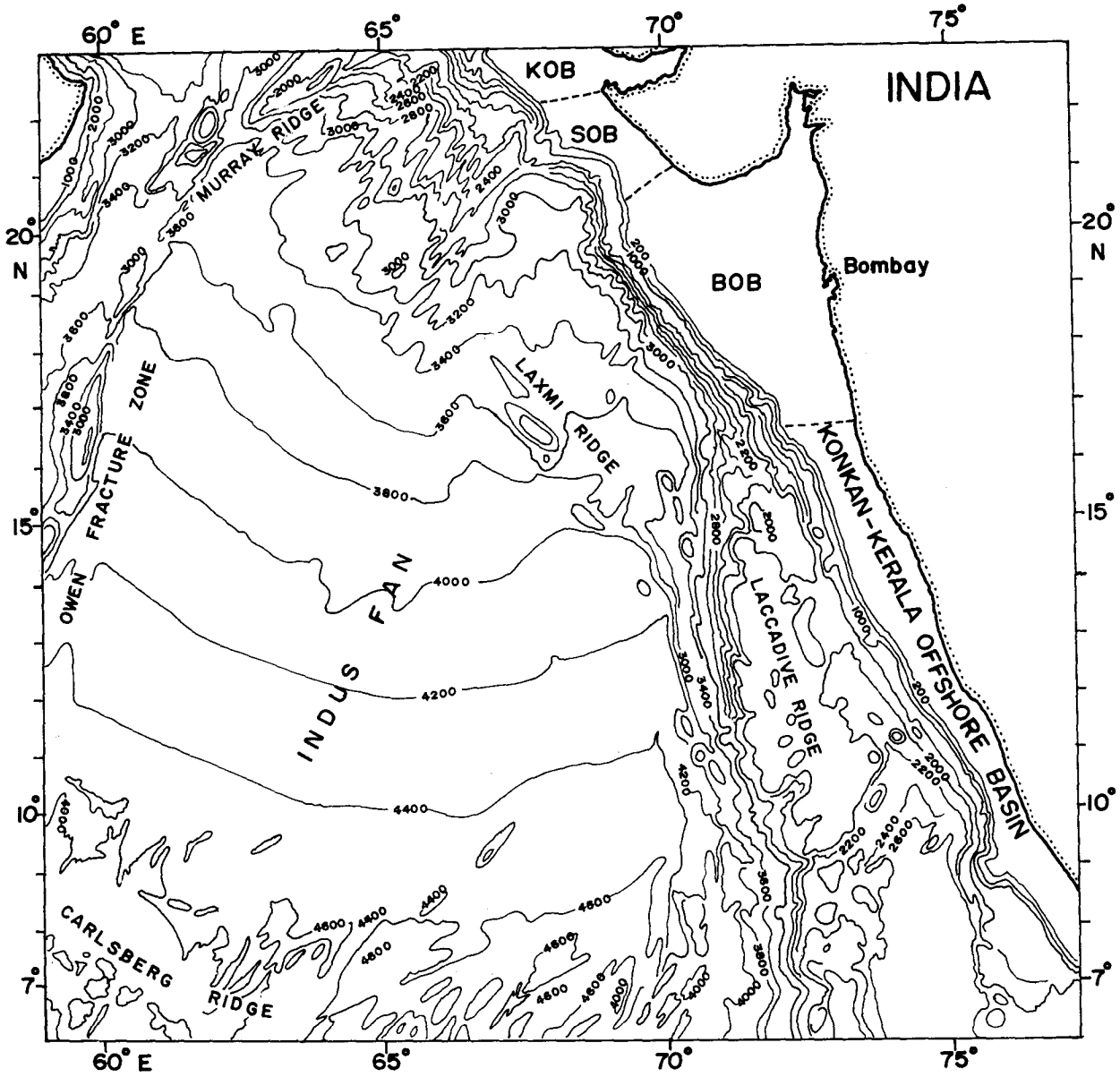

Figure 2.2 Bathymetry (contour interval 200 m) of the study area and adjoining region (after Kolla and Coumes, 1990). Prominent bathymetric features such as the aseismic Laccadive and Laxmi Ridges, the active Carlsberg Ridge, Owen Fracture Zone and its northern extension the Murray Ridge, and the Indus Fan are labeled. KOB=Kutch Offshore Basin, SOB=Saurashtra Offshore Basin, BOB=Bombay Offshore Basin.

parallel to the ancient Precambrian structural and tectonic grain of the Indian subcontinent. Ramaswamy and Rao (1980), Rao and Srivastava (1984), Singh and Lal (1993), Pandey and Dave (1998) from seismic reflection data and drill well results of Konkan-Kerala basin, have interpreted i) progradation of shelf since the Miocene, ii) Eocene to Middle Miocene succession of limestone, shale and sandstone, iii) Late Miocene to Recent succession of shale and claystone. End of Middle Eocene and Early Oligocene are identified by them as regional hiatuses in this area.

The DSDP Site 219, located on the crest of the Laccadive Ridge, indicated shallow water Upper Paleocene limestone, sandstone and siltstones succeeded by Eocene chalk and ooze (Whitmarsh et al., 1974). The DSDP Sites 220 and 221 located in the WAB indicated that i) the Middle Eocene age of the oldest sediment overlying the oceanic basalt at Site 221 and ii) an age of 51 m.y. for the oldest sediments at Site 220 suggesting an older age for the underlying oceanic basalt (Whitmarsh et al., 1974). Naini and Talwani (1982), Kolla and Coumes (1990) have interpreted the oceanic nature of the basement west of the Laccadive Ridge and rifted transitional crust between the shelf and the Laccadive Ridge. Biswas (1988, 1989) has suggested that the boundary between the oceanic and the continental crust may lie close to the continental slope.

2.4 EVOLUTION OF THE CONTINENTAL MARGIN OF WESTERN INDIA AND THE EASTERN ARABIAN SEA

The development of the western margin basins is related to reactivation of major faults along Precambrian trends during Late Triassic-Early Jurassic rifting of the Gondwanaland (Biswas, 1982). Whereas, the opening of the Arabian Sea is linked to the break up of the Seychelles-Mascarene plateau from India during the Early Paleocene (Besse and Courtillot, 1988). Therefore, in the following paragraphs the opening of the Indian Ocean in general and Arabian Sea in particular are discussed.

The unified Gondwanaland in the southern hemisphere was comprised of present day South America, Africa, Arabia, Madagascar, Sri Lanka, India, Australia and New Zealand (Figure 2.3). The Gondwanaland has broken into several fragments from the

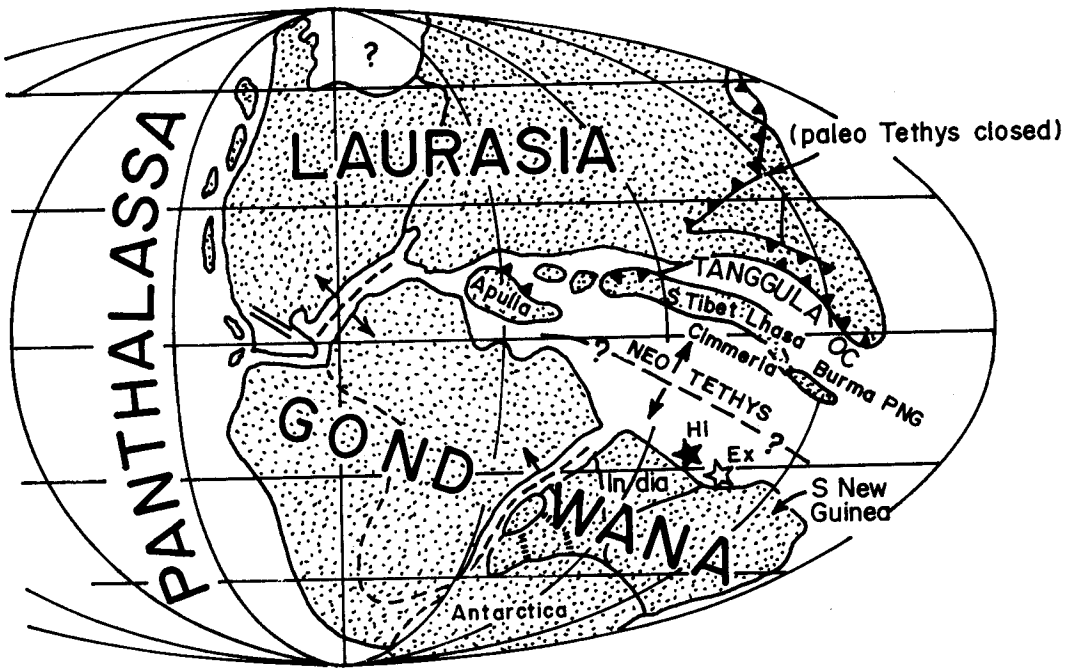

Figure 2.3 Reconstruction of continents and oceans during Jurassic time (Gradstein and von Rad, 1991). Ex=Exmouth Plateau, Hi=Tethys Himalaya, PNG=Papua-New Guinea.

Jurassic to the Recent and the consequences are the several minor and major plate boundary reorganizations with greater implications in the evolution of the crust of the Indian Ocean and the adjoining margins. Several earlier studies have described the break up and rift-drift history of the part of the Gondwanaland and their reconstruction for different geological pasts primarily based on marine geophysical results such as identified seafloor spreading magnetic anomalies, transform faults, fracture zones and paleomagnetic data (McKenzie and Sclater, 1971; Larson, 1975; Exon and Willcox, 1978; Norton and Sclater, 1979; Veevers, 1986; Besse and Courtillot, 1988; Scotese et al., 1988; Duncan, 1990; Gradstein and von Rad, 1991; Royer et al., 1992). Results of these studies have revealed the following major tectonic episodes from the break up of Gondwanaland that affected the Indian subcontinent since the Jurassic:

1. The breakup of Gondwanaland into Eastern Gondwanaland (Madagascar-Seychelles-India-Antarctica-Australia) and Western Gondwanaland (South America-Africa) is believed to have commenced during the Early Jurassic.

2. The breakup of eastern Gondwanaland followed by the initiation of the seafloor spreading processes in the Argo Abyssal Plain since Late Jurassic, 156 Ma (ODP Site 765) has paved the way for the formation of the present Indian Ocean floor (Figure 2.3).

3. The Madagascar-Seychelles-India has rifted from Antarctica-Australia fragment of East Gondwanaland in the Late Mesozoic (anomaly M11, 133.5 Ma). This separation occurred along the old Eastern Ghat trend of eastern India and India-Madagascar started drifting in a northwest direction. Uplift associated with the rifting has tilted the peninsular India to the west and the major river drainage started flowing from east to west (Cox, 1989; Kent, 1991; Subrahmanya, 1994). This drainage pattern persisted until the rifting of Madagascar from western India.

4. The breakup of Australia from Antarctica started during Middle Cretaceous (95±5 Ma). At the same time India separated from Africa-Arabia-Madagascar and evolution of the Mascarene basin started by initiation of seafloor spreading

(anomaly 34, 83 Ma) and northward propagation of rifting between eastern Madagascar and western side of Seychelles-India. Since then India started moving rapidly towards north. The fluvial system reoriented to the east due to uplift associated with this rifting and the rivers, which once drained from east to west into the Arabian Sea, started draining from west to east into the Bay of Bengal. The Middle Cretaceous (95±5 Ma) is widely recognized for the first major plate reorganization in the Indian Ocean.

5. The opening of the Arabian Sea has commenced during the Late Cretaceous-Early Tertiary when the spreading ridge system in the Mascarene basin ceased spreading and jumped to the north separating the Seychelles from India (Figure 2.4). As a result, Seychelles was transferred to the African plate. During this time one of the largest continental flood basalts, Deccan Traps have erupted and covered vast area of the central and western India and the Seychelles. The India's northward movement was unchanged inspite of the tectonic events, eruption of Deccan basalt and ridge jump, and the drift rate has remained constant ~13.5 cm/yr between 83 and 48 Ma (Duncan and Hargraves, 1990).

6. The rapid northward movement of India has dropped considerably consequent to continental collision between India and Eurasia during the Middle Eocene (Patriat and Achache, 1984). Thus coincides with cessation of the spreading in the northeast Indian Ocean after the formation of anomaly 19 (Royer et al., 1991; Krishna et al., 1995). The spreading ridge, fossiled just after Chron 19 and known as the Wharton Ridge, has jumped to the south (Liu et al., 1983). As a result, the Australian and Indian plates became a single plate that is now known as Indo-Australian plate. This period is recognized as the second major plate reorganization event in the Indian Ocean.

7. The northward moving Indian plate over the Reunion hotspot has resulted in emplacement of the volcanics of the Laccadive-Maldives-Chagos and Mascarene plateau and prograded ages of volcanics with younger ages to the south (Duncan and Hargraves, 1990). The northern Chagos Bank (49 Ma) and much of the

Saya-de-Malha Bank (47 Ma) are generated while hotspot was located near or on a spreading segment of the Central Indian Ridge. Geochemical data from Site 713 indicated mixing of melts from hotspot and mid-ocean ridge basalt (MORB) source. At anomaly 13, 34 Ma, the Reunion hotspot centered under a segment of the Central Indian Ridge (Figure 2.4). Due to the migration of the spreading system to the northeast, the Reunion hotspot was transferred from the Indian plate to the African plate. As a result, volcanic build up of the Chagos-Laccadive Ridge stopped. Since then to the Present, the hotspot is in intraplate position and building the eastern Mascarene plateau.

8. Since the second major plate reorganization, the plate boundaries in the Indian Ocean began to assume a modern aspect. The younger tectonic events since then include opening of the Gulf of Aden for ~10 Ma (Laughton et al., 1970b; Stein and Cochran, 1985), onset of intraplate deformation (around Upper Miocene, 7-8 Ma) in the Central Indian Ocean (Weissel et al., 1980; Bull, 1990; Neprochnov, Gopala Rao et al., 1998), separation of Arabia from Somalia and cessation of motion along the Owen Fracture Zone (Wiens et al., 1985).

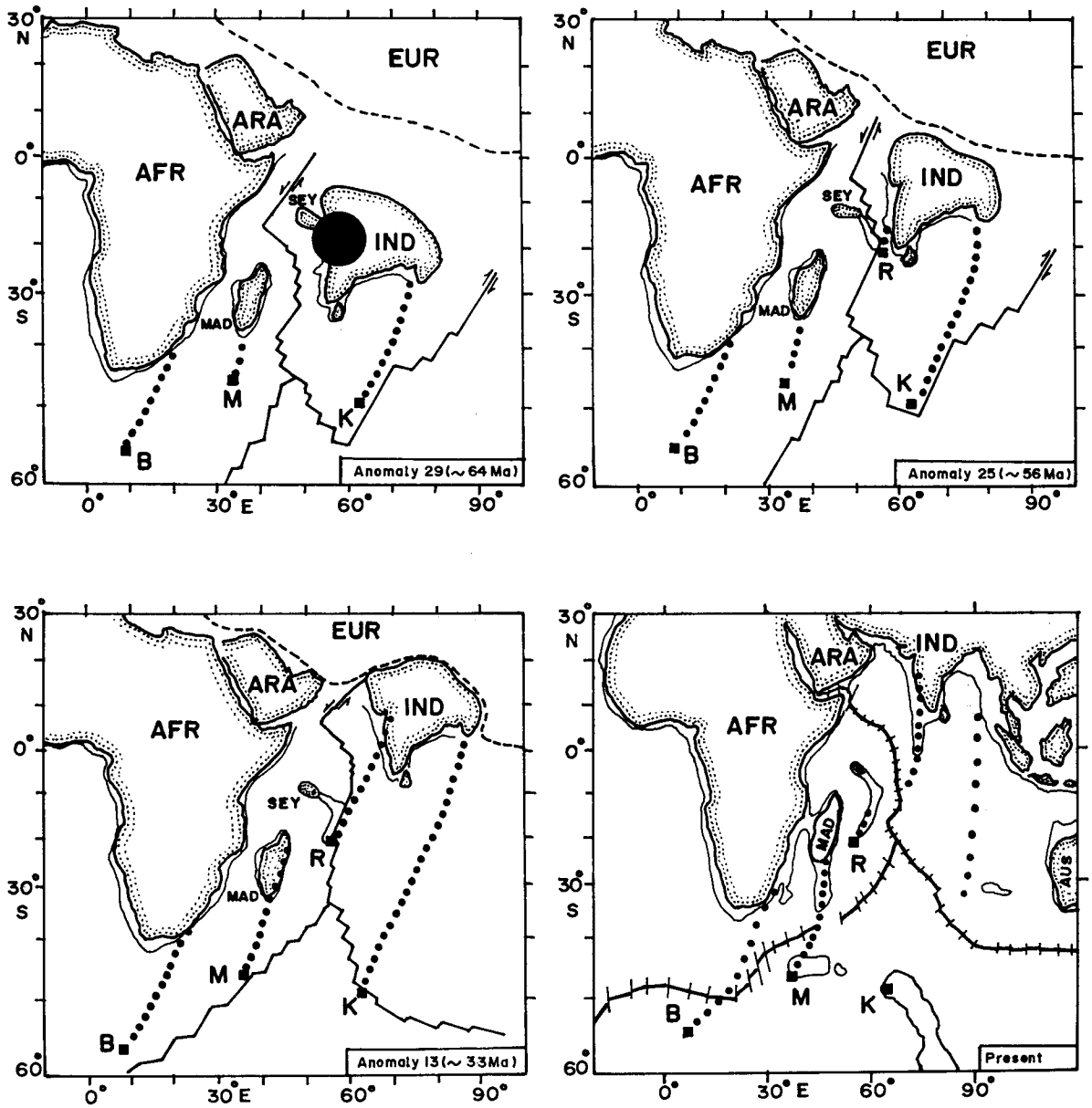

Figure 2.4 Paleogeographic reconstructions of the western Indian Ocean for anomaly 29 (~63 Ma), Anomaly 25 (~56 Ma), Anomaly 13 (~33 Ma) and Present (compiled from Scotese et al., 1988; Duncan, 1990). Large dark circle indicates eruption of massive volumes of the Deccan flood basalts. Small solid circles and squares represent past track and present location of hotspots respectively. B=Bouvet hotspot; M=Marion hotspot, K=Kerguelen hotspot, R=Reunion hotspot, EUR=Eurasia, IND=India, AFR=Africa, MAD=Madagascar, SEY=Seychelles.

CHAPTER 3

CHAPTER 3

ACQUISITION, PROCESSING AND PRESENTATION OF MARINE GEOPHYSICAL DATA

3.1 INTRODUCTION

The geophysical data (Table 3.1) used in this thesis were mostly collected in six cruises of ORV Sagar Kanya and one cruise of chartered vessel DSV Nand Rachit during 1983-92. The bathymetry and magnetic data collected onboard chartered vessel MV Polar Circle, on her way to Antarctica and back during First Indian Expedition to Antarctica in 1981-82, were also used. Bathymetry, gravity, magnetic and multichannel seismic reflection data collected onboard ORV Sagar Kanya were recorded both in digital and analog forms. While, bathymentry and magnetic data collected onboard DSV Nand Rachit and MV Polar Circle were recorded in analog form as there was no onboard facility for digital recording of the data. A detail description of the layout of cruise tracks, geophysical equipment used, processing and presentation of data are given below:

3.2 LAYOUT OF THE CRUISE TRACKS

As mentioned in Chapter 1, one of the main objectives of the present study is to identify seafloor spreading type linear magnetic anomalies in the Western Arabian Basin, to derive a plausible tectonic model for its evolution and its implications on the evolution of the western continental margin of India. In order to achieve the objectives, emphasis was laid on the proper orientation of the cruise tracks. Thus, bathymetry and magnetic data in the Western Arabian Basin were collected along tracks approximately parallel to the reported seafloor spreading direction and, therefore, orthogonal to the trend of the magnetic lineations of the oceanic crust (Figure 3.1). The above orientation of the tracks was selected because of the fact that the magnetic anomalies are best reflected when surveyed perpendicular to the lineation pattern. Apart from these closely

Table 3.1 Type of data acquired during cruises and used in the present study.

Vessel	Cruise Id.	Bathymetry	Gravity	Magnetic	Seismic
Sagar Kanya	SK05	√	-	√	-
Sagar Kanya	SK12	√	√	√	√
Sagar Kanya	SK22	√	√	√	-
Sagar Kanya	SK50	√	-	√	-
Sagar Kanya	SK64	√	-	√	-
Sagar Kanya	SK79	√	-	√	-
Nand Rachit	NR05	√	-	√	-
Polar Circle	PC01	√	-	√	-

Table 3.2 Type of data obtained from NGDC and used in the present study.

Vessel	Cruise Id.	Bathymetry	Gravity	Magnetic	Seismic
Atlantis II	A20	-	-	√	-
Charles Darwin	CD	√	-	√	-
Conrad	C9	√	-	√	-
Conrad	C17	√	√	√	-
Glomar Challenger	GL-leg 23	√	-	√	-
HMS Owen	OW	-	-	√	-
Vema	V19	√	√	√	-
Vema	V33	√	√	√	-
Vema	V34	√	-	√	-
Vema	V35	√	√	√	-
Vema	V36	√	√	√	-
Wilkes	WI33			√	-
Wilkes	WI34	-	-	√	-

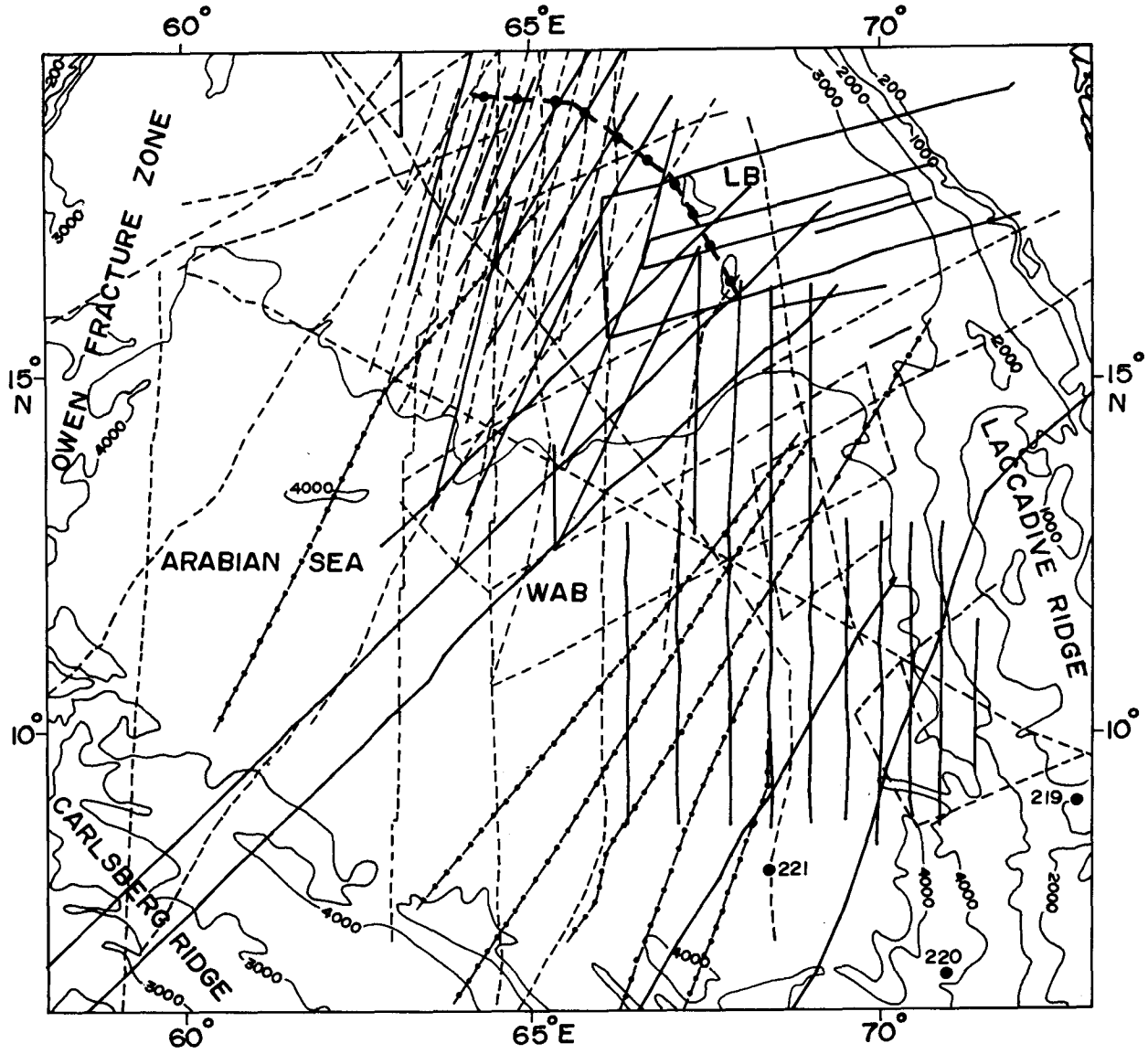

Figure 3.1 Location of cruise tracks in the study area. Solid lines indicate tracks along which bathymetry and magnetic data were acquired onboard ORV Sagar Kanya and chartered research vessels. Dashed and dashed-dotted lines represent data obtained from National Geophysical Data Center (NGDC) and from published maps (Udintsev, 1975; Mercuriev et al., 1995) respectively. Thick solid lines with solid circles represents axis of the Laxmi Ridge. Locations of DSDP Sites are shown with large solid circles. Bathymetric contours are in meters. WAB=Western Arabian Basin, LB=Laxmi Basin.

spaced profiles, magnetic and bathymetry data were also collected along two regional profiles (Figure 3.2) extending from the Western Arabian Basin to the Eastern Somali Basin across the Carlsberg Ridge to provide constraints on spreading history of the Arabian Sea. About 20000 line kilometers (lkm) of bathymetry and magnetic data are analyzed for detailed study of the seafloor spreading magnetic anomalies.

In addition to these data, about 2400 lkm of bathymetry and gravity and about 720 lkm of regional multichannel seismic reflection data covering the important geological provinces of the southwestern continental margin of India are also analyzed to study crustal structure (Figure 3.3). Most of the profiles are orthogonal to the reported trend of the main structural feature of the margin and constitute the primary data base of this part of the study area.

A summary of the quantum of marine geophysical data collected during the cruises of Indian and chartered vessels and utilized in the present investigations are as follow:

Type of data		Quantum of data (line kilometers)
Bathymetry	:	22400
Magnetic	:	22400
Gravity	:	2400
Multichannel seismics	:	720

3.3 OTHER SOURCES OF GEOPHYSICAL DATA

The digital data available with National Geophysical Data Center (NGDC), Colorado, USA in the study area (Table 3.2) are also complemented in the present work. Besides, some other published magnetic profiles (Udintsev, 1975; Schlich, 1982; Mercuriev et al., 1995) have also been used in this study.

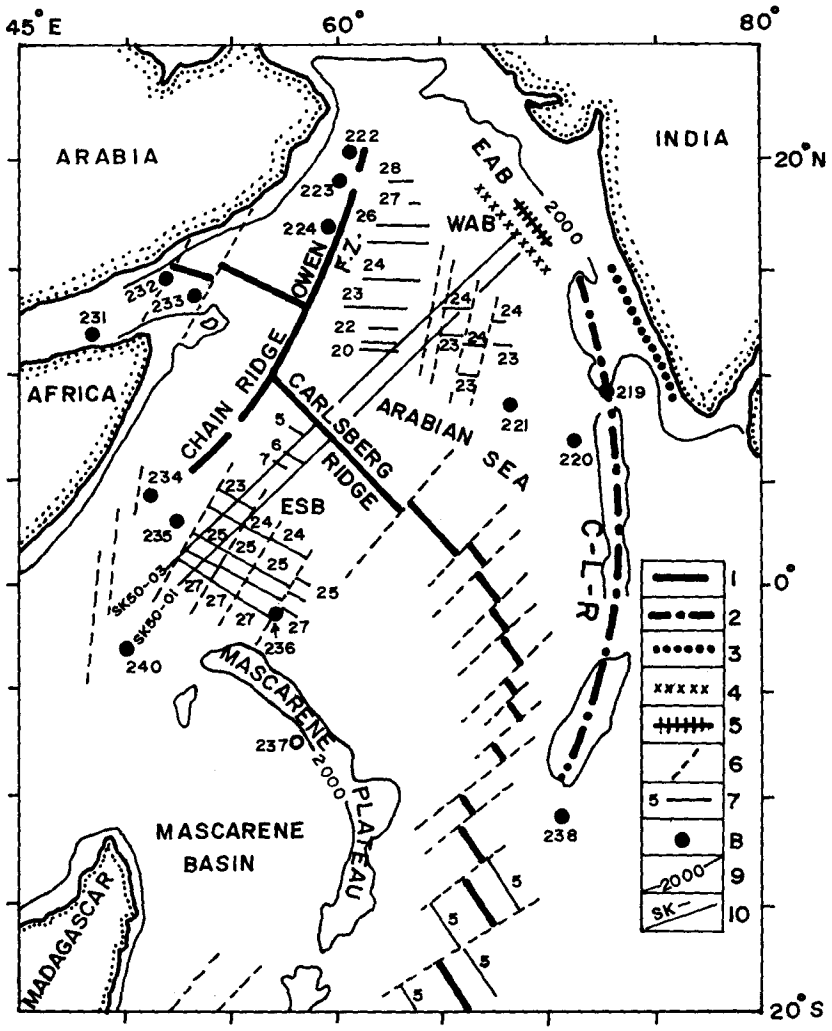

Figure 3.2 Location of two regional profiles (SK50-01 and SK50-03) extending from the Western Arabian Basin (WAB) to Eastern Somali Basin (ESB) across the Carlsberg Ridge. Magnetic lineations and main structural features are compiled from Naini and Talwani, 1982 and Schlich, 1982). 1=Mid-Ocean Ridge crest, 2=Chagos-Laccadive Ridge, 3=Prathap Ridge, 4=Laxmi Ridge, 5=Basement Ridge, 6=Fracture Zones, 7=Magnetic lineations, 8=DSDP Sites, 9=bathymetric contours in meters, 10= Surveyed tracks. EAB=Eastern Arabian Basin.

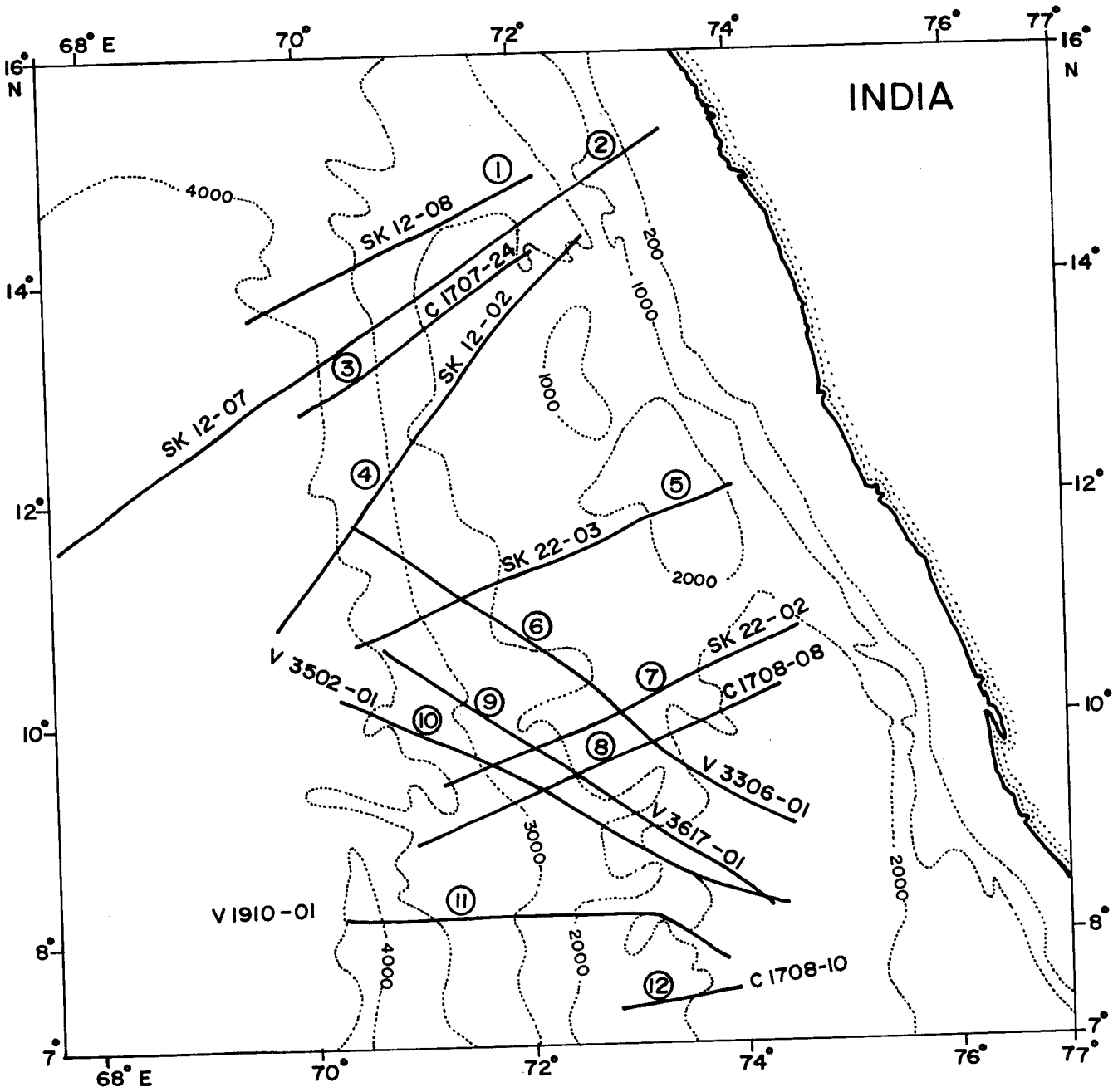

Figure 3.3 Location of cruise tracks on the southwestern continental margin of India. Bathymerty and gravity data were acquired along these tracks. Multichannel seismic reflection data were collected along track SK12-07. Renumbered profiles (number in circle) are used in Chapter 6.

3.4 GEOPHYSICAL EQUIPMENT USED FOR DATA ACQUISITION

3.4.1 NAVIGATIONAL EQUIPMENT

During the cruises, the positions along the track lines were obtained with different types of navigation equipment. A dual channel satellite receiver MX 1107 was used to obtain positions along the track lines during cruises of DSV Nand Rachit and MV Polar Circle. Whereas, a Magnavox Series 5000 Integrated Navigation System (INS) was used to obtain positions along the track lines during cruises of ORV Sagar Kanya. The INS system used a Magnavox dual channel Satellite navigator (model MX 1107) and Global Positioning System (GPS) as primary navigational aid. A brief description of these systems is as follows:

3.4.1.1 SATELLITE NAVIGATION SYSTEM

The Satellite Navigation System (MX 1107) comprised of dual channel satellite receiver, data entry key board, display unit, digital processor and antenna. The system makes use of the satellite signals transmitted from the U.S. Navy Navigation Satellite System (NNSS), often known as the Transit Satellites, to compute the position of the vessel. The Transit Satellite System consists of six polar orbiting Satellites at an altitude of about 600 nautical miles. These Satellites transmit very stable 400 and 150 MHz signals which are phase modulated with several types of information. A part of the message from the satellite signal contains the navigation data which precisely describes the position of the satellite as a function of time.

The transit satellites travel roughly at a speed of 4 miles/s and this motion with respect to an observer on the earth causes a Doppler shift in the radiated 400 and 150 MHz signals. This Doppler shift is measured by the satellite receiver to compute the slant range between the observer and the satellite. The slant range and the satellite position data are used to compute the position of the receiver onboard the vessel at that time. Thus accurate position fixing can be achieved only when the satellite passes above the horizon of the observer. The availability of satellite fix depends on the latitude of

operation and varies between 30 minutes at poles to 110 minutes at the equator. The satellite receiver computes the position of the vessel in between the satellite passes with the aid of gyro and speed log information. These positions are called as the dead reckoning positions. The accuracy of the position during a satellite fix is about ± 50 m RMS and the positional accuracy deteriorates during dead reckoning process.

3.4.1.2 GLOBAL POSITIONING SYSTEM

The basic system of Global Positioning System (GPS) consists of a satellite signal receiver MX 4400 with a microprocessor and an antenna. The system is based on a set of satellites called as NAVSTAR (Navigation System with Time and Ranging) satellites. These satellites orbit the earth at an altitude of about 10900 nautical miles with an orbital period of 12 hours. This system is based on 18 satellites in six orbital planes. These orbits are configured to make a satellite covering the earth in such a way that at least four satellites are in line of sight from any point at a given time.

Position determination involves recovery of Time of Arrival (TOA) measurement on satellite signal and the use of satellite ephemeris to compute the position of the satellite being tracked. Navigation is accomplished by using Kalman filter, a software based navigation model stored in receiver processor. It provides continuous navigation solutions based on TOA and Doppler measurements. Satellite derived position has an accuracy of ±15 meters RMS. The dead-reckoning process may not be required as the GPS provides 24 hours coverage. However, the MX 4400 satellite receiver has the capability of providing dead-reckoning positions from the speed and heading information of the vessel.

3.4.1.3 INTEGRATED NAVIGATION SYSTEM

The Magnavox series 5000 Integrated Navigation System (INS) provides an accurate real time navigation, generalized data logging and facilities for real time display of the acquired navigation and geophysical data. A high speed minicomputer (Hewlett Packard HP 2117 F) serves as the controlling unit in the system. The minicomputer

provides interfacing of the navigation sensors, and of the data logging display and command/control peripherals. Prior to the installation of GPS receiver, the basic reference for the INS was the transit satellites. The system integrates the position of the vessel obtained from several navigational aids such as MX 1107 satellite receiver, the GPS receiver, Omega etc. The computer estimates the dead reckon positions in between the satellite fixes at desired interval using the speed of the vessel from the Doppler sensor (DOLOG system/sonar of A/S Krupp Atlas, FRG) and course of the vessel from the ship's gyro compass. The accuracy of the primary navigation system during an appropriate satellite pass is expected to be around 32 meters, as suggested by the manufacturer. Besides logging of the data on magnetic tape, the INS also provides the navigational data to the various onboard interfaced scientific equipment for data processing. A schematic network of the INS is shown in Figure 3.4.

3.4.2 ECHOSOUNDER

The sea bottom topography of the study area has been inferred using bathymetry data. The data were acquired using the echosounders available onboard the vessels. M/s Honeywell ELAC (Germany) Narrow Beam Sounder (NBS) and deep sea echosounder systems (Figure 3.5) were used during the cruises of ORV Sagar Kanya. M/s Raytheon (USA) deep sea echosounder was used during the cruises of DSV Nand Rachit and MV Polar Circle. The operating frequency of the above mentioned systems was selected as 12 KHz.

The basic principle of the echosounder system is to continuously transmit acoustic pulses and receive the reflected signal from the seabed. The time elapsed between the transmission and reception of the acoustic pulse is measured. The elapsed time is converted into depth considering the velocity of sound (1500 m/s) in sea water.

3.4.3 PROTON PRECESSION MARINE MAGNETOMETER

Proton precession marine magnetometer model G-801/3 of M/s EG&G Geometrics (USA) was used to measure earth's total intensity magnetic filed data along

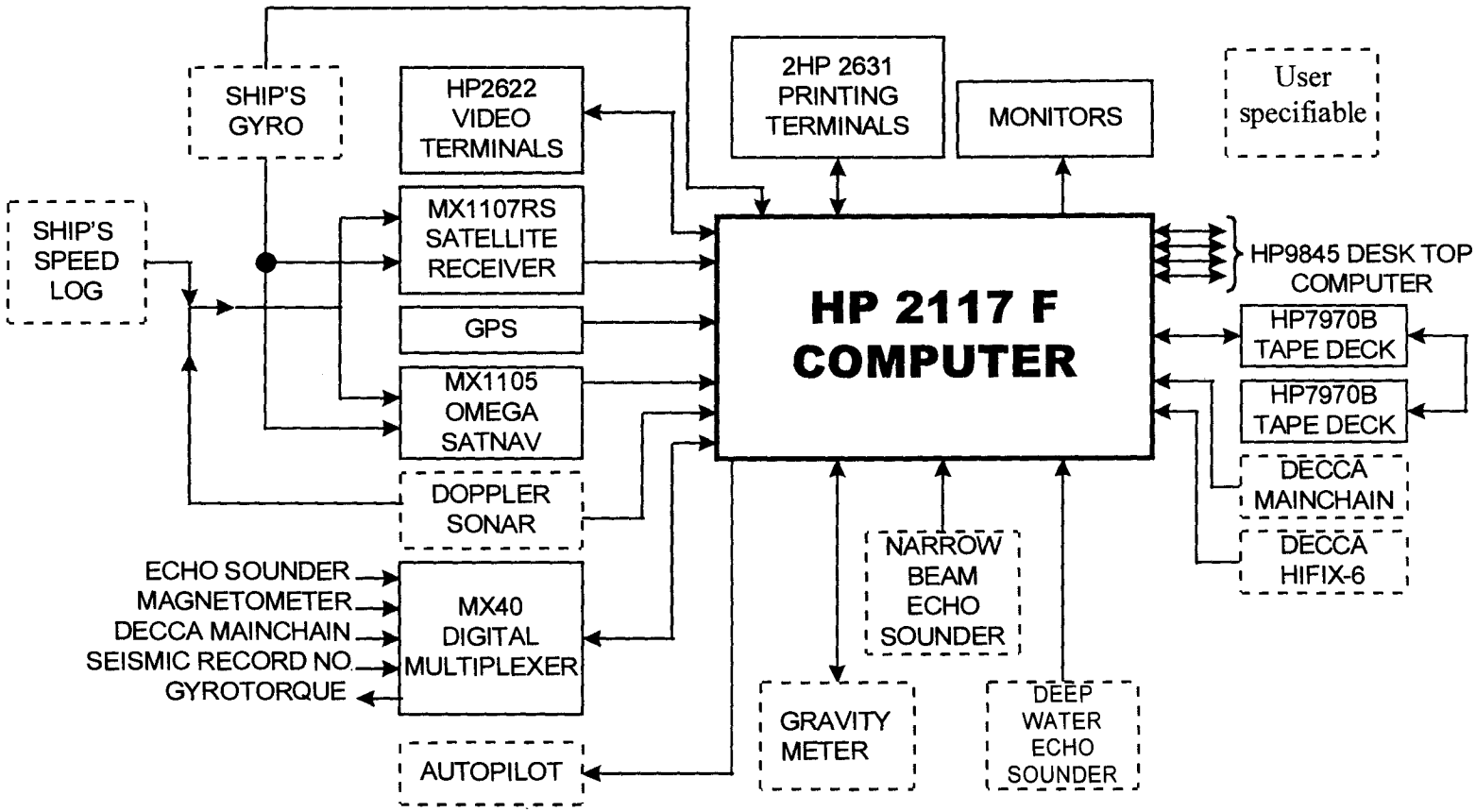

Figure 3.4 Schematic block diagram of the Integrated Navigation System (INS) onboard ORV Sagar Kanya.

Figure 3.5 Echosounder systems used for measuring depth to the seafloor.

the track lines. The magnetometer consists of a sensor with cable, electronic console and a recorder (Figure 3.6). The sensing element consists of solenoidally wound coils with balancing trim turns to minimize noise pickup from remote sources. The coil is immersed in a hydrocarbon fluid rich in protons (e.g. kerosene). The electronic console includes a circuitry to process the precession signal, sensor interfacing, signal amplification, phase lock and frequency multiplication, frequency counting, counter gate length control and system control functions.

The proton precession magnetometer operates on the principle of nuclear magnetic resonance to produce a measurement of the total magnetic intensity i.e., the scalar magnitude of the ambient field. In the proton magnetometer sensor, a uniform magnetic field is created by passing a current through a coil surrounding a small volume of proton rich hydrocarbon fluid (kerosene). The spinning protons act as a small magnetic dipoles and align themselves in the direction of the applied field. If the applied field is suddenly removed, the spin of the aligned protons causes them to precess at an angular velocity ω, known as the Larmor precession, in phase about the direction of the ambient earth's magnetic field at a rate which is proportional to the total magnetic intensity (T) of the earth. This can be written as:

$$\omega = \gamma_P T$$

Therefore, the frequency of precession f can be written as:

$$f = \gamma_P T/2\Pi$$

or, $$T = 2\Pi f/\gamma_P$$

Where γ_P is the gyromagnetic ratio of the proton. γ_P is known to high precision and is independent of the surrounding or chemical composition. Its value obtained by Driscoll and Bender (1958, 1958a) and adopted by IUGG is given as:

$$\gamma_P = 2.67513 \times 10^{-4} \text{ Oersted}^{-1} \text{ sec}^{-1}$$

or, $$\gamma_P = 0.267513 \text{ gamma}^{-1} \text{ sec}^{-1}$$

Therefore, $$T = 23.4874 \times f \text{ gamma}$$

Thus, if the frequency of precession can be measured, the field strength is determined. The precession frequency f is independent of the direction of the spins with

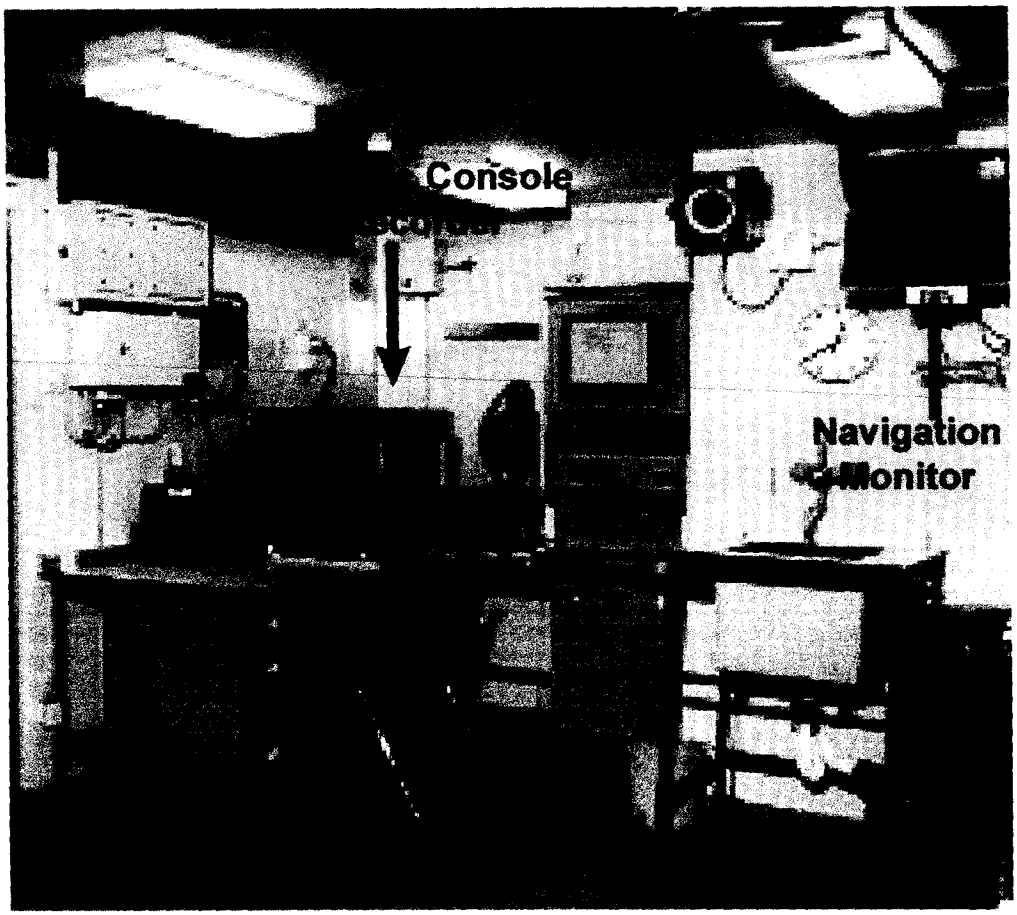

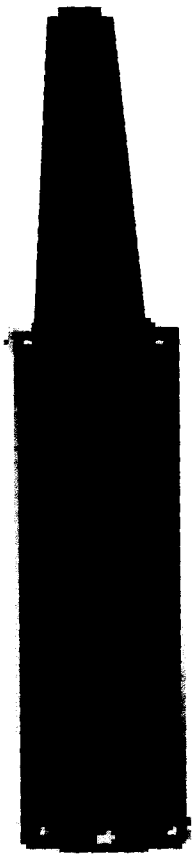

SENSOR

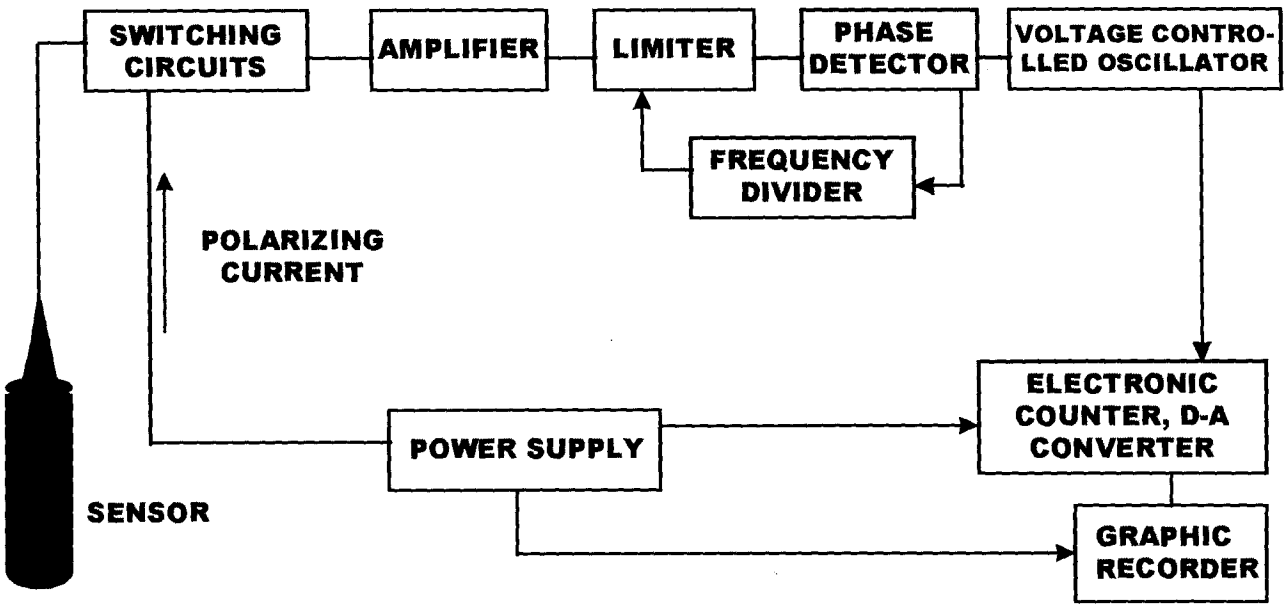

Figure 3.6 Proton precession marine magnetometer system (Geometrics G801/3) used to measure the earth's total magnetic field. The bottom part of the figure illustrates the schematic diagram of various modules of the system.

respect to the earth's magnetic field. The signal amplitude is variable and it is maximum when the spins are normal, zero when they are parallel to the direction of the earth's magnetic field. Precise frequency measurement was made by detecting a signal from the precession of proton. The modulated signal was amplified to a suitable level and the frequency was measured.

The total intensity magnetic field data were collected by towing the sensor behind the vessel. The towed length of the cable was generally kept three times the ship's length to avoid the magnetic noise generated by the magnetic material of the ship. During the cruises of ORV Sagar Kanya, data were recorded in analog form with 100 and 1000 gamma full scales, and simultaneously in digital form on magnetic tape at a sampling rate of 6 sec. Whereas, during cruises of DSV Nand Rachit and MV Polar Circle the data were recorded only in analog form at the same sampling rate of 6 sec. All the data were recorded with an accuracy of 1.0 nT. The digital display of the data on the console helped to monitor the quality of acquired data.

3.4.4 SEA GRAVIMETER

Gravity data were acquired using M/s Bodenseewerk (Germany) sea gravimeter system KSS 30 onboard ORV Sagar Kanya. The system consists of three major subsystems: GSS 30 gravity sensor subsystem, KT 30 stabilization subsystem and ZE 30 data handling subsystem (Figure 3.7). These subsystems are briefly described in the following paragraphs:

3.4.4.1 GSS 30 GRAVITY SENSOR SUBSYSTEM

The gravity sensor (Figure 3.7) is located at a level 2.15 meters above the ship's hull. It uses a non-astatized spring-mass assembly also known as '*Zero Length*' spring as basic gravity detector. The measuring system is housed in the thermostatized/pressure tight and magnetically shielded compartment. This system, based on a vertical sensor, consists of a tube-shaped mass guided by 5 threads in friction less manner. The motion of the sensor mass is limited to one degree of freedom in vertical direction. The constant

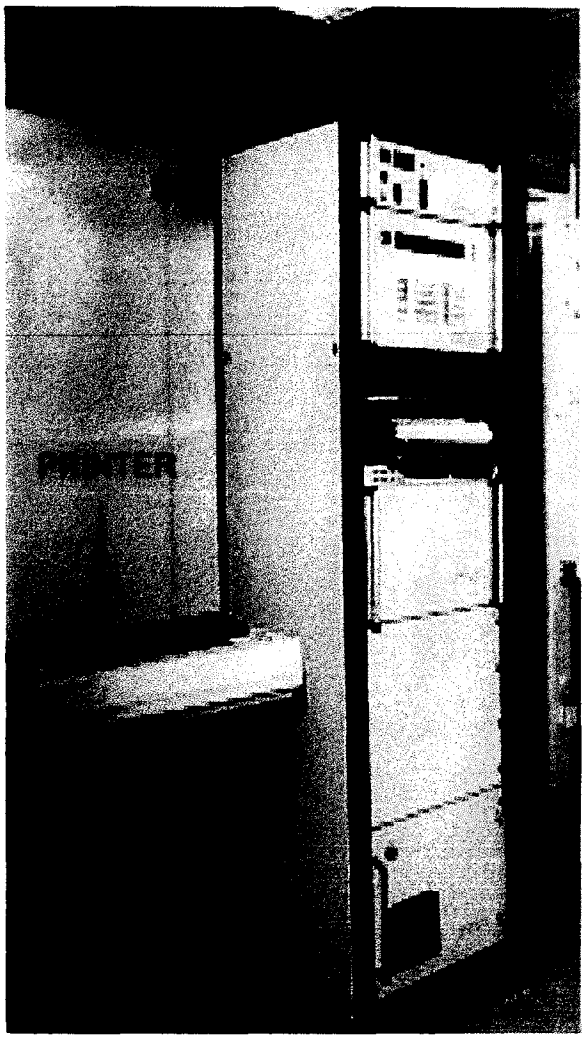

DATA HANDLING SUBSYSTEM

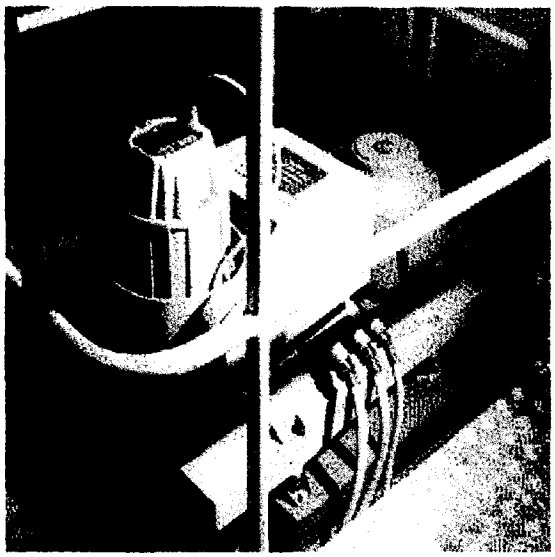

GRAVITY SENSOR & STABILIZATION SUBSYSTEMS

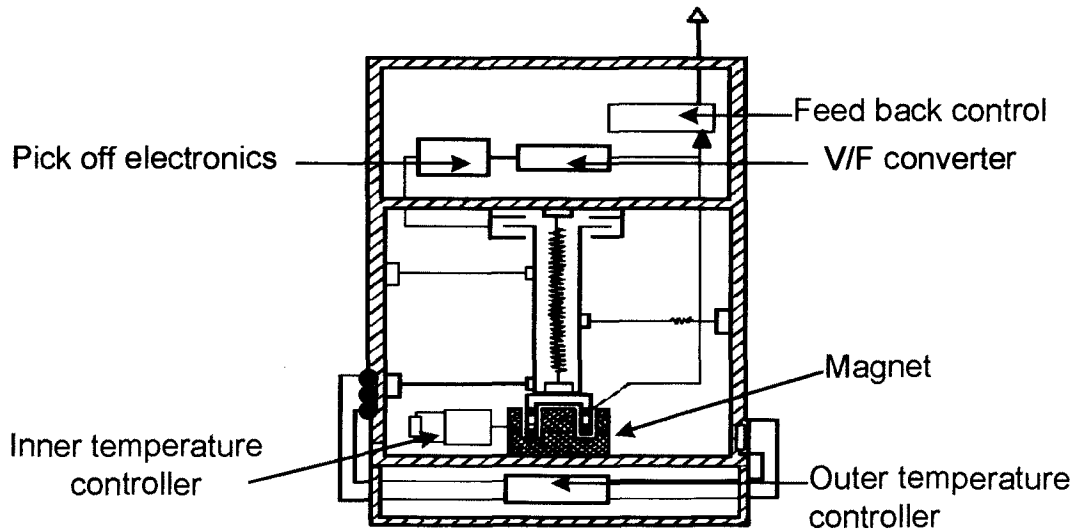

Figure 3.7 Marine gravimeter (Bodenseewerk KSS 30) system along with sensor mounted on gyrostabilized platform. The bottom part of the figure shows the principal elements within the sensor.

gravity acceleration 'g' is compensated by a mechanical spring, whereas gravity changes are detected by an electromagnetic system.

3.4.4.2 KT 30 STABILIZATION SUBSYSTEM

The stabilization subsystem (Figure 3.7) consists of the platform (KT 30), vertical gyro (K 30) and platform electronic (KE 30) which is part of the data handling subsystem. The stabilization of the gravity sensor GSS 30 on moving ship is performed by the gyro stabilized platform for pitch and roll. The stabilization of the gravity sensor with high dynamic accuracy is the basis for all gravity measurements. The basic principle of operation of the vertical gyro is to keep the spin axis of the gyro near the true vertical by means of the erection control-loop.

3.4.4.3 ZE 30 DATA HANDLING SUBSYSTEM

The data handling subsystem (Figure 3.7) mainly consists of a central processor and the interface to the peripheral equipment. It supports all equipment for filtering, logging, preprocessing and self testing of gravity measurements. It also supports the control electronics of the platform and monitor registration facilities. It receives all navigation data from the navigation computer necessary for gyro erection, turn maneuver compensation and on-line preprocessing of gravity data. During on-line processing Eotvos correction, Free-air correction and Bouguer corrections are applied to the measured gravity to compute Eotvos corrected gravity and Free-air and Bouguer anomalies. ZE 30 block diagram along with interfaced peripheral equipment is shown in Figure 3.8.

The gravimeter system was calibrated to check the performance of the system before start of the cruise. After calibration of the system, the gravity measurement at harbour is made while the ship is at the berth. The measured gravity and absolute gravity values at harbour are entered into the system. The absolute gravity value at different berths of Mormugao harbour were determined by tying to the nearest network of known gravity bases. The continuous gravity data were recorded on magnetic tape at a

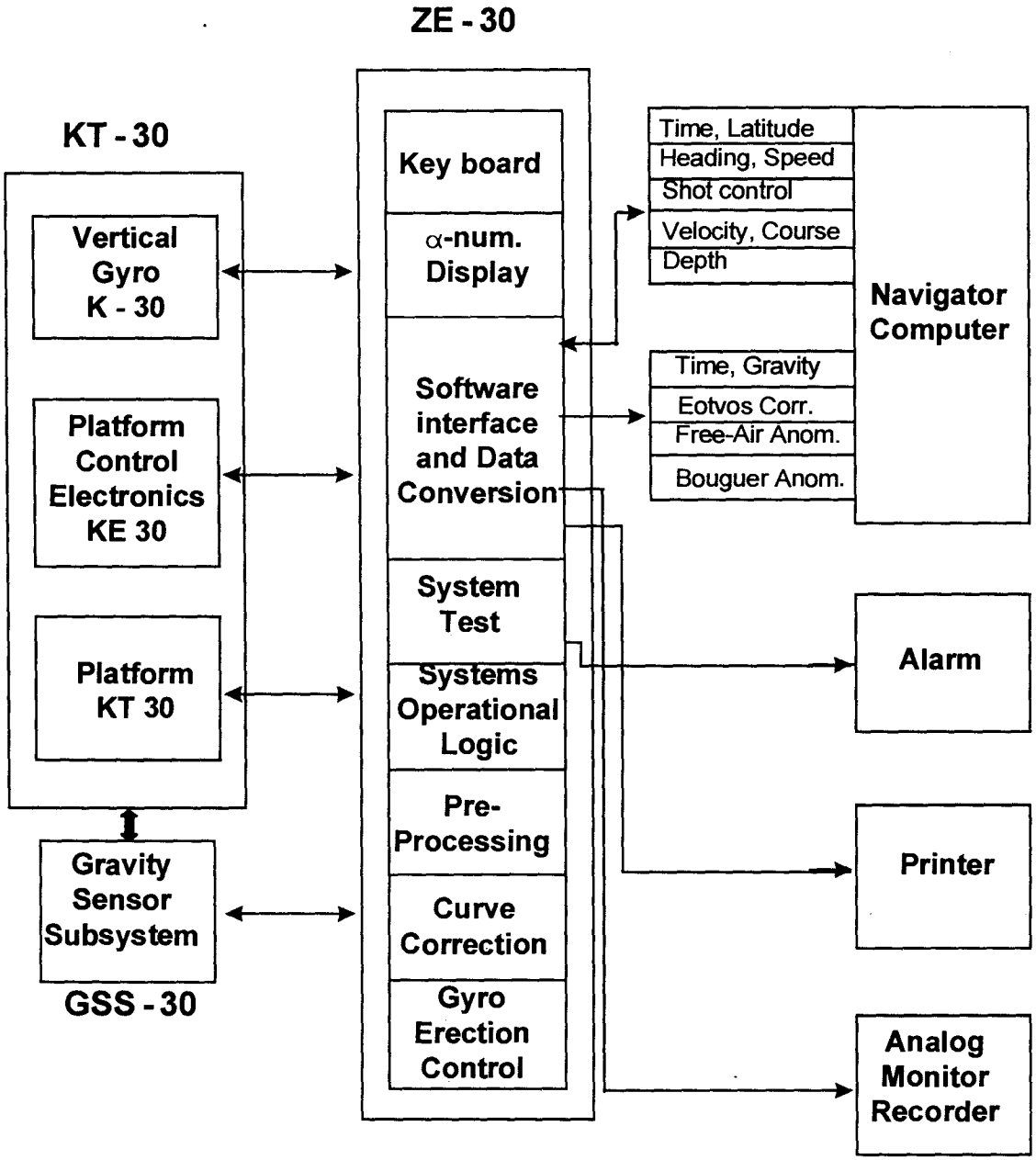

Figure 3.8 Block diagram showing marine gravimeter system (KSS 30) and peripheral equipment.

sampling rate of 3 sec. The data were also recorded on a 2-channel strip chart recorder and printed at every 5 minutes interval on the teletype printer for monitoring purpose. Most of the gravity data were acquired at an average speed of 5.0 knots along with seismic surveys, otherwise acquired at an average speed of 8.0 knots in a sea state less than 3 to keep the accelerations along the pitch and roll axes of the gravimeter sensor due to ship motion within acceptable limits. These are continuously monitored from the outputs (analog and digital) of the accelerometers mounted on the gravimeter gyro-stabilized platform. The accuracy of the system is about 0.02 mGal which is the minimum change in gravity that can be detected. However, the effective accuracy which depends on the accuracy of navigation and sea conditions is about 0.8 to 1.0 mGal.

3.4.5 MULTICHANNEL SEISMIC REFLECTION SYSTEM

Multichannel seismic reflection data were acquired using the Digital Field System (DFS) V of M/s Texas Instruments INC., USA onboard ORV Sagar Kanya. During the cruises the ship maintained a speed of approximately 4-5 knots and navigated by transit satellites. 12 fold subsurface coverage was achieved during the surveys using 24-channel seismic streamer with 32 hydrophones per group spaced at 25 m. The following parameters were used for recording the data :

Recording Parameters :

Source

Type of air gun	:	VLA and VLF
Array type	:	D-array (linear array)
Total volume (litre)	:	7.98
Number of guns	:	7 (Variable sizes)
Operating pressure (bar)	:	150
Depth below mean sealevel (m)	:	10
Shot interval (m)	:	25

Instrument

System	:	DFS - V
Record length (ms)	:	8000
Sampling Interval (ms)	:	4
Band pass filter (Hz)	:	8-64
Recording format	:	SEG - B
Notch filter	:	Out

Streamer

Type	:	SHHN 4 T
Number of channels	:	24
Group interval (m)	:	25
Number of hydrophones	:	32/Group
Depth below mean sealevel (m)	:	10
Near offset (m)	:	175
Far offset (m)	:	750

The seismic reflection method involves in principle measurement of travel time of seismic pulses. A short elastic pulse in the frequency range 10-100 Hz is transmitted which is capable of penetrating sedimentary strata of the survey area. After reflection from the horizons existing within the strata, the reflected signals are detected by hydrophones which are placed in the streamer and connected to the recording system. A schematic diagram of seismic reflection system at sea is shown in Figure 3.9. In the following paragraphs, a brief description of seismic source and different modules of the DFS V recording system are presented.

3.4.5.1 SEISMIC ENERGY SOURCE

D-type Array consisting of seven air guns of M/S Prakla-Seismos GMBH, Germany was used as energy source. It consists of three air guns type VLA and four air guns type VLF and form a linear array. The distances between individual guns and their volume (Figure 3.10a) were selected in such a way that the generated signals represent a good approximation to a spike. The guns were hooked to a U-form rail like suspension onboard ORV Sagar Kanya. The air supply hoses and the electrical cables are combined

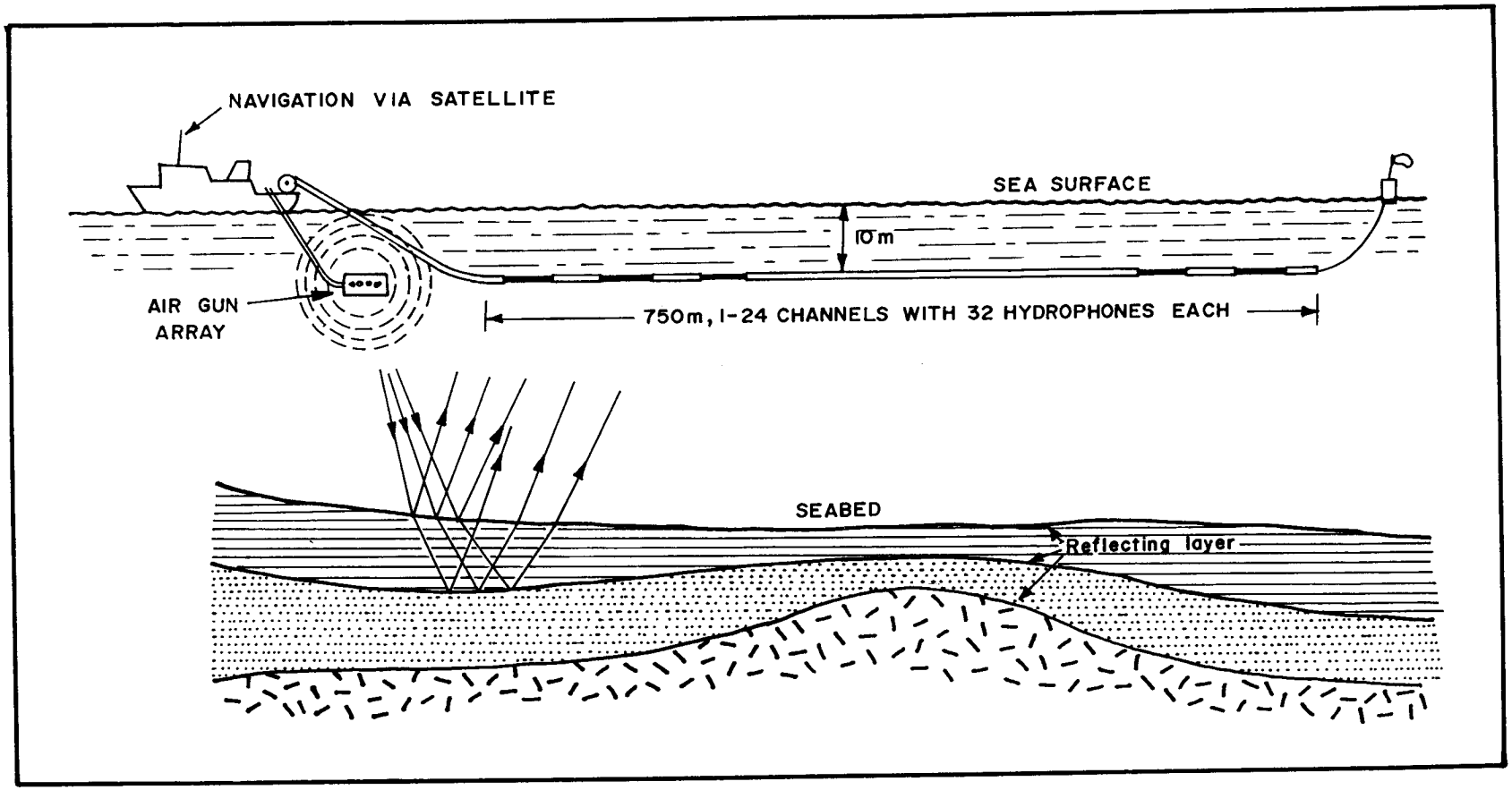

Figure 3.9 Schematic diagram showing seismic reflection data acquisition at sea.

to form one unit and called electro-pneumatic air gun connecting cable. This connects the array to the filling station and electronic cabinet (VZAC). The air gun array was towed behind the ship at a depth of 10 m. The filling station; a control, safety and storage station; is located between air gun and compressor. Shipboard compressors supply air at 150 bar pressure through an air hose into the upper section of the air guns. The highly compressed air pushes the two-part piston of the guns down into the lower position as illustrated in Figure 3.10b. Compressed air is gradually forced through the nozzle in the piston rod, filling the chamber at the bottom of the air gun. The pressures above the upper and below the lower piston are therefore identical. Since the area of the upper piston is greater than that of the lower piston, the net power will press downwards giving the piston a stable position as shown in Figure 3.10b. The air gun is fired by an electrical signal sent through the cable to the magnetic valve at the top of the air gun. This causes some of the air in the upper chamber above the piston to be forced via the magnetic valve through the channel on the extreme right and down on the upper side of the upper piston causing the net power which previously pressed downwards suddenly to press upwards. This causes the piston to accelerate upwards at great speed (Figure 3.10c) and most of the air below the lower piston in the chamber is released into the surrounding water. The air posses great volume-acceleration causing it to transmit the required pressure wave.

3.4.5.2 DIGITAL FIELD SYSTEM

The DFS V is comprised of three interconnected modules, viz. analog module, controller module and tape transport, used to record seismic data. The data come from blast-generated sound pulses which are sensed as they echo back from seabed and subsurface layers. These sounds are picked up by hydrophones and transmitted to the DFS V. The different modules of DFS V system (Figure 3.11) are briefly described in the following paragraphs:

The analog module controlled by the controller module, receives the signal from hydrophone and provide input line filtering, analog amplification and filtering,

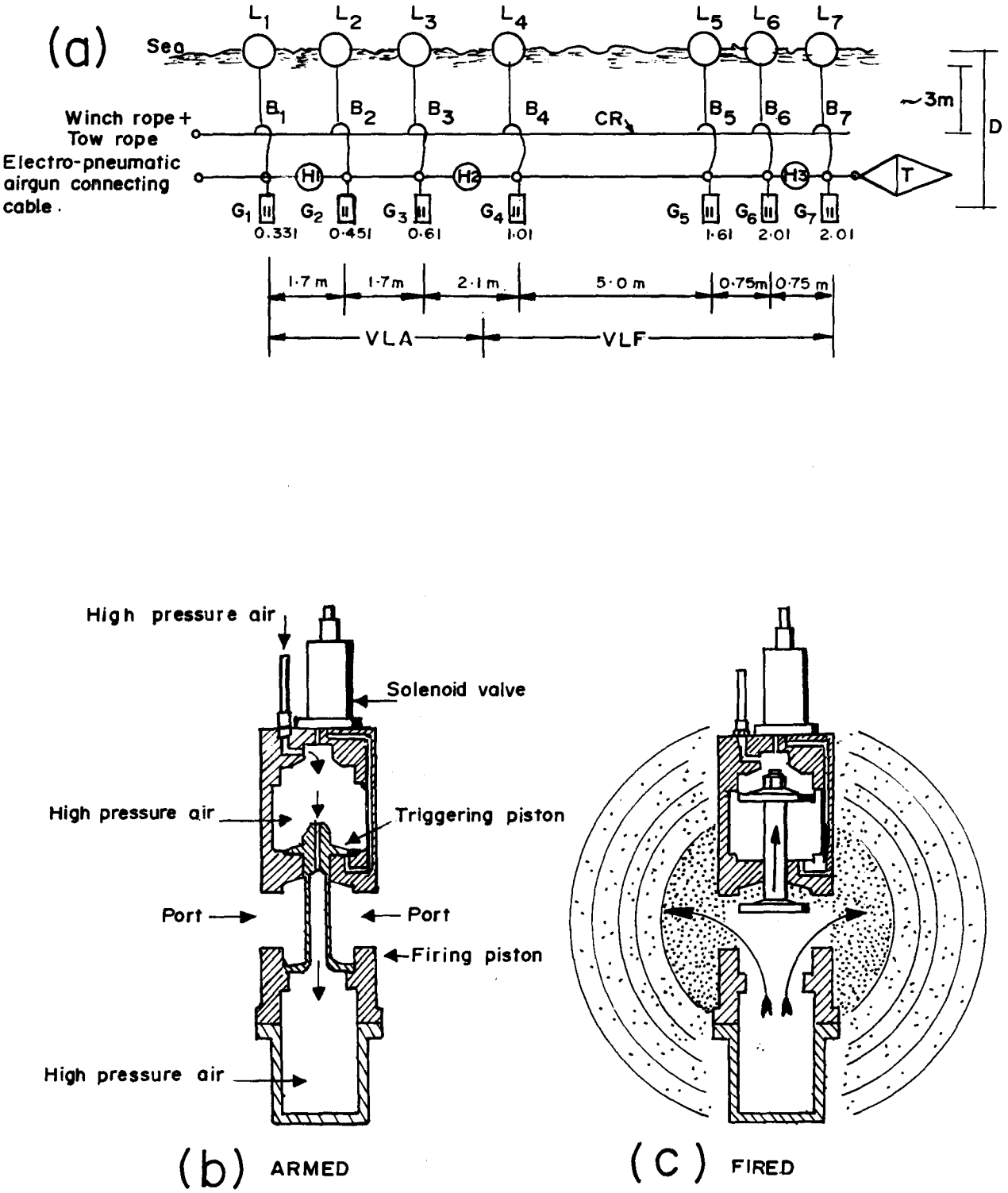

Figure 3.10 Air guns array layout and principle of operation at sea. L1-L7 : locations of floating balloons, D : array depth, T : rope tautener, H1-H3 : time break hydrophones, G1-G7 : air guns with related volumes in liters, B1-B7 : carrying bows, CR : connecting rope.

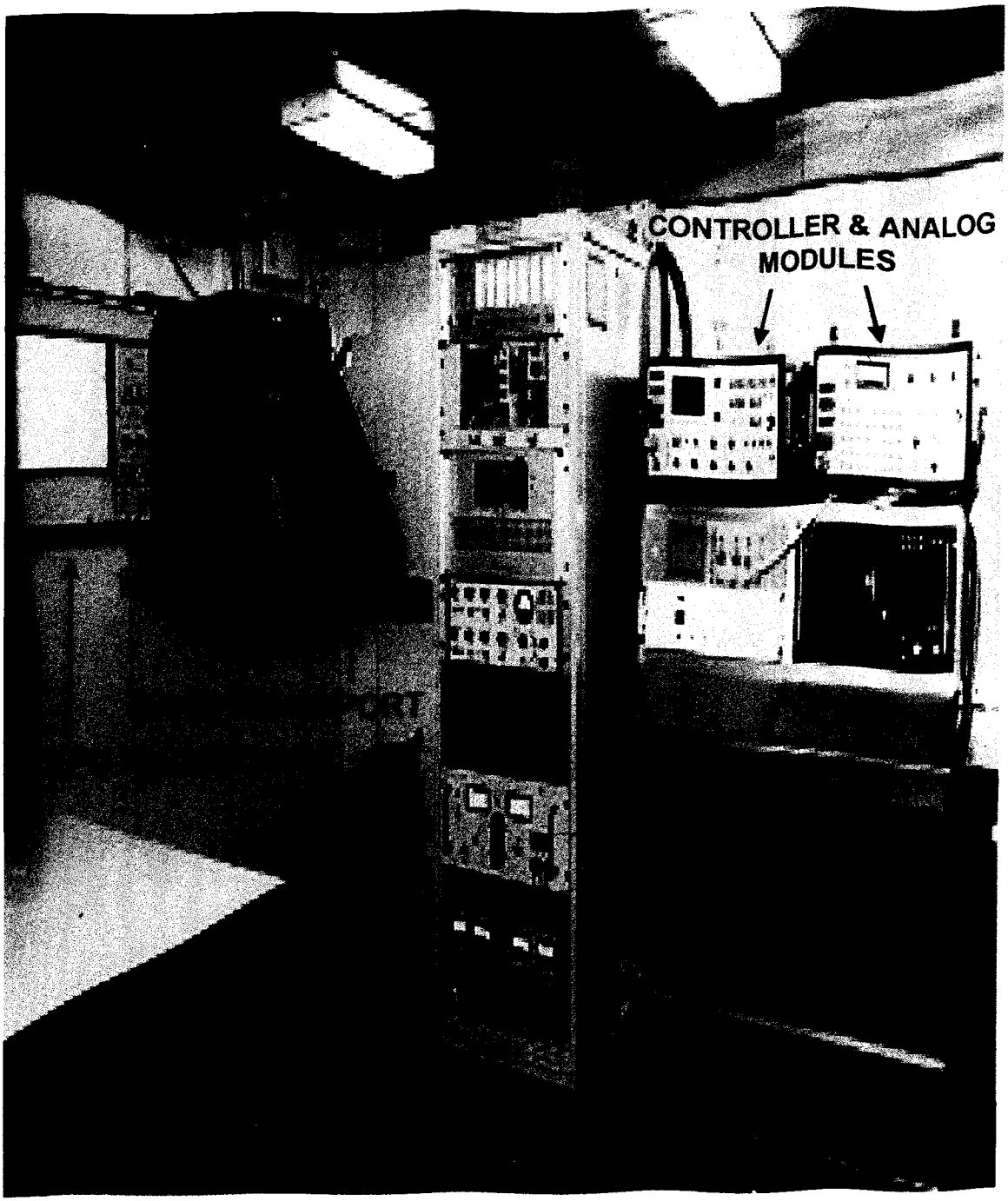

Figure 3.11 Seismic reflection data acquisition system (Digital Field System V) onboard ORV Sagar Kanya.

multiplexing and Analog to Digital (A/D) conversion. Finally, the digital information (both the gain of the amplifier and the digital output of the A/D converter) is transmitted serially to the controller module where the data is formatted and transmitted to the Tape Transport module.

The controller module provides system timing, digital gain, D/A conversion, demultiplexing, playback filtering and camera driving. The controller module functions can be broadly grouped in two categories; i) data and, ii) control. The data are bits and signals derived from the seismometers through A/D converter and the floating point amplifier. The control signals are those derived from the internal clock generators and the programs plugs and switch settings. These signals advance the data bits through the system.

The tape transport module records the digital data received from controller module on magnetic tape. The seismic data are recorded on one-half inch width tape, 1600 BPI using IBM-compatible 9-track dual-gap heads. There are two magnetic tape drives, tape drive 2 starts automatically when the tape on drive 1 is full. This is particularly important in marine surveys where the interval between two shots can be as little as 10 sec. An EPC model 4603 graphic recorder was used for recording the near channel (channel No. 1) data continuously in analog from on a dry thermal paper for quality control.

3.5 PROCESSING AND PRESENTATION OF DATA

As mentioned earlier, the geophysical data acquired onboard ORV Sagar Kanya are in digital form, whereas, the bathymetry and magnetic data acquired onboard chartered vessels are in the form of analog records and navigational print outs. These data have been processed using three different approaches depending on the mode of collection and type of data. The digital data are processed using Magnavox supplied software on both onboard HP 1000 general purpose computer and Norsk Data computer, ND-570 at National Institute of Oceanography, Goa. The analog data are

processed following a scheme of processing (Kamesh Raju et al., 1986) on ND-570 computer. The multichannel seismic reflection data which requires specialized processing, were processed on ND-570 computer system. In the following sections, a brief description of various steps of processing involved in each of these approaches is presented:

3.5.1 PROCESSING OF DIGITAL DATA

3.5.1.1 NAVIGATION DATA

The navigation data collected during the cruises consist of data obtained mostly from transit satellites and from GPS. The position information obtained from transit satellites are accurate during satellite passes and less accurate during dead reckoning which is computed by INS during data acquisition with the aid of gyro and speed log information. Due to obvious reason the dead reckon positions are at variance with the position obtained during satellite fix. The error estimate between dead reckon position and the position obtained during a satellite fix is used to correct all the dead reckon positions obtained between two satellite fixes. The positions obtained with 24 hours GPS coverage do not have such problem, however, the data was checked by plotting it on graphic monitor and erroneous values, if any, are deleted. All the position data are corrected and edited prior to processing of other geophysical data and generating track plot.

3.5.1.2 BATHYMETRY DATA

The digital depth data of echosounder some times recorded as erroneous data. These errors arise due to a variety of reasons resulting from a combination of instrument errors, sea conditions and bottom topography. It is therefore necessary to check recorded data before they are actually used for presentation and interpretation. The quality check are accomplished by displaying the depth data on the graphic monitor and the erroneous data points are edited/deleted from the data file. The edited depth data are

corrected for variation of the sound velocity in sea water using Matthew's table (Carter, 1980). The corrected depth data are used for presentation and interpretation in this study.

3.5.1.3 MAGNETIC DATA

The total intensity magnetic field measurement including digital magnetic data obtained from NGDC are reduced to residual magnetic anomalies by subtracting the International Geomagnetic Reference Field (IGRF) calculated at each observation point for appropriate epochs as regional filed (IAGA Division V, Working Group 8, 1992). As is normally the case with deep sea surveys, diurnal correction for the daily variation of the earth's magnetic filed was not applied. The reduced magnetic data are presented as profiles along the ship's tracks and as projected profiles in Chapters 4 and 5. The original interpretation are carried out on the computer plotted profiles along track lines at a scale of 1:3500000 on Mercator chart.

3.5.1.4 GRAVITY DATA

As mentioned earlier, the ZE 30 data handling subsystem of gravimeter performs on-line processing of gravity data. The quality of processed gravity data mainly depend on the accuracy of the navigation data. The navigation data supplied by INS to ZE 30 during on-line processing are accurate only during satellite passes and less accurate during dead reckon. In view of the above, the measured gravity data are post processed using corrected navigation data. The following formulae are used during processing:

$$F = (G_V - G_H)K + G_{ABS} - G_N + E$$

where G_V is the measured gravity in mGal at actual position

G_H is the measured gravity in mGal at harbour

K= 0.9090 which is the gravimeter sensor constant

G_{ABS} is the absolute gravity in mGal at harbour

G_N is the normal gravity in mGal computed from International Gravity Formula

E is the Eotvos correction in mGal

The normal gravity is computed by the International Gravity Formula (Garland, 1979) which can be written as:

$$G_N = 978.03185\ (1 + 0.005278895\ \sin^2\phi + 0.000023462\ \sin^4\phi)$$

where ϕ is the geographical latitude.

For Eotvos correction (E) the following formula (Nettleton, 1976) is used:

$$E = 7.508\ V \sin\alpha \cos\phi + 0.004154\ V^2$$

where V is the speed of the ship in knots in the direction of course

ϕ is the geographical latitude

α is the course of the ship

Bouguer gravity anomaly (B) is computed from following formula:

$$B = F + B_K$$

where B_K is the Bouguer correction in mGal which is calculated from following formula:

$$B_K = \delta_\Delta \times G_N \times D \times 4.25976 \times 10^{-8}$$

Where δ_Δ is the density difference between earth crust and sea water, and D is the water depth in meter.

In the present study only Free-air gravity anomalies are used for interpretation. Bouguer gravity anomalies are not used here due to uncertainties in assuming the crustal densities. The Free-air anomalies are plotted along the profiles and presented in Chapter 6.

3.5.2 PROCESSING OF ANALOG DATA

The analog records of bathymetry and total magnetic intensity data are digitized using digitizer board. The digitization are accomplished by manually moving the digitizer's cursor along the curve defining the data and picking the representative data points by activating the cursor switch. This procedure has resulted in digitized values at random time intervals. At places of rapid variations, the data points are sampled at very closely spaced intervals in order to ensure true representation of the field data. After digitizing each segments of the record, the digitized data are checked using graphics

display to detect erroneous values and to check the quality of digitization. The digitized values are converted into time series data by linearly interpolating the data in between the digitized points. Thus, two separate time series data files, both bathymetry and total magnetic intensity, are generated. The time series data contain common reference parameters such as ship code, date, time, start of line, end of line etc.

As mentioned, the navigation data were obtained based on transit satellite. The positions are accurate only during satellite fix and the accuracy of positioning deteriorates during dead-reckoning process. During post processing of navigation data only good satellite fixes are considered and the position in between the satellite fixes are computed. This process involved computation of distance, speed and course in between the satellite position fixes over a spherical surface, by taking into account the WGS-72 spheroid constants. While compiling good satellite fixes, the positions at the start of a line and at places of sudden speed increase and course change are also taken, in order to avoid erroneous interpolation of navigation data. From these position data, time series navigation data are generated. The time series navigation data too contain reference parameters such as ship code, date, time, start of line, end of line etc. in addition to position data, speed, course etc.

Finally, the time series data of bathymetry, total magnetic intensity and navigation are merged using the above mentioned reference parameters. The merged data file thus contains ship code, line code, latitude, longitude, speed, course, water depth, total magnetic intensity data etc. This data file are then used to apply position related corrections as mentioned in sections 3.5.1.2 and 3.5.1.3 to compute corrected bathymetry and residual magnetic anomalies.

3.5.3 PROCESSING OF MULTICHANNEL SEISMIC REFLECTION DATA

The processing of multichannel seismic reflection data are carried out using NORSEIS seismic data processing software on Norsk Data ND-570 computer system. The basic objective of all seismic processing is to convert the information recorded in

the field into a form that facilitates geological interpretation. The data initially recorded in multiplexed mode on magnetic tape are transformed into a seismic section comparable in many ways to a geological structural section. The important step of processing is to eliminate or at least suppress all noise (defined as signal not associated with primary reflections) and to present the reflections on the record sections with the greatest possible resolution. The processing sequence of all necessary processes are shown as schematic diagram in Figure 3.12. The mandatory processes shown in solid boxes are in a fixed sequence. Most optional processes can vary in position within this fixed sequence. Stacking velocities of the subsurface layers were derived from semblance analysis of four adjacent CDP gathers at selected areas along each line. The processed seismic reflection data are presented as stack section in Chapter 7.

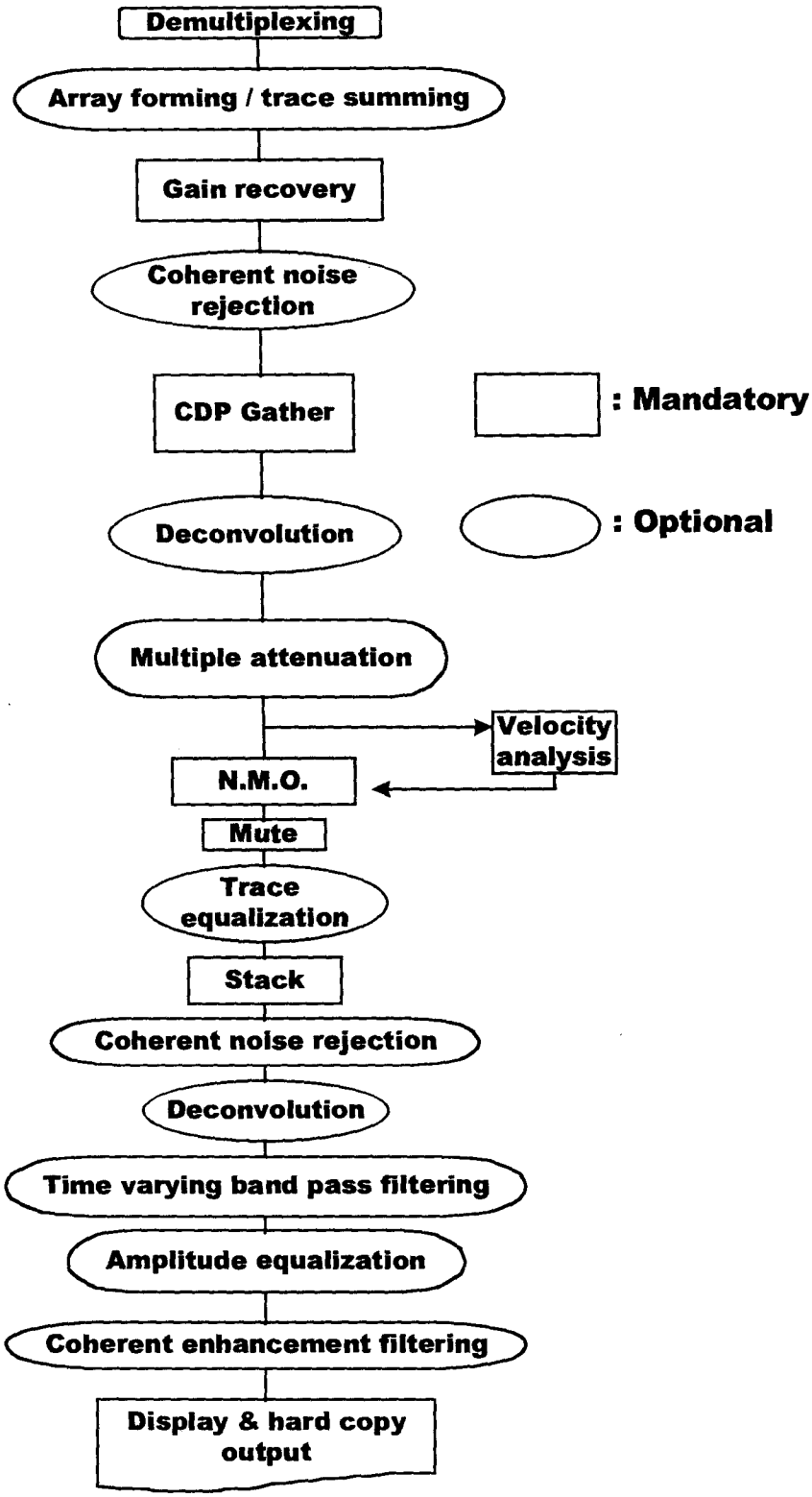

Figure 3.12 Processing sequence followed to process the multichannel seismic reflection data using NORSEIS seismic software package on ND - 570 computer.

CHAPTER 4

CHAPTER 4

IDENTIFICATION OF SEAFLOOR SPREADING MAGNETIC ANOMALIES

4.1 INTRODUCTION

Magnetic anomalies observed in the oceans are quite different from those observed over land and on the continental shelves. The anomalies in the oceans i) have short wavelength and high amplitude that appear as linear or greatly elongated on anomaly maps, and ii) can be easily correlated with reverse and normal polarity intervals of the geomagnetic polarity time scale. Thus, their identification and correlation with geomagnetic polarity time scale is vital for dating the ocean floor. In order to interpret the marine magnetic anomalies in time and space, it is necessary to correlate and identify the magnetic anomaly pattern based on Vine-Matthews hypothesis of seafloor spreading. A brief summary of the hypothesis is presented in the following section:

4.2 VINE-MATTHEWS HYPOTHESIS OF SEA FLOOR SPREADING

At the mid-ocean ridges, the oceanic lithosphere splits and magma is outpoured continuously. To accommodate the newly generated magma, the solidified part of the older magma moves away from the ridge axes. It is known as seafloor spreading process. At subduction zones the old oceanic lithosphere is consumed in the asthenosphere to accommodate the newly created lithosphere such that the surface area of the earth remains constant (Figure 4.1). The most definitive evidence for seafloor spreading process comes from study of the linear magnetic anomalies that characterizes the ocean floor. The solidified part of the lithosphere acquires the then magnetization while cooling through curie isotherm of about 520°C in oceanic areas. The observed pattern of the magnetic anomalies in the north Atlantic (Heezen et al., 1953; Keen, 1963), the Antarctic (Adams and Christoffel, 1962), and the Indian Ocean (Heirtzler,

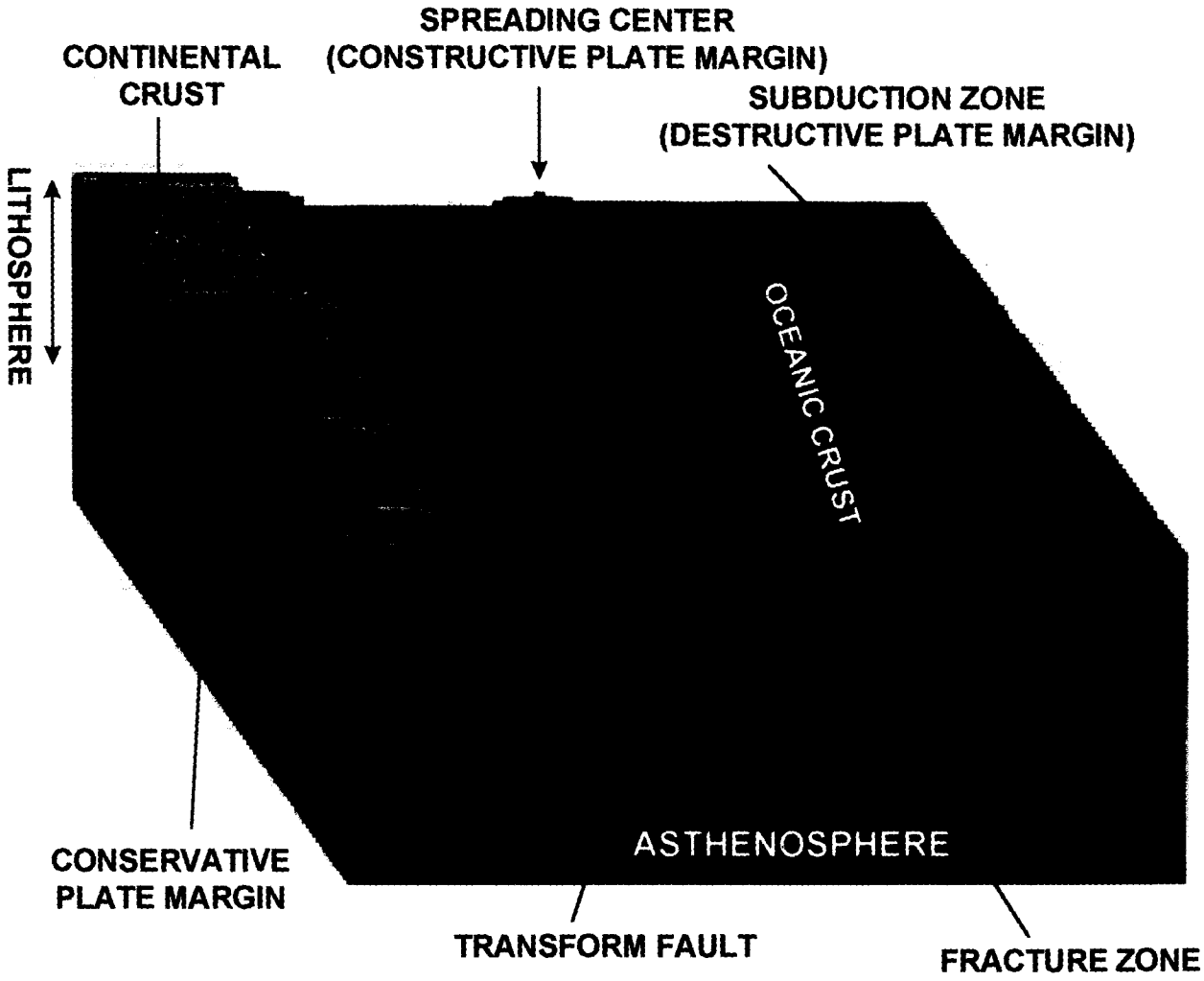

Figure 4.1 Diagram showing the basic concepts of seafloor spreading and plate tectonics.

1961; Matthews, 1963) have shown pronounced central anomaly associated with the median valley of the mid-ocean ridges and short period anomalies along the flanks of the ridges. The investigations of early sixties in the northeast Pacific Ocean revealed ridge parallel anomalies in the form of high and low magnetic strength (Mason, 1958; Mason and Raff, 1961; Raff and Mason, 1961; Vacquier et al., 1961). These are known as 'magnetic stripes'. The regular and continuous stripes were also found over most of the ocean floors (Cox, 1973). However, their origin remained a complete mystery for quite some time. The first successful attempt to account for the 'stripes' was made by F.J. Vine (then a graduate student at Cambridge University) and D.H. Matthews (his supervisor), in 1963 and independently by Morley and Larochelle in 1964.

They have explained them in light of the theory of seafloor spreading (Hess, 1960, 1962; Dietz, 1961) with reversals of the earth's magnetic field (Cox et al., 1963a). This is known as the Vine-Matthews hypothesis of seafloor spreading. As the earth's magnetic field reverses periodically and seafloor spreading occurs, the generated oceanic crust paralleling the crest of the ridge get magnetized normally and reversely. The crust with normal and reverse polarities caused the successive stripes of increase or decrease in the total intensity depending on the ambient magnetic field. The schematic illustration of the Vine and Matthews concept is shown in Figure 4.2.

The hypothesis was at first received with some skepticism. Later, it was received wide acceptance during 1965-1967 due to increased evidence for the stripes of magnetic anomalies from large investigations which led to the development of the plate tectonic theory (Vine and Wilson, 1965; Vine, 1966). The theory accounts the crust formed at mid-ocean ridges and moves away from them is controlled by the convective currents of the mantle material.

It may be mentioned that the discovery of reversal of the earth's magnetic field was one of the most profound discoveries in terms of its impact on the earth-sciences. The most important application of the chronology of reversals is to provide the calibration needed for the interpretation of marine magnetic anomalies. In the following

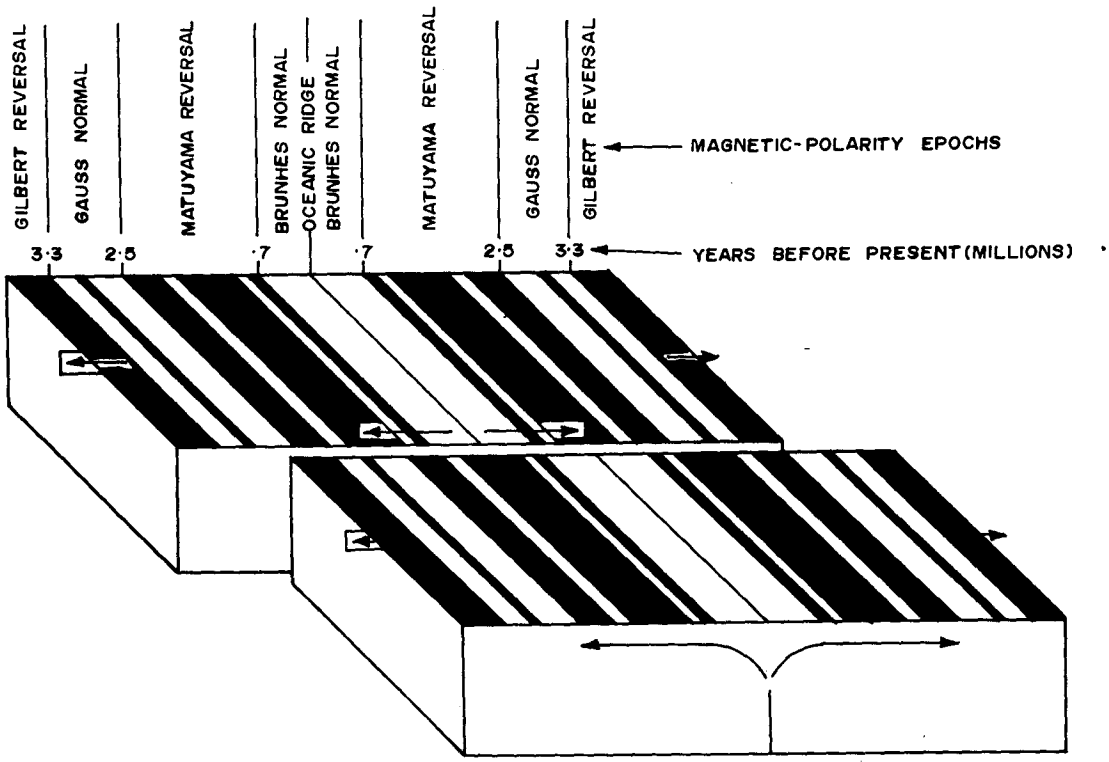

Figure 4.2 Schematic diagram showing Vine and Matthews concept of seafloor spreading. Asthenosphere mantle material rises under a spreading center to produce oceanic lithosphere. As this moves sideways, it cools past the Curie point of magnetic minerals in the rocks and acquires the ambient earth's magnetic field. Solid black and white stripes represents normally and reversely magnetized oceanic crustal blocks generated during reversals of earth's magnetic field.

section, the chronology of reversal of the earth's magnetic field is described.

4.3 GEOMAGNETIC POLARITY TIME SCALE

The geomagnetic field has two stable dipole states. A normal state in which the magnetic field over the earth's surface undergoes minor variations about a northerly direction as it is doing at present. A reversed state in which the direction is generally southerly. The field switches back and forth between the two stable states at varied intervals. When asthenospheric mantle material rises in a narrow zone along the ridge axis and cools through the Curie point of the major magnetic minerals, it acquires magnetization in the polarity of the earth's magnetic field that prevails at the time. As a result they contain information of the magnetization which can be used to determine the time of origin of the rocks and thus provides a basic data in time and space which are required for understanding the tectonic processes.

Brunhes has first discovered reversals of the earth's magnetic field as early as 1906. Mercanton (1926) and Matuyama (1929) have provided the timing of magnetic reversals. Matuyama's study, based on available age information of the rock samples, has revealed that during early part of the Quaternary period the earth's magnetic field was reversely magnetized and that has gradually changed over to normal state. Subsequent investigations of Hospers (1954), Khramov (1957), Sigurgeirsson (1957), and Cox (1959) have confirmed the reversals and soon made to realize the need for the geomagnetic polarity reversal time scale.

Because the geomagnetic field is a global phenomenon, the field-reversal theory requires that transitions from one magnetic polarity to another must occur at exactly the same time over the entire earth. This necessitated to determine ages of the rocks as they are the most important information needed to propose calibrated time scale for the magnetic reversals. The development of different dating techniques (particularly Potassium-Argon method) in the late 1950's have made it possible to determine ages for the volcanic rocks where magnetic polarities have been determined. Cox et al. (1963a,

b), for the first time, have proposed time scale for geomagnetic reversals making use of the Potassium-Argon (K-Ar) dates. Further, discovery of short polarity event of duration as small as 10^5 years within the major polarity intervals have led to modify the time scale. Such polarity intervals were termed polarity epochs which is defined as time intervals during which the field is entirely or predominantly of one polarity (Cox et al., 1964). They were named after the early workers in the field of geomagnetism e.g. Brunhes, Matuyama, Gauss, Gilbert, while the short duration polarity events (short intra-epoch fluctuations) were named after the sites of their discovery (Cox et al., 1964). A polarity epoch may contain several polarity events and can be dominantly reversed (e.g. the Brunhes), dominantly normal (e.g. the Matuyama), or mixed. With the discovery of evidence for more and more reversals, it was realized that the length of time between reversals varies continuously over a wide range from very short events to long polarity epochs. By the late 1960's the time scale of reversals were extended back to about 4.5 million years from the combined magnetic data, and dating of volcanic rocks and deep-sea sediments (Cox et al., 1968; Cox, 1969).

While Heirtzler et al. (1968) proposed a magnetic polarity reversal time scale for the Late Cretaceous to Recent, about 75 Ma (anomaly 32), based on the distribution of oceanic magnetic anomalies on a few long magnetic profiles. This time scale was derived by assuming that all the linear magnetic anomalies are parallel to the ridge axes, and due to geomagnetic field reversals as hypothesized by Vine and Matthews (1963). It was deduced by considering a constant spread rate of 1.9 cm/yr (Dickson et al., 1968) and distance of the model magnetized bodies from the axial zone of spreading i.e. ridge axis in the South Atlantic. The available date of 3.35 m.y. of the Gauss-Gilbert magnetic polarity boundary is taken as basis for extrapolating the ages of the magnetic reversals backward in time. The geomagnetic polarity time scale of Heirtzler et al. (1968) was confirmed by the deep sea drilling results from Joint Oceanographic Institutes for Deep Earth Sampling (JOIDES) investigations in the South Atlantic (Maxwell et al., 1970). This time scale has been widely accepted for interpreting the magnetic anomalies of the world oceans. It has been further improved for still short duration intervals of magnetic reversals and precise dating of the earlier identified anomaly numbers.

Age calibration has been the focus for changes to the geomagnetic polarity time scale of LaBrecque et al. (1977). Subsequent calibration efforts added more control points based on developing magneto-biostratigraphic ties, and relaxed the implicit assumption of constant spreading in the South Atlantic to smaller time scales (Ness et al., 1980; Lowrie and Alvarez, 1981; Harland et al., 1982; Berggren et al., 1985; Haq et al., 1988).

Cande and Kent (1992) proposed a geomagnetic polarity time scale for the Late Cretaceous and Cenozoic based on an analysis of marine magnetic data from the world's major oceanic ridge systems. This scale is based on nine age calibration tie points evenly distributed at approximately 10 m.y. intervals (Table 4.1) which was fitted with a cubic spline approximation to interpolate the age of polarity intervals. At these tie points the magnetic anomalies are correlated with the ages determined from biostratigraphic studies of oceanic basement and basal sediments (Figure 4.3). Linear interpolated ages were assigned for the in between anomaly numbers from magnetic profiles. Additional small-scale anomalies (tiny wiggles) that represent very short polarity intervals or intensity fluctuations of the dipole field have been incorporated.

Cande and Kent (1995) again refined their 1992 geomagnetic polarity time scale with more precise age data and proposed a new time scale. It uses an age of 65 Ma (instead of 66 Ma as used by them in 1992) for the Cretaceous-Tertiary boundary as recorded in marine (Swisher et al., 1992; Dalrymple et al., 1993) and non-marine (Swisher et al., 1993) sediments. Secondly, it uses an astronomical age of 5.23 Ma (Hilgen, 1991; Langereis et al., 1994) for the older boundary of subchron 3n.4n rather than 2.6 Ma for the younger boundary of chron 2A (Matuyama/Gauss boundary). The re-revised age calibration for geomagnetic polarity time scale is presented in Table 4.2 and the revised time scale is presented in Table 4.3.

Table 4.1 Age calibrations for Geomagnetic Polarity Time Scale (after Cande and Kent, 1992).

Polarity Chron	South Atlantic Distance (km)	Age (Ma)
2An(0.0)	41.75	2.6
5Bn(0.0)	290.17	14.8
6Cn.2r(0.0)	501.55	23.8
13r(.14)	759.49	33.7
21n(.33)	1071.62	46.8
24r(.66)	1221.20	55.0
29r(.3)	1364.37	66.0
33n(.15)	1575.56	74.5
34n(0.0)	1862.32	83.0

Note: For more precise correlation, the fractional position within a chron or subchron is referred to by the equivalent decimal number appended, within parentheses, to the chron or subchron name. As examples, the younger end of chron 29n is designated as 29n(0.0) whereas, the older end of chron 29n is conveniently designated as 29r(0.0) since it is equivalent to the younger end of chron 29r. A level within chron 29r and 3/10 from its younger end is designated as 29r(0.3).

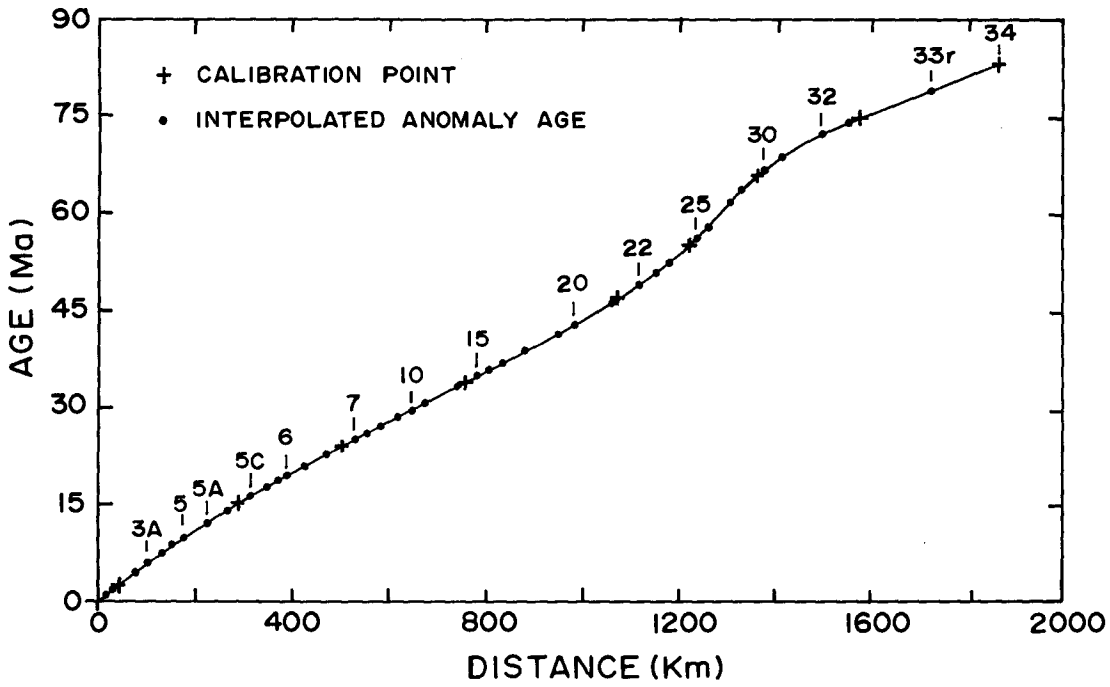

Figure 4.3 Ages of magnetic anomalies determined by interpolation of ages of nine age calibration points (after Cande and Kent, 1992).

Table 4.2 Revised age calibrations for Geomagnetic Polarity Time Scale (after Cande and Kent, 1995)

Polarity Chron	South Atlantic Distance (km)	Age (Ma)
3n.4(0)	84.68	5.23
5Bn(0.0)	290.17	14.8
6Cn.2r(0.0)	501.55	23.8
13r(.14)	759.49	33.7
21n(.33)	1071.62	46.8
24r(.66)	1221.20	55.0
29r(.3)	1364.37	65.0
33n(.15)	1575.56	74.5
34n(0.0)	1862.32	83.0

Note: For more precise correlation, the fractional position within a chron or subchron is referred to by the equivalent decimal number appended, within parentheses, to the chron or subchron name. As examples, the younger end of chron 29n is designated as 29n(0.0) whereas, the older end of chron 29n is conveniently designated as 29n(o) or 29r(0.0) since it is equivalent to the younger end of chron 29r. A level within chron 29r and 3/10 from its younger end is designated as 29r(0.3).

Table 4.3 Geomagnetic Polarity Time Scale from Late Cretaceous to Recent (after Cande and Kent, 1995)

Normal Polarity Interval (Ma)	Polarity Chron
0.000 - 0.780	1n
0.990 - 1.070	1r.1n
1.770 - 1.950	2n
2.140 - 2.150	2r.1n
2.581 - 3.040	2An.1n
3.110 - 3.220	2An.2n
3.330 - 3.580	2An.3n
4.180 - 4.290	3n.1n
4.480 - 4.620	3n.2n
4.800 - 4.890	3n.3n
4.980 - 5.230	3n.4n
5.894 - 6.137	3An.1n
6.269 - 6.567	3An.2n
6.935 - 7.091	3Bn
7.135 - 7.170	3Br.1n
7.341 - 7.375	3Br.2n
7.432 - 7.562	4n.1n
7.650 - 8.072	4n.2n
8.225 - 8.257	4r.1n
8.699 - 9.025	4An
9.230 - 9.308	4Ar.1n
9.580 - 9.642	4Ar.2n
9.740 - 9.880	5n.1n
9.920 - 10.949	5n.2n
11.052 - 11.099	5r.1n

Normal Polarity Interval (Ma)	Polarity Chron
11.476 - 11.531	5r.2n
11.935 - 12.078	5An.1n
12.184 - 12.401	5An.2n
12.678 - 12.708	5Ar.1n
12.775 - 12.819	5Ar.2n
12.991 - 13.139	5AAn
13.302 - 13.510	5ABn
13.703 - 14.076	5ACn
14.178 - 14.612	5ADn
14.800 - 14.888	5Bn.1n
15.034 - 15.155	5Bn.2n
16.014 - 16.293	5Cn.1n
16.327 - 16.488	5Cn.2n
16.556 - 16.726	5Cn.3n
17.277 - 17.615	5Dn
18.281 - 18.781	5Dn
19.048 - 20.131	6n
20.518 - 20.725	6An.1n
20.996 - 21.320	6An.2n
21.768 - 21.859	6AAn
22.151 - 22.248	6AAr.1n
22.459 - 22.493	6AAr.2n
22.588 - 22.750	6Bn.1n
22.804 - 23.069	6Bn.2n
23.353 - 23.535	6Cn.1n
23.677 - 23.800	6Cn.2n
23.999 - 24.118	6Cn.3n
24.730 - 24.781	7n.1n

Normal Polarity Interval (Ma)	Polarity Chron
24.835 - 25.183	7n.2n
25.496 - 25.648	7An
25.823 - 25.951	8n.1n
25.992 - 26.554	8n.2n
27.027 - 27.972	9n
28.283 - 28.512	10n.1n
28.578 - 28.745	10n.2n
29.401 - 29.662	11n.1n
29.765 - 30.098	11n.2n
30.479 - 30.939	12n
33.058 - 33.545	13n
34.655 - 34.940	15n
35.343 - 35.526	16n.1n
35.685 - 36.341	16n.2n
36.618 - 37.473	17n.1n
37.604 - 37.848	17n.2n
37.920 - 38.113	17n.3n
38.426 - 39.552	18n.1n
39.631 - 40.130	18n.2n
41.257 - 41.521	19n
42.536 - 43.789	20n
46.264 - 47.906	21n
49.037 - 49.714	22n
50.778 - 50.946	23n.1n
51.047 - 51.743	23n.2n
52.364 - 52.663	24n.1n
52.757 - 52.801	24n.2n
52.903 - 53.347	24n.3n

Normal Polarity Interval (Ma)	Polarity Chron
55.904 - 56.391	25n
57.554 - 57.911	26n
60.920 - 61.276	27n
62.499 - 63.634	28n
63.976 - 64.745	29n
65.578 - 67.610	30n
67.735 - 68.737	31n
71.071 - 71.338	32n.1n
71.587 - 73.004	32n.2n
73.291 - 73.374	32r.1n
73.619 - 79.075	33n
83.000 -118.000	34n

4.3.1 POLARITY CHRON NOMENCLATURE

The polarity chron nomenclature proposed by Cande and Kent (1995) have been used in this study. A brief summary is described here.

The longest intervals of predominantly one polarity is referred by the corresponding anomaly number followed by the suffix 'n' for normal polarity or 'r' for the preceding reversed polarity interval. If these chrons are subdivided into shorter polarity intervals, they are referred as subchrons and are identified by appending, from youngest to oldest, to the primary chron name and adding an n for a normal polarity interval, or r for a reverse interval. As an example, the three normal polarity intervals of anomaly 6C (chron 6Cn) are denoted as 6Cn.1n, 6Cn.2n and 6Cn.3n subchrons. Similarly, the reversed interval preceding (older than) subchron 6Cn.1n is referred as subchron 6Cn.1r. In the figures, the normal polarity is denoted as 'N' instead of 'n' for clarity.

4.4 COMPUTATION OF SYNTHETIC MAGNETIC ANOMALIES

Identification of the linear magnetic anomalies and their correlation with the synthetic anomalies of the crust are important for systematic mapping of the ages of the ocean floor. Synthetic anomalies are generated based on geomagnetic polarity time scale and spreading rate of the ocean floor. The magnetic model of the ocean crust thus consists of normally and reversely magnetized rectangular stripes. The shape of magnetic anomalies generated using above model depends mainly on two factors: i) the azimuth and latitude of the ridge generating the anomalies and the present azimuth and latitude of anomalies where it is observed, and ii) the thickness and susceptibility of the magnetized oceanic crust which produces the magnetic anomalies.

If the seafloor spreads in E-W direction i.e. spreading ridge trends N-S as in the Northeast Pacific or the South Atlantic, the anomalies are observed at latitude where they are originated. Therefore, the pattern of observed anomalies remains the same since there is no change in the magnetic inclination at the time of generation and observation

of anomalies. In contrast, if the magnetized crust moves to the north or south as a result of spreading process and the re-orientation of the ridge axis, the shape of the observed anomalies change as a result of change in the magnetic inclination at the time of generation and observation of the anomalies. In the northeast Arabian Sea, trend of the ancient spreading direction was ~NNE and the magnetized crustal block had drifted substantially towards north from its original location (McKenzie and Sclater, 1971). Under these circumstances, it is essential to take into account the magnetic parameters existed at the time of generation of the anomalies. To overcome this problem, McKenzie and Sclater (1971) suggested a method to compute synthetic magnetic anomaly by taking into account for the changes in latitude and azimuth for the spreading ridge at the time of generation and observation of the anomalies. In the present study, a FORTRAN program is developed to compute synthetic magnetic anomalies using the concept of Vine and Matthews (1963). This program is basically based on: i) Talwani and Heirtzler's (1964) program for the computation of magnetic anomalies caused by two dimensional structures of arbitrary shape and, ii) the method described by McKenzie and Sclater (1971) and Vacquier (1972). Therefore, the synthetic magnetic profiles, as they would be observed at the present latitude and orientation, are computed from geomagnetic polarity reversal chronology and assumed spreading rates for original latitude and orientation of the ridge.

The shape of the anomalies is also dependent on the product of the thickness and the susceptibility of oceanic layer (McKenzie and Sclater, 1971). The thickness of magnetized layer, is usually taken as constant (layer 2 of the oceanic crust). It could even extend down to the Curie isotherm limit for magnetism which is about 575°C (Vine, 1968). Bott (1967) suggested that layer 2 of the oceanic crust, which is 2 km thick on an average, is the main source of the magnetic anomalies. This source of magnetic anomalies lie within layer 2 because layer 1 consists of effectively non-magnetic sediments and layer 3 is too deep to explain the anomalies. But, Cande and Kent (1976) proposed a two layer approximation of the basaltic layer and suggested that the rapidly cooled top 500 m of the layer 2 contributes to about three quarters of total

amplitude of the magnetic anomalies. Whereas, the slowly cooled lower layer which experiences delayed acquisition of magnetization contributes to one quarter. Vacquier (1972) suggested that the thickness of the model stripe could be anything between 0.5 and 2.5 km. In the case the shapes of the calculated anomalies are not seriously affected by the assumed thickness of the model because the oceanic crust is generally occur at 4 km water depth.

Furuta et al. (1987) suggested that a 0.6 km thick pillow lava of the upper most oceanic crust is the main source of marine magnetic anomalies. There is no general agreement on the thickness and susceptibility of the basaltic layer which produces the magnetic anomalies (McKenzie and Sclater, 1971; Talwani et al., 1971).

Measurements of the susceptibility of the pillow lavas dredged from ridge axis have revealed an average susceptibility of 0.05 cgs units and is sufficient to produce the observed magnetic anomalies if the thickness of layer is 400 m (Irving et al., 1970; Marshall and Cox, 1971). But, recent magnetic investigations in the ocean revealed that the anomaly pattern is not altered inspite of layer 2 being absent. Talwani et al. (1971) have suggested that in a region of unknown magnetization and magnetic layer thickness, relatively thick blocks with low magnetization or thin blocks with large magnetization can be ascribed to generate the synthetic anomalies. However, constant thickness and magnetization parameters are preferred.

In the present study, synthetic magnetic anomalies are computed by considering 2 km thick oceanic layer 2 with a susceptibility of 0.01 cgs units (McKenzie and Sclater, 1971). Since the shape and sequence of the anomalies are governed by Vine and Matthew's model and the geomagnetic polarity time scale, the observed and synthetic profiles are correlated by primarily considering shape of the anomalies.

It is observed that the magnetic anomalies in the northern Arabian Sea are negative over normally magnetized crust, akin to the crustal magnetization in the southern hemisphere. The oceanic crust in the northern Arabian Sea was formed in southern magnetic latitudes with low inclination and drifted to present latitude. Since the

shape of the observed anomalies are affected by the change in the magnetic inclination at the time of generation, the anomalies are negative over normally magnetized crust. Figure 4.4 shows synthetic magnetic profiles generated for a ridge striking E-W at a latitude of 20°S and observed at various latitudes. From this exercise, it is seen that changes in the shapes of the anomalies occur when the seafloor moves across the magnetic equator. Positively magnetized blocks give rise to negative anomalies when observed in the northern hemisphere. These factors are considered while generating the synthetic anomalies of the crustal model of the Arabian Sea.

4.5 IDENTIFICATION OF SEAFLOOR SPREADING MAGNETIC ANOMALIES

The Western Arabian Basin (WAB) and the Eastern Somali Basin (ESB) are conjugate oceanic basins created during symmetric seafloor spreading along the Carlsberg Ridge. Identification of linear magnetic anomalies in both the basins as well as on the Carlsberg Ridge may provide a complete evolutionary history of the Arabian Sea. In the present study a detailed identification of magnetic anomaly in the WAB is carried out based on closely spaced profiles. To provide a reasonable constraints on the evolution of this basin, identification of magnetic anomalies along two regional profiles across the Carlsberg Ridge are also carried out. In the following sections, identification of anomalies are described.

4.5.1 PALEO-LATITUDE FROM ANOMALY SHAPE AND AMPLITUDE

McKenzie and Sclater (1971) have suggested that the oceanic crust of the Arabian Sea, east of the Owen Fracture Zone is generated at 10^0S and drifted to a considerable distance northwards since its formation. Whitmarsh (1974) has considered that the oceanic crust of the WAB was generated at 13^0S to compute synthetic magnetic profile for correlation and identification of anomalies on observed profiles. To calculate the paleo-latitude of the oceanic crust of the WAB the observed anomalies are compared with calculated anomalies from the Vine-Matthews block model formed at different latitudes. In this exercise a large number of synthetic anomaly profiles are generated

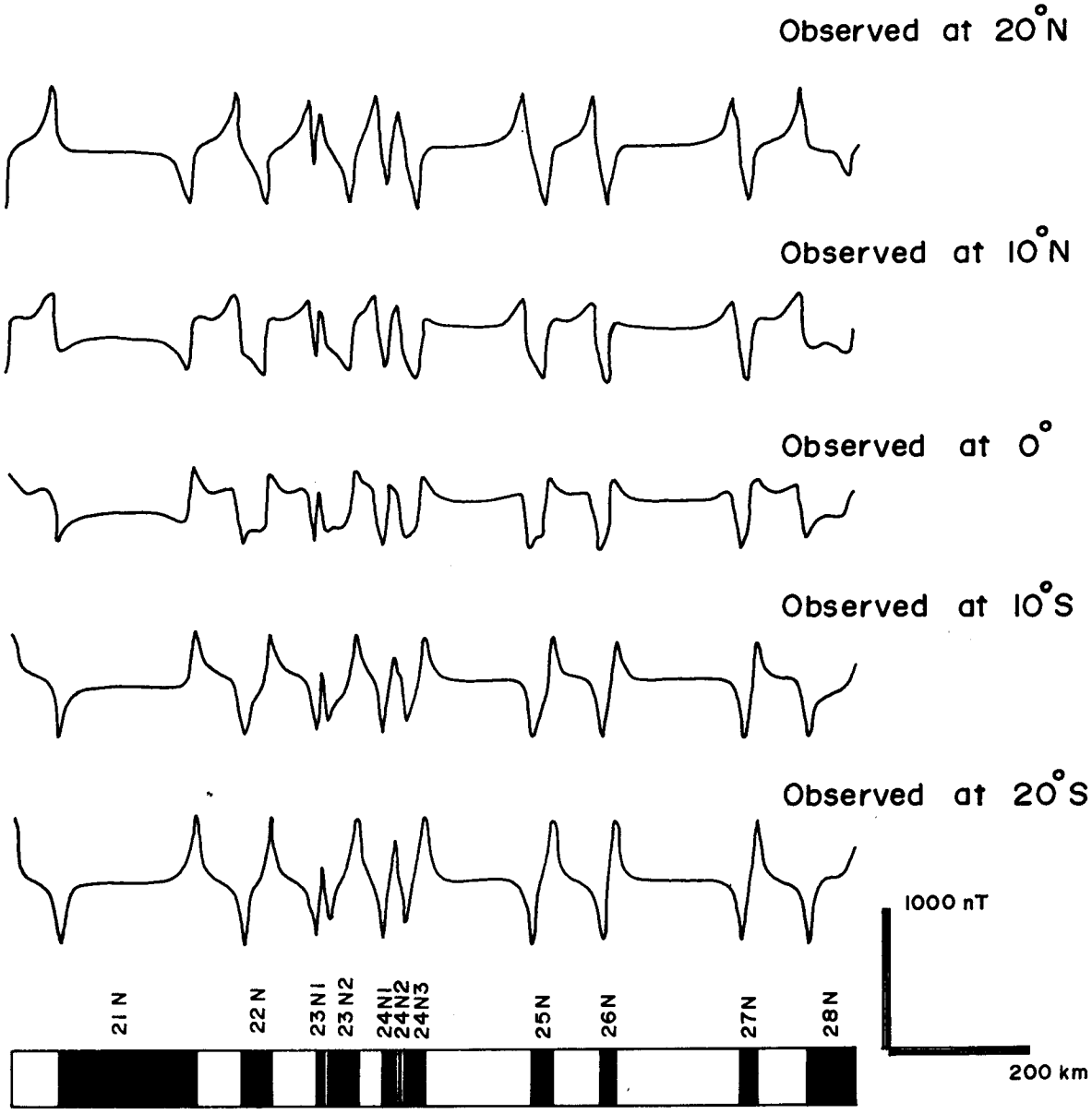

Figure 4.4 Synthetic magnetic profiles generated for a ridge striking east-west at 20°S and observed at various latitudes. Note that major changes in the shapes of the anomalies occur when the seafloor moves across the magnetic equator. Positively magnetized block give rise to negative anomalies when observed in the northern hemisphere.

considering the position of observation at 13^0N, 65^0E for many different latitudes and strikes of the paleo-spreading ridge in an attempt to reproduce the observed anomalies. Few of the many profiles calculated in this way are shown for comparison in Figure 4.5. It is seen that the shapes of the anomalies (relatively negative anomalies due to normally magnetized block) thus calculated i) have pronounced peak at the left if generated at 20°S or 30°S, ii) are almost symmetrical and very slightly higher on the left if generated at 10^0S, and iii) have peak at the right if generated at the equator. It is further seen that the observed profiles are almost symmetrical though very slightly higher on the left. The shapes of anomalies in the WAB are well correlatable to the model anomalies generated by a ridge striking N75^{0}W at 10^0S. Therefore, a N75^0 W striking ridge at a paleo-latitude of 10^0S is considered for computing the synthetic magnetic anomalies for the WAB area.

4.5.2 IDENTIFICATION OF MAGNETIC ANOMALIES IN THE WESTERN ARABIAN BASIN

The identification of magnetic anomalies of the WAB is primarily based on identification of fine-scale structure of anomalies 23 and 24 followed by striking pair of negative anomalies 25 and 26 separated from others by a flat region with no anomalies. In the recent geomagnetic polarity time scale (Cande and Kent, 1995), the anomaly 23 is characterized by a younger short span (0.168 m.y.) of normal, a brief span (0.101 m.y.) of reverse and a large span (0.696 m.y.) of older normal polarity. Whereas, in the geomagnetic polarity time scale of Heirtzler et al. (1968), the anomaly 23 is defined as a single large span (0.9 m.y.) of normal polarity. Similarly, anomaly 24 is characterized by a small trough (tiny wiggle) within the two larger troughs of anomaly 24. This is due to the fact that anomaly 24 consists of three sub-chrons i.e. a brief normal polarity interval flanked by two closely spaced relatively long normal polarity intervals. Presence of these sub-chrons results in a distinct shape of anomaly 24. In the geomagnetic polarity time scales (Heirtzler et al., 1968; LaBrecque et al., 1977; Berggren et al., 1985; Cande and Kent, 1995) the normal polarity epochs of anomalies 25 and 26 are separated on both sides by a very long (more than 2.0 m.y.) period of reversed polarity epochs (i.e. reverse

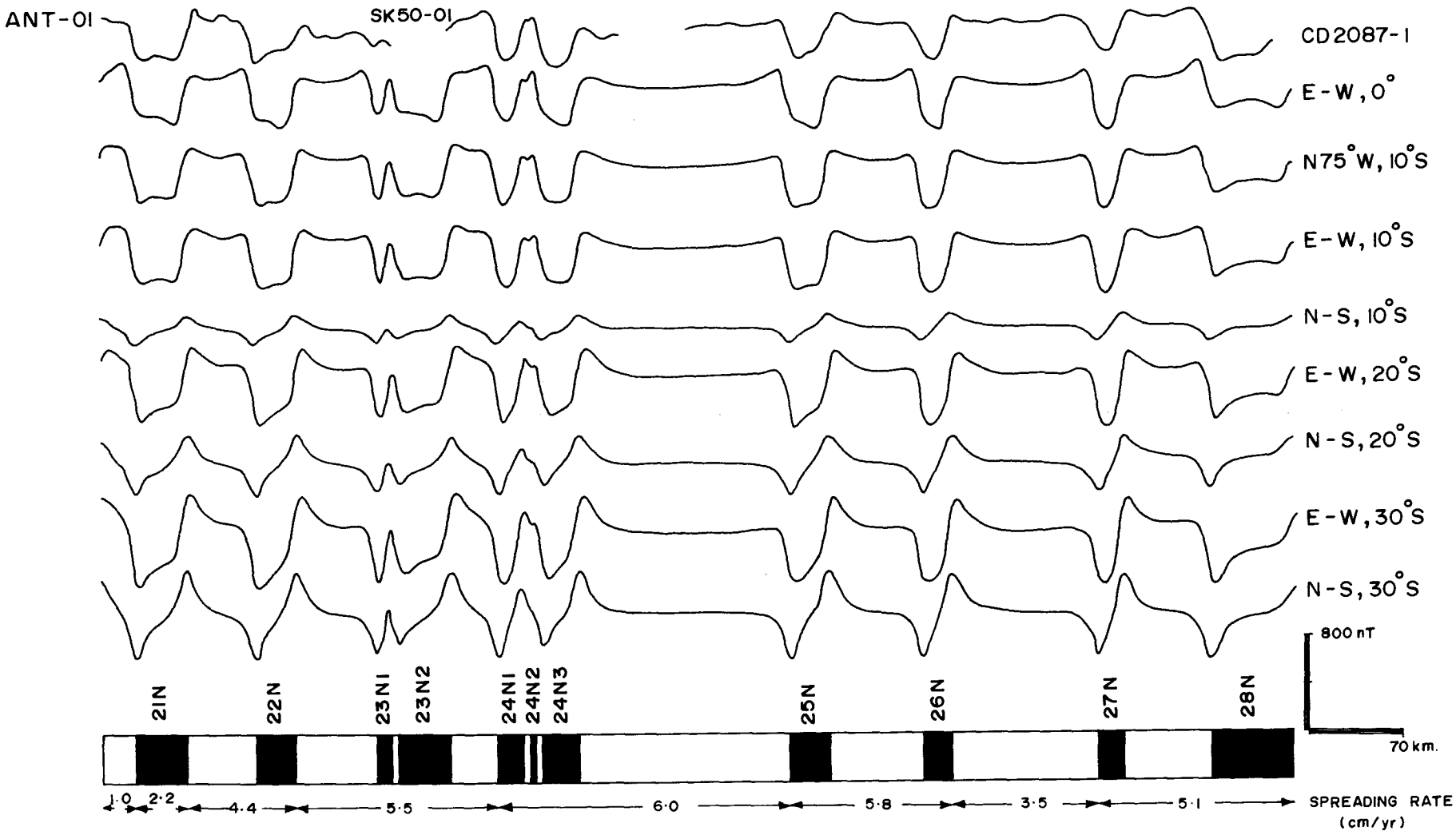

Figure 4.5 Comparison of the observed profiles (ANT-01, SK50-01, CD2087-1) with the synthetic magnetic profiles. Synthetic profiles are computed for a ridge with different strikes and paleo-positions and presently observed at 13°N and 65°E. Note that the shapes of observed anomalies are well correlatable with synthetic anomalies computed for a ridge striking N75°W at 10°S.

polarity between anomalies 24 and 25; reverse polarity between anomalies 26 and 27), thereby making this part of the anomaly sequence very distinctive. Using geomagnetic polarity time scales (Heirtzler et al., 1968; LaBrecque et al., 1977; Berggren et al., 1985; Cande and Kent, 1995) and an assumed half spreading rate (6.0 cm/yr), synthetic profiles are generated for anomalies 23 through 27 (Figure 4.6). It can be seen that except for the synthetic profile generated using Heirtzler et al. (1968), other three scales results in a distinct shape of anomaly 23. Similarly, a distinct shape of anomaly 24 can be seen except for the profiles generated using geomagnetic polarity time scales suggested by Heirtzler et al. (1968) and LaBrecque et al. (1977). Whereas, anomalies 25 and 26 are very distinct in all the synthetic profiles computed using all the above mentioned time scales. These remarkably large and distinctive anomalies discussed above are used as a key indicators for identification of anomalies on observed profiles in the WAB.

The identifications of magnetic anomalies of the WAB are carried out by comparing the observed anomalies with synthetic anomalies. The observed anomalies are projected at an azimuth of 360°. The synthetic magnetic anomaly for the WAB are generated for a ridge striking N75°W at a latitude of 10°S and now observed at 13°N, 65°E. Magnetized layer (susceptibility 0.01 cgs units) is considered flat and 2 km thick with its top at 5.5 km depth below sea surface. The recent geomagnetic polarity time scale and polarity chron nomenclature proposed by Cande and Kent (1995) have been used to assign magnetic anomaly numbers on observed profiles.

The computed synthetic magnetic profiles and undisturbed portions of the representative observed magnetic profiles are shown in Figure 4.7. The spreading rates between anomalies are estimated during repeated trials so as to obtain a good match between the synthetic profile and the undisturbed segments of the observed anomaly profiles. From the best fit model, it is found that the half spreading rates vary from 1.0 to 6.0 cm/yr between anomalies 18N and 28N.

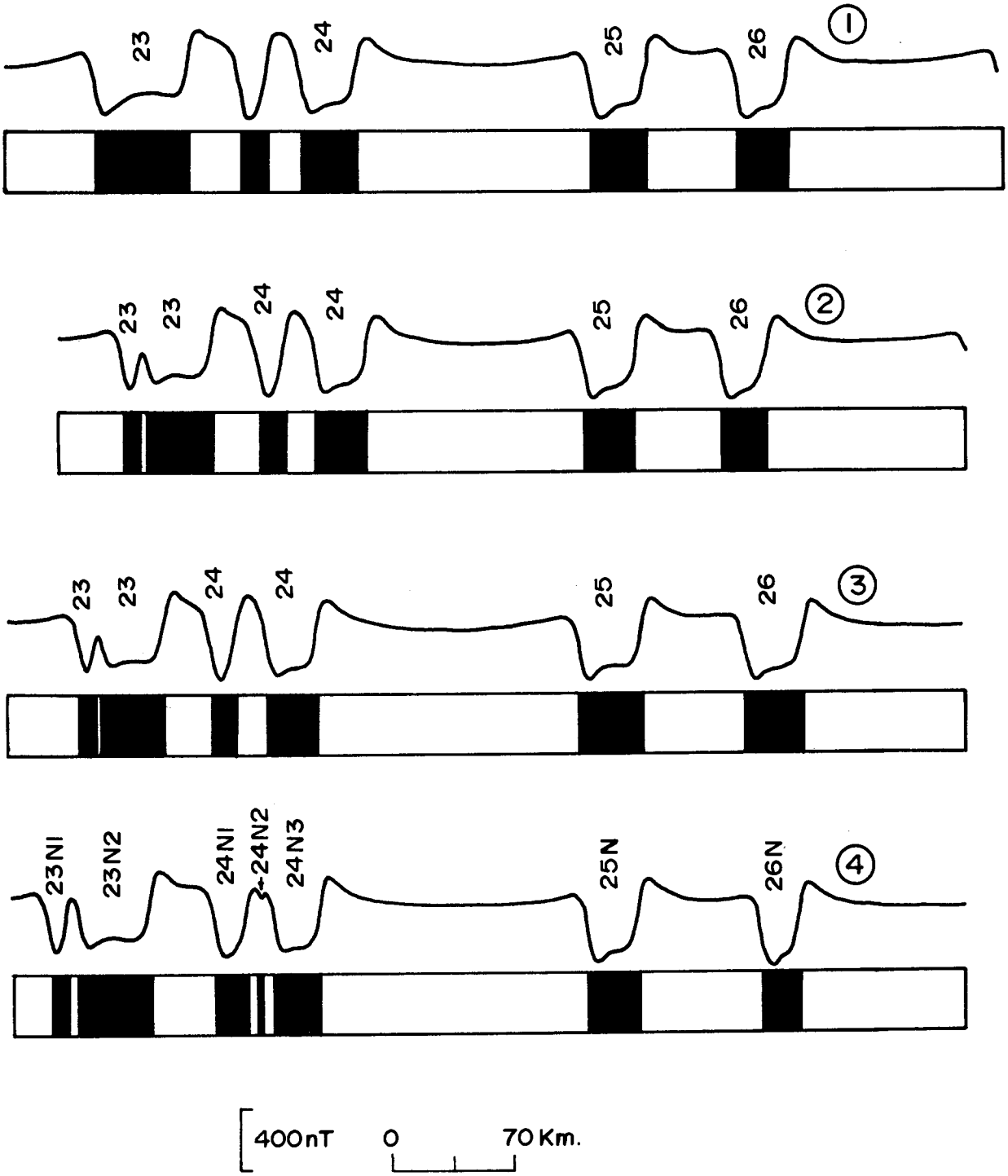

Figure 4.6 Synthetic magnetic profiles (half-spread rate 6.0 cm/yr) to demonstrate the shape of the anomalies 27 through 23. Different magnetic polarity reversal time scales used to generate synthetic magnetic profiles (number in circle) are: Heirtzler et al. (1968) for profile 1; LaBreque et al. (1977) for profile 2; Berggren et al. (1985) for profile 3 and Cande and Kent (1995) for profile 4. The fine scale structure of anomaly 24 in profile 4 and anomaly 23 in profiles 2, 3 and 4 can be distinctly seen. Other details as per Figure 4.8.

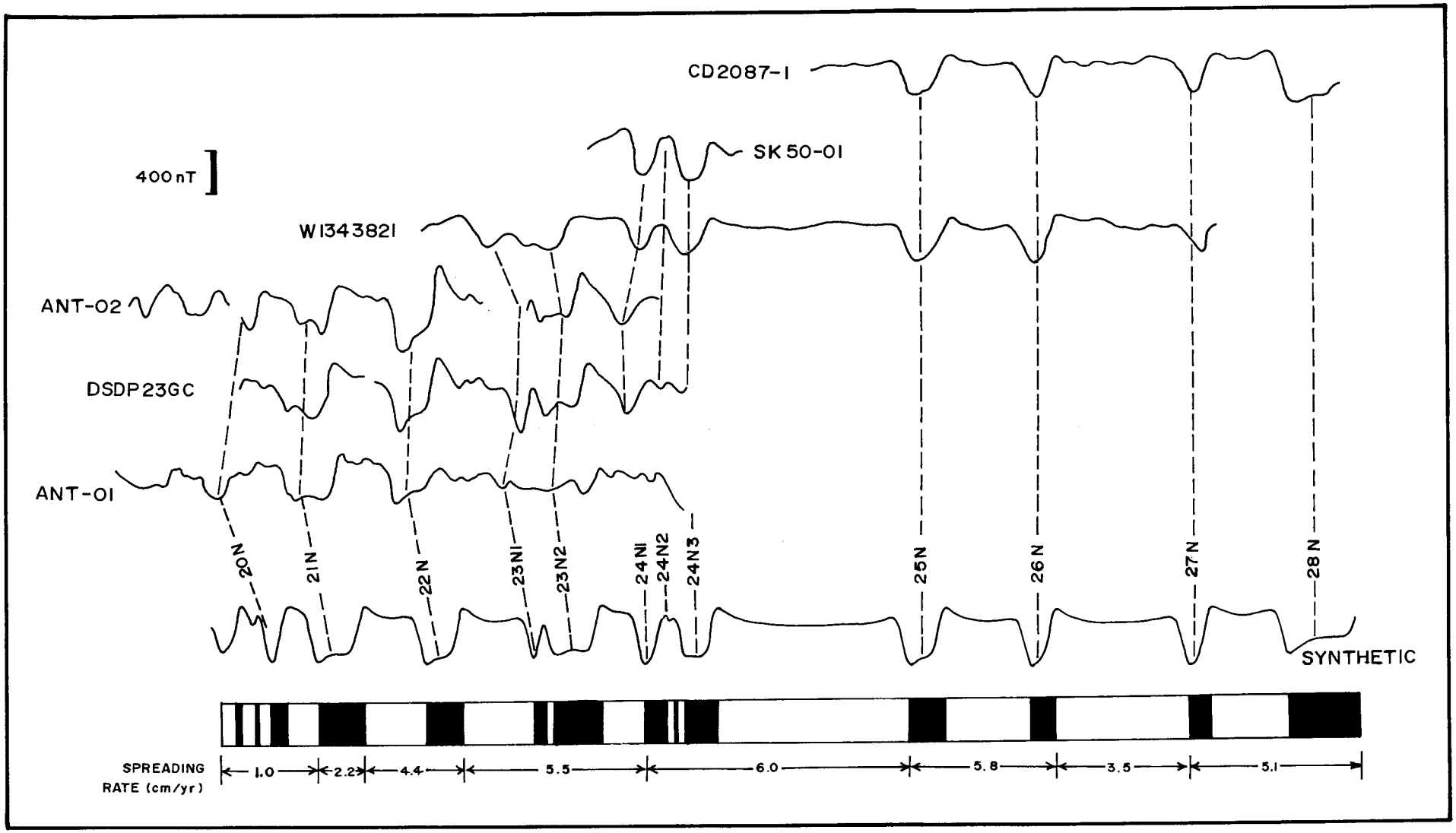

Figure 4.7 Synthetic and undisturbed portions of the representative observed magnetic profiles in the Western Arabian Basin. The location of profiles is shown in Figures 4.8 and 4.9. Observed profiles are projected at an azimuth of 0°N. Synthetic magnetic profile is computed for a ridge striking N75°W at a latitude of 10°S and now observed at 13°N, 65°E. Normally magnetized blocks are indicated by solid black. Magnetized layer (susceptibility 0.01 cgs units) is flat, 2.0 km thick with its top at 5.5 km below the sea surface. Magnetic anomaly identifications are according to the geomagnetic polarity reversal time scale and polarity chron nomenclature proposed by Cande and Kent (1995).

4.5.2.1 *PRE-ANOMALY 24 LINEATIONS IN THE WESTERN ARABIAN BASIN*

The identification of E-W set of pre-anomaly 24 lineations in the northwestern part of the WAB was initially proposed by McKenzie and Sclater (1971) and later mapped by Naini and Talwani (1982). However, identification of anomaly 28, which is considered to be the oldest anomaly of the basin, was not identified unambiguously. Further, over a large part of this area (i.e. from 66°E up to the vicinity of the Laxmi and Laccadive Ridges) no pre-anomaly 24 lineations are mapped. Later with the help of additional data, Miles and Roest (1993) confidently mapped a segment of magnetic lineation generated during normal polarity event north of anomaly 27N in the areas adjacent and (sub)parallel to the E-W trending Laxmi Ridge segment between 63°40' and 66°E, and identified the lineation as anomaly 28N. With the integration of new profiles to the published data, the magnetic data in the northern WAB (north of 15°N) became dense (Figure 4.8), which permitted some obvious inter-profile anomaly correlations. The extension of lineation 28N as well as other pre-anomaly 24 lineations eastwards up to about 70°E could be mapped (Figure 4.8). It may be noted that all over the area adjacent to the southern boundary of the Laxmi Ridge, only the early part of the anomaly 28 could be mapped, whereas for the other pre-A24 lineations well demarcated boundaries of the magnetized blocks could be mapped. Based on distribution of the identified magnetic lineations, the pre-anomaly 24 sequence broadly is divided into western, central and eastern subsets. The western set of lineations 24N1-28N are well developed and they can be traced as long continuous east-west trending segments almost up to the vicinity of the Owen Fracture Zone. In the central set (between 65°30' and 67°30'E), the lineations 28N-25N trend NW-SE and is oblique to the local trend of the Laxmi Ridge. The eastern set (i.e. eastward from 67°30'E) of the lineations again trends E-W and the southward extension of the physiographic expression of the Laxmi Ridge appears to be truncated by lineation 28N. Further, unlike the E-W trending western set of lineations 28N-25N, the central and eastern set of same lineations occur as short segments. Anomalies 28N-25N are mapped with a fair degree of confidence at least up to about 68°30'E. But further eastwards it becomes difficult to identify

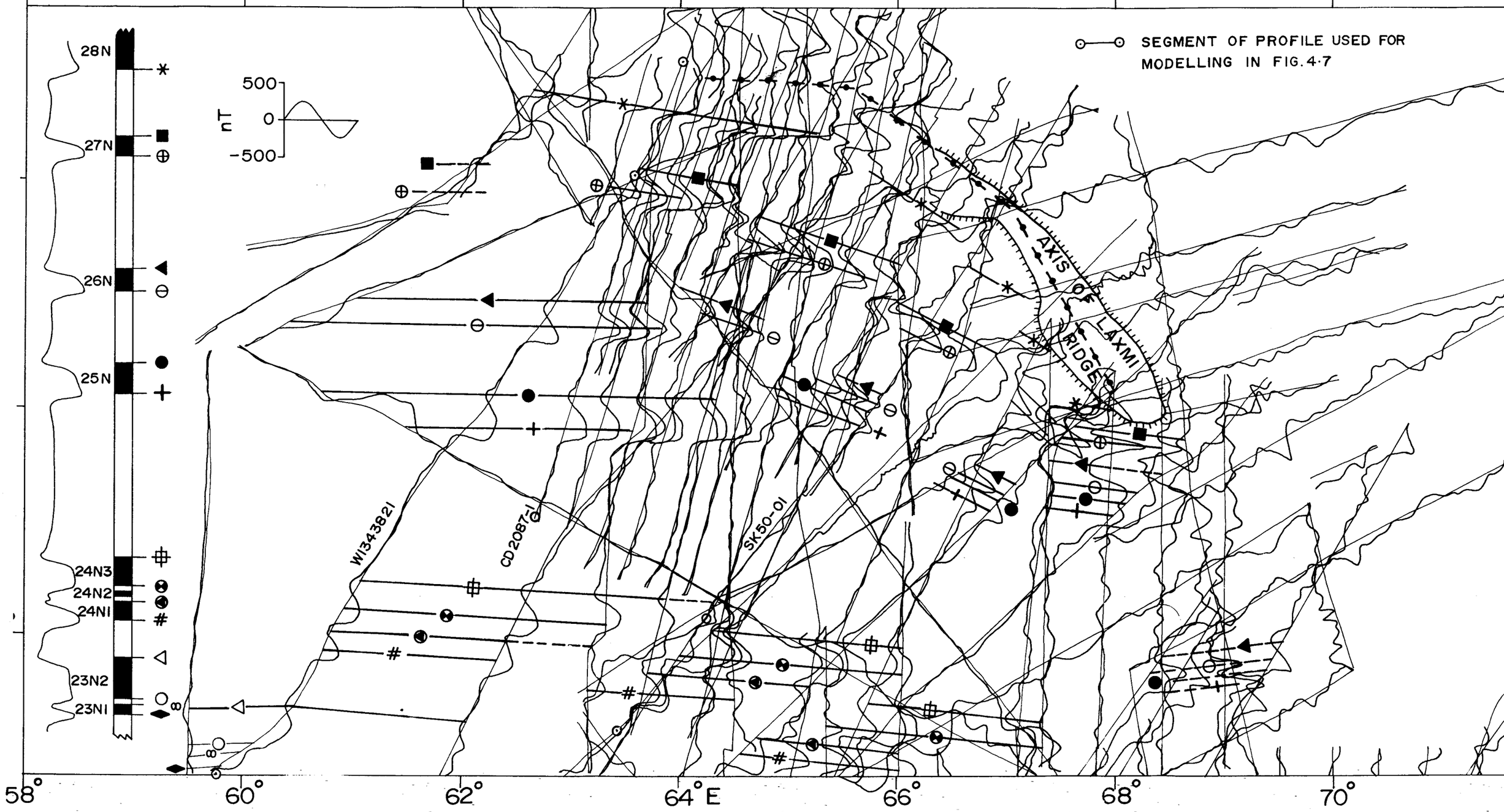

Figure 4.8 Pre-anomaly 24 lineations in the Western Arabian Basin. Magnetic anomalies are plotted perpendicular to the ship's tracks. The trend and extension of magnetic lineations are defined by younger and older boundaries of the normally magnetized blocks, and are shown by solid lines with symbols corresponding with the appropriate magnetized block of the synthetic profiles. Dashed lines represent inferred extension of magnetic lineations. Left: synthetic magnetic profile computed for a ridge striking N75°W at latitude of 10°S and now observed at 13°N, 65°E. Normally magnetized blocks are indicated by solid black. Magnetized layer (susceptibility 0.01 cgs units) is flat, 2.0 km thick with its top at 5.5 km below the sea surface. Magnetic anomaly identifications are according to the geomagnetic polarity reversal time scale and polarity chron nomenclature proposed by Cande and Kent (1995). Only those tracks which have been used in the Figure 4.7 are labeled here.

confidently this set of lineations.

It may also be noted that the identification of NW-SE trending central set of lineations 26N-25N differs from Miles and Roest (1993). With available additional data, it was possible to map them more precisely and identifying the trend in the study area. The 26N and 25N are identified as the prominent lineations occurring between the confidently identifiable lineations 24N3 and 27N (Figure 4.8). It is noticed that the amplitude of anomalies 26N and 25N east of 65°E is relatively less as compared to the areas in the west. Further, the width of the eastern and central set of lineations 28N-25N in general and 26N-25N in particular is distinctly less compared to the width of the E-W trending western set of same lineations. It is also observed that in the western part of the WAB area the offsets in the magnetic lineations are distinctly oblique, whereas in the eastern part of this area such offsets are not discernible (Figure 4.8).

4.5.2.2 *POST - ANOMALY 25 LINEATIONS IN THE WESTERN ARABIAN BASIN*

The post-anomaly 25 lineations of the southern part of the WAB are characterized by the presence of numerous relatively closely spaced magnetic anomalies. Possibly, due to this situation and the paucity of data, the seafloor spreading magnetic anomalies remained sparsely mapped in all earlier studies in this area. In the present study, the fine scale structure of the anomalies 24 and 23 are used as key indicators to establish identifications of magnetic anomalies on observed profiles. Using the diagnostic shapes of anomalies 23 and 24 including tiny wiggle within anomalies 24, anomalies 24N3 through 18N1 are identified in many profiles (Figure 4.9). However, it is observed that it is rare to get the entire normal and reverse sub-chron sequences of anomalies 24 through 18 on every profile. Most of the profiles depict only a portion of this sequence and in places it is difficult to identify them due to presence of additional normal events. In such areas, identifications are extended by inter-profile correlation of anomalies which are obvious, and demarcated the appropriate edge of the magnetized block even when the magnetic signature of only one of the edges of the block are identifiable. It is

Figure 4.9 Post-anomaly 25 lineations in the Western Arabian Basin. Magnetic lineations are plotted perpendicular to the ship's tracks. The trend and extension of the magnetic lineations are defined by younger and older boundaries of the normally magnetized blocks, and are shown by solid lines with symbols corresponding with the appropriate magnetized block of the synthetic profiles. Dashed lines represents inferred extension of magnetic lineations. Left: synthetic magnetic anomaly profile computed for a ridge striking N75°W at latitude of 10°S and now observed at 13°N, 65°E. Normally magnetized blocks are indicated by solid black. Magnetized layer (susceptibility 0.01 cgs units) is flat, 2.0 km thick with its top at 5.5 km below the sea surface. Magnetic anomaly identifications are according to the geomagnetic polarity reversal time scale and polarity chron nomenclature proposed by Cande and Kent (1995). Thick dashed line represents Fracture Zones (FZ). Only those tracks which have been used in the Figure 4.7 are labeled here.

°E 60° 62° 64° 66° 68° 70° 72°

14° 12° 10° N 8° 6°

500
0
-500

24N3
24N2
24N1
23N2
23N1
22N
21N
20N
19N1
18N1

221

220

DSDP23GC

ANT-02

ANT-01

FZ

SEGMENT OF PROFILE USED FOR MODELLING IN FIG. 4·7

interesting to observe that the offsets in the post-anomaly 25 lineations are oblique similar to pre-anomaly 25 lineations.

4.5.3 VALIDATION OF IDENTIFIED MAGNETIC ANOMALIES IN THE WESTERN ARABIAN BASIN

In the Arabian Sea, DSDP23GC is the only profile which passes through DSDP Site 221 and also intersects many of the magnetic lineations of this area. Therefore, this profile is used to validate the anomaly identifications. However, earlier workers were not unanimous regarding the identification of the two prominent anomalies which lie immediate north and south of DSDP site 221. The anomaly immediately north of this site was identified as anomaly 20 by Whitmarsh (1974) based on the Middle Eocene age of the oldest sediment (46 m.y.) overlying the basement at this site and the geomagnetic polarity reversal time scale proposed by Heirtzler et al. (1968). Schlich (1975) has identified it as anomaly A22. His identification of this anomaly was however based on comparable characteristic shapes of the anomalies 24 and 23 observed in the Crozet and Madagascar basins and the anomalies on DSDP23GC profile. Naini and Talwani (1982) apparently considered these anomalies as isolated ones and did not assign any identification to them. Based on additional profiles, it is observed that the two prominent anomalies located immediate north and south of Site 221 on profile DSDP23GC, are not isolated ones but are confidently correlatable from one to other. These anomalies are parallel to other lineations in this area and occur immediately next to and south of the anomaly 23 identified in the present study. Therefore, they have been identified as anomalies 22N and 21N (Figure 4.9).

The identified magnetic anomalies show that the location of DSDP Site 221 falls on the reversely magnetized oceanic crust between anomalies 22N and 21N. The corresponding magnetic age of this reversely magnetized crust is about 48 m.y. according to the recent magnetic polarity reversal time scale (Cande and Kent, 1995). This age is closely comparable to the 46 m.y. micropaleontological age (Whitmarsh, 1974) of the oldest sediment overlying the basaltic crust at Site 221. It is further noted (Table 4.4) that at this site the depth to the basement predicted from the cooling plate

Table 4.4 Comaprision of observed and predicted basement depths at DSDP Site 221.

Observed basement depth (dc1) after sediment load correction.	4828 m
Basement depth (dc2) predicted by cooling plate model.	4779 m

1) $dc1 = dw + ts\{(\rho s - \rho m)/(\rho w - \rho m)\}$ after Crough (1983).

Where, water depth (dw) = 4650 m, sediment thickness (ts) = 270 m, and average sediment density (ρs) = 1.8 g/cm^3 are from DSDP Site 221 after Whitmarsh et al. (1974). Water density (ρw) = 1.03 g/cm^3, and mantle density (ρm) = 3.3 g/cm^3 are assumed.

2) $dc2 = 2700 + 300\ (t)^{1/2}$ after Hays (1988)

Where, t = 48 m.y. age of the oceanic crust inferred from the present study.

model (Parson and Sclater, 1977) agrees well with the depth to the basement (after sediment load correction) determined from drill well results. This age and crustal depths compatibility, further strengthens the validity of the updated magnetic anomaly identifications (i.e. anomalies 22N and 21N) proposed in this study. Using the identification as constraints, the anomalies 28N through 18N1 are identified and thus able to validate their correlation on several profiles (Figures 4.8 and 4.9).

4.5.4 IDENTIFICATION OF YOUNGER ANOMALIES ACROSS THE CARLSBERG RIDGE

The magnetic anomalies observed on two regional profiles SK50-01 and SK50-03 can be broadly grouped into three zones. They are: i) a zone of relative high frequency short wavelength anomalies, observed over the axial part of the Carlsberg Ridge, ii) a zone of large distinctive anomalies observed towards both extremities on the profiles, and iii) the relative magnetic quite zone observed between the above two zones (Figure 4.10). Further, the bathymetric and magnetic profiles across the ridge show a large negative central magnetic anomaly (~500 nT) associated with the prominent bathymetric depression of the median valley (Figure 4.10). Correlation between profiles SK50-01 and SK50-03 suggests that the central anomaly and median valley have a N30°W trend, which is quite different from the reported general trend (N50°W) of the Carlsberg Ridge in the area (McKenzie and Sclater, 1971). However, after careful examination of the adjacent VEMA and OWEN profiles, it is observed that the axial anomalies in this area do indeed trend nearly N50°W and that a persistent right lateral offset must be present between profiles SK50-01 and SK50-03 (Figure 4.11). To accommodate this offset pattern, a fracture zone is postulated. The fracture zone offsets the entire younger sequence of anomalies.

For the purpose of identification of anomalies, synthetic magnetic profile is generated for a ridge striking $N50^0W$ at 7^0N (Figure 4.12). In this area, anomaly 5 is well developed and is easily identifiable. With the help of the synthetic anomaly profile and identifications proposed by previous workers, in addition to the large axial anomaly

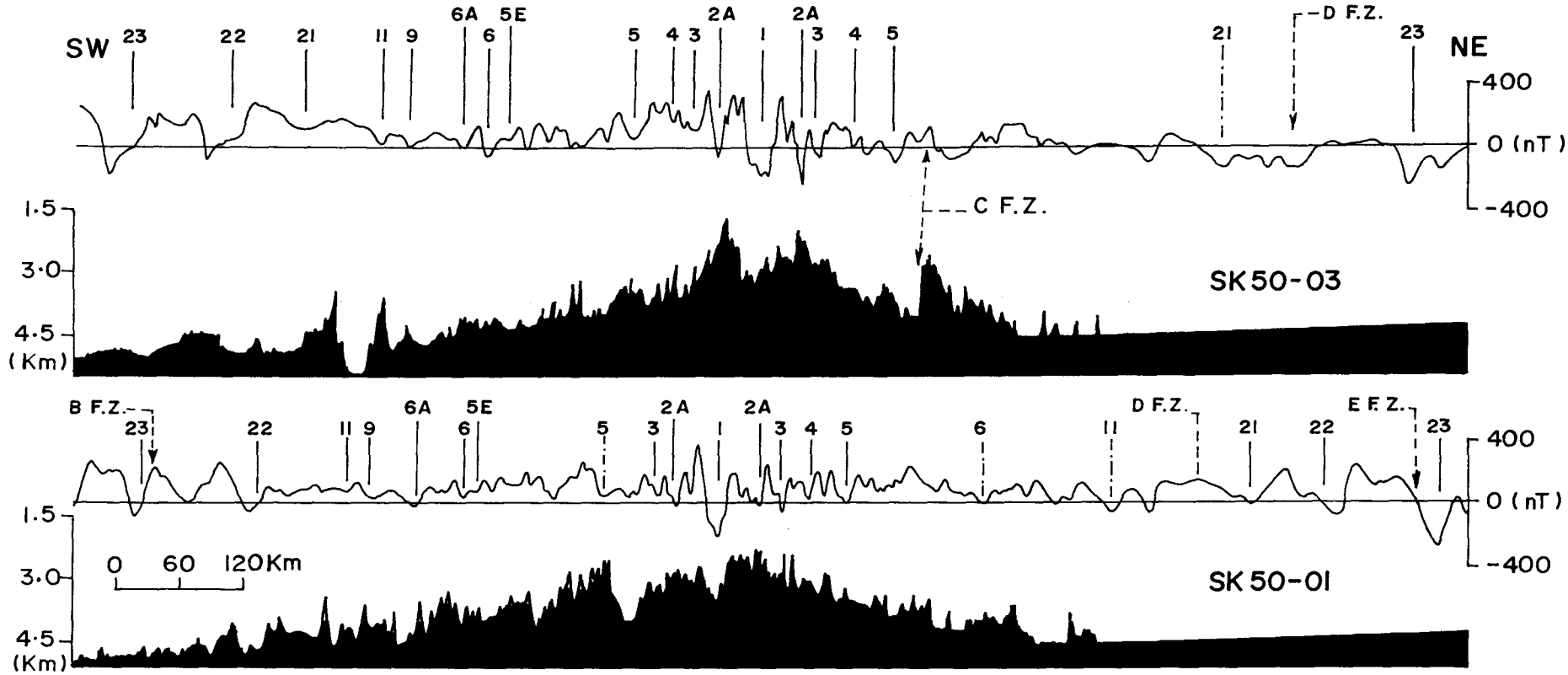

Figure 4.10 Stacked bathymetric and magnetic anomaly profiles across the Carlsberg Ridge. Observed profiles are stacked with respect to an arbitrary reference line A-B. Fracture Zones (FZ): B, D and E (previous studies), C (present study).

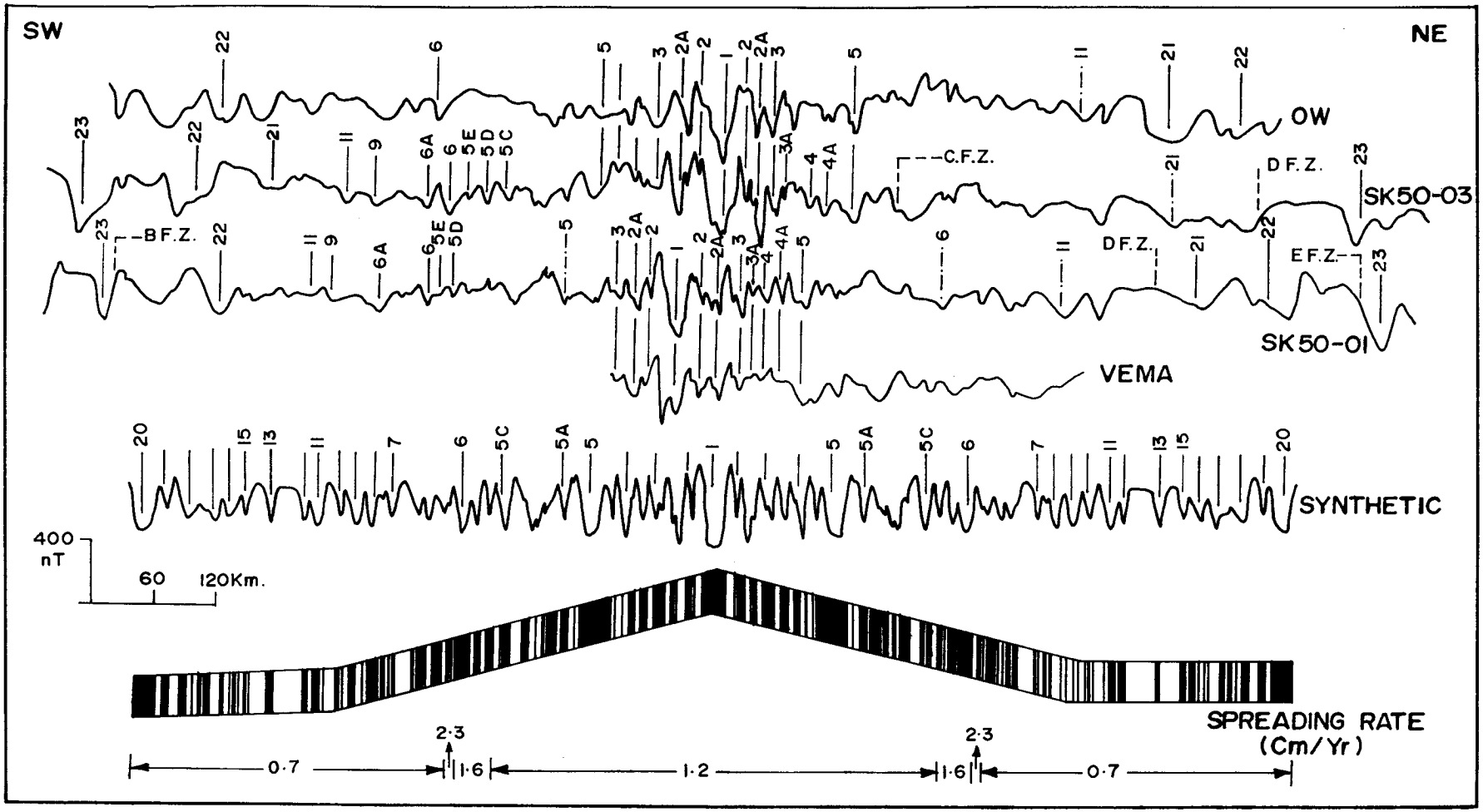

Figure 4.11 Magnetic anomalies across the Carlsberg Ridge, plotted perpendicular to the survey tracks. Fracture Zones (FZ): B, D and E (previous studies), C (present study). A-B represents an arbitrary reference line used for stacking. Dashed-dotted lines represent questionable identifications.

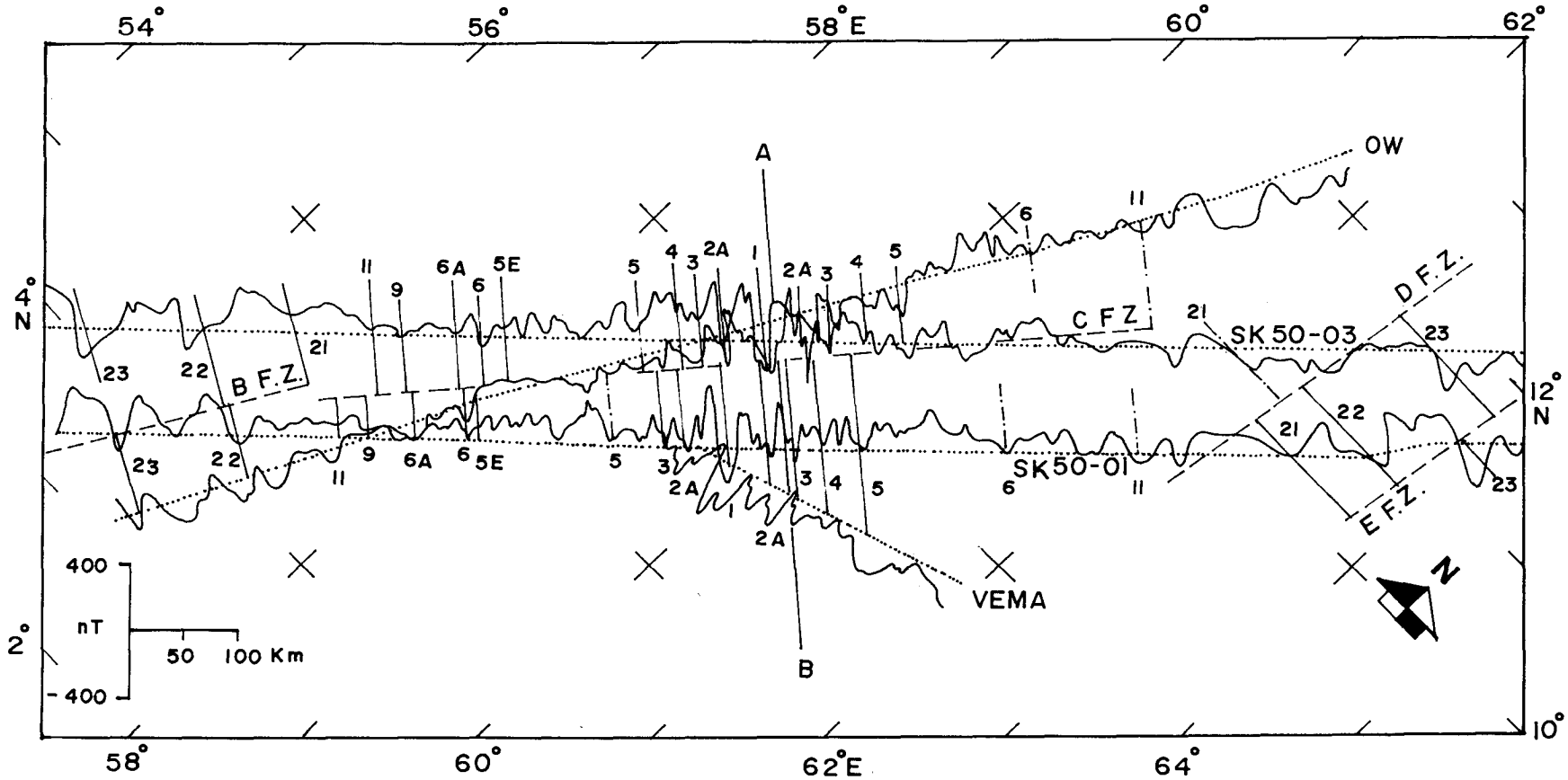

Figure 4.12 Synthetic and observed magnetic anomalies across the Carlsberg Ridge. Observed profiles are projected at an azimuth of 040°. Synthetic profile is generated for a ridge striking N50°W at 7°N with variable spreading rate. Magnetic anomaly identifications are according to the reversal time scale of Berggren et al. (1985). Fracture Zones (FZ): B, D and E (previous studies), C (present study).

1, anomalies 2, 2A, 3, 3A, 4, 4A, 5, 5C, 5D, 5E, 6 and 6A are identified. The best fit between the synthetic anomaly and the observed anomalies indicates a variable half spreading rates, i.e. 1.2 cm/yr between anomalies 1 and 5C, 1.6 cm/yr between anomalies 5C and 6, 2.3 cm/yr between anomalies 6 and 6A, and 0.7 cm/yr beyond anomaly 6A. Up to anomaly 5, the spreading rate estimated in this study remain the same as that reported by McKenzie and Scatter (1971). However an increase in the spreading rate between anomalies 5C and 6A is also discernible. Beyond anomaly 6A, the anomalies are of low amplitude and difficult to identify. However, a careful comparison between the observed anomalies and the synthetic anomalies (Figure 4.13) reveals a few pre-anomaly 6A lineations which are also parallel to the present day spreading axis. The anomaly segments corresponding to these lineations show very good correlation and match well with the synthetic anomalies (Figures 4.11 and 4.13) generated between 6A and 11, at half spreading rate (0.7 cm/yr). Anomalies 6, 9 and 11 are identified confidently on the southwestern flank of the Carlsberg Ridge, whereas, identification of these anomalies on the northeastern flank of the ridge are tentative. The identification of anomalies between 21 and 11 on both the flanks of the ridge are difficult due to quite nature of observed magnetic anomalies.

As mentioned earlier, a fracture zone offsetting the axial magnetic anomalies is postulated. It can be seen that this fracture zone offsets the anomalies up to chron 11 on both the flanks of the Carlsberg Ridge. This right lateral offset is of the order of 50 km and the length of the fracture zone is about 720 km. The presence of a prominent bathymetric scarp (Figure 4.10) immediately after anomaly 5 on profile SK50-03 (northeastern limb) indicates the location where the profile crosses a fracture zone.

4.6 NEW CONSTRAINTS FOR SPREADING HISTORY OF THE ARABIAN SEA

Identification of magnetic anomalies in the Western Arabian Basin and across the Carlsberg Ridge provides new constraints on the seafloor spreading history of the Arabian Sea. As mentioned earlier, identification of oldest anomalies in the Western Arabian Basin and its conjugate Eastern Somali Basin could not be conclusively

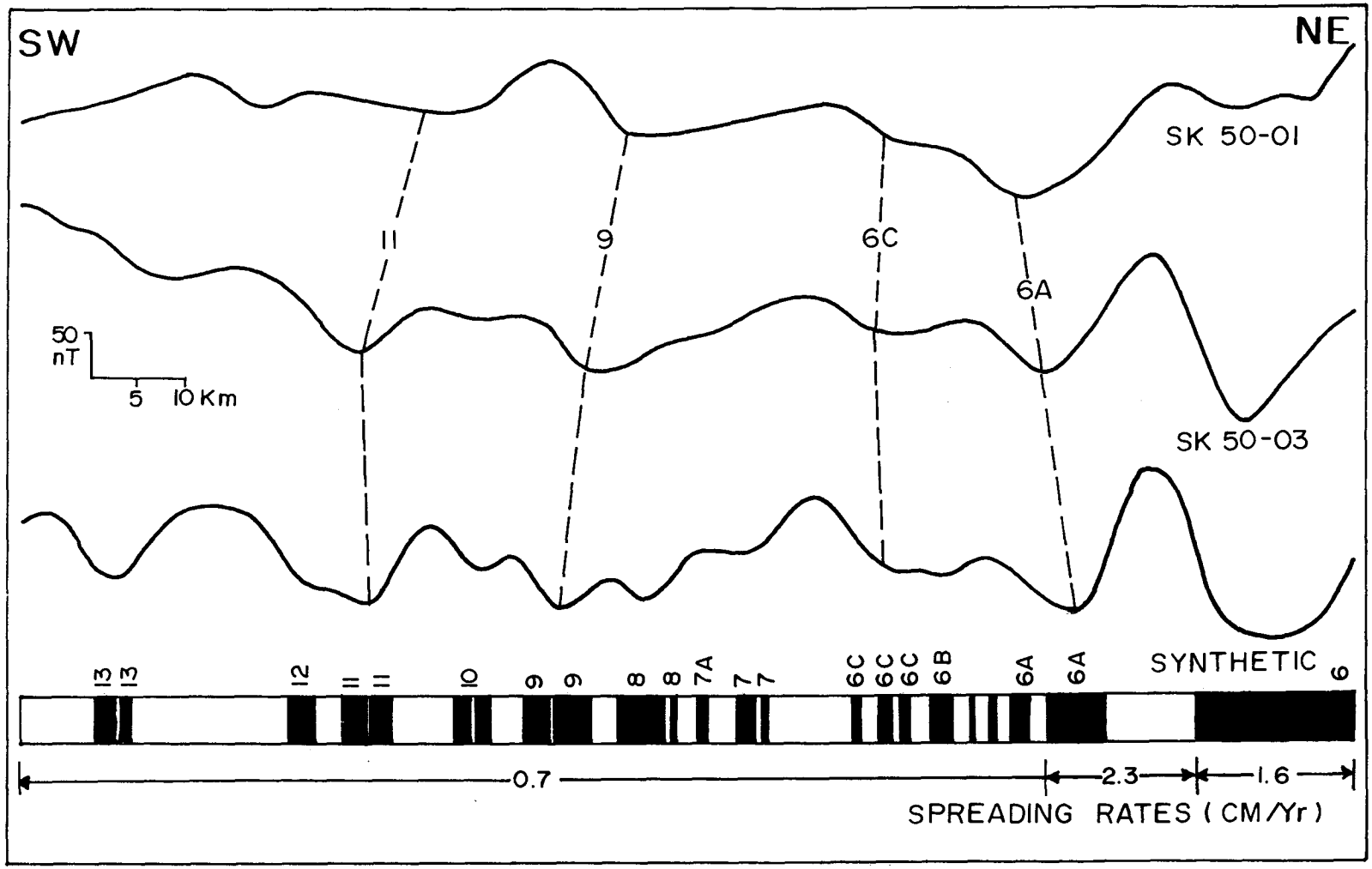

Figure 4.13 Observed post-anomaly 6 segment of profile on the southwestern flank of the Carlsberg Ridge and corresponding synthetic anomaly to demonstrate the identification of magnetic anomalies 11 through 6A. Parameters for synthetic profile computations are as in Figure 4.11.

identified by earlier workers. The identification of magnetic anomalies presented in this studies suggest that anomaly 28N is the oldest anomaly in this basin. It is therefore inferred that the spreading episode which was responsible for the creation of the Western Arabian Basin and Eastern Somali Basin commenced at anomaly 28N(~63 Ma).

As discussed earlier, anomaly 21N is confidently identified in both Western Arabian Basin and Eastern Somali Basin on the regional profiles SK50-01 and SK50-03. Immediately after anomaly 21N, a magnetic quiet zone is present. However, anomaly 18N is also identified in the eastern part of the WAB. In view of the above, it appears that the magnetic quiet zone starts at anomaly 18N. This magnetic quiet zone in the Arabian Sea is considered to represent a period when spreading either completely ceased or was reduced to an imperceptible rate. It is therefore concluded that anomaly 18N (~39 Ma) mark the end of the older phase of spreading in the Arabian Sea. Further, gradual drop in half spreading rate from 5.5 cm/yr at anomaly 23 to 1.0 cm/yr at anomaly 18N is observed. Lowering of spreading rate during the same period was also observed along the Central and Southeast Indian Ridges (Patriat and Segoufin, 1988). Following Patriat and Achache (1984), this decrease in the spreading rate is likely to be associated with the closure of the Neotethys to north of the India and, thus, indicate the onset of the soft collision of India with the southern margin of Eurasia.

The magnetic quiet zone mentioned earlier starts after anomaly 18N and terminates against a lineation parallel to the present day spreading axis which is identified in this study as anomaly 11N. This suggests that the younger phase of the spreading in the Arabian Sea in its present geometry commenced just before anomaly 11N (~30 Ma). Elsewhere, in the Indian Ocean anomaly 18 was mapped extensively and considered to mark the time when this ocean began to assume its modern aspect. The absence of anomalies between 18N and 11N indicates that the younger phase of spreading in the Arabian Sea commenced much later, i.e. shortly before anomaly 11N. Further, the hiatus in spreading in the Arabian Sea was for only 9 m.y. (i.e. between anomalies 18N and 11N) which is much shorter than previously believed.

CHAPTER 5

CHAPTER 5

PALEO-PROPAGATING RIDGES IN THE WESTERN ARABIAN BASIN

5.1 INTRODUCTION

The most convincing evidences for seafloor spreading, continental drift and plate tectonics come from the configuration of linear magnetic anomalies of the oceans. For the first time, existence of linear magnetic stripes of the seafloor (Mason and Raff, 1961; Raff and Mason, 1961) have been identified from marine magnetic investigations of the north-west coast of the America. Vine and Matthews (1963) have proposed a model to explain the origin of these stripes. According to the model, the alternate stripes of positive and negative magnetic anomalies are caused by ocean floor spreading and reversals of the Earth's magnetic field. This was one of the most important early attempt towards development of the rigid-plate hypothesis. Later, Vine and Wilson (1965), Wilson (1965) and Vine (1966) have shown that i) these anomalies are symmetrical and could be correlated with similar anomalies throughout the world ocean as well as with the geomagnetic reversal time scale, and ii) the anomalies are offset along transform faults and their fossil traces known as fracture zones (Figure 5.1). This pattern was constructed assuming that the transform offset was inherited from the original configuration of the spreading ridge boundary and the ridge consists of impenetrable end points for the two ridge segments which abut against the offset. The simple pattern of geometry of ridge segments and transform offset (Figure 5.1) has led to the development of the concept of seafloor spreading and plate tectonics, and has provided a useful model to explain the gross configurations of seafloor features and plate motions. In the late seventies and early eighties, deviations to this model have increasingly been proposed in the Atlantic and Pacific Oceans where adequate data were available for reinterpretation. The existence of several major seafloor lineations that are oblique to both relative and absolute plate motions have been observed. These observations

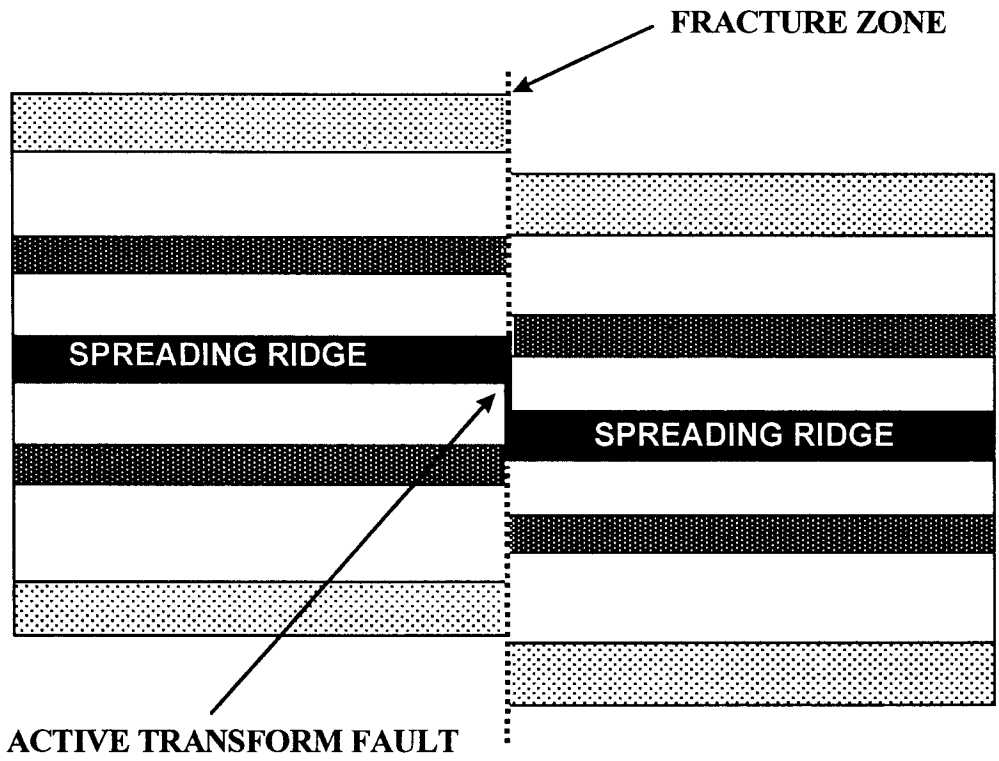

Figure 5.1 Magnetic stripe pattern generated by seafloor spreading at a stable spreading ridge-transform fault system. Alternate shaded and white blocks indicate normal and reversed magnetized stripes.

enabled the study of new aspects of seafloor spreading processes beyond the simplified model of ridge segments and transform faults. Previous workers have interpreted the oblique anomaly offsets as a result of faulting either due to plate non-rigidity or due to relative motions of several microplates (Raff and Mason, 1961; Vine, 1968; Elvers et al., 1973; Carlson, 1976; Farrar and Dixon, 1980). However, they could not satisfactorily explain the observations within the framework of plate tectonic theory, which became much more evident with the addition of magnetic profiles world wide. This necessitated development of new models to explain the oblique offsets and other complexities associated with magnetic lineations that seemed incompatible with plate tectonic theory. Finally, Shih and Molnar (1975) and Hey (1977) have proposed the propagating rift hypothesis to explain the oblique offsets in magnetic anomaly pattern and other lineaments that are oblique to both relative and absolute plate motions.

As mentioned in Chapter 4, the magnetic lineations in the Western Arabian Basin (WAB) exhibit offsets at many places. In all earlier studies, such offsets have been interpreted in terms of fracture zones orthogonal to the magnetic lineations. The existence, trend and extent of the fracture zones proposed earlier are somewhat speculative and poorly constrained. The magnetic lineations mapped in the present study, interestingly, do not support the existence of such orthogonal fracture zones at most places. Instead, it depicts oblique offsets. Several magnetic anomaly profiles commonly show closely or far apart spacing of magnetic lineations compared to predicted symmetrical pattern indicating missing or extra crust. Further, it is strongly suspected that the then nearby Reunion hotspot had a thermal influence on the accretion process of the Early Tertiary oceanic crust of the WAB. As a result, the magnetic anomaly pattern in the WAB is much more complex than believed so far.

In this chapter, it is shown that i) the WAB contains several paleo-propagating ridges similar to those observed in other oceans of the world, ii) a combination of seafloor spreading and ridge propagation offer a simple and convincing explanation for most of the complex magnetic anomaly pattern observed in this area, and iii) accretionary process of the Early Tertiary oceanic crust of the WAB is influenced by the

propagating ridges and the then nearby Reunion hotspot. A brief summary of the propagating rift hypothesis is presented in the following section.

5.2 THE PROPAGATING RIFT HYPOTHESIS

Shih and Molnar (1975) and Hey (1977) independently proposed the propagating rift hypothesis as a mechanism of producing oblique termination of magnetic lineations. According to the hypothesis, propagation progressively occurs when a lithospheric plate breaks and a new spreading center forms. The term propagating rift means non-instantaneous rifting and is considered synonymous with progressive or asynchronous rifting. Propagating rifts are extensional plate boundaries that progressively break through rigid lithosphere. If the rifting advances to the seafloor spreading stage, propagating seafloor spreading centers follow behind, gradually extending through the rifted lithosphere. A propagating rift occurs when one segment of a spreading center at a ridge-transform-ridge plate boundary grows at the expense of the other and the transform fault migrates along the ridge axis.

Although the conceptual mechanism appears to be simple, this hypothesis has significant implications for both large and fine scale plate tectonic evolution. It explains i) the existence of many seafloor and continental margin lineaments that are oblique to both relative and absolute plate motion which previously seemed incompatible with plate tectonic theory (Hey et al., 1980), ii) why some continental margins are not parallel to seafloor isochrons (Vink, 1982) and, iii) the large scale reorganization of some seafloor spreading system as well as formation of some transient microplates. For further discussion on the subject, the terms ridge propagation/propagating ridge/propagator are used in this study to infer propagating seafloor spreading center to distinguish from the propagating tectonic rifting.

The rift propagation has been explained with the three basic variations of propagating spreading center geometry and is shown in Figures 5.2 and 5.3. Figure 5.2 explains a "discontinuous propagation model" proposed by Hey (1977). In this model at

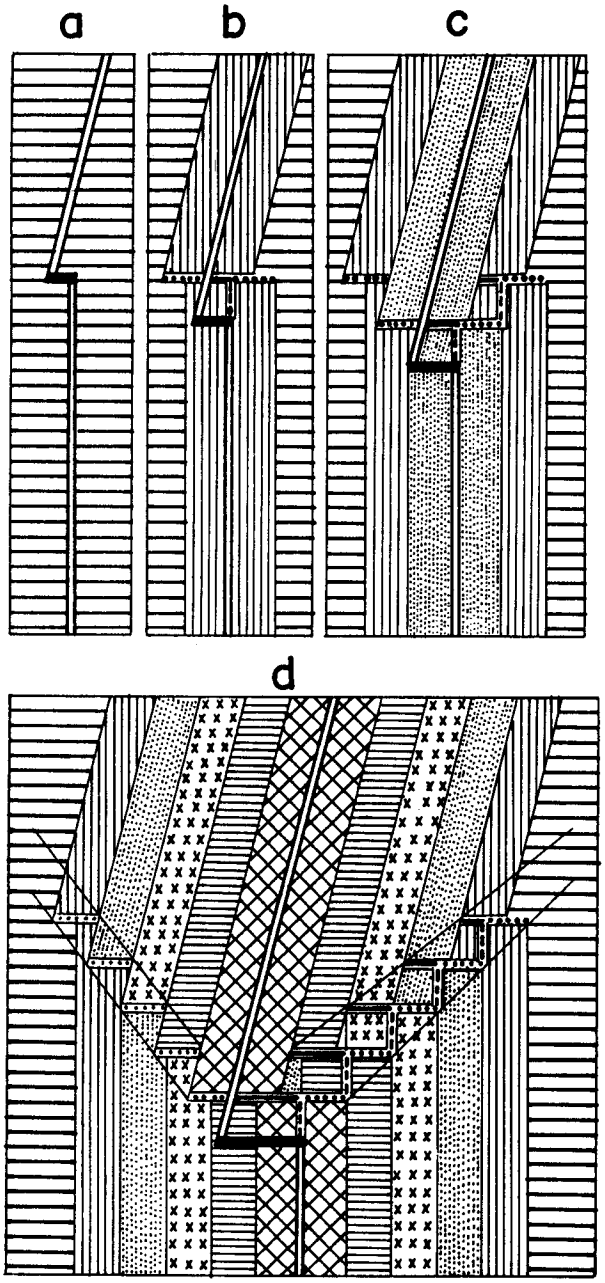

Figure 5.2 Schematic diagram showing step wise evolution of propagating rift (after Hey, 1977). (a) The initial situation where two spreading center segments, trending in slightly different directions, offset by a transform fault; (b,c) The new rift extends instantaneously for a short distance, then spreads symmetrically for a while, then extends instantaneously for another short distance. This process occurs in a systematic fashion; (d) The V-pattern of en-echelon fossil spreading centers and fracture zones formation due to propagation. Double lines are active spreading centers. Isochrons are stippled. Thick lines connecting double lines are active transform faults. Dashed lines are fossil spreading centers. Thin lines are fossil transform faults created by propagating rift. Dotted lines are fracture zones that are inactive extensions of these fossil transform faults.

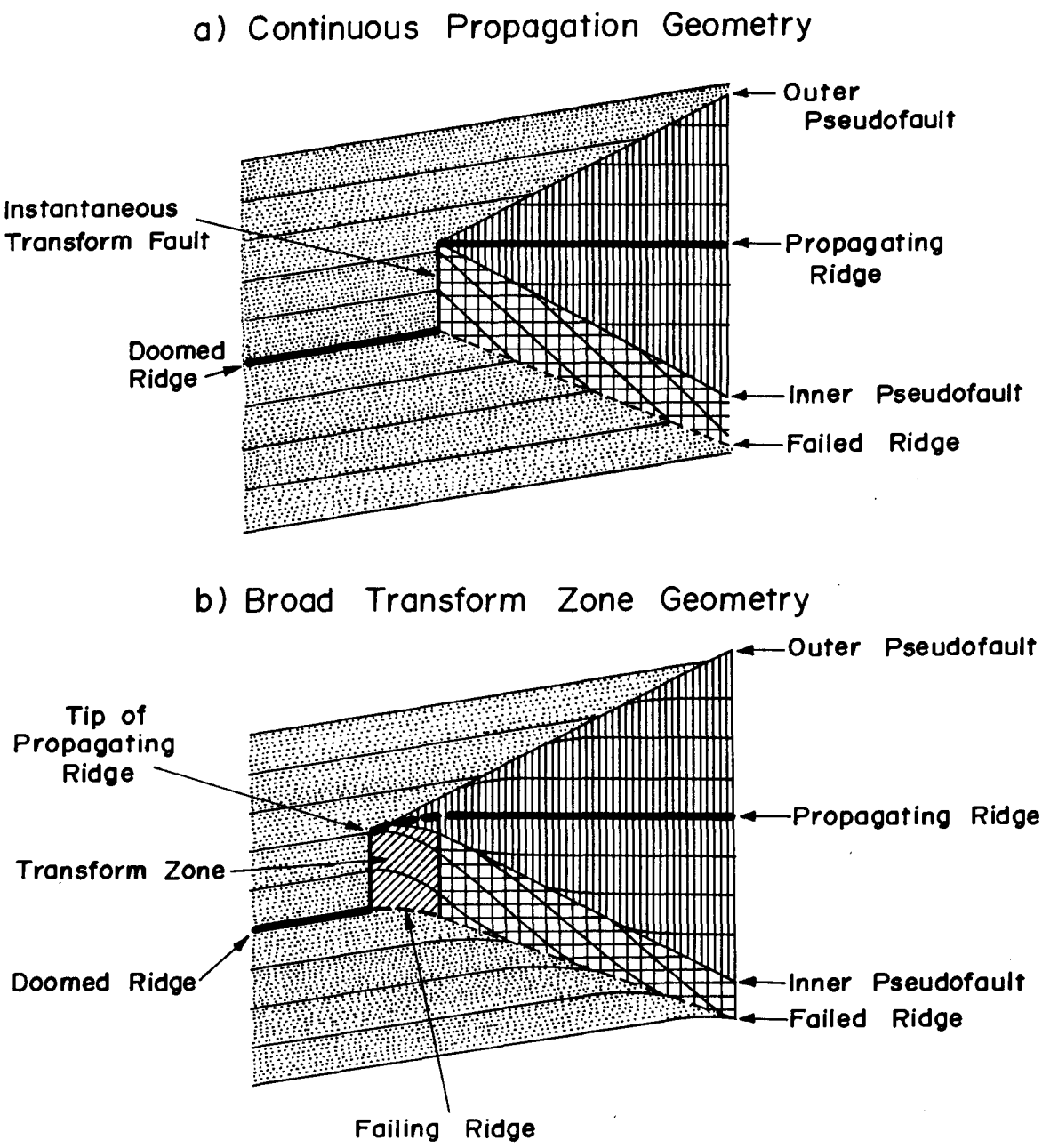

Figure 5.3 (a) Continuous, and (b) broad transform zone propagating ridge model. Propagating ridge lithosphere is marked by vertical lines, normal lithosphere created at the doomed ridge is indicated by dots and transferred lithosphere is crossed hatched. Area covered by oblique lines between propagating and receding (doomed) ridges in (b) represent transform zone.

regular intervals, the left spreading ridge propagates downward, takes over the spreading for a new length of ridge and establishes a transform fault at its tip. In other words this scenario emerges as a result of a sequence of spreading center jump, propagating along the spreading center and is connected to the old (dying) spreading center by a new transform fault. As a result, the former transform fault becomes inactive (fossilized)) and is added to one of the plates along with a segment of the old (extinct) spreading center. The amount of propagation down the axis of the spreading is related to the length of the extinct part of the ridge. As this process is repeated, the new spreading center grows in length and the old one shrinks. The length of the isochrons changes accordingly. Fossilized transform faults and spreading centers are consistently added to the same plate, resulting in asymmetric accretion to the plate. This process produces an en-echelon failed ridge segment, fossil transform faults and fracture zones frozen into progressively younger lithosphere.

A second model known as "continuous propagation model" was subsequently suggested by Hey et al. (1980) where spreading ridge propagates continuously. Figure 5.3a shows the pattern of lithospheric blocks and tectonic elements produced when propagation, rift failure and lithosphere transfer are all continuous and simultaneous. In this model, a transform fault migrates continuously with the propagator tip and thus pseudofaults are formed instead of fracture zones because the transform fault would only exist instantaneously at one place. This idealised geometry assumes an instantaneous transfer of lithosphere. The orientation of isochrons and crustal structures in the zone of transferred lithosphere can be predicted (Hey et al., 1986) from the mathematical description for continuous propagation geometry of Figure 5.4 (Table 5.1). Geologically more plausible continuous propagation model (Hey et al., 1980, 1986; McKenzie, 1986) is shown in Figure 5.3b. In this model, the propagation is continuous, however, some finite time is required for the propagating ridge spreading rate to increase from zero to the full rate and for the rate on the failing ridge to decrease to zero. In this model, instead of a continuously migrating transform fault, there would be a broad transform zone between the propagating and failing spreading ridge axes.

Table 5.1 Mathematical description for continuous propagating ridge geometry as shown in Figure 5.4 (after Hey et al., 1986).

Equations	Constraints
$OFF = PR \mp \theta_o$	
$IPF = PR \pm \theta_i$	
$FR = PR \pm \beta$	
$TL = PR \pm \phi$	
$\theta_o = TAN^{-1} (SV_o/PV)$	$0 < \theta_o < 90$
$\theta_i = TAN^{-1}(SV_i/PV)$	$0 < \theta_i < 90$
$\alpha = PR - DR$	$-90 < \alpha\ 90$
$\beta = TAN^{-1}(TAN\ \theta_i \mp TAN\alpha)$	$-90 < \beta < 90$
$\phi = TAN^{-1}(TAN\ \theta_i + TAN\ \theta_o \mp TAN\ \alpha)$	$-90 < \Phi < 90$

Where, PR: Propagating ridge azimuth, DR: Doomed/receding ridge azimuth, OPF: Outer pseudofault azimuth, IPF: Inner pseudofault azimuth, TL: Transferred lithosphere isochron azimuth, SV: Spreading half rate, PV: Propagation rate, Subscript o and i indicate outer and inner pseudofault respectively. The offset between the propagating and failing ridge is either left or right lateral, which causes sign changes in the equations. The top sign in above equations represent the left-lateral case and bottom sign is for right lateral case.

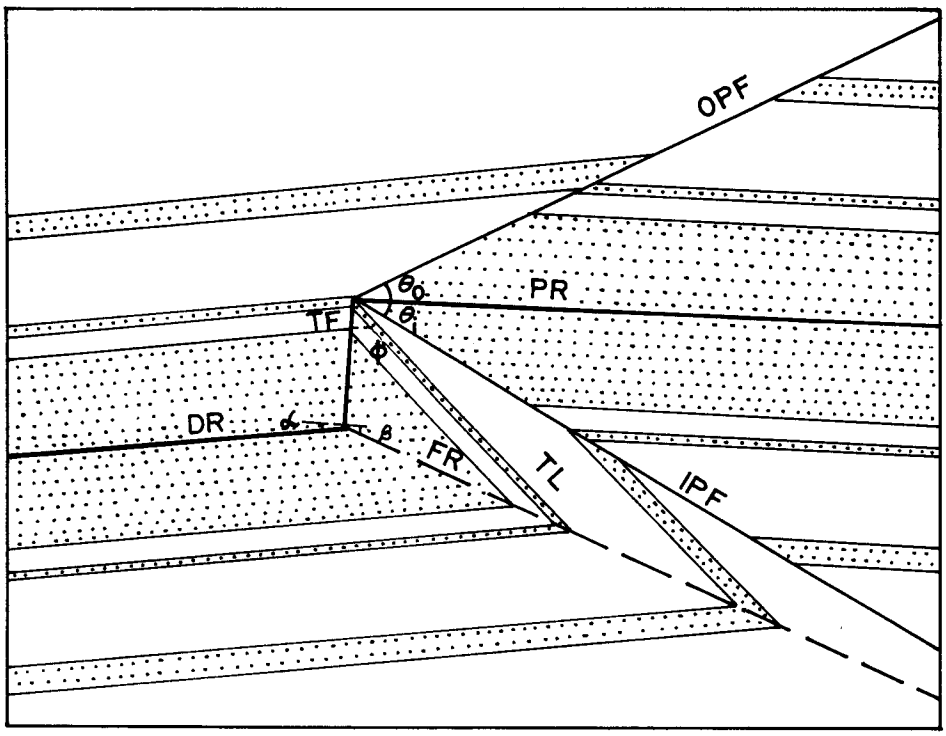

Figure 5.4 Idealized geometry of a continuous propagation showing various parameters used in equations in Table 5.1. Normally magnetized areas are stippled. PR: propagating ridge, OPF: outer pseudofault, IPF: inner pseudofault, DR: doomed ridge, FR: failed ridge (long dashed lines), TL: transferred lithosphere, TF: transform fault.

The propagating rift hypothesis is only a minor modification towards understanding of seafloor spreading. It explains satisfactorily in a simple way many diverse imperfections associated with magnetic anomaly patterns. It also provides a better insight into the processes by which spreading ridge forms and adjusts to changing conditions. The nomenclatures of the various tectonic and lithospheric elements of the propagating ridge system are given in Appendix A.

5.3 IDENTIFICATION OF PALEO-PROPAGATING RIDGES IN THE WESTERN ARABIAN BASIN

As outlined earlier, the magnetic lineations in the WAB exhibit offsets at many places. In the previous studies, these offset patterns were accommodated by invoking the presence of number of fracture zones. However, due to sparse data coverage, the trend and location of these fracture zones were not adequately constrained. Therefore, they were considered as features orthogonal to the general trend of the magnetic lineations of the area. The magnetic lineations mapped in the present study, interestingly, do not support the existence of such orthogonal fracture zones in most of the places. Instead, it depicts obviously recognisable oblique offsets (Figures 5.5a,b). These oblique offsets are clearly discernible between lineations 28N through 25N and 24N3 through 23N1.

The oblique offsets of the magnetic lineations are inferred to be the diagnostic feature of the propagating ridges (Hey, 1977; Hey et al., 1980, 1986; Hey and Wilson, 1982; Auzende et al., 1994; Morgan and Sandwell, 1994). In the north-western WAB area, Miles and Roest (1993) reported presence of two such oblique offsets of the magnetic lineations and proposed a two phased propagating ridge model. The present studies of closely spaced magnetic profiles particularly to the east of the area studied by Miles and Roest (1993) have led to identification of nine more such major oblique offsets within the sequence of lineations 28N-20N and precise location of the two propagators identified by Miles and Roest (1993).

The observed oblique offsets are interpreted as inner pseudofaults of the paleo-

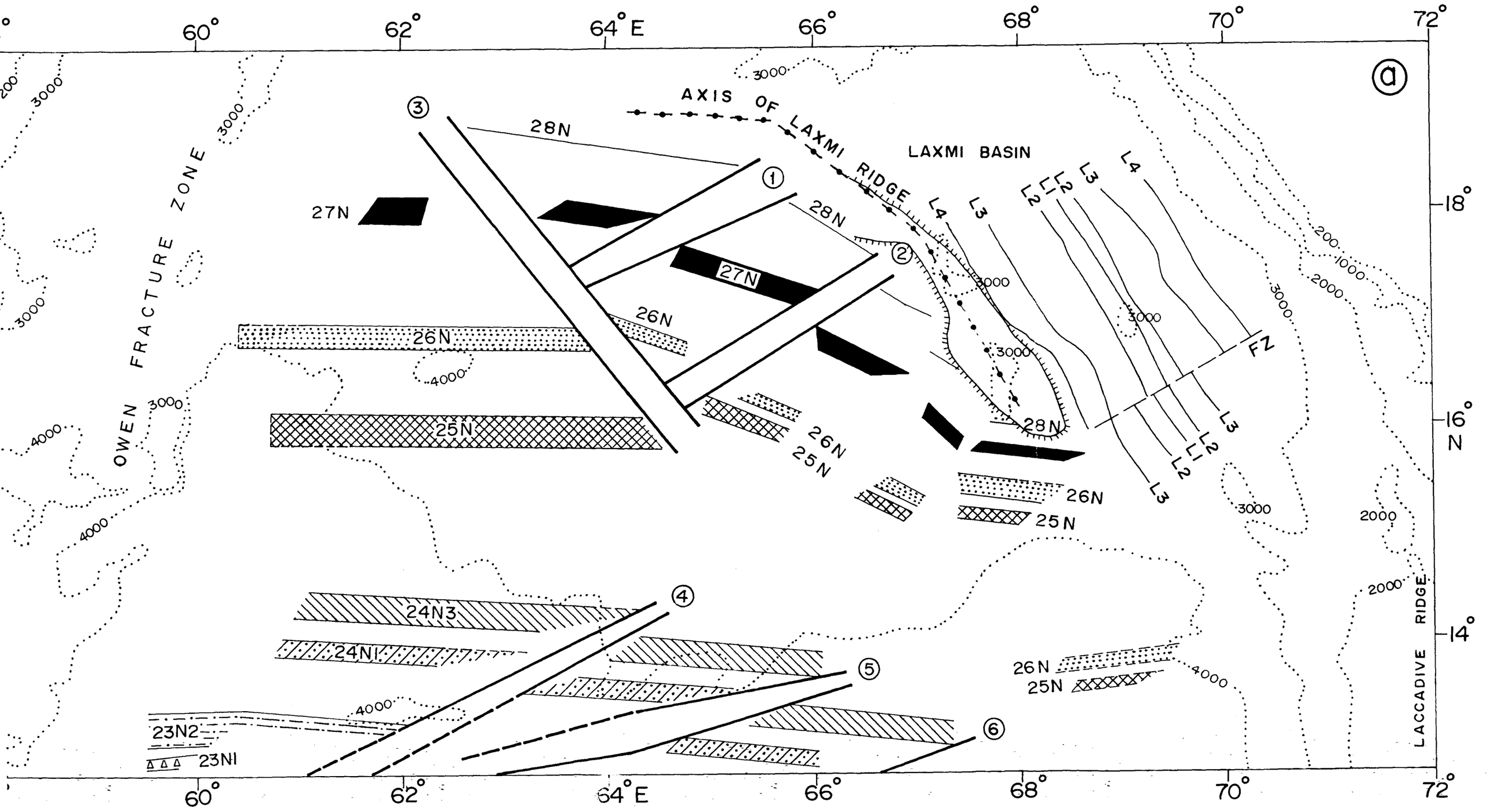

Figure 5.5 (a) Pre-anomaly 25 magnetic lineations and tectonic interpretation in the Western Arabian Basin. Diagonal offsets of magnetic lineations are interpreted pseudofaults. Numbers in circles refer to the propagator which generated the adjacent pseudofault. Dotted lines represent bathymetric contour in meters. L1-L4 and FZ represent Laxmi Basin magnetic lineations and fracture zone respectively.

Figure 5.5 (b) Post-anomaly 25 magnetic lineations and tectonic interpretation in the Western Arabian Basin. Diagonal offsets of magnetic lineations are interpreted pseudofaults. Numbers in circles refer to the propagator which generated the adjacent pseudofault. Dotted lines represent bathymetric contour in meters. FZ: Fracture Zone.

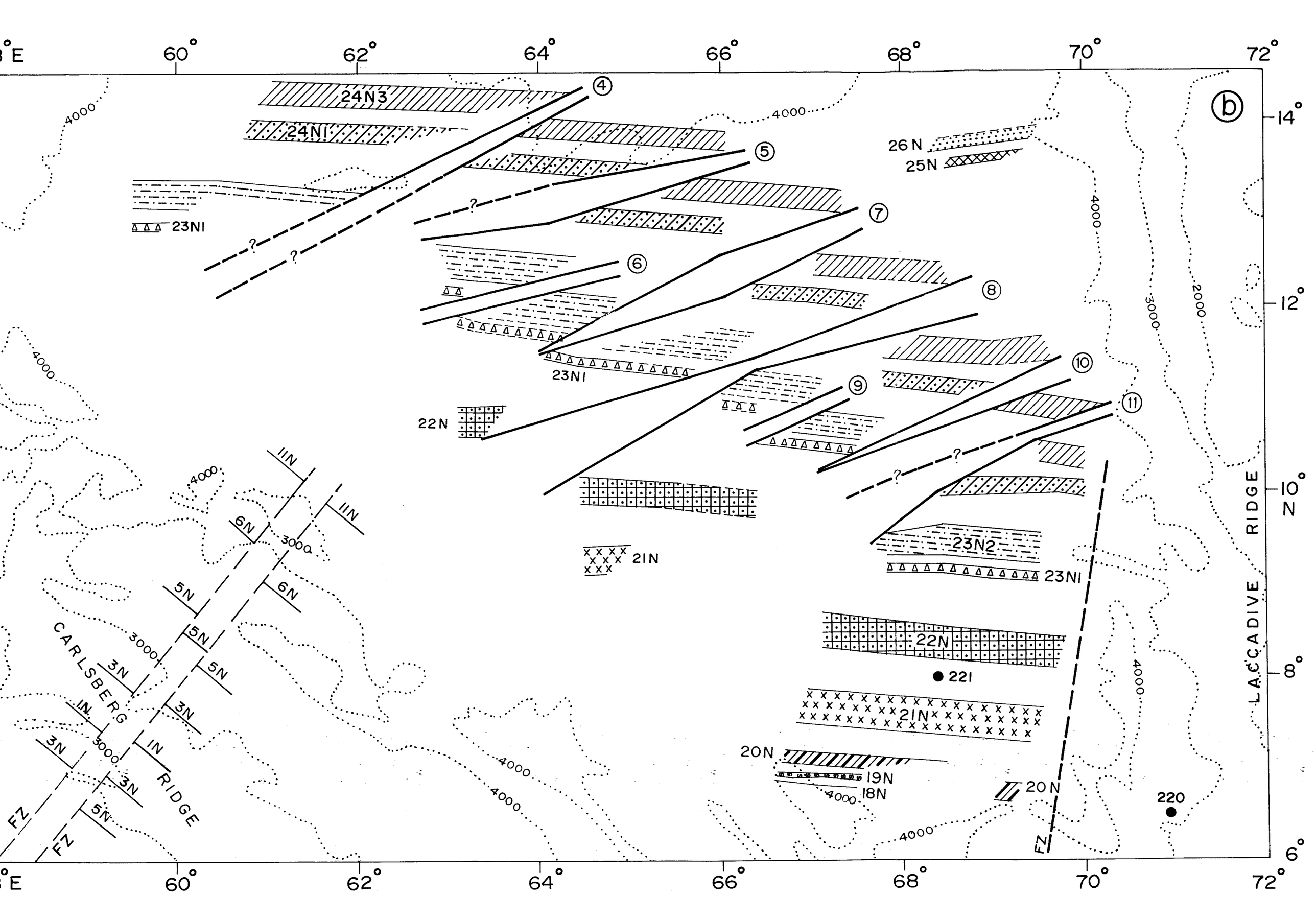
60°
62°
64°
66°
68°
70°
72°
14°
12°
10°
8°
6°
N
E
b
4000
3000
2000
24N3
24N1
23N1
26N
25N
22N
21N
23N2
19N
18N
20N
221
220
IIN
6N
5N
3N
IN
CARLSBERG RIDGE
LACCADIVE RIDGE
FZ

propagating ridges in this area following the propagating ridge model of Hey et al. (1980). It is inferred that inner pseudofault is available in the WAB on the Indian plate of these propagating ridges. While, its conjugate outer pseudofault is expected to be in the conjugate Eastern Somali Basin on the African plate. For reference to the text and figures, the pseudofaults are numbered according to the paleo-propagators (PR) which generated them (Figure 5.5a,b).

5.4 CHARACTERISTICS OF INFERRED PALEO-PROPAGATING RIDGES OF THE WESTERN ARABIAN BASIN

Based on the identification of linear magnetic anomalies and their offset in the WAB, eleven major paleo-propagating ridges have been inferred. The location of these propagators along with tectonic and main structural features of the region are presented in Figure 5.6. Based on analysis of the propagators, their main characteristics are listed in Table 5.2. In the following paragraphs, some salient features of these characteristics in relation to regional tectonics are described to understand the dynamics of ridge propagation in the WAB.

The depth to basement map (Naini, 1980) of the WAB indicates that i) region of deepest basement (~7.0 km) is centred around 15°N, 65°E, and ii) the shallow basement depth (~4 km) occurs along base of the western flank of the Laccadive Ridge and SW flank of the Laxmi Ridge. Overall, the basement depth distribution pattern of the WAB defines i) a conspicuous westward dipping E-W basement trend south of 15°N, and ii) a general southwest-ward dipping basement with NE-SW to ENE-WSW trend southwest of the Laxmi Ridge. It is seen (Figure 5.6, Table 5.2) that ten of the eleven propagators have propagated down the regional basement gradient. Only one propagator (PR-3) has propagated up the regional basement gradient. The correlation between propagation direction and along-axis topographic gradient was first suggested by Hey et al. (1980) and Morgan and Parmentier (1985). Since then, it has been observed in many areas of the world oceans (Table 5.3). As discussed above, the direction of paleo-ridge propagation is well correlatable with regional basement gradient of the WAB. Therefore,

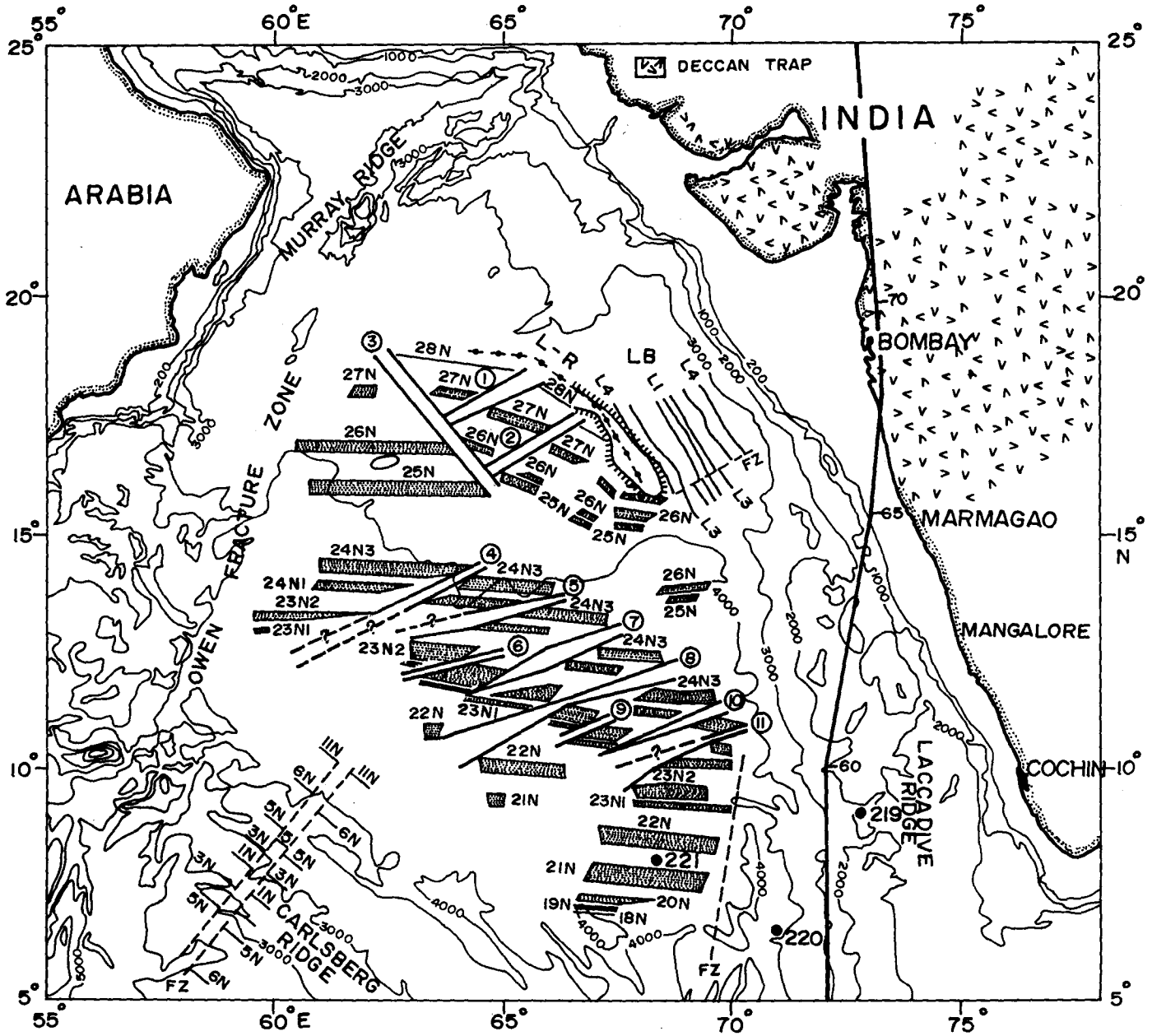

Figure 5.6 Summary map showing identified magnetic lineations, fracture zones and pseudofaults in the study area. Number in circles refer to the propagator which generated the adjacent pseudofault. Bathymetric contours are in meters. L1-L4 and FZ represent Laxmi Basin (LB) magnetic lineations and fracture zone respectively. Solid circle with short thin line represents axis of the Laxmi Ridge (L-R). Location of DSDP Sites (219, 220 and 221) are shown with solid circle. Computer-modeled Reunion hotspot track is shown with thick solid line. Numbers along the hotspot track are predicted ages in Ma (Shipboard Scientific Party, 1988).

Table 5.2 Characteristics of paleo-propagating ridges of the Western Arabian Basin

PR No.	Prop. [1] Dir.	Offset[2]	θ[3]	Vspr[4]	Vprop[5]	Vprop/ Vspr[6]	D/U[7]	Away/Towards[8] hotspot
PR1	288	R-L	52	5.1	3.98	0.39	D	Away
PR2	292	R-L	56	4.8	3.24	0.34	D	Away
PR3	092	L-L	52	4.7	3.67	0.39	U	Towards
PR4	275	R-L	30	6.0	10.39	0.87	D	Away
PR5	275	R-L	22	5.8	14.36	1.24	D	Away
PR6	280	R-L	23	5.5	12.96	1.18	D	Away
PR7	275	R-L	26	5.8	11.89	1.03	D	Away
PR8	274	R-L	22	5.8	14.36	1.24	D	Away
PR9	277	R-L	28	5.5	10.34	0.94	D	Away
PR10	282	R-L	30	6.0	10.39	0.87	D	Away
PR11	272	R-L	25	5.8	12.44	1.07	D	Away

Where superscript used in the table represents:

1 Propagation direction in degree clockwise from north.

2 Offset (R-L: Right Lateral, L-L: Left Lateral).

3 Average angle(θ) in degree between a single propagator wake and ridge axis.

4 Average half spreading Rate (Vspr) in cm/yr.

5 Propagation rate(Vprop) in cm/yr. Vprop= Vspr/Tanθ after Hey et al.(1986).

6 Ratio of propagation rate to full spreading rate.

7 Propagated Down (D) or Up(U) along regional basement gradient.

8 Propagated Away/Towards with respect to computer modelled Reunion hotspot track.

Table 5.3 Compilation of characteristics of some of the propagating ridges in the world oceans

Location of PR[1]	PR Dir.[2]	Offset[3]	Spread. Rate[4]	Propag. Rate[5]	PR/SR[6]	D/U[7]	Nearby Hotspot[8]	Away/Towards hotspot[9]	References[10]
1. Galapagos region (Pacific Ocean)									
i) 2.6°N, 95.6°W	W	R-L	5.8	5.2	0.90	D	Galapagos	Away	Hey et al. (1986)
ii) 2.5°N, 93.0°W	W	R-L	5.5	-	-	D	Galapagos	Away	Christie and Sinton (1981)
iii) 0.8°N, 87.2°W	E	R-L	6.4	-	-	D	Galapagos	Away	Christie and Sinton (1981)
2. Easter microplate region (Pacific Ocean)									
i) 25.0°S, 112.4°W	N	L-L	12.0	15.0	1.25	D	Easter	Away	Naar and Hey (1986)
ii) 24.0°S, 119.9°W	N	L-L	-	-	-	D	Easter	Away	Naar and Hey (1986)
iii) 23.5°S, 111.8°W	N	L-L	-	-	-	D	Easter	Away	Naar and Hey (1986)
iv) 26.8°S, 114.2°W	SE	-	7.0*	10.0	1.43	D	Easter	Towards	Naar and Hey (1986); Hey et al. (1985)
3. Western Arabian Basin (Northwest Indian Ocean)									
i) Propagators 1-2 and 4-11	W	R-L	9.6-12.0	6.48-14.36	0.33-1.44	D	Deccan-Reunion	Away	**Present study (Table 5.2)**
ii) Propagator 3	E	L-L	9.4	7.74	0.39	U	Deccan-Reunion	Towards	**Present study (Table 5.2)**

1=Location of propagating ridge tip, 2=Direction of propagating ridge (N: north, S: south, E: east, W: west, SE: southwest), 3=offset (L-L: left lateral, R-L: right lateral, 4=Full spreading rate (cm/yr), 5=Propagation rate (cm/yr), 6=Ratio of propagation rate to full spreading rate, 7=Propagated Down (D), Up(U) along regional basement gradient. 8=Name of the hotspot influenced the accretion process, 9=Ridge propagation towards or away with respect to hotspot.

the result of this study provide further support to the observation that propagating ridges propagate down the basement topographic gradient.

It is interesting to observe that out of the eleven paleo-propagating ridges inferred in this study area, ten were propagated westward and only one (PR3) was propagated eastward. In many areas of the world oceans it has been observed that the propagating ridges normally migrate outwards from the proximity of hotspots (Hey et al. 1980; Morgan and Parmentier, 1985; Naar and Hey, 1986; Karsten and Delaney, 1989; Brozena and White, 1990). The westward propagators of the study area are possible due to their proximity to a hotspot. Earlier studies have suggested a spatial as well as temporal proximity of a hotspot with the Early Tertiary seafloor spreading regime of the WAB area. The Indian plate is considered to have come over the Reunion hotspot around 70 Ma. The Deccan Trap volcanic province of the Indian peninsula and the volcanic buildup offshore are considered to represent the volcanic trace formed during the northward motion of the Indian plate over this Reunion hotspot (Whitmarsh, 1974; Morgan, 1981; Shipboard Scientific Party, 1988). Therefore, it is inferred that the westward propagation of most of the propagators is due to their proximity to the then Reunion hotspot.

It can be seen (Table 5.2) that the propagation rate of propagators PR1 to PR3 varies from 3.24 to 3.98 cm/yr with an average rate of 3.63 cm/yr. Whereas, the propagation rate of propagators PR4 to PR11 varies from 10.34 to 14.36 cm/yr with an average rate of 12.14 cm/yr. The propagators PR1 to PR3 were active during pre-anomaly 24N3 period and propagators PR4 to PR11 were active during post-anomaly 25 period. The relative increase in propagation rate of the post-anomaly 25 propagators may be due to decrease in the lithospheric resistance faced by them. During pre-anomaly 24 period, the propagating ridges were oblique to the receding ridges. Therefore, they cut into progressively older and thicker crust and faced increased lithospheric resistance. Whereas, in the case of post-anomaly 25 period, the propagating ridges as well as the receding ridges were parallel, therefore the propagators cut through crust of approximately same age without encountering increase in the lithospheric resistance.

Possibly, this relative decrease in lithospheric resistance to the post-anomaly 25 propagators resulted in a rapid propagation. However, other possibility, such as presence of large stress field as a cause of this increased propagation rate also can not be ruled out.

5.5 RIDGE PROPAGATION AND ASYMMETRIC CRUSTAL ACCRETION IN THE WESTERN ARABIAN BASIN

Crustal accretion in the oceans normally takes place due to symmetric or asymmetric spreading across the ridges. However, repeated ridge propagation can also lead to an asymmetric accretion of the crust. The systematic ridge propagation in a preferred direction can lead to overall asymmetric accretion which is related to the direction of ridge propagation and overall orientation of the spreading segments (Hey et al., 1980, 1986). In the Western Arabian Basin two categories of plaeo-propagators are inferred (Figure 5.6). In first category, the spreading ridge segments with right lateral offset propagated towards west. Whereas, in second category the spreading ridge segments with left lateral offset propagated towards east. In both these cases, the part of lithosphere of the African plate are added to the Indian plate due to paleo-ridge propagation. A schematic diagram depicting the accretion process is shown in Figure 5.7. The lithosphere formed on the receding ridge was progressively transferred from the African plate to the Indian plate by the westward as well as the eastward paleo-propagating ridges (Figure 5.7a,b). This has created a regional asymmetric crustal accretion, which has been inferred from the identified magnetic anomaly pattern. The general description of the propagators is presented in a more detailed manner in the following paragraphs.

In the northern WAB the PR1 and PR2 began to propagate westward at anomaly 28N time, ~63 Ma (Figure 5.6). Sometime between anomalies 27N and 26N the westward propagation of PR1 has ceased. About this time, the corresponding failing ridge rejuvenated and began to propagate eastward as PR3. The PR2 although started at the same time as PR1, ceased much later when it met with the eastward propagating

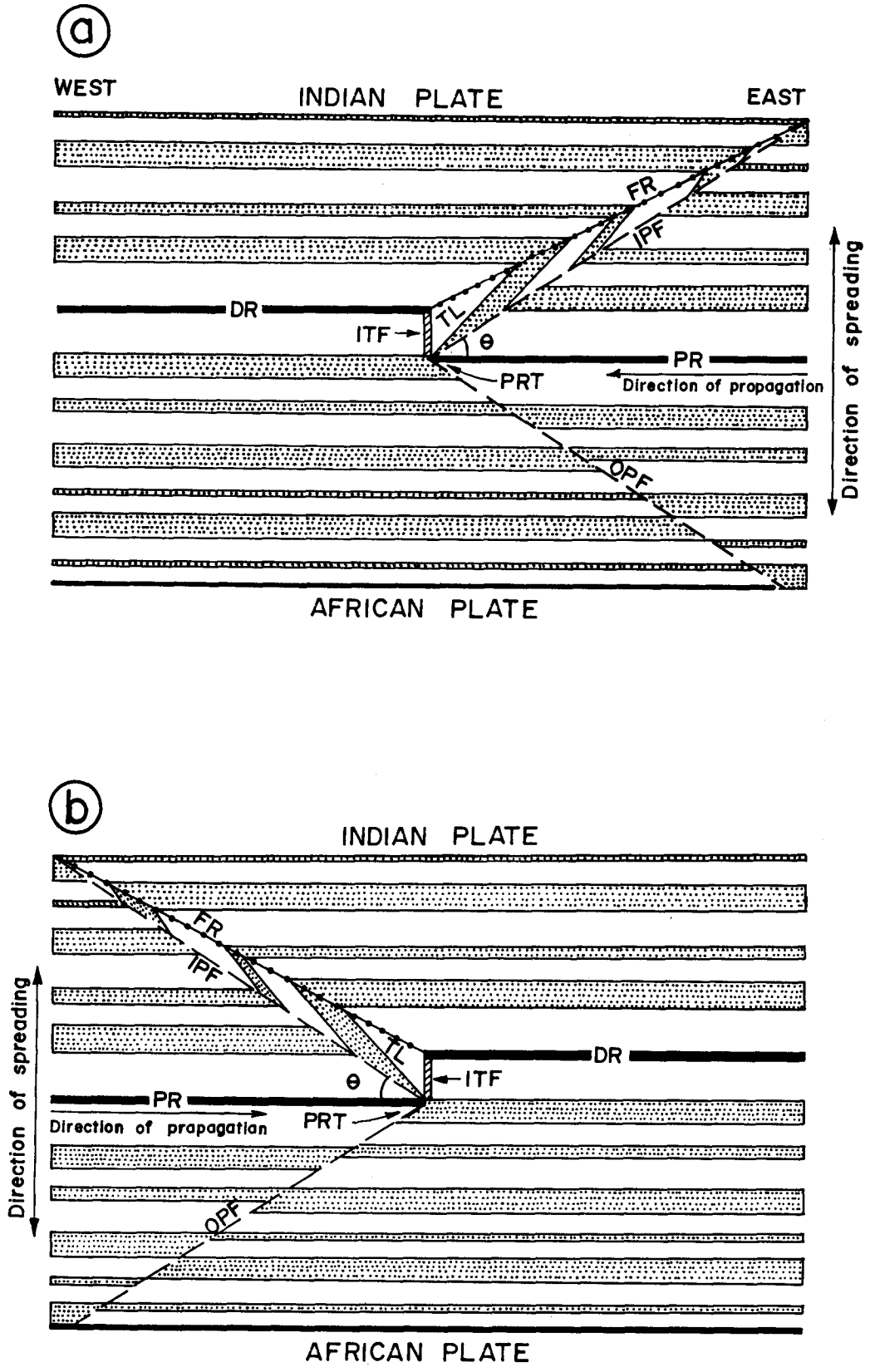

Figure 5.7 Schematic model illustrating (a) westward ridge propagation, and (b) eastward ridge propagation. In both cases, part of the lithosphere formed on the receding ridge (doomed ridge) progressively transferred from the African plate to the Indian plate, and thereby created a regional asymmetry in crustal accretion. Normally magnetized area are shown with dots. PR: propagating ridge, DR: doomed ridge, FR: failed ridge, TL: transferred lithosphere, IPF: inner pseudofault, ITF: instantaneous transform fault.

PR3 shortly after anomaly 25N. The eastward propagating PR3 is likely to have terminated sometime between anomalies 25N and 24N3.

In the southern WAB, eight post-anomaly 25N propagators (PR4-PR11) are inferred. All of them were propagated westward and at least six of them appear to have been coeval. They started shortly before 24N3 (~53 Ma) and remained active at least up to the time of anomaly 23N1 (~50.7 Ma). Whether these propagators continued until the time of anomaly 20 or later needs additional data to be ascertained. The geometry of the propagating ridges inferred in this study suggests that; i) in the northern WAB, the growing ridge had different azimuth as compared to the receding ridge, ii) in the southern WAB, the growing as well as receding ridges remained approximately in the same azimuth and, iii) in all these cases of ridge propagation, the propagating ridges had transferred the crust from the African plate to the Indian Plate. Although most of the propagators systematically propagated for quite long time (anomalies 24N3-22N), the pseudofaults change in their azimuth probably reflecting a change in the spreading rate and or propagation rate.

In the study area only the central set of magnetic lineations 28N through 25N trend NW-SE, whereas all other lineations trend approximately E-W (Figure 5.5a). This possibly suggests that the spreading segment, which was responsible for the origin of the central set of lineations, was initially inconsistent with the general spreading direction of the region. Further, the width of the lineations 28N-25N appears to reduce gradually from west to east giving an impression of fanning of the anomalies. The lineations orientation do not clearly indicate systematic westward fanning, therefore, it is unlikely that it is a case of fanning of the lineation due to a nearby pole of rotation. The anomalous accretionary scenario of the anomalies 28N-25N in the east might have resulted during the reorientation of the NW-SE trending central spreading segment as discussed above by a complex process of ridge propagation and ridge jump.

5.6 CAUSES OF RIDGE PROPAGATION

Ridge propagation occurs to create a stable state when some excessive forces cause instabilities on a spreading system. So far, mainly two mechanisms have been proposed for ridge propagation; i) a ridge propagates away from areas of anomalously shallow seafloor which may reflect excessive magma activity such as hotspots (Hey et al., 1980; Morgan and Parmentier, 1985), or ii) it propagates in response to changes in plate motion (Hey and Wilson, 1982; Wilson et al., 1984). The former, the hotspot driven model, fits well with the ridge propagation in many areas of world's oceans (Table 5.3). For example, all four well-documented active propagating ridges along the Galapagos spreading center in the Pacific Ocean are propagated away from the Galapagos hotspot (Hey et al., 1980; Wilson and Hey, 1995). Similarly, on the Easter microplate area, the clearest example of propagation is also away from the Easter hotspot (Schilling et al., 1985; Naar and Hey, 1991). The two most recent episodes of ridge propagation on the Juan de Fuca Ridge were in opposite direction i.e. away from the Cobb-Axial Seamount hotspot (Johnson et al., 1983; Karsten and Delaney, 1989). However, in this area the relationship of earlier propagators to hotspot activity is less clear (Hey and Wilson, 1982). The second mechanism of ridge propagation advocates that ridge propagation is a consequence of changes in plate motion (Hey et al., 1980; Wilson et al., 1984; Wilson, 1988). However, Morgan and Sandwell (1994), based on large database of ridge propagation, suggested that a persistent along-axis gradient produces ridge propagation while changes in plate motion determine the offset direction and offset distance of the propagating ridges. A noticeable change in plate motions leads to the rapid growth of the offset at propagating ridges as the new ridge axis forms more nearly perpendicular to the new spreading direction than does the retreating ridge axis. Their inference is further supported by other studies that show evidence for propagation in the absence of significant changes in spreading direction (Macdonald et al., 1984; 1988).

The observed relationship between hotspots and ridge propagation has suggested that propagation might result from the flow of partial melts or mantle material away

from a hotspot (Hey and Vogt, 1977; Schilling et al., 1982; Vogt et al., 1983). Spreading ridge propagates away from areas of high tensile stress produced by thermal or dynamic uplift due to hotspots (Hey et al., 1980). In general, cracks in an elastic medium propagate away from areas of high tensile stress in the direction perpendicular to maximum local tensile (least compressive) stress (Lawn and Wilshaw, 1975; Pollard and Aydin, 1984). Morgan and Parmentier (1985) have developed a fracture mechanics model and suggested that ridge propagation occurs because of excess gravity sliding stresses produced by the hotter and thus more buoyant asthenosphere and shallow seafloor associated with the hotspot.

Although many spreading ridges appear to propagate in response to hotspot related stresses, ridge may also propagate due to stresses produced otherwise. In the Arabian Sea, the paleo-ridge propagation is most likely due to the Reunion hotspot driven stresses.

The evidence of ridge propagation in the Western Arabian Basin attains particular importance due to several reasons. Firstly, it demonstrates the necessity of re-examination of magnetic anomalies in the conjugate Eastern Somali Basin in order to achieve a more refined and complete evolutionary history of the Indian Ocean in general and the Arabian Sea in particular. Secondly, the propagating ridge hypothesis although is about two decades old, still there is paucity of published instances of their identification over relatively older oceanic crust. The well preserved magnetic fabric of the Early Tertiary oceanic crust of the Western Arabian Basin will therefore become one of such rare examples. Thirdly, due to the temporal and spatial proximity of the propagators with the then Reunion hotspot, this area may provide a candidate site for detailed study of the processes of systematic ridge propagation under the influence of hotspot.

CHAPTER 6

CHAPTER 6

MODEL STUDIES OF FREE-AIR GRAVITY ANOMALIES

6.1 INTRODUCTION

Model studies of free-air gravity anomalies under constraints from known geological and geophysical results are important to decipher the crustal densities and structure. The studies of the Chagos-Laccadive Ridge (C-L-R) system, a major physiographic feature of the eastern Arabian Sea, are limited and mostly confined to the southern part of it. The Laccadive Ridge, northern part of the C-L-R paralleling the west coast of India, is one of the most poorly studied portion of the C-L-R. At present, its nature, structure and mode of compensation is not well constrained mainly due to the scarcity of marine geophysical data.

In this Chapter admittance analysis of gravity and bathymetry data and two-dimensional modeling of the gravity data over the ridge are carried out using constraints from the results of the Deep Sea Drilling Project (Site 219), seismic reflection and refraction. The aim of the study is to i) determine the transfer function which describes the relationship between gravity and bathymetry, ii) interpret this transfer function in terms of various isostatic models, iii) determine density and structure of the crust, and iv) use the inferred model of isostasy, density and crustal structure to provide constraints on mode of compensation, nature and origin of the Laccadive Ridge to improve understanding of the evolution of the western continental margin of India in particular and the Arabian Sea in general.

6.2 METHODOLOGY

6.2.1 ADMITTANCE ANALYSIS OF GRAVITY AND BATHYMETRY DATA

Bathymetry and gravity data of geological feature is often characterized by a linear frequency response function or admittance. The method of quantitatively determining the state of isostasy of a geological feature was developed by Dorman and Lewis (1970). Later McKenzie and Bowin (1976) and Watts (1978) extended the technique of admittance analysis to deep sea gravity and bathymetry data. This method assumes that free-air gravity anomalies are caused by topography and its compensation and attempts to determine a function which, when convolved with topography, produces the gravity anomaly. The advantage of this method is that this function may be derived from observational data, independent of a particular isostaic model. Once the function has been determined, it can be interpreted in terms of simple models of isostasy.

The isostatic response method simply involves the derivation of a filter, which is convolved with the bathymetry in the space domain, produces a series which resembles the observed gravity, again in the space domain. This process can be represented in the space domain using the convolution operator, *, as:

$$g(x)=f(x)*b(x) \quad \text{----------(6.1)}$$

Where, b(x) is the series representing bathymetry, f(x) is the series representing the filter and g(x) is the free-air gravity series. The above convolution in the space domain is equivalent to multiplication in spatial frequency domain.

$$G(k_n)=Z(k_n)B(k_n) \quad \text{----------(6.2)}$$

Where, $G(k_n)$, $Z(k_n)$ and $B(k_n)$ are the discrete Fourier transform of g(x), f(x) and b(x) respectively. $Z(k_n)$ is known as the admittance or transfer function and the wave number $k_n=2\pi/\lambda$ where λ is the wavelength. The equation (6.2) can be re-written as:

$$Z(k_n)=G(k_n)/B(k_n) \quad \text{----------(6.3)}$$

However, the function $Z(k_n)$ obtained in this way is influenced by noise in the gravity field particularly at short wavelengths. The noise present in any data may be due to measurement error, data reduction procedure or variation in the structure of the linear system under consideration. In the presence of noise a better estimate of $Z(k_n)$ according to McKenzie and Bowin (1976) can be obtained from:

$$Z(k_n)=C(k_n)/E_b(k_n) \quad \text{----------(6.4)}$$

where,
$$C(k_n)=\frac{1}{2N}\sum_{n=1}^{N} G_n(k_n)B_n(k_n)^{**} \quad \text{----------(6.5)}$$

$$E_b(k_n)=\frac{1}{2N}\sum_{n=1}^{N} B_n(k_n)B_n(k_n)^{**} \quad \text{----------(6.6)}$$

Where, the symbol, **, denotes the complex conjugate. $C(k_n)$ is the cross spectrum of the gravity and the bathymetry, $E_b(k_n)$ is the power spectrum of bathymetry and N is the total number of gravity and bathymetry profiles. In this case the admittance is given by the cross spectrum of the gravity and bathymetry divided by the power of the bathymetry. The filter f(x) can be obtained in the space domain by inverse Fourier transforming the admittance estimate. The estimate still contains noise and some form of spectral smoothing must be applied. McKenzie and Bowin (1976) subdivided their profiles into a number of smaller segments and obtained admittance estimates for each segments. They then averaged over all the segments. A problem with this approach to smoothing is that each segment will contain a slightly different geological signal and they can not be isolated after averaging. Another approach was adopted by Dorman and Lewis (1970), Banks and Swain (1978) and McNutt (1979) who applied smoothing in the spatial frequency domain by averaging about particular wavelengths. The method used in this study is that of Watts (1978) where smoothing has been accomplished by using many profiles crossing the particular feature of geological interest. An independent estimate of the cross spectrum and power spectrum of gravity and bathymetry are

obtained for each profile. These spectra are summed and the resulting averaged spectra are used to obtain a single admittance function. By this procedure the filter or admittance is obtained for a single geological feature.

In addition to determining the filter, there are several relevant checks on the quality of the admittance function. McKenzie and Bowin (1976) suggested the estimation of following parameters to verify the quality of admittance function.

The phase of admittance($\phi(k_n)$) defined by:

$$\phi(k_n)=\tan^{-1}[Im\{Z(k_n)/Re(Z(k_n)\}] \quad \text{----------(6.7)}$$

Since $Z(k_n)$ is expected to be real therefore $\phi(k_n)$ should be close to zero.

Another useful parameter is the coherence (γ^2) which is the measure of the portion of the observed gravity that can be directly attributed to the bathymetry. The coherence is given by:

$$\gamma^2(k_n)=\{N(CC^*/E_bE_g)-1\}/(N-1) \quad \text{----------(6.8)}$$

Where, N is the number of profiles, $C=C(k_n)$ is the complex cross spectrum of bathymetry and gravity and can be estimated from equation (6.5). $E_b=E_b(k_n)$ is the power spectrum of bathymetry and can be estimated from equation (6.6). $E_g=E_g(k_n)$ is the power spectrum of gravity and is given by:

$$E_g(k_n)= \frac{1}{2N} \sum_{n=1}^{N} G_n(k)G_n(k)^* \quad \text{----------(6.9)}$$

Further, the coherence can be used to separate the energy spectrum into two parts and is given by:

$$\text{Coherent energy}= \gamma^2(k_n)E_{g,}(k_n) \quad \text{----------(6.10)}$$

$$\text{Incoherent energy}= \{1-\gamma^2(k_n)\}E_{g,}(k_n) \quad \text{----------(6.11)}$$

The coherent energy is defined as that part of energy in the gravity that is caused by the bathymetry and the most confident determination of $Z(k_n)$ can be made where the coherent energy dominates. It is worth mentioning that the results of the computations

are a filter or admittance which reproduces the gravity from the bathymetry over the feature which is being examined. The admittance is based completely on the observed relationship between gravity and bathymetry and is not tied to any isostatic model. However, as were shown by Dorman and Lewis (1970), Lewis and Dorman (1970), McKenzie and Bowin (1976), Walcott(1976), Banks et al. (1977), Watts (1978), and Louden (1981), the admittance can be easily compared with the isostatic models based on different hypothesis of compensation.

6.2.2 TWO-DIMENSIONAL GRAVITY MODEL

Two-dimensional model of the density distribution along profile SK12-07 (Figure 6.1) beneath the Laccadive Ridge is constructed to satisfy the free-air gravity anomalies. To construct the model, thickness of the sediments and the depth to the basement are taken from the interpreted seismic reflection profile presented in Chapter 7. The seismic velocities along the profile are constructed from the projected positions of the published refraction results (Naini, 1980). The seismic velocities are converted to densities following Nafe and Drake (1963) velocity-density relationship. The seawater and upper mantle densities of 1.03 and 3.3 g/cm^{-3} respectively are considered. An algorithm by Talwani et al. (1959) is used to compute the free-air gravity anomalies of the assumed crustal model. The computed gravity anomalies are then compared to the observed anomalies, and the model is refined until a satisfactory fit is achieved. A reasonable fit between the computed and the observed gravity anomalies, within the constrains from the seismic reflection and refraction results, is obtained with a misfit of individual point generally less than 5% of the observed values.

6.3 ESTIMATION AND ANALYSIS OF ADMITTANCE FUNCTION

The method discussed in the previous section has been used to estimate the admittance function over the Laccadive Ridge. A total of 12 profiles of bathymetry and free-air gravity anomaly across the ridge between 8° and 16°N are selected for analysis. The location of the profiles are shown in Figure 6.1. All the profiles are 384 km long,

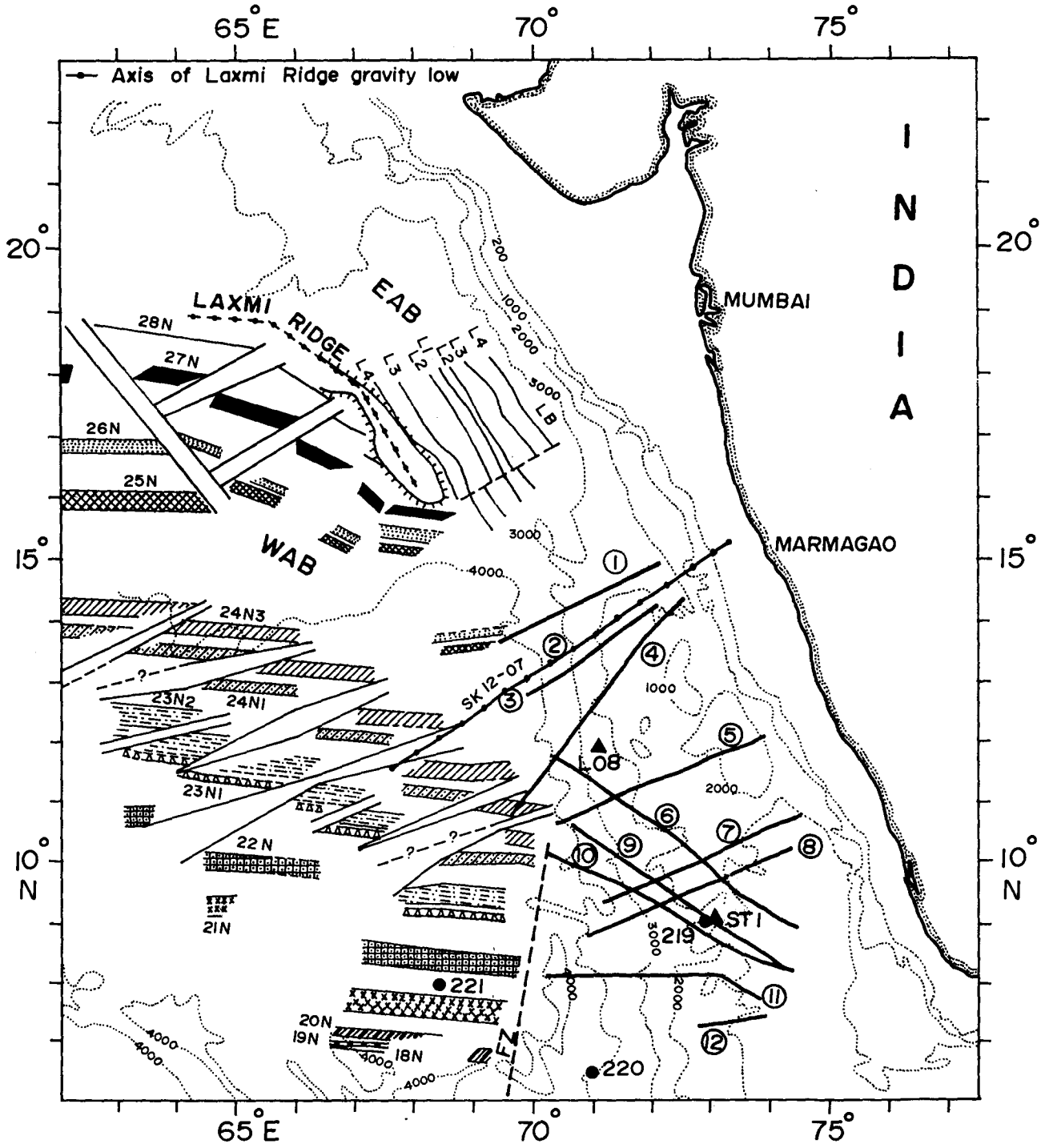

Figure 6.1 Location of free-air gravity anomaly and bathymetry profiles (number in circle) across the Laccadive Ridge. Magnetic lineations are defined by younger and older boundaries of the normally magnetized blocks. Diagonal offsets of magnetic lineations are interpreted pseudofaults. Dotted lines represent bathymetric contour in meter. DSDP Sites are shown with solid circles. ST1 and L08 are refraction stations. LB=Laxmi Basin, L1-L4=Laxmi Basin magnetic lineations, EAB=Eastern Arabian Basin, WAB=Western Arabian Basin.

centered over the peak of the ridge to ensure that the admittance calculated is applicable to the ridge and not to the nearby oceanic as well as continental crust. Both bathymetry and free-air gravity anomaly data are projected normal to the strike of the ridge and are shown in Figure 6.2.

Before applying the discrete Fourier transform to the data, both bathymetry and gravity data are sampled at 1.5 km interval. Spline interpolation is used to get samples at the equal intervals, as a result noise introduced due to sampling is very small and is considered to be within the limits of errors in the data acquisition. Mean and regional trend are removed from each of the bathymetry and gravity profiles. This procedure eliminates the long wavelength (> 500 km) regional signal from the observed data. This is necessary because the long wavelength regional variation is not important compared to the wavelength of the ridge. A cosine taper for 10% of the length of the profile at both the ends is applied to avoid discontinuity and finally zeros are added to make the series length an integral power of 2. The later was necessary so that the fast Fourier transform algorithm (Cooley and Tukey, 1965) could be used. Profile no. 12 extends up to mid-point of the ridge therefore a mirror image of data set was generated to get full length. Finally the complex admittance function was calculated using equation (6.4). The coherence, phase, and the coherent and incoherent energies were also calculated as checks on the reliability of the admittance amplitude. These parameters are plotted as function of wave number and presented in Figures 6.3 and 6.4.

The $\log_{10}$ of admittance amplitude is smooth for wavenumbers less than ~0.5 km^{-1} which corresponds to wavelengths greater than ~13 km. This relative smoothness of admittance indicates that the same signal is associated with all profile and the smoothing procedure certainly reduces noise. The phase of admittance is close to zero for these wavenumbers, a situation implying the admittance is real. At greater wavenumbers ($k>0.5$ km^{-1}), the phase of the admittance fluctuates about zero and progressively becomes noisy. The coherence is high for wavenumbers $k<0.5$ km^{-1}, indicating that a significant portion of the energy in gravity can be attributed to bathymetry at these wavenumbers. At higher wavenumbers ($k>0.5$ km^{-1}) the coherence

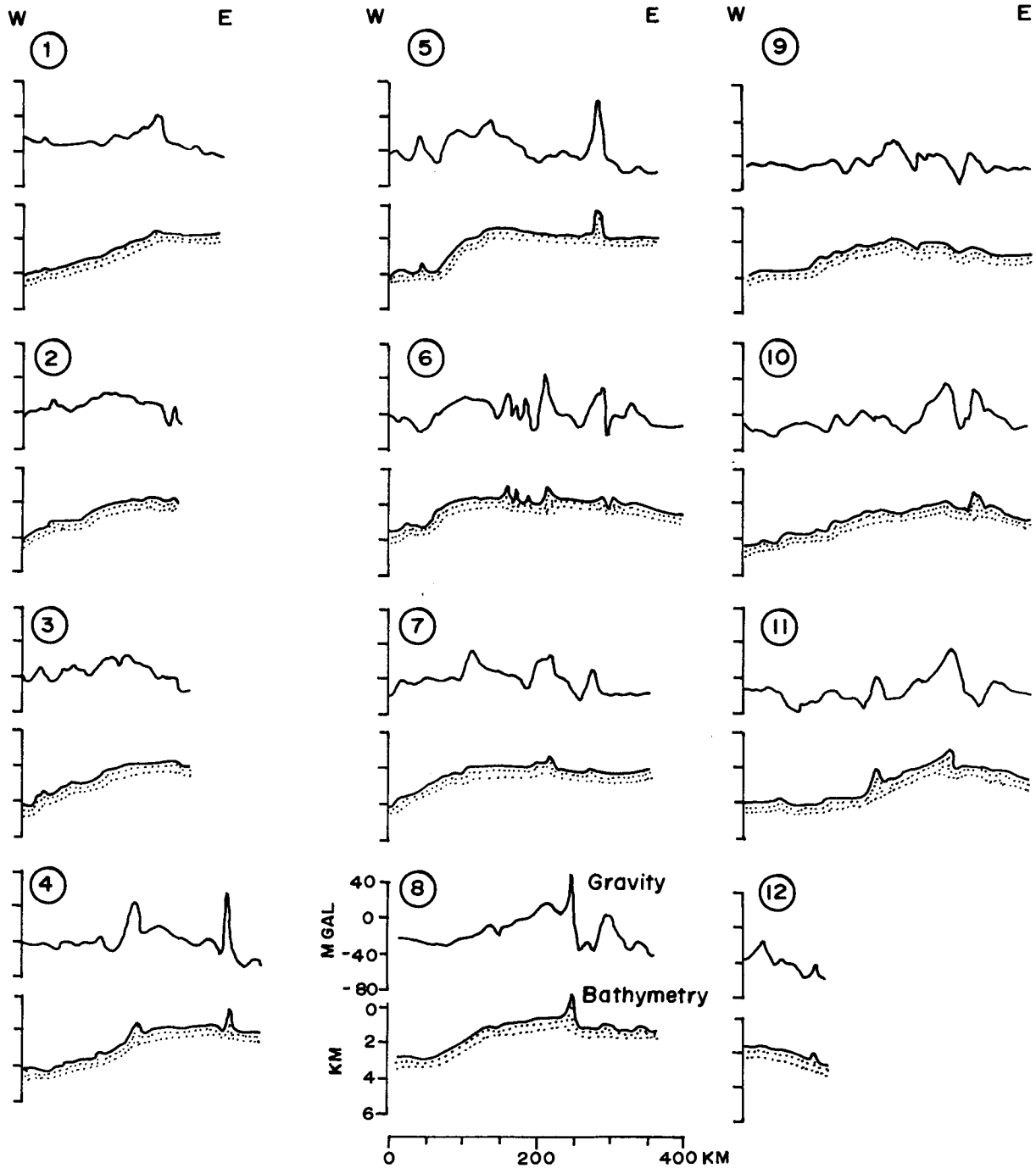

Figure 6.2 Observed free-air gravity anomaly and bathymetry profiles projected perpendicular to the trend of the Laccadive Ridge. Number in circle represents profile number shown in Figure 6.1.

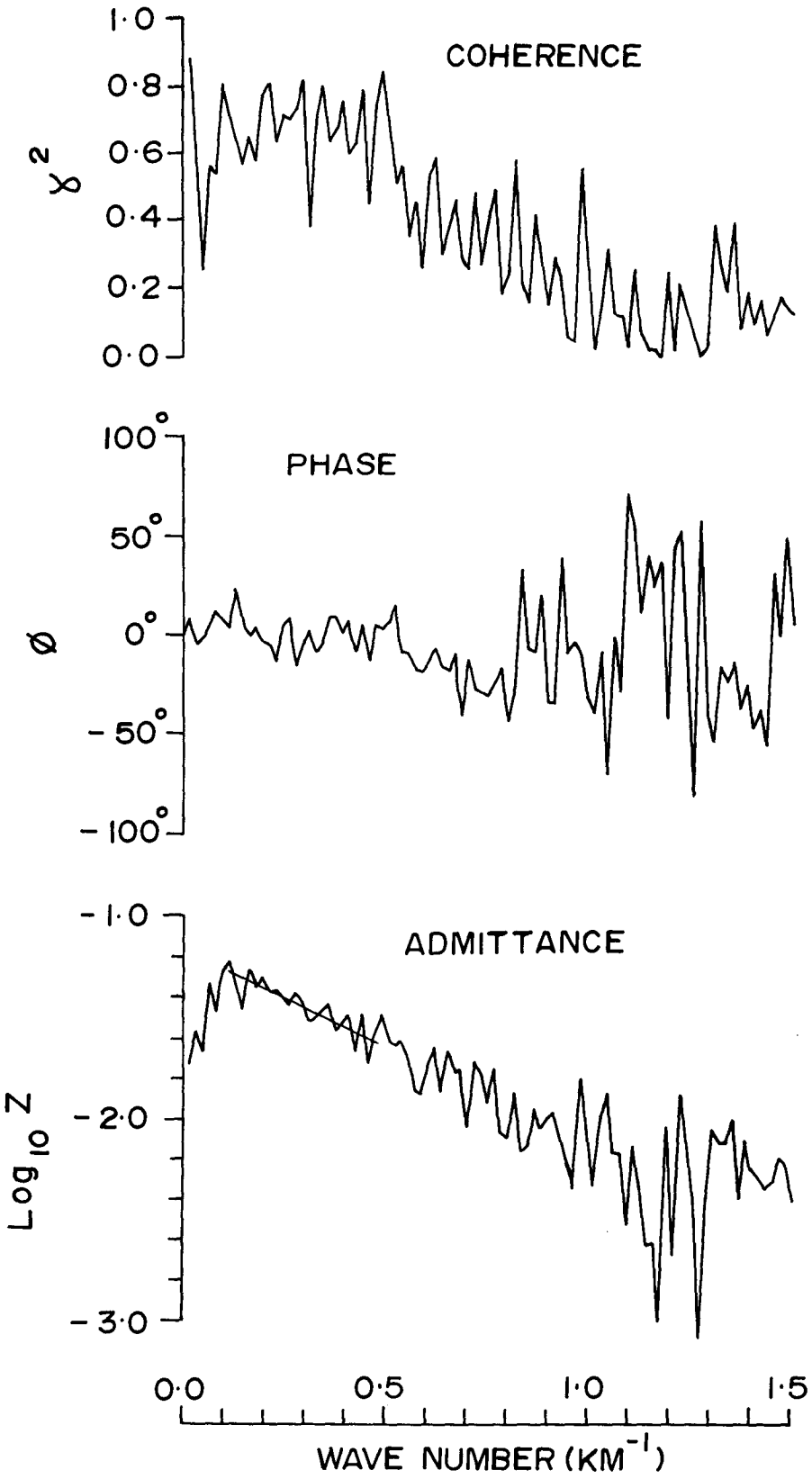

Figure 6.3 The coherence, phase (in degree) and $\log_{10}$ of the amplitude of the admittance determined from the gravity and bathymetry profiles shown in Figure 6.2. The dashed line on the $\log_{10}$ (admittance amplitude) is a best fit line of the observed admittance for $57>\lambda>12$ km. The slope of this line gives an estimate of the mean water depth of 2.429 km and density of the topographic relief of 2.85 g/cm^3. The actual mean depth is 2.478 km.

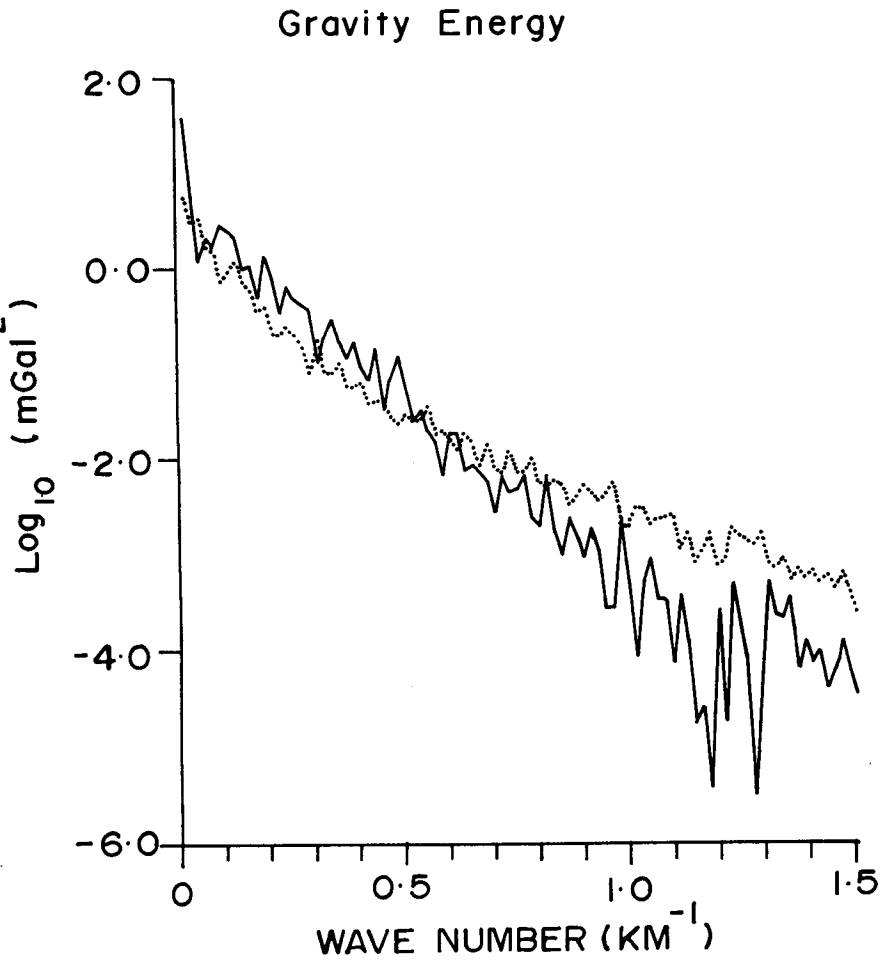

Figure 6.4 The coherent (solid line) and incoherent (dotted line) energy calculated from the gravity and bathymetry profiles shown in Figure 6.2.

plot is rather noisy which suggests that the assumption of simple one-dimension relationship between gravity and bathymetry breaks down at these wavenumbers. The gravity energy has been divided into coherent and incoherent part (Figure 6.4). The coherent energy is a measure of the energy in the gravity field which is caused by topography. Whereas, the incoherent energy is a measure of the energy due to other effects such as instrument noise and non two-dimensionality of the geological feature. For $k<\sim0.5$ km^{-1} ($\lambda>\sim13$ km) the coherent energy is dominant and for $k>\sim0.5$ km^{-1} the incoherent energy dominates. These results suggest that the admittance for wavenumber less than 0.5 km^{-1} is physically significant and can be compared with models. However it was observed that the admittance and coherence associated with strong random errors are biased to abnormally low values. Low coherence can either show that a significant portion of the energy in the observed gravity can not be assigned to bathymetry, or that strong noise occurs on both data sets at considered wavelengths (Forsyth, 1985; Dalloubeix et al., 1988). Final confirmation of the quality of the admittance estimate can be obtained from a comparison of the observed gravity and calculated free-air gravity anomalies. The predicted gravity in frequency domain is estimated using the equation (6.2). Inverse Fourier transform of the product of admittance and bathymetry spectrum gave the predicted gravity in time domain. Figure 6.5 shows the observed bathymetry, predicted gravity (or filtered bathymetry), observed gravity and the difference between observed and predicted gravity. The values on the right of each residual profiles indicate the Root Mean Square(RMS) deviation of the gravity anomaly. The close similarity between observed and predicted gravity profiles indicates that the observed admittance function adequately represent the relationship between gravity and topography for the Laccadive Ridge. However, some of the large residuals associated with short wavelength shallow peak of the ridge do exist in the residual gravity profiles. Perhaps, these residuals emphasizes features with unusual density contrasts at or below the ocean bottom. Since these differences are small, the observed admittance function can be interpreted with some confidence in terms of different isostatic models.

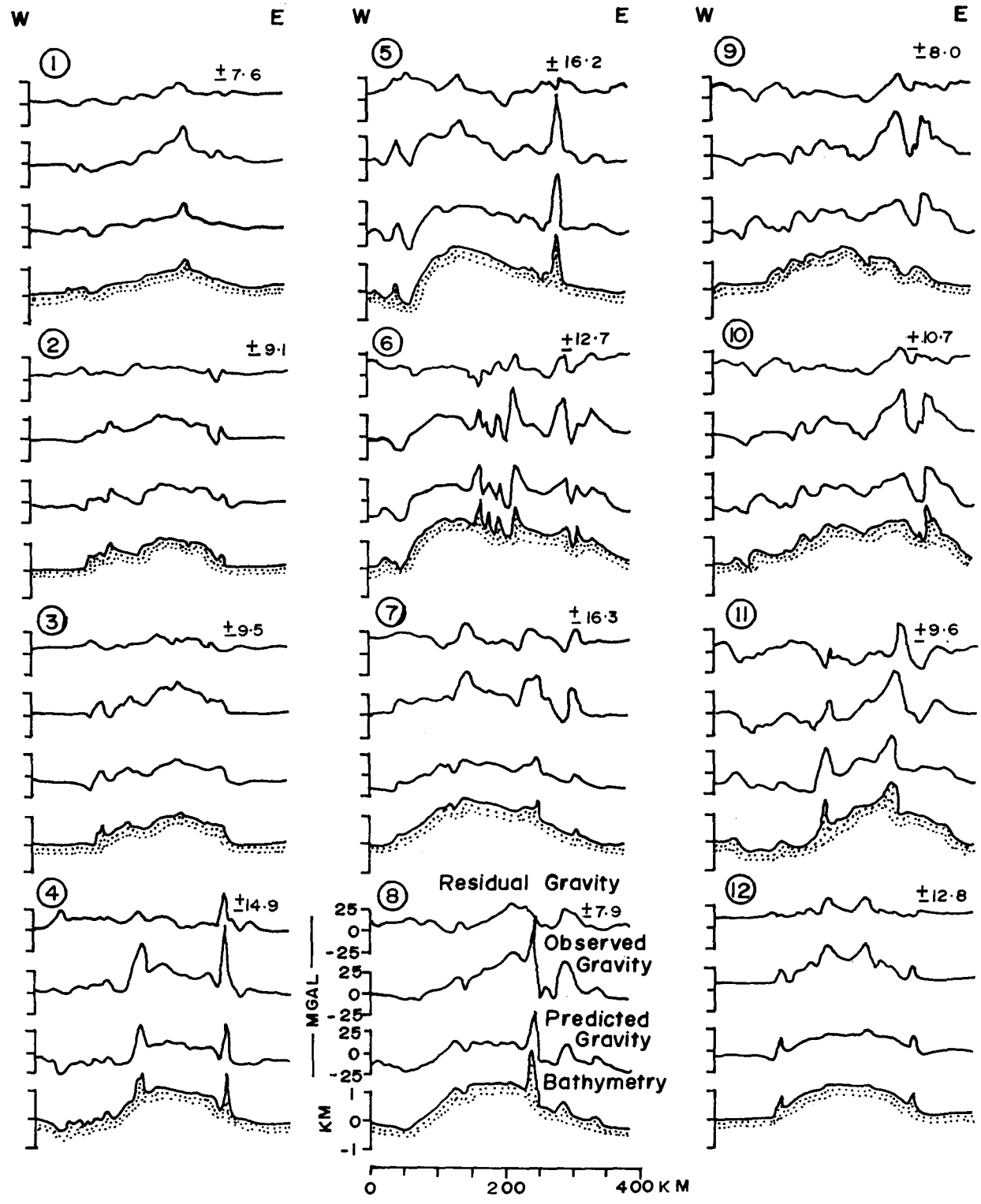

Figure 6.5 Observed bathymetry, predicted gravity, observed gravity and residual gravity profiles across the Laccadive Ridge. The observed gravity and bathymetry profiles are plotted after removing their mean and trend. The root-mean squared difference between the observed and predicted gravity are shown to the right of the residual gravity. Number in circle represents profile number. Location of the profiles is shown in Figure 6.1.

6.4 INTERPRETATION OF ADMITTANCE FUNCTION

In order to get a meaningful result about the nature of isostatic compensation, it is necessary to compare the observed admittance with the admittance derived from theoretical models. The simplest model for explaining the observed admittance values is to assume that the gravity anomalies are only due to the seafloor topography and that the topography is uncompensated. The admittance expressing the relationship of gravity to uncompensated topography is given (McKenzie and Bowin, 1976; Watts, 1978; McNutt, 1979) by:

$$Z(k_n)=2\pi G(\rho_b - \rho_w)\exp(-k_n d) \quad \text{----------(6.12)}$$

Where, G is the gravitational constant, ρ_b is the density of the topography, ρ_w is the density of the sea water, and d is the mean water depth of the topography.

A plot of $\log_{10}$ of admittance against wavenumbers should therefore yield a straight line and thus estimates of ρ_b and d can be made from the intercept and slope (McKenzie and Bowin, 1976). The slope of the line is given by 0.4343d and the intercept is given by $\log_{10}\{2\pi G(\rho_b-\rho_w)\}$. The value ρ_b and d are derived from a least square fit of the decreasing admittances with increasing wavenumbers. A best fit straight line for the admittance for $0.11<k<0.51$ gives estimates of d = 2.429 km and ρ_b = 2.85 g cm^{-3}. The straight best fit line is shown in Figure 6.3. The estimate of d matches well with the observed mean water depth (2.478 km). Due to non availability of direct measurements of rock densities of the Laccadive Ridge, the estimated value of ρ_b is constrained using seismic refraction results (Francis and Shor, 1966, Naini, 1980) and velocity-density relationship (Nafe and Drake, 1963). The refraction stations ST1 (9.0833°N, 73.066°E) and L08 (11.9067°N, 71.1750°E) located on the Laccadive Ridge detected the following crustal layers:

Station: ST1

Layer velocity (km/s)	3.85	5.00	6.84	7.97
Layer thickness (km)	1.87	2.90	10.60	

Station: L08

Layer velocity (km/s)	1.65	2.12	4.40	5.60	6.30	7.20
Layer Thickness (km)	0.41	0.42	0.66	1.49	4.69	8.40

According to the Nafe-Drake velocity-density relationship, the igneous crustal velocities of 5.0-7.20 km/s of the Laccadive Ridge correspond to the densities of 2.52-2.90 g/cm^3 which compares well with the estimated value of ρ_b. The close compatibility of estimated ρ_b and d with the independently obtained values are an indication that the admittance between k_n =0.11 and k_n =0.51 can be related to the real geological situation. Although the low wavenumber ($0.11< k_n<0.51$) portion of the $\log_{10}$ of admittance can be well represented by straight line, at very short wavenumbers ($k_n<0.11$) the amplitude of the admittance deviates from the model of uncompensated bathymetry. In other words, the uncompensated topography model does not fit the observed admittance values at very shorter wavenumbers. It is expected from the equation (6.12) that the admittance should continue to increase as the wavenumber decreases. But the observed behavior is quite different i.e. observed admittance decreases with decreasing wavenumbers. This can be seen in Figure 6.3. The rapid decrease of admittance at shorter wavenumbers (i.e. at longer wavelengths) is due to isostatic compensation. Since this will produce long wavelength topography without corresponding gravity anomalies (McKenzie and Bowin, 1976; Watts, 1978), it is therefore desirable to compare observed admittance at shorter wavenumbers (i.e. at longer wavelengths) with theoretical values derived from models of isostatic response.

According to the theory of isostasy, masses in different vertical columns above a particular depth, called depth of compensation, are equal. There are two main types of crustal isostatic models: one in which compensation is achieved by lateral density variations (Pratt-Hayford model) and the other in which compensation results from changes in crustal thickness (Airy and flexure models). The two most commonly used models in admittance analysis have been the Airy and flexure models (McKenzie and Bowin, 1976; Watts, 1978; Louden, 1981; Karner and Watts, 1982; Tamsett, 1984;

Young and Hill, 1988). In this study too the observed admittances is interpreted in terms of the Airy and flexure models of isostasy.

6.4.1 AIRY MODEL

In an Airy or local isostatic model (Airy, 1855), compensation is accomplished by variations in the thickness of a constant density layer of mean thickness (Figure 6.6). The theoretical admittance for the simple Airy model of compensation is the sum of the admittance due to the density contrast between the crust and mantle at the Moho (McKenzie and Bowin, 1976). The resulting admittance is given by:

$$Z(k_n)=2\pi G(\rho_b - \rho_w)\exp(-k_n d)\{1-\exp(-k_n T_c)\} \text{----------(6.13)}$$

Where T_c is the distance below seafloor at which compensation is assumed to occur. For simple Airy isostasy, T_c is approximately the average crustal thickness. The parameters used in the computation of theoretical curves of admittance for the Airy model of isostatic compensation are listed in Table 6.1.

Theoretical curves of admittance for the Airy model of isostatic compensation for various crustal thickness using equation (6.13) are shown in Figure 6.7 together with the observed admittances. The vertical bars on the admittance estimates in this figure represents the standard errors calculated by:

$$\sigma^2=[1/(\gamma^2-1)/2N] \text{ ----------(6.14)}$$

It is observed that at wavenumbers 0.05 km^{-1}, the admittance as well as coherence values are biased to abnormally low values. These parameters indicate that the gravity is not simply related to the bathymetry at this wavenumber and the admittance coefficient at this wavenumber should therefore be neglected when comparing the observed admittance with theoretical curves. The observed admittance values for wavenumbers less than ~0.08 km^{-1} i.e. wavelengths greater than ~80 km (neglecting third admittance coefficient) fall between T_c=15 km and T_c=20 km with an

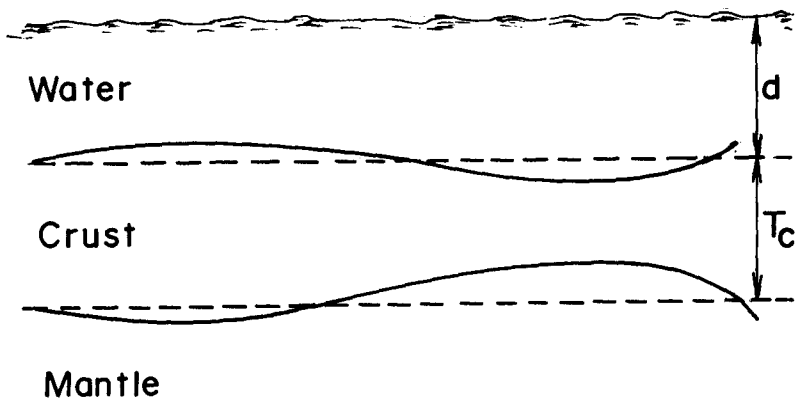

Figure 6.6 Sketch of the model to calculate the admittance for Airy compensation. The d and T_C are mean ocean depth and mean thickness of the crust respectively. ρ_W and ρ_b are densities of sea water and crust. Values of these parameters are listed in Table 6.1.

Table 6.1 Summary of the parameters used in the calculation of admittance function for Airy and Plate models of isostatic compensation.

Parameters	Symbol used	Numerical Value
Mean water depth of topography	d	2.478 km
Thickness of crustal layer 2	T_2	1.5 km
Mean thickness of crust	T_c	16.0 km
Density of sea water	ρ_w	1.03 g cm^{-3}
Density of crustal layer 2	ρ_2	2.6 g cm^{-3}
Density of crustal layer 3	ρ_3	2.9 g cm^{-3}
Density of upper mantle	ρ_m	3.4 g cm^{-3}
Universal Gravitational constant	G	6.67×10^{-8} dyne cm^2 g^{-2}
Young's modulus	E	10^{12} dyne cm^{-2}
Acceleration due to gravity	g	981 cm sec^{-2}

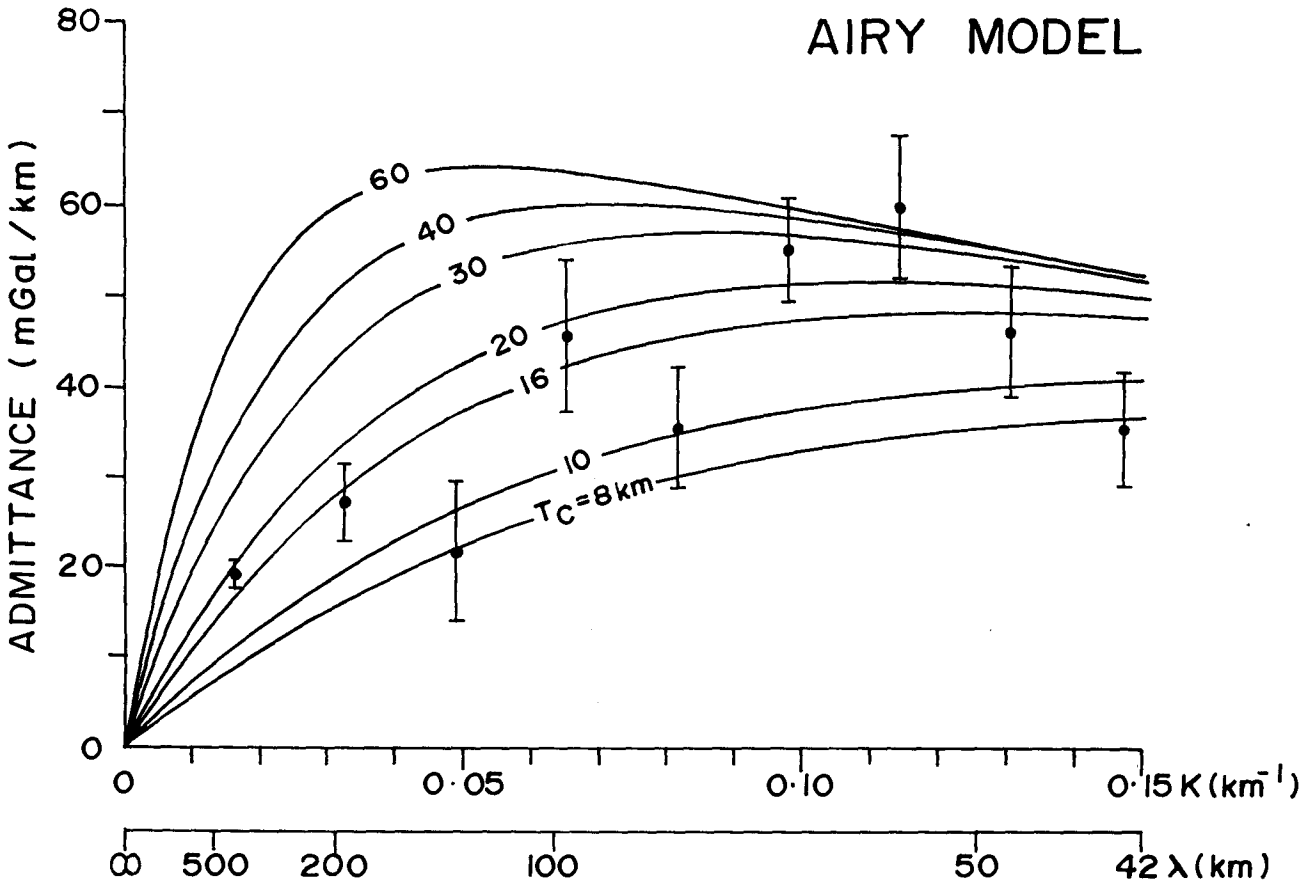

Figure 6.7 Observed admittance values (solid circles) for the Laccadive Ridge compared with the theoretical admittance curves (solid line) for Airy model of isostasy for T_C ranging from 8 to 60 km. The vertical bar on each solid circle indicates standard error. The theoretical models are based on the parameters summarized in Table 6.1.

average of ~17 km. Seismic refraction results at stations ST1 (9.0833°N, 73.0667°E) and L08 (11.906°N, 71.175°E) on the crest of the Laccadive Ridge suggest total igneous crustal thickness of 13.5 and 14.6 km respectively (Francis and Shor, 1966; Naini and Talwani, 1982). The average crustal thickness (~17 km) estimated from the admittance analysis in the present study is higher but comparable to above seismic refraction results.

6.4.2 PLATE MODEL

In a flexural isostatic model, topographic features are treated as loads on a thin elastic plate underlain by weak fluid and compensation occurs on a regional basis because loads are partially supported by the lateral strength of the lithosphere. The extent to which the lithosphere can support load is characterized by the flexural rigidity or, equivalently, the effective elastic thickness (EET) of the plate. McKenzie and Bowin (1976) gave an expression for the admittance of this model. Watts (1978) altered this model slightly to include an additional crustal layer between the basement and the mantle layers. The basic elements of this model are outlined in Figure 6.8. The admittance for this model is given by:

$$Z(k_n)=2\pi G(\rho_2 - \rho_w)\exp(-k_n d)[1-\{\exp(-k_n T_2)(\rho_3 - \rho_2) + \exp(-k_n T_c)(\rho_m - \rho_3)\}/ \{(\rho_m - \rho_2)+4(\rho_m - \rho_w)Mk'^2AB^{-1}\}] \quad (6.15)$$

Where T_2 is the thickness of layer 2 of the ocean crust, T_c is the mean thickness of the crust, ρ_3 is the density of layer 3 of ocean crust, ρ_m is the density of the upper mantle.

$$M=E/(3gT_e(\rho_m-\rho_w)/2)$$

where, E and T_e are the Young's modulus and effective plate thickness respectively.

$$k'=k\,T_e/2$$

$$A=\{\sinh 2k'/2k'\}^2-1$$

$$B=\{\sinh 4k'/4k'\}^2+1$$

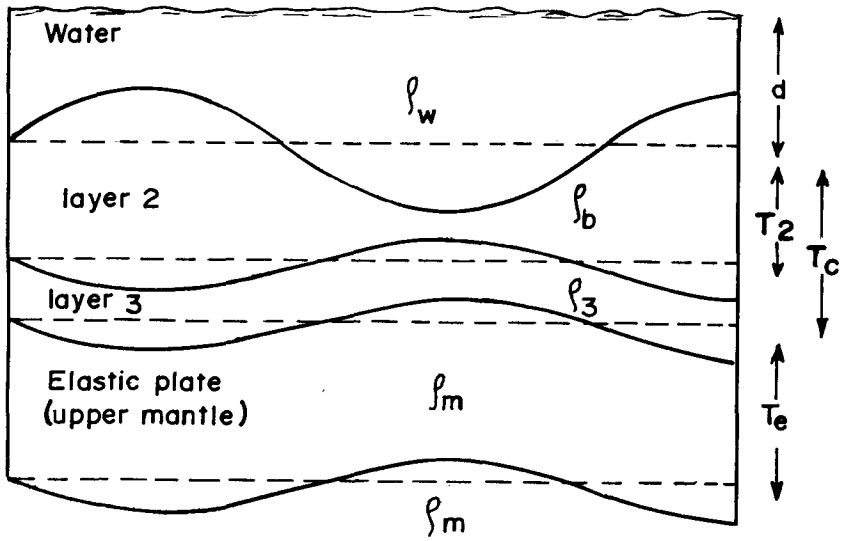

Figure 6.8 Sketch of the model to calculate the admittance for elastic plate compensation. d is mean ocean depth. t and t2 are the mean thickness of the crust and of the crustal layer 2. ρ_W, ρ_b , ρ_3 and ρ_m are the densities of sea water, crustal layer 2, crustal layer 3 and the upper mantle respectively. T_e is the effective elastic thickness of the lithosphere. Values of these parameters are listed in Table 6.1.

The calculated admittance curves for the plate model of compensation using the equation (6.15) are compared with the observed values in Figure 6.9. The parameters used in the computation of theoretical curves of admittance for the above model of isostatic compensation are listed in Table 6.1. The error bars (vertical bars) in the admittance estimates in Figure 6.9 represent the standard error calculated by the equation (6.14). The observed admittance values for wavenumbers less than ~0.08 km^{-1} i.e. wavelengths greater than ~80 km (neglecting third admittance coefficient) fall between T_e=2 km and T_e=10 km with a best fitting average elastic plate thickness of ~5 km.

6.5 RESULTS OF TWO-DIMENSIONAL GRAVITY MODEL STUDIES

Two-dimensional model studies of the free-air gravity anomalies along profile SK12-07 is carried out to interpret crustal structure across the central western continental margin of India. The best fit model obtained after several iterations is shown in Figure 6.10. The inferred model suggests that the maximum igneous crustal thickness below the Laccadive Ridge is ~17 km. It is higher than the normal oceanic crustal thickness. The anomalous crustal thickness is possible in areas of crustal extension during continental rifting. The crustal thickness gradually decreases towards offshore reaching an average value of ~6 km in the west of the Laccadive Ridge where, thinned crust of the ridge (~16 km) is juxtaposed with the known Early Tertiary normal oceanic crust (~6 km). It may be mentioned that the free-air gravity anomalies show a rising trend west of the location where the two crusts are juxtaposed.

6.6 MODE OF COMPENSATION AND NATURE OF THE LACCADIVE RIDGE

The origin of the C-L-R is attributed to various processes such as transform faulting, micro-continent tectonics and a hotspot trace. Naini and Talwani (1982) suggested that the northern part of the C-L-R north of the equator is of continental origin. However, the Deccan Trap volcanic province of the western India and the offshore Chagos-Laccadive Ridge is considered to represent the volcanic trace formed

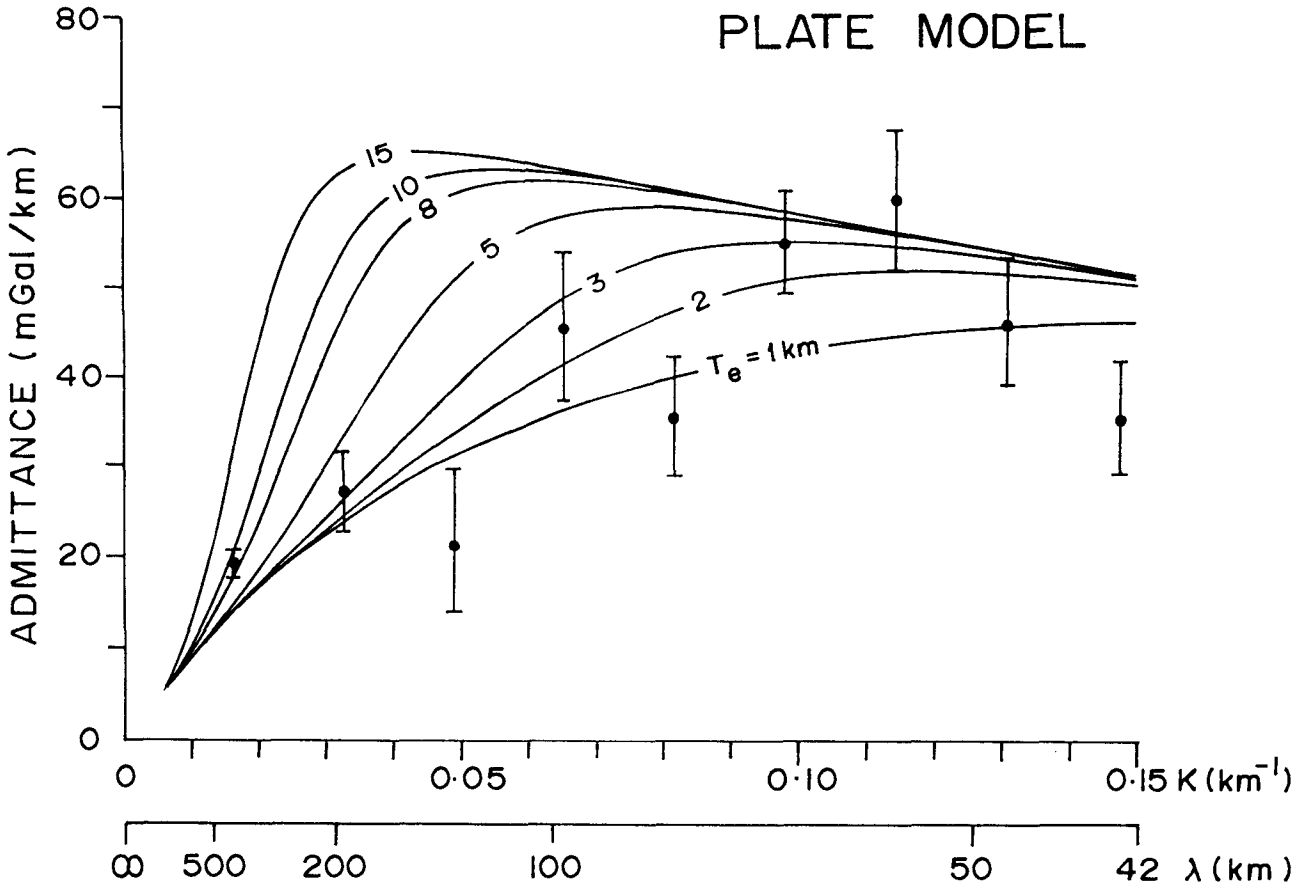

Figure 6.9 Observed admittance values (solid circles) for the Laccadive Ridge compared with the theoretical admittance curves (solid line) for Plate model of isostasy for Te ranging from 1 to 15 km. The vertical bar on each solid circle indicates standard error. The theoretical models are based on the parameters summarized in Table 6.1.

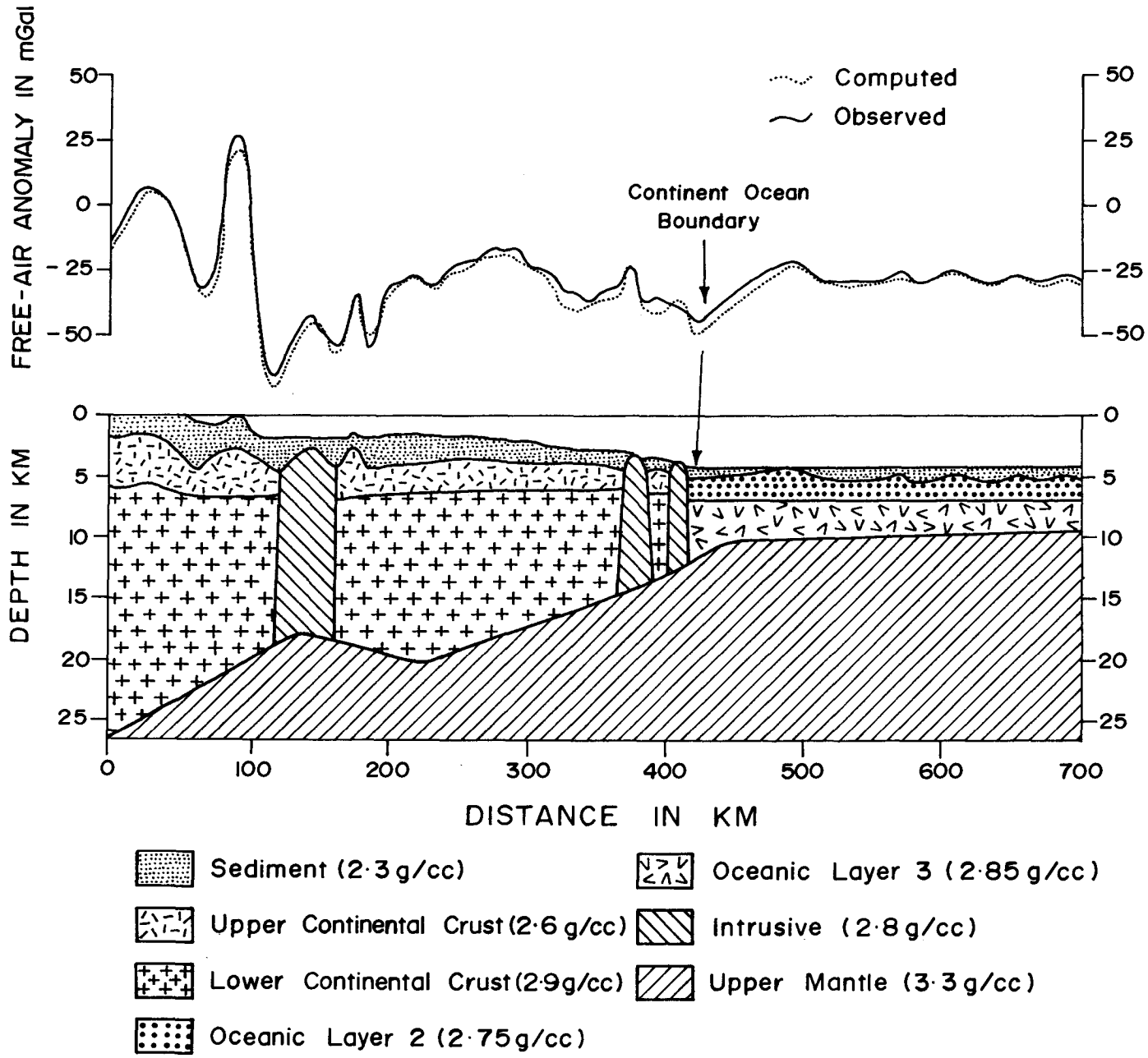

Figure 6.10 Two-dimensional gravity modeling and interpreted crustal structure along profile SK12-07. Layer thickness and their densities are constrained from interpreted seismic section presented in Chapter 7 and published refraction results.

during the northward motion of the Indian plate over the Reunion hotspot (Whitmarsh, 1974; Morgan, 1981, Shipboard Scientific Party, 1988; Richards et al., 1989; Duncan, 1990). Based on result of DSDP Site 219 located on the crest of the Laccadive Ridge, Detrick et al. (1977) have shown that the C-L-R has subsided at rates similar to that of normal oceanic crust. Ashalatha et al. (1991), based on admittance analysis of gravity and bathymetry data over the C-L-R south of 10°N, have shown that the ridge was emplaced near a spreading center.

The admittance analysis over the Laccadive Ridge suggests that the crustal thickness of the ridge varies between 15 and 20 km with an average value of ~17 km for the Airy model of isostasy. The result agrees well with few available seismic refraction results (Francis and Shor, 1966; Naini and Talwani, 1982). Whereas, admittance estimates assuming an elastic plate model suggests ~5 km of effective elastic thickness. Such a low elastic plate thickness may imply that the ridge was either emplaced over a young lithosphere near spreading ridge or on older lithosphere which was later thermally rejuvenated to reset its effective elastic thickness. The emplacement over a young lithosphere near spreading center appears to be unlikely because the Reunion hotspot was close to or on a spreading center at ~49 Ma and was building the northern Chagos Bank and Saya-de-Malha Bank (Duncan, 1990). The thermal rejuvenation due to hotspot requires residence of the plume beneath the lithosphere for a certain period of time (Kent et al., 1992). A reduction in effective elastic plate thickness of the Cape Verde Rise in the South Atlantic Ocean (Young and Hill, 1986; McNutt, 1988) and the Magellan seamounts in the Pacific Ocean (Smith et al., 1989) are reported where the entire lithosphere column was reheated due to hotspot. Considering the very fast movement of the Indian Plate (13.5 cm/yr) over the Reunion hotspot between 83 and 48 Ma (Duncan and Hargraves, 1990), thermal rejuvenation due to hotspot may be insufficient to change the effective elastic plate thickness. Therefore, emplacement over older oceanic lithosphere is unlikely. In view of these results, it is inferred that local isostatic compensation by the Airy mechanism is an appropriate model of compensation of the topography of the Laccadive Ridge.

Based on crustal structure and density distribution inferred from the admittance and two-dimensional gravity model studies, a continental origin for the Laccadive Ridge is suggested. Further, the ocean-continent boundary is inferred to lie immediately west of the Laccadive Ridge (Figure 6.10). An integrated interpretation based on the results from bathymerty, gravity, multichannel seismic reflection along with published results are presented in Chapter 8 to substantiate the above inferences.

CHAPTER 7

CHAPTER 7

MULTICHANNEL SEISMIC REFLECTION STUDIES

7.1 INTRODUCTION

The study of continental margin leads to understand the continental breakup and rifting, key issues to decipher the crustal structure and tectonics. The continental break-up, in general, is associated with crustal thinning, volcanism, rifting and drifting. The process of rifting causes development of several structural features and sedimentary basins. The western continental margin of India, an Atlantic-type (passive), consists of several large sedimentary basins (Figure 7.1). The Bombay offshore basin is one among them with proven resource potential, while the Konkan-Kerala basin is considered as potential prospects area. An understanding of the geological processes and tectonic events, which have caused the formation of present continental margin of India in space and time, is critical for a plausible assessment of the non-living resource potentials. Detailed geological and geophysical surveys of this margin have been mostly confined to the shelf for the purpose of commercial exploration of non-living resources. Lately there is an increased quest for exploration in the deep water areas. Marine geophysical studies of the basins and structural features will also enable to unfold the untold tectonic history of a margin to a possible extent.

In this chapter, multichannel seismic (MCS) reflection data along a regional profile (SK12-07) across the western continental margin off Goa coast are analyzed to understand the depositional patterns of sediments and nature and structure of crust of the margin (Figure 7.1). The profile runs nearly perpendicular to the strike of the main structural features of the margin: the outer shelf, shelf-margin basin, the Laccadive Ridge and the eastern part of the Western Arabian Basin (WAB). The processed multichannel seismic section is analyzed to identify the seismic sequence boundaries and

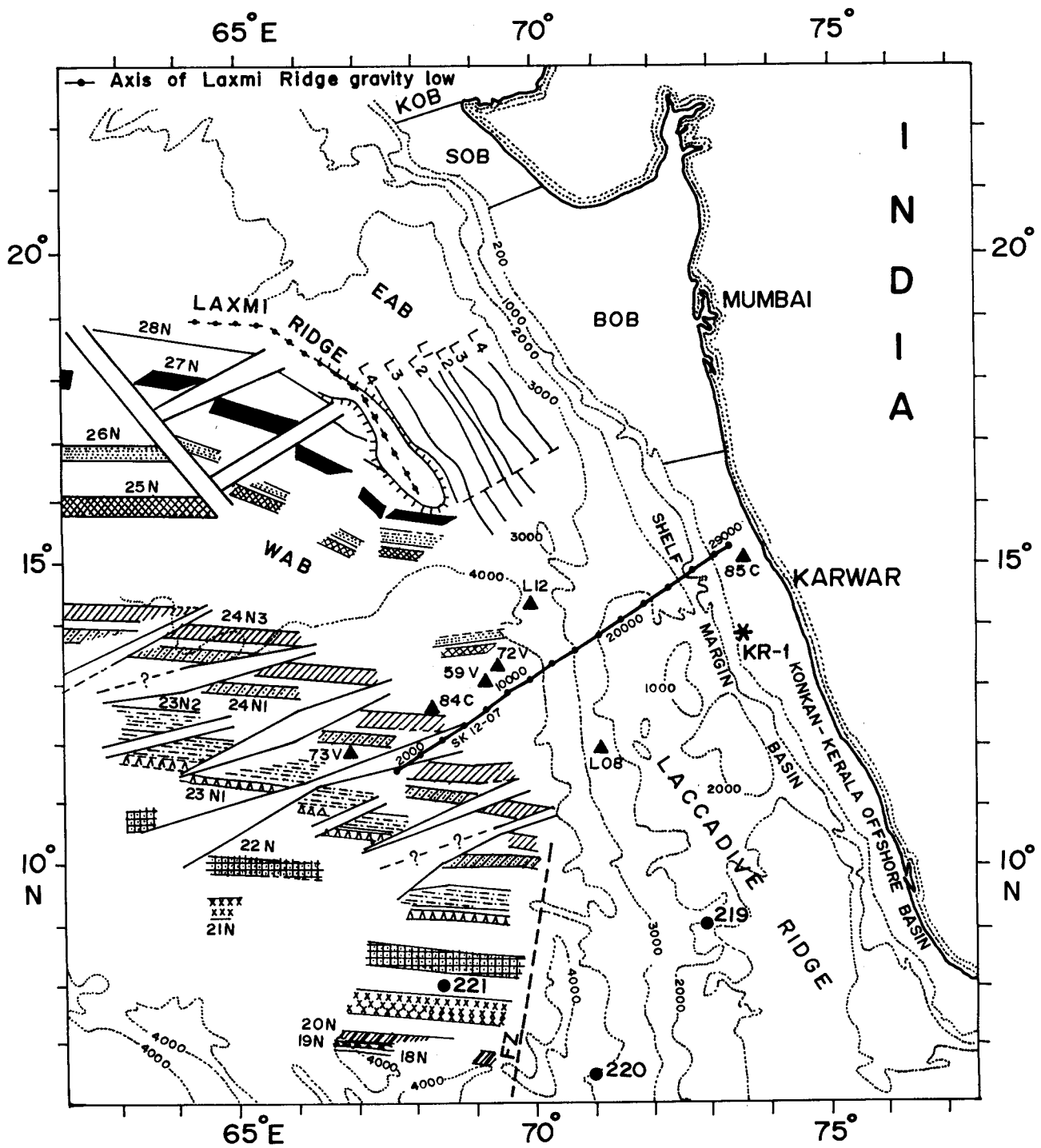

Figure 7.1 Generalized tectonic map of the Eastern Arabian Sea. Magnetic lineations (28N through 18N) are from the present study. Diagonal offsets in the magnetic lineations are interpreted pseudofaults. Dotted lines represent bathymetric contour in meters. Location of DSDP Sites (219-221) are shown as solid circles. Refraction stations (after Francis and Shor, 1966; Naini and Talwani, 1982) are shown as solid triangles. Star denotes drill-well location (KR-1). Multichannel seismic reflection profile (SK12-07) is shown as solid line with dots. EAB=Eastern Arabian Basin; WAB=Western Arabian Basin; L1-L4=Laxmi Basin magnetic lineations. KOB=Kutch Offshore Basin, SOB=Saurashtra Offshore Basin, BOB=Bombay Offshore Basin

seismic facies within seismic sequences. The seismic sequence boundaries are subdivisions of a seismic section into packages of concordant reflections separated by surfaces of discontinuity, which can be interpreted as depositional sequences. Whereas, the seismic facies, within seismic sequences, are groups of seismic reflections whose parameters (configuration, amplitude, continuity, frequency and interval velocity) differ from adjacent groups. Each parameter provides considerable information on nature, structure etc. of the reflecting surface. For example, the reflection configuration reveals a gross stratification pattern from which depositional process, erosion and paleotopography can be inferred. Reflection continuity is closely associated with continuity of strata. Continuous reflections suggest wide spread uniformly stratified deposits. Reflection amplitude contains information on the velocity and density contrast of individual interfaces/reflectors and their spacing. Frequency is a characteristic of nature of seismic pulse and is related to spacing of reflectors or lateral changes in interval velocity. The geometry and the inter-relationship of the seismic reflectors provide evidences on spatial and temporal variations in sedimentation and related tectonics.

The reflection boundaries between seismic sequences have been picked up in the basins of the study area, where thick sedimentary column is available and continued them on either side of the basinal areas, and thus lateral continuity of the sequences has been established. The bases of selection of the sequence boundaries are i) high amplitude reflector, and ii) continuous reflector marking the change in the seismic reflection pattern above and below its surface. As there is no drill-hole information available in the deep water region of the seismic profile, the results of the Deep Sea Drilling Project (DSDP) Site 219, located ~550 km south of present seismic profile on the crest of Laccadive Ridge (Figure 7.1), are considered to infer the nature and ages of the seismic sequences. Further, the seismic facies of present seismic section are compared with the published regional seismic facies results (Rao and Srivastava, 1984). The studies reveal that the pack of the sediments consists of six seismic sequences, referred as H1, H2, H3, H4, H5 and H6, H1 being the oldest. The ages are assigned to the sequence boundaries on the basis of results of drill well (KR-1) published by Oil and Natural Gas Corporation

Limited (ONGCL) located on the outer shelf of Karwar coast (Singh and Lal, 1993; Pandey and Dave, 1998) and DSDP Site 219 (Whitmarsh et al., 1974).

7.2 ANALYSIS OF SEISMIC REFLECTION DATA

The regional multichannel seismic reflection profile SK12-07 is ~720 line kilometers long and covers outer shelf, shelf margin basin, Laccadive Ridge and eastern part of the WAB. The profile is shot from west to east, that is, from deep sea to outer shelf region. The water depths along the profile vary between ~50 m on the shelf and ~4300 m in the deep sea region. In the following sections, the analysis of seismic reflection data is presented starting from outer shelf to deep sea.

7.2.1 OUTER SHELF

The outer shelf, from land to seaward side (east to west), consists of a gentle sloping continental shelf where the water depth varies from ~50 to ~200 m. The present day shelf edge, which follows ~200 m isobath, is distinct and easily discernible. On the outer shelf, the seismic sequences are identified as top of H2, H3, H4+H5 and H6 between shot points 29000 and 27000 (Figure 7.2). The thickness of sequences H3, H4+H5 and H6 vary from 0.2 to 0.7 s, 0.05 to 0.13 s, and 0.1 to 0.26 s two-way travel time (TWT) respectively. The seismic sequences H4 and H5 could not be resolved on the outer shelf, hence they are put together. The sequence H1 and the base of the sequence H2 could not be identified on the shelf area as it is highly masked with multiples. Therefore, top reflector of the sequence H2 is considered to represent the acoustic basement in this area which is distinctly uneven, high amplitude, discontinuous to continuous reflector. The sequence H3 consists of variable amplitude, nearly parallel and good to fairly good reflection continuity. Lower parasequences of the sequence H3 onlap onto the top reflector of the sequence H2. Further, a distinct change in the reflection pattern above the sequence H3 is observed, where the sequences H4+H5 display low amplitude, parallel and relatively continuous in short segments. The sequence H6 is of low amplitude and nearly acoustically transparent. The sequences

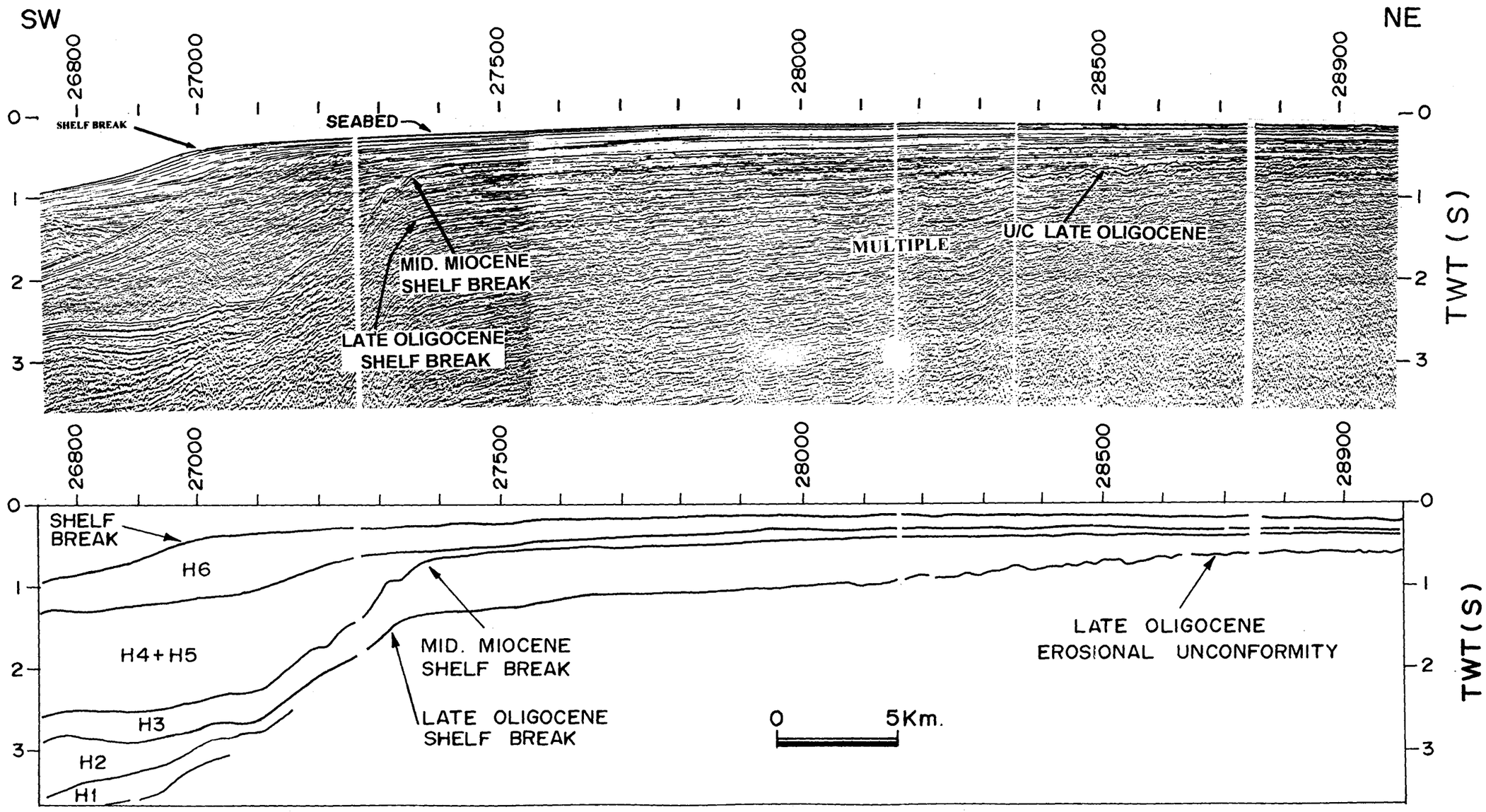

Figure 7.2 Multichannel seismic reflection record and interpreted line drawing across the outer shelf showing seismic sequences H1-H6, present and paleo-shelf breaks and Late Oligocene erosional unconformity. Location of profile is shown in Figure 7.1.

H4+H5 and H6 together indicate typical sigmoidal reflection configuration near the shelf break region indicating shelf progradation. The distinct change in the reflection pattern above sequence H3 may represent a marked change in sedimentation pattern. The observed change in the gradient of sequences H2 and H3 at shot point 27350 marks the paleo-shelf edges, whereas the change in the gradient of top of sequence H6 at shot point 27000 marks the present day shelf edge. It is ~8 km west of the paleo-shelf edge indicating that the shelf is prograded towards west by ~8 km in this area.

7.2.2 SHELF MARGIN BASIN

The sedimentary basin lying between the shelf break in the east and eastern flank of the Laccadive Ridge in the west is known as shelf margin basin which is observed between shot points 27000 and 22400 (Figures 7.3 and 7.4). The basin has a width of about 115 km on this profile. For the purpose of the present study, the shelf margin basin is divided into two parts, that are eastern and western basins separated by a flat topped structural high, also known as shelf margin high, shown between shot points 25850 and 25300 in Figures 7.3 and 7.4. The structural high rises to ~550 m from the adjacent seafloor of the eastern basin and ~1700 m from the adjacent seafloor of the western basin and modifies the continental slope.

In the eastern basin, the water depths vary between 900 and 1000 m (Figure 7.3). In this basin, seismic sequences H1, H2, H3, H4, H5 and H6 are identified. The base of sequence H1 is of high amplitude, uneven and deepens towards center of the basin. This reflector is considered as acoustic basement. Thickness of sequences H1, H2, H3, H4, H5 and H6 varies from 0.3 to 0.8 s, 0.25 to 0.9 s, 0.4 to 0.68 s, 0.45 to 0.65 s, 0.2 to 0.6 s and 0.3 to 0.48 s TWT respectively. The seismic sequence H1 consists of discontinuous reflection configuration and divergent towards center of the basin. The sequence H2 consists of discontinuous, low frequency and high amplitude reflections. Whereas the sequence H3 consists of very good to fairly good reflection continuity, high amplitude and nearly parallel. The sequence H4 consists of high amplitude, low frequency, and discontinuous reflections. While the sequence H5 consists of low

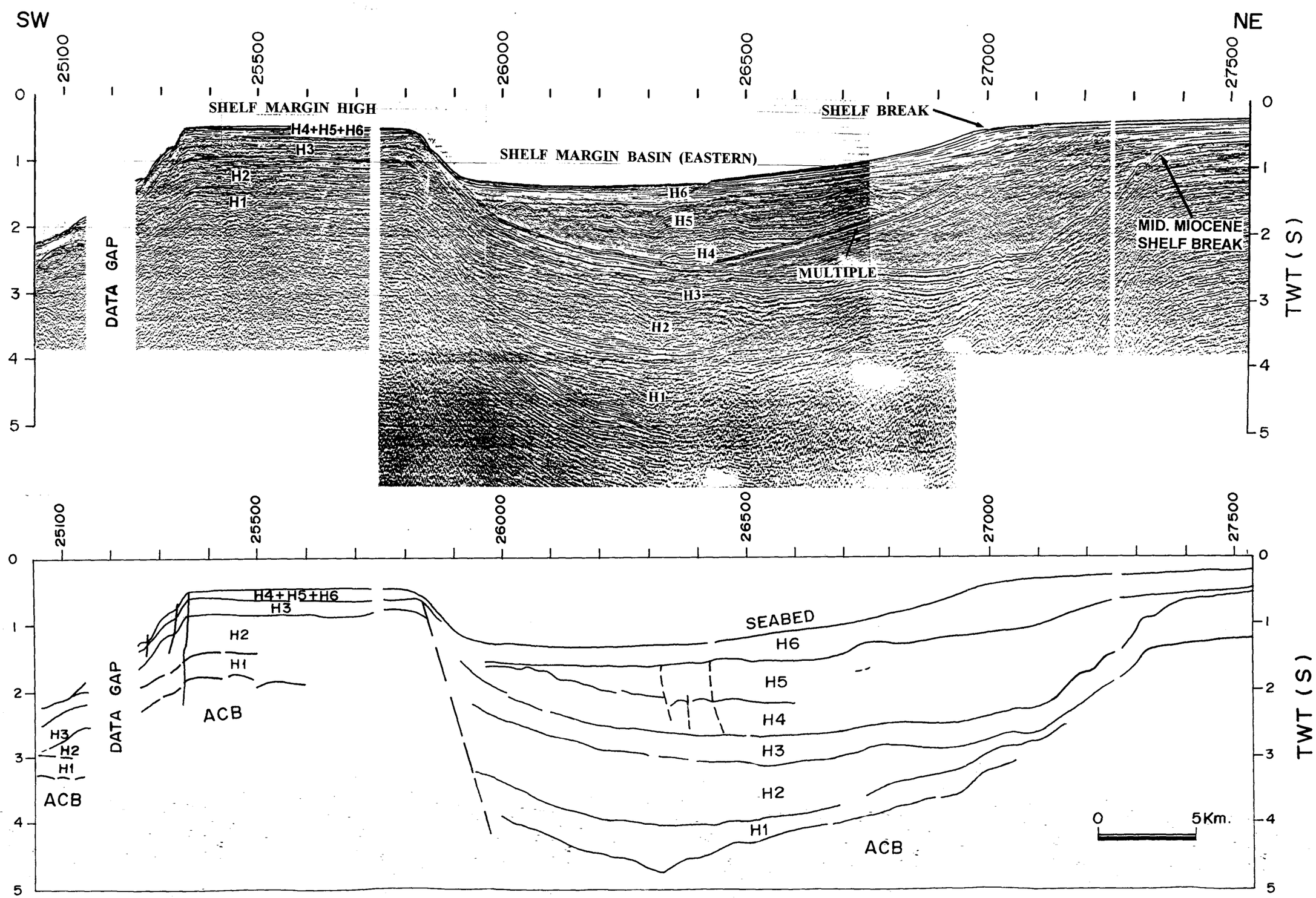

Figure 7.3 Multichannel seismic reflection record and interpreted line drawing across the shelf margin basin (eastern) showing seismic sequences H1-H6, present and paleo-shelf breaks and shelf margin high. Location of profile is shown in Figure 7.1.

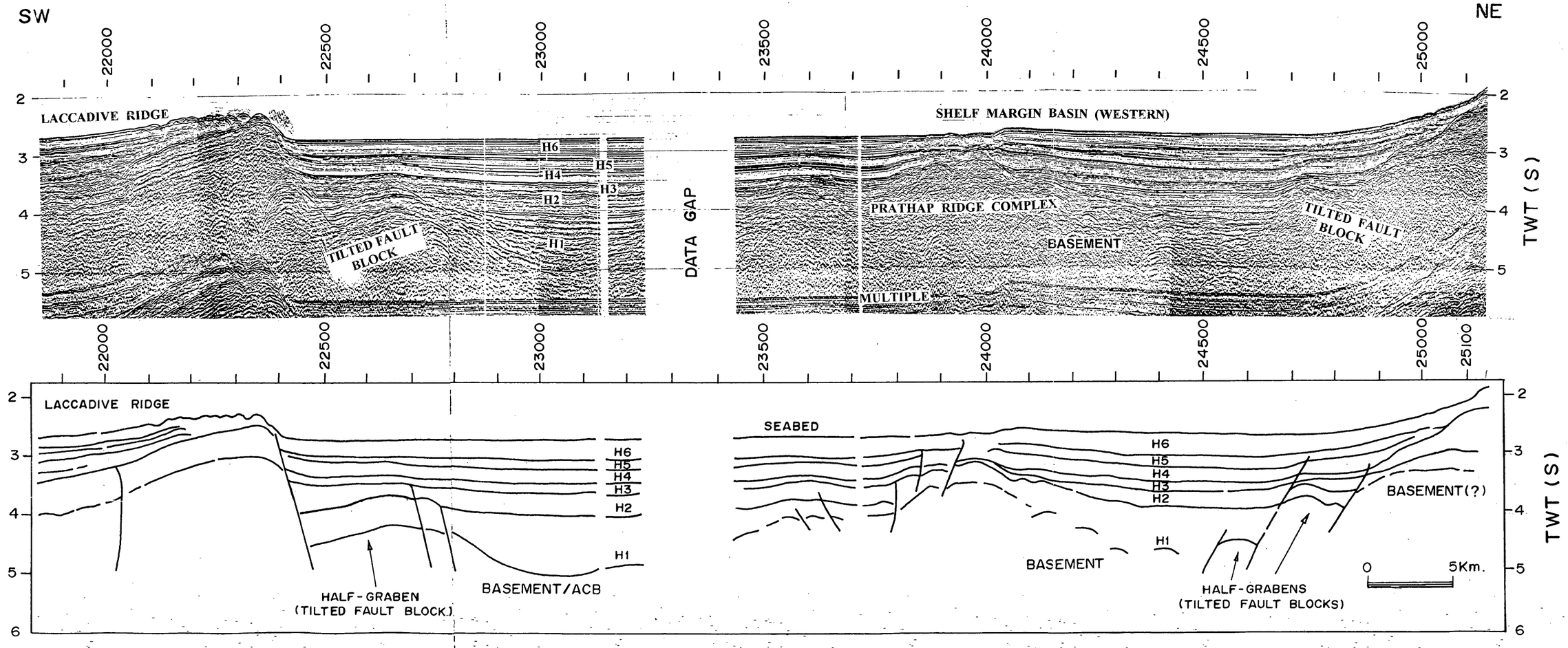

Figure 7.4 Multichannel seismic reflection record and interpreted line drawing across the shelf margin basin (western) showing Prathap Ridge Complex, half grabens (tilted fault blocks), eastern flank of the Laccadive Ridge and seismic sequences H1-H6. Location of profile is shown in Figure 7.1.

amplitude and continuous. The reflectors within sequence H5 are folded and faulted, whereas the reflectors of sequence H4 are relatively less distorted. The diffraction pattern observed near the structural high within the sequences H4+H5 may represent the slumped material from the high. The reflectors of sequence H6 are continuous and parallel.

The structural high is ~14 km wide and is bounded by near vertical faults. Over the structural high, the seismic sequences H3, H4+H5 and H6 are observed. The seismic sequences H1 and H2 over the structural high could not be traced due to the presence of multiples.

The western basin, observed between the structural high and the eastern flank of the Laccadive Ridge, is ~72 km wide in 2000 and 2100 m water depths (Figure 7.4). In this basin, seismic sequences H1, H2, H3, H4, H5 and H6 are identified. Thickness of sequences H1, H2, H3, H4, H5 and H6 varies from 0.1 to 0.9 s, 0.1 to 0.4 s, 0.1 to 0.2 s, 0.18 to 0.28 s, 0.09 to 0.2 s and 0.2 to 0.35 s TWT respectively. The reflector at the base of sequence H1 is hyperbolic with vertices at varied depths. At the eastern and western ends of the basin, tilted reflecting surfaces at about 1.1 s TWT subsurface depth are noticed. They are fault bounded and tilted away from the center of the basin (Figure 7.4). In the center of the basin between shot points 24070 and 23800, the hyperbolic reflections occur at shallow subsurface depth with a relief of ~1.6 s TWT (Figure 7.4). This rise is identified as 'Prathap Ridge Complex'. The feature was identified earlier by Naini (1980). The sequence H2 consists of low to high amplitude and discontinuous reflections. The sequence H3 consists of irregular and high amplitude reflections. The reflections mark the high energy conditions, possibly due to the turbidites. The nature of the reflectors within sequence H4, H5 and H6 vary across the basin and are weak to reflection free.

7.2.3 LACCADIVE RIDGE

The Laccadive Ridge occurs between 1650 and 2100 m water depth in the study area and is bounded on the east between shot points 22500 and 22300 by a scarp (Figure 7.4). The western end of the ridge between shot points 12400 and 12100 is marked with large positive relief (~600 m) in the seafloor topography (Figure 7.6). The ridge is ~260 km wide and gradually deepens to the west. On the ridge, seismic sequences H1 (top), H2, H3, H4, H5 and H6 are identified. The reflection patterns of these sequences differ from the pattern of the sequences on the shelf and shelf margin basin. The sequences H2, H3, H4, H5 and H6 are 0.06 to 0.2 s, 0.15 to 0.5 s, 0.09 to 0.25 s, 0.07 to 0.15 s and 0.11 to 0.24 s (TWT) thick respectively. The reflections from the basement could not be identified due to presence of interbedded multiples. A prominent reflector, characterized by high amplitude, discontinuous reflection configuration with numerous diffraction hyperbolae, is identified all along the ridge. This reflector is identified as top boundary of sequence H1 and marks high acoustic impedance contrast with overlying sediments (Figure 7.5). Below this reflector, a less distinct, parallel to sub-parallel reflection pattern is observed within the sequence H1. The sequence H2 consists of weak and discontinuous reflectors at places, otherwise it is acoustically transparent. The sequence H3 reflectors are discontinuous to chaotic and low amplitude. The sequence H4 consists of continuous, parallel and low amplitude reflection pattern, which marks a distinct change in the depositional environment above sequence H3. The sequence H5 is acoustically transparent except the upper part of it, which consists of near parallel, continuous and high amplitude reflectors. The reflectors of sequence H6 are weak and discontinuous in a limited extent otherwise they are acoustically transparent.

On the crest of the Laccadive Ridge, two low relief axial graben like features associated with block faulting are observed, one of them lie between shot points 18800 and 18400 (Figure 7.5). Most of the seismic sequences occur within the grabens. Besides, two structural highs are observed towards the western end of the Laccadive Ridge between shot points 14300 and 13700, and 12600 and 12100 below thin veneer

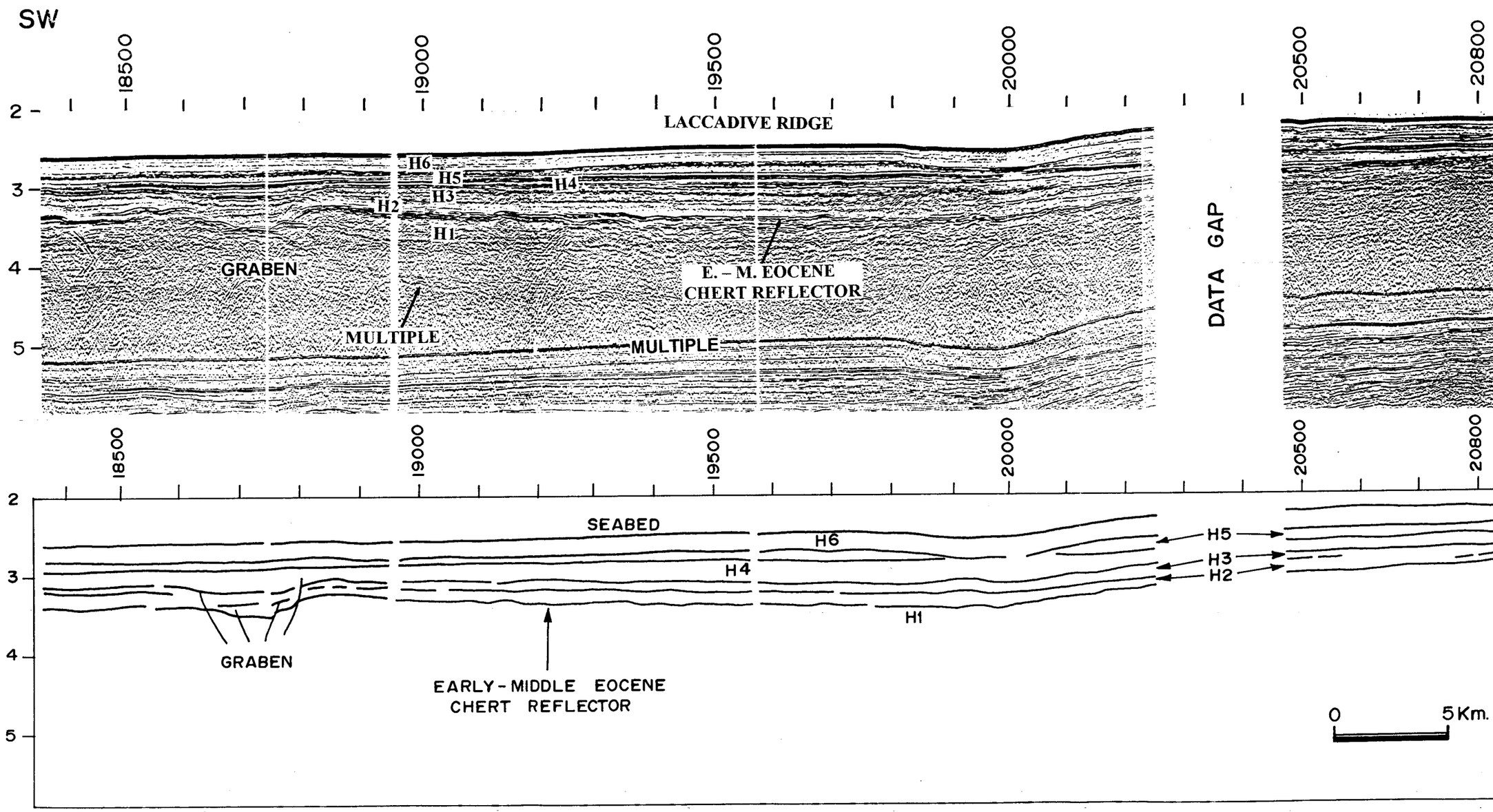

Figure 7.5 Multichannel seismic reflection record and interpreted line drawing over the Laccadive Ridge showing seismic sequences H1-H6, graben like feature and prominent Early-Middle Eocene chert reflector. Location of profile is shown in Figure 7.1.

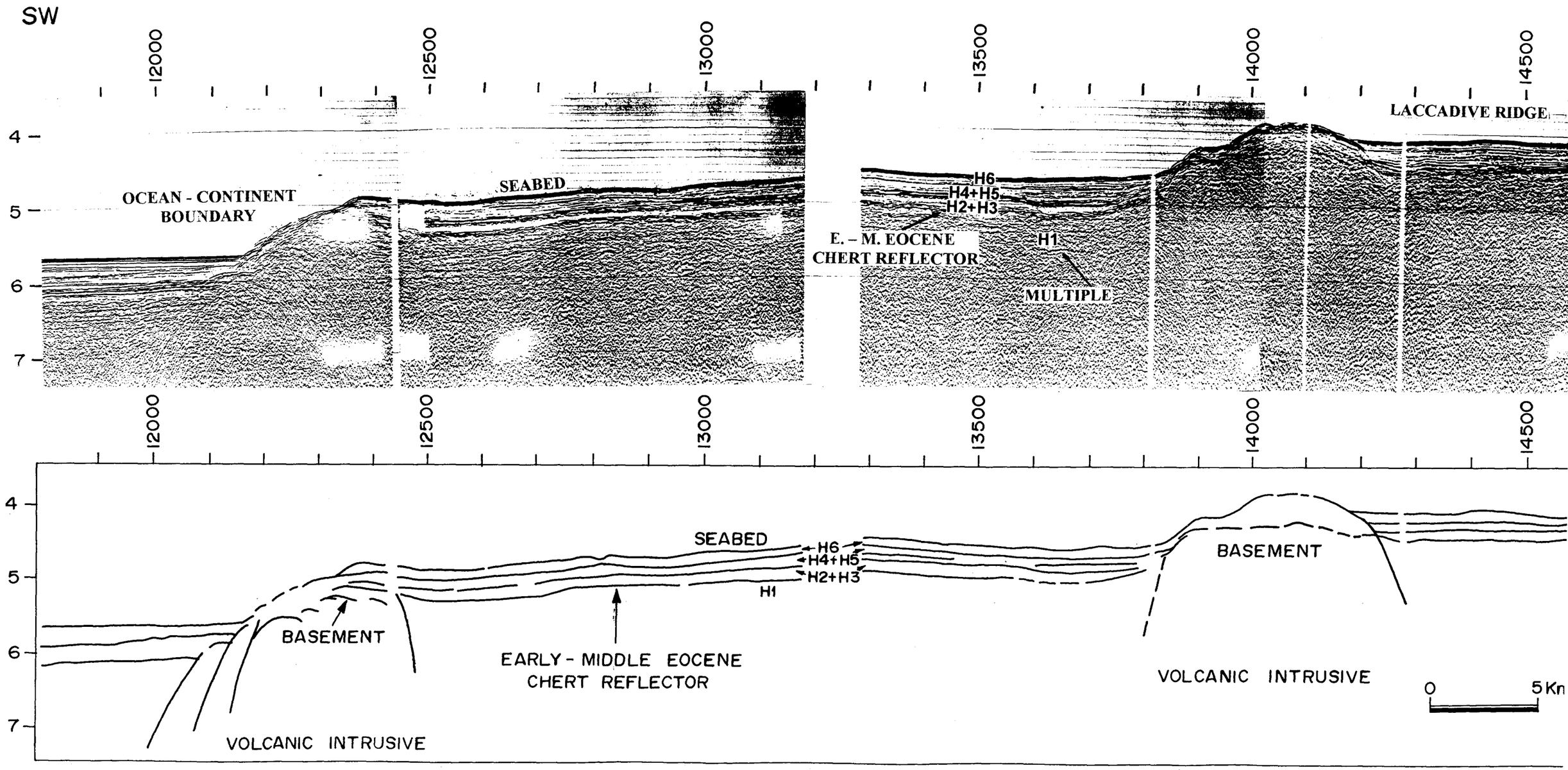

Figure 7.6 Multichannel seismic reflection record and interpreted line drawing towards seaward edge of the Laccadive Ridge showing seismic sequences H1-H6, prominent Early-Middle Eocene chert reflector, volcanic intrusives and inferred ocean-continent boundary. Location of profile is shown in Figure 7.1.

of sediments (Figure 7.6). Between shot points 20300 to 19800 the sequence H5 is eroded and, thus, form two lens shaped structures between shot points 20600 to 20000, and 19900 to 19100 on either side of the erosional feature. It is 25-30 km wide and is overlain by sequence H6. The feature is even seen in the seabed topography as bathymetric low of 100 to 110 m. The feature is most probably due to erosion resulted from paleo-contour currents paralleling the ridge and is visible even in the present day seafloor topography. The transition from the western extremity of the Laccadive Ridge with the WAB is marked by a steep fall (~600 m) in seafloor topography.

7.2.4 WESTERN ARABIAN BASIN

The Western Arabian Basin (WAB), west of the Laccadive Ridge, lies between water depths of 4200 and 4300 m water depth along the profile (Figures 7.6 and 7.7). The seismic section in the WAB is not interpreted in terms of seismic sequences as the depositional environment significantly differs from the regions described earlier. Nevertheless, it consists of two well-defined units. The lower part is separated from the upper part by a reflector of medium to low amplitude reflections and denoted by 'R'. In this basin, the reflectors are nearly parallel, continuous, high to medium amplitude (Figure 7.7). The reflectors of the upper part onlap onto reflector 'R' (Figure 7.6) all along this basin. Thus, the reflector 'R' marks a boundary separating the lower and upper seismic sequences. The basement in the WAB mostly consists of high amplitude, hyperbolic and discontinuous reflections, indicating that the basement is oceanic in nature. However, at places the reflection patterns are discontinuous and high amplitude associated with diffraction and appear to be similar to the reflections of the H1 top observed over the Laccadive Ridge. The sediments carpeting the basement are ~1.2 s TWT maximum thick.

7.3 INTERPRETATION

The most prominent structures on the seismic section along profile SK12-07 are i) paleo-shelf edge, ii) present day shelf edge, iii) shelf margin basin, iv) Prathap Ridge,

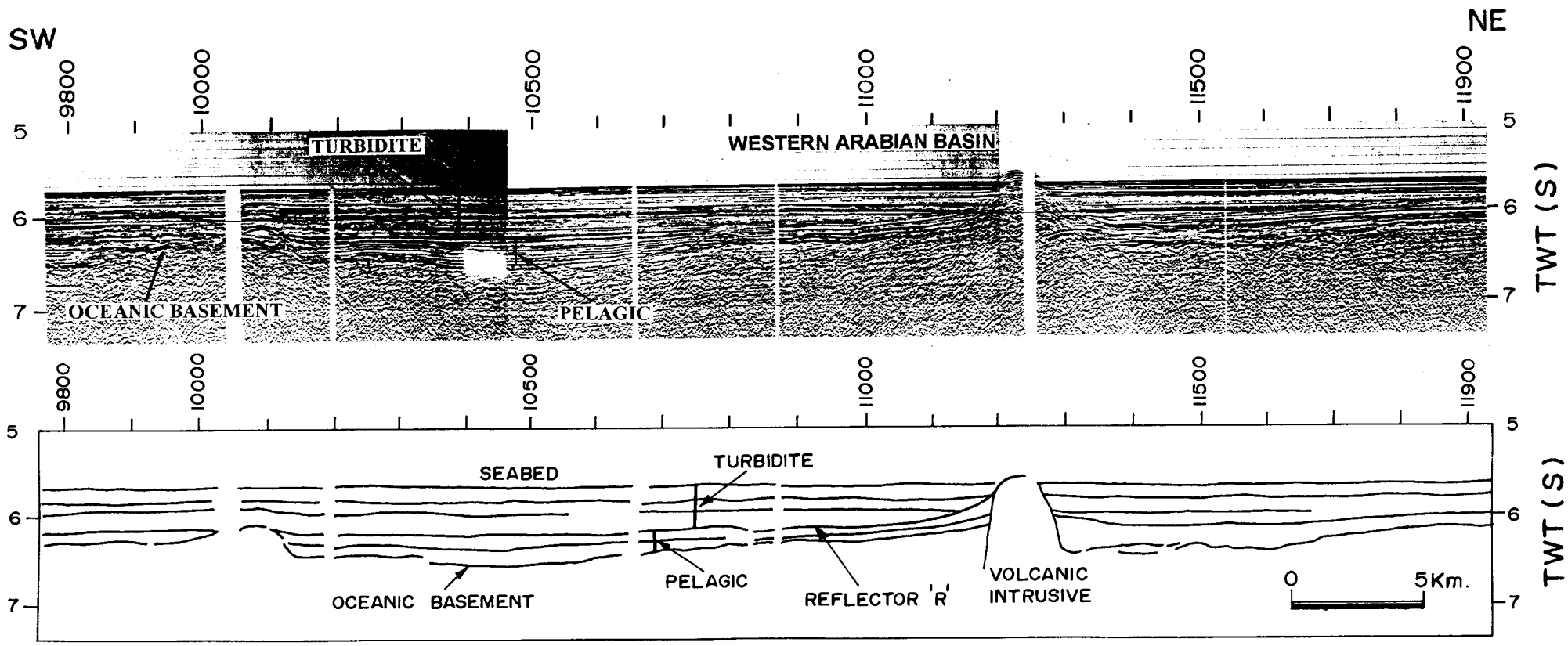

Figure 7.7 Multichannel seismic reflection record and interpreted line drawing across the Western Arabian Basin showing oceanic basement, pelagic and turbidite sediments separated by reflector 'R' of Middle-Late Oligocene age. Location of profile is shown in Figure 7.1.

v) Laccadive Ridge, and vi) WAB, west of the Laccadive Ridge. They can be grouped broadly into three major tectonic zones: i) the outer shelf and shelf margin basin, ii) the Laccadive Ridge and iii) the WAB. In all the tectonic zones except the WAB, six major seismic sequences H1, H2, H3, H4, H5 and H6 are identified where H1 is the oldest. The ages for these sequences have been assigned following i) the published litho-stratigraphic results of Konkan-Kerala shelf (Singh and Lal, 1993; Pandey and Dave, 1998), ii) correlating the identified seismic sequence boundaries with global sealevel curve (Haq et al., 1987), and iii) the published results of DSDP Site 219. The correlated sequences boundaries using above criteria are shown in Figures 7.8 and 7.9. Thus, the sequences H1, H2, H3, H4, H5 and H6 may represent Paleocene to Late Eocene, Late Eocene to Late Oligocene, Late Oligocene to Middle Miocene, Middle Miocene to Middle Pliocene, Middle Pliocene to Late Pleistocene and Late Pleistocene to Recent respectively. Wherever, the crystalline or volcanic basement could not be identified, the lower most reflector is denoted as the acoustic basement and interpreted as the lower boundary of sedimentary column. The crystalline basement along the profile is identified in a part of shelf margin basin and the WAB. The basement could not be identified on the shelf and on the Laccadive Ridge because of the interference from multiples.

It is observed that the sedimentation pattern in the tectonic zones is not the same. In the shelf margin basin, the sediment is ~3.55 s TWT maximum thick. Whereas, it is 0.9 s and 1.2 s TWT over the Laccadive Ridge and the WAB respectively. In the following sections, the seismic results are interpreted starting from outer shelf to deep sea.

7.3.1 SHELF AND SHELF MARGIN BASIN

One of the important feature of the shelf and shelf margin basin is the paleo-shelf edge which is prograded seaward side by ~8 km from the present day shelf edge. It is referred as the Middle Miocene paleo-shelf edge on correlation with the published results (Ramaswamy and Rao, 1980; Biswas and Singh, 1988; Singh and Lal, 1993). The reflector depicting the paleo-shelf edge, top of seismic sequence H3, is very distinct

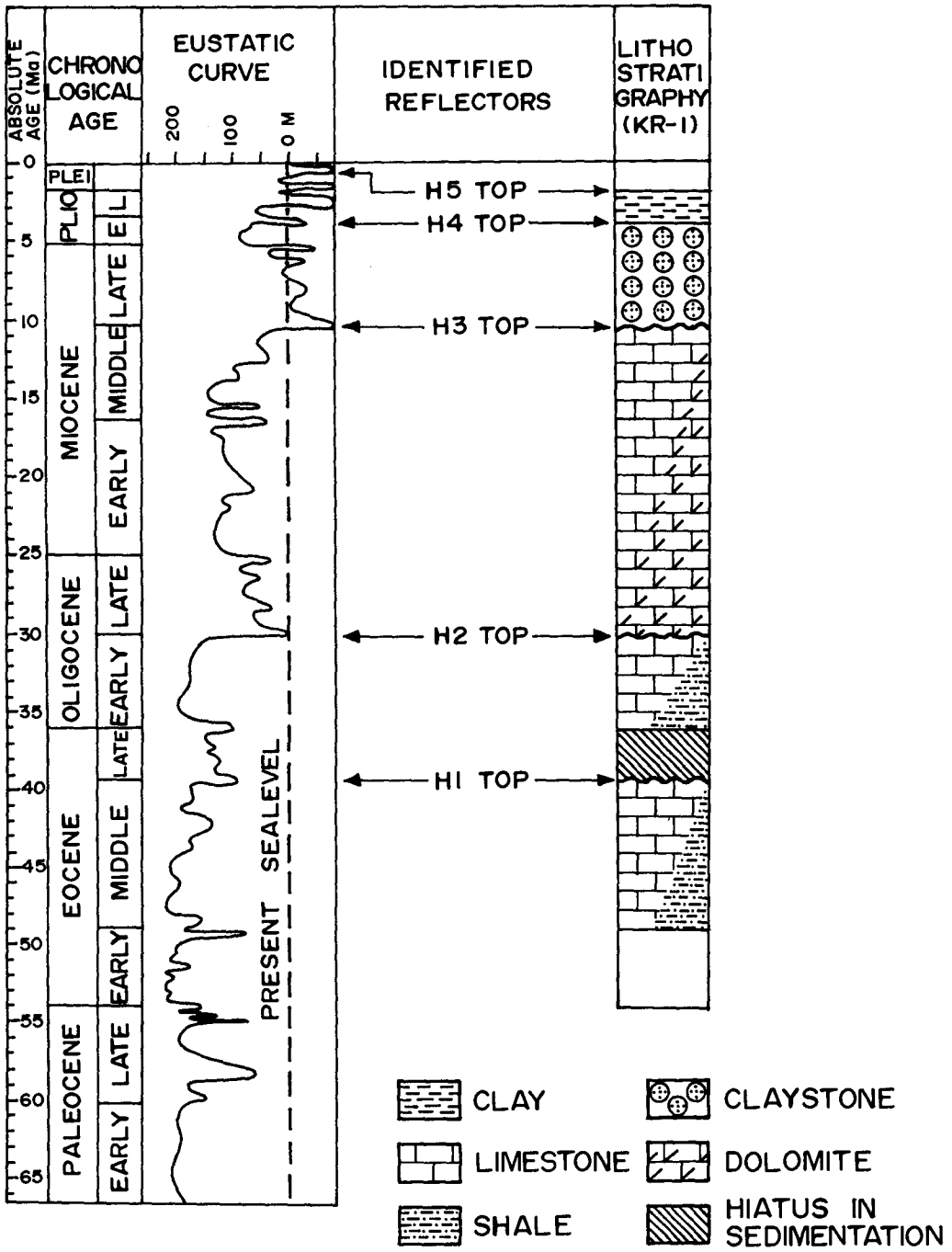

Figure 7.8 Correlation of seismic sequences (H1-H5) of the present study with the published lithostratigraphy (after Singh and Lal, 1993; Pandey and Dave, 1998) and Eustatic sealevel curve (after Haq et al. 1987).

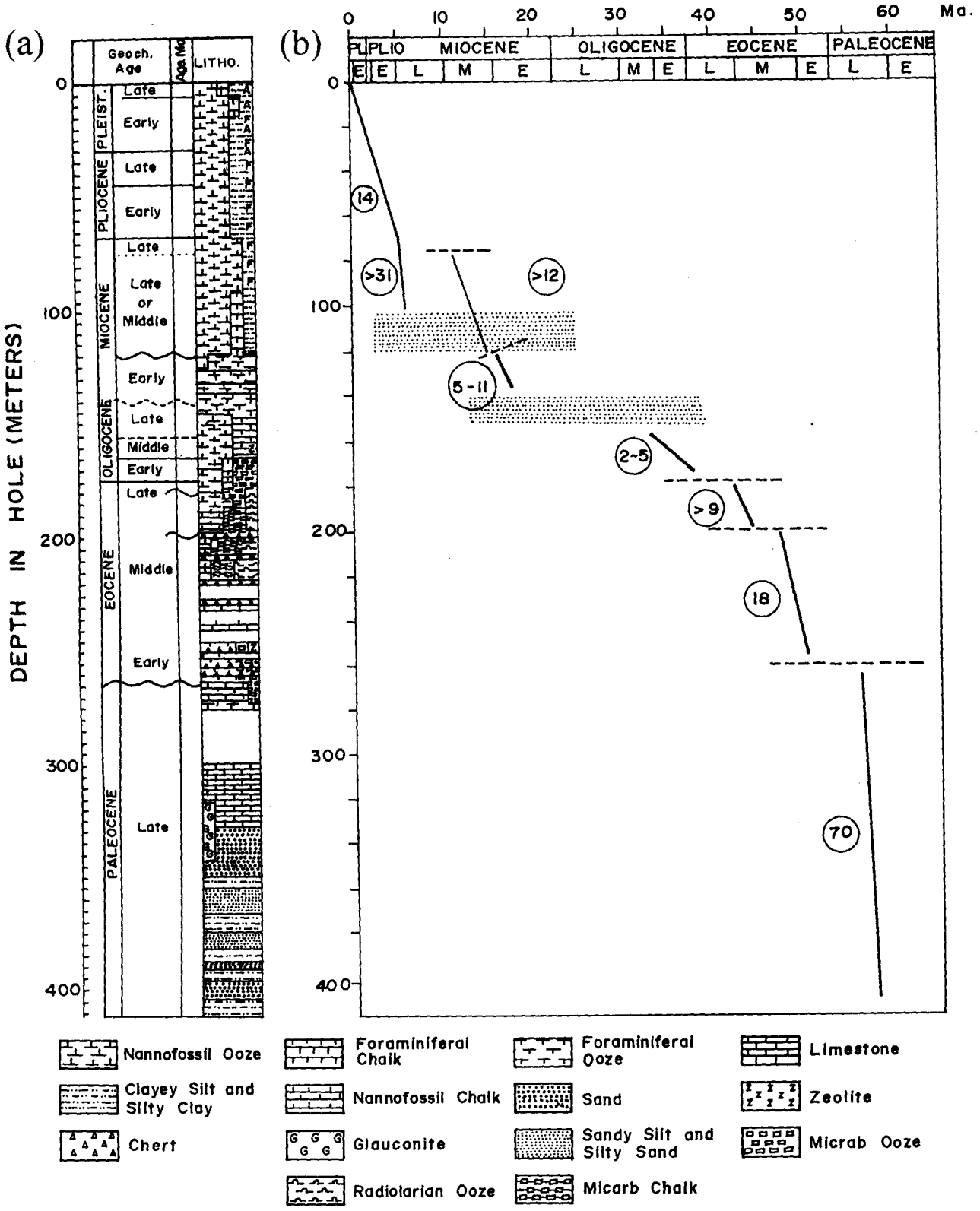

Figure 7.9 (a) Lithostratigraphy and (b) sedimentation rate curve at DSDP Site 219 (after Whitmarsh et al. 1974). In the sedimentation rate curve, the stippled pattern shows uncored intervals and values inside the circle represent sedimentation rate in meters/million years.

and marks change from continuous parallel to acoustically transparent reflections above it to low frequency, high amplitude, discontinuous reflection pattern of the underlying sequences (Figures 7.2, 7.3 and 7.4). The age of the top of sequence H3 is therefore inferred as the Middle Miocene. It forms a well defined boundary of the sequences and constrain the seismic stratigraphy determination in the study area. This change in the reflection pattern suggests a change in the depositional environment also. Increased precipitation is a general phenomenon due to intense Indian monsoon during post Middle Miocene. It might have resulted in enhanced weathering and erosion of the onshore areas and larger terrigenous sediment flux in to the eastern Arabian Sea. Deposition of the resulting clastics onto the western margin of India might has resulted in decrease of the relative carbonate deposition. Thus, it is possible to distinguish from reflection pattern itself carbonate-dominated sediments of the Late Paleocence to Middle Miocene, to terrigenous-dominated sediments of the Late Miocene to Recent. The change from carbonate to terrigenous dominated sedimentation appears to be related to regional changes in climate during the post-Middle Miocene. Earlier studies (Rao and Srivastava, 1984; Nair et al., 1992; Singh and Lal, 1993; Whiting et al., 1994) suggested that i) the Upper Paleocene to Late-Middle Miocene sequence consists of marine carbonates with interspersed shale layers, and ii) an episode of clastic-dominant margin growth during post Middle Miocene (Figure 7.8).

Moreover, the chaotic reflection pattern of sequence H3 especially in the western part of the shelf margin basin reflects the high energy conditions and rapid sediment flux. It leads to suggest that the sequences overlying H3 consist of mainly clastic sediments and below it are carbonate dominant sediments. Due to heavy influx of clastic sediments, a thick pack of prograded sediments has piled up in the slope region resulting in seaward progradation of shelf edge and sigmoidal reflection pattern in the area.

Another prominent reflector, H2 top below the sequence H3, is identified on the shelf and in the shelf margin basin. This reflector at about 0.35 s depth on the outer shelf is uneven and discontinuous. The parasequences of sequence H3 onlap onto it (Figure 7.2). Due to onlapping nature of the reflectors onto this surface, H2 top is inferred as

erosional unconformity. At the shelf edge region, it marks the paleo-shelf edge. Considering the refraction results of Site 85C (Figures 7.1 and 7.2) and TWT for H2 top, the estimated depth of H2 top below the present sea level is ~450 m. The surface might be exposed to sub-areal or wave base erosion. The Late Oligocene age of the unconformity is suggested for the sequence boundary underlying the H3 sequence. Haq et al. (1987) have interpreted major drop in eustatic sea level (~200 m) at the end of Lower Oligocene (Figure 7.8). Whiting et al. (1994) inferred a characteristic Late Oligocene to Early Miocene rapid increase in subsidence rate of this margin based on subsidence curves obtained from drill-holes of the shelf region of western continental margin of India. Subsequent sedimentation during transgressive sealevel has given rise to the onlapping sequences. The seismic section of continental shelf and slope region (Figure 7.2), thus, shows three distinct shelf edges; Late Oligocene, Middle Miocene and Present. There is no lateral shift in the location of the Late Oligocene to Middle Miocene shelf edges. The Late Oligocene to Middle Miocene sediment deposition of shelf and slope region inferred from the present studies corresponds to an aggradational phase. Whereas, the Middle Miocene to Recent sedimentation is dominated by progradation.

The reflection pattern of sequences H1 and H2 appears to be similar to the reflection pattern of the sequence II of Rao and Srivastava (1984). Based on interval velocities, they opined that the sequence II may represent carbonate sedimentation and was developed during stable platform conditions. Widespread formation of carbonate sediments was facilitated by less clastic inputs during the Middle to Late Eocene (Nair et al. 1992). The drill well KR-1 on the shelf of Karwar coast shows Eocene to Middle Miocene limestone, shale and sandstone (Singh and Lal, 1993) (Figures 7.1 and 7.8). Aubert and Droxler (1996) have reported temperate climate during the Paleocene and Eocene times which facilitated the accumulation of thick shallow water carbonates along the western continental margin of India and Maldives. The discontinuous, low frequency and high amplitude reflection of the seismic sequences H1 and H2 represent the carbonate accumulation during stable platform conditions. In view of the results and observed reflection pattern in the shelf margin basin, sequence H1 is most likely

limestone sequences and the sequence H2 is alternate bands of limestone and shale. Singh and Lal (1993), based on drill well (KR-1) results, have inferred that end of the Middle Eocene and the Early Oligocene are marked by regional hiatuses. A well-developed regional unconformity of Oligocene age has been reported by Gopala Rao et al. (1997) in the Bay of Bengal and attributed its development due to eustatic sea level changes. As mentioned earlier, the hiatus at the close of the Early Oligocene is identified as the Late Oligocene unconformity, H2 top. Therefore, the prominent top reflector of seismic sequence H1 underlying sequence H2 appears to be of Late Eocene age.

The seismic sequences H4 and H5 of the shelf margin basin, overlying the Middle Miocene (H3 top) reflector, consist of parallel reflectors. The sediment of these sequences are most likely deposited in relatively low energy and high stand oceanographic conditions during the post Middle Miocene. They have been inferred as clastics. Based on mass accumulation rates of the terrigenous component of the deep sea sediments found in the DSDP and Ocean Drilling Program (ODP) sites in the northern Indian Ocean, Rea (1992) has inferred two distinct sediment influx maxima in the Late Miocene (9-6 Ma) and Middle Pliocene (4-2 Ma). Stow et al. (1990), based on facies analysis of sediments of closely spaced ODP Leg 116 Sites in the distal Bengal Fan, suggested another phase of major Himalayan uplift during the Upper Pleistocene (~1.0 Ma). Considering the results, eustatic sealevel curve of Haq et al. (1987) and drill-hole results of Site KR-1, it is inferred that the top reflector of sequences H4 and H5 may represent the Middle Pliocene and Late Pleistocene ages respectively (Figure 7.8). It may be noted that the reflectors of H4 and H5 sequences in the eastern basin are folded and faulted. The sequence H5 is extensively folded and faulted, whereas, the underlying sequence H4 is relatively less distorted. The sequence H6 overlying the sequence H5 consists of near parallel continuous reflectors and devoid of these features. In general, the sediments of shelf margin basin have been deposited in two different environments. A stable shallow water platform conditions with less clastic inputs has facilitated the carbonates deposition during Eocene-Oligocene. A high terrigenous flux has influenced the margin due to Indian monsoon and subsiding shelf during post Middle Miocene. The shelf margin high might have acted as a barrier for westward flow of the increased

clastics during the post Middle Miocene period. The subsiding basin could not keep pace with the increased sedimentary input particularly after Middle Pliocene. As a result the sedimentary sequences are folded and faulted which are well reflected in parasequences of sequence H5 compared to the sequence H4.

7.3.2 LACCADIVE RIDGE

Correlations of the seismic sequences of the Laccadive Ridge with that of the shelf and shelf margin basin have been attempted due to similarities among them, eventhough they are quite apart and separated by the shelf margin basin. As discussed earlier, the top of the seismic sequence H1 over the Laccadive Ridge is a very prominent reflector due to its high acoustic impedance contrast with the overlying sediments and is easily identifiable across the ridge. The summary report of DSDP Site 219 depicting lithological units, ages and unconformities along with sedimentation rates are shown in Figure 7.9. The results of drilling have indicated chert layer of the Early and Middle Eocene age with a P-wave velocity of ~4.0 km/s (Whitmarsh et al., 1974). This layer is similar in reflection pattern to the top of seismic sequence H1 observed in the study area. Considering the reflection pattern of the present seismic section and published P-wave velocity over the Laccadive Ridge (Naini and Talwani, 1982), Early-Middle Eocene age is assigned to the top boundary of the sequence H1 and identified as chert reflector. Numerous diffraction hyperbolas observed along the surface suggests a highly irregular surface. The deeper less distinct reflections, observed below the top boundary of sequence H1 over the ridge, is attributed to the shallow water Paleocene sandstone/conglomerate on correlation with the results of the DSDP Site 219. The chert reflector over the Laccadive Ridge is considered to represent acoustic basement as the deeper reflections are possibly masked by presence of interbedded multiples. Therefore, depth to the crystalline basement is still unknown. However, considering the refraction results over the ridge (Naini and Talwani, 1982) at Sites L08 and L12 (Figure 7.1), it is inferred that the basement may lie at ~1.7 km depth below the chert reflector in this area.

The reflection pattern of sequence H2 is different from the underlying sequence H1. The top reflector of the sequence H2 is characterized by relatively high amplitude and continuous reflections. The Late Oligocene is marked by a major fall in the eustatic sealevel and change in sedimentation pattern. It has resulted in an erosional unconformity, H2 top of the shelf area. It is quite likely that the H2 top over the ridge represent Late Oligocene unconformity. Whitmarsh et al. (1974) has speculated an unconformity at the end of Oligocene. Due to non-recovery of drilled sediments of the period, they were unable to confirm its exact age. The overlying thin seismic sequence H3 indicate very less sedimentation. This observation is well supported by less sedimentation rate observed in the Late Oligocene to Middle Miocene period. Therefore, Middle Miocene age can be assigned to the top of the H3 sequence which is also a prominent reflector in the shelf and shelf margin basin representing an unconformity. As discussed earlier that two post Miocene sediment influx maxima have occurred during the Middle Pliocene and Late Pleistocene in the Arabian Sea and the Bay of Bengal. Therefore, the post Middle Miocene seismic sequences i.e. H4 and H5 observed over the ridge may correspond to the Middle Pliocene and Late Pleistocene respectively.

The graben like feature observed on the crest of the Laccadive Ridge system perhaps reflects the faulting. Whitmarsh et al. (1974) and Gopala Rao et al. (1987) indicated the presence of steep offsets in the chert reflector. They concluded that these features are possibly caused by draping of chert reflector over the pre-existing rough topography, the greater relief of which was attributed to the vertical offsets of the fault zones. Their inferences is further supported by the presence of several seabed scarps with NNE trend at Site 219.

7.3.3 WESTERN ARABIAN BASIN

The hyperbolic reflections associated with the basement in the WAB suggest oceanic basement, which is well supported by identification of the Early Tertiary magnetic lineations as discussed in Chapter 4. However, at places to the east of the

WAB, the reflection patterns appear to be similar to that identified due to chert reflector over the Laccadive Ridge. The DSDP Site 220 investigations in the WAB inferred oceanic basalt immediately below the chert reflector. This leads to suggest that even though the oceanic basement at places is not reflected in the seismic section, it is expected to lie just below the chert layer masking reflections of the real basement. As mentioned earlier the sedimentary column in the WAB is divided into two parts by a reflector 'R'. This reflector marks a major unconformity surface in this basin. According to the results of the DSDP Site 221, lying much south of the SK12-07, illite-rich sediments characteristic of Indus Fan sedimentation started depositing in the distal Arabian Sea by the Middle-Late Oligocene (Weser, 1974). Considering the Late Paleocene-Early Eocene age of the oceanic crust and deposition of Indus Fan sedimentation during the Middle-Late Oligocene, it is inferred that the reflector 'R' may represent the Middle-Late Oligocene age. Earlier Patriat and Achache (1984), Patriat and Segoufin (1988), and Royer and Sandwell (1989) have suggested that the hard collision between the Indian and the Eurasian plates occurred during the Middle Eocene. This might have resulted in the formation and initial uplift of the Himalayas. Since then, several other episodes of Himalayan uplift occurred (Valdiya, 1984; Kolla and Coumes, 1987; Cochran, 1990; Stow et al., 1990). The time difference (~9 m.y.) between initial uplift and the Indus Fan sedimentation appears to be related to the development of the drainage system for the transportation of detritus sediments onto the fan area. Considering DSDP results (Whitmarsh et al., 1974), it is inferred that the sediments below reflector 'R' are deposited due to pelagic sedimentation and the sediments above reflector 'R' are turbidites deposited due to the Indus Fan sedimentation.

CHAPTER 8

CHAPTER 8

EVOLUTION AND TECTONIC HISTORY OF THE EASTERN ARABIAN SEA SINCE THE EARLY TERTIARY

The present marine geophysical investigations have revealed the crustal structure of the western continental margin of India along profile SK12-07 and the seafloor spreading in the Western Arabian Basin. The crust of the margin is mantled by the sediments of six seismic sequences of Paleocene to Late Eocene, Late Eocene to Late Oligocene, Late Oligocene to Middle Miocene, Middle Miocene to Middle Pliocene, Middle Pliocene to Late Pleistocene and Late Pleistocene to Recent including three unconformities. The Late Eocene, Late Oligocene and Middle Miocene unconformities are inferred due to the Indian and Eurasian plate collision, eustatic sealevel changes and Himalayan orogeny. The sediments of the area to the west of the Laccadive Ridge consist of pelagic overlain by turbidites.

The detail marine magnetic investigations of the Western Arabian Basin have revealed i) the Early Tertiary linear magnetic lineations 28N (~63 Ma) through 18N (~39 Ma), ii) the half spread rates varying from 6.0 to 1.0 cm/yr, iii) paleo-propagators and iv) pause or slow spread rates between Middle Eocene and Early Oligocene. The Reunion hotspot and collision of Indian and Eurasian plates have influenced the spread rates and accretionary processes of the crust of the Western Arabian Basin. The results are utilized to interpret the nature, origin and evolution of the crust of the Eastern Arabian Sea.

8.1 NATURE AND ORIGIN OF THE WESTERN ARABIAN BASIN

The Western Arabian Basin is underlain by oceanic basement where well developed Early Tertiary linear magnetic anomalies 28N (~63 Ma) through 18N (~39

Ma) are identified and presented in Chapter 4. The crustal structure along profile SK12-07, based on analysis of multichannel seismic reflection data and two-dimensional gravity model studies, is presented in Chapter 6. The interpreted crustal model of the Western Arabian Basin suggests that the maximum sediment thickness is ~1.4 km and the oceanic crustal thickness (layer 2 + layer 3) varies between 5.0 and 7.0 km. The oceanic crustal and velocity structure published by Raitt (1963), Shor et al. (1970) and White et al. (1992) have been compiled and presented in Table 8.1. It revealed that the normal oceanic crust consists of three distinct layers 1, 2 and 3. Layer 1 consists of variable thickness of sediments which was not listed in the Table 8.1. Layer 2 exhibits a wide range of seismic velocities and is commonly identified as the extrusive basaltic lavas and dikes formed at the spreading center. Layer 3 consists of gabbroic rocks underlying the diabase and exhibits consistent seismic velocities between 6.5 and 7.2 km/s. Comparison of the 5-7 km igneous crustal thickness inferred from the present study with that of other areas of the world oceans (Table 8.1) reveals a normal oceanic crustal structure of the Western Arabian Basin. Further, nearby seismic refraction stations (59V, 84C, 73V) along profile SK12-07 in the area reveal P-wave velocity of 1.7-3.7 km/s for Layer 1, 5.5-5.7 km/s for Layer 2, and 6.6 km/s for Layer 3 (Figures 8.1 and 8.2). This indicates that Layer 3 in the Western Arabian Basin exhibits consistent seismic velocities and lies within the P-wave velocity bounds for normal oceanic crust. Whitmarsh et al. (1986) suggested that the presence or absence of Layer 3 velocities is widely recognized as a good discriminant between normal oceanic and thinned continental crusts.

8.2 NATURE AND ORIGIN OF THE LACCADIVE RIDGE

The interpreted crustal model (Figure 6.10 of Chapter 6) has revealed that maximum igneous crustal thickness over the ridge is ~17 km which is overlain by sediments of ~2.5 km maximum thickness. The P-wave velocities at refraction stations L08, L12 and 72V, located on the ridge, vary between i) 1.6 and 4.4 km/s in sedimentary column, ii) 5.5 and 5.7 km/s within upper crust, iii) 6.3 and 6.4 km/s within middle crust, and iv) 7.2 and 7.3 km/s within the lower crust (Figures 8.1 and 8.2).

Table 8.1 Compilations of normal oceanic crustal structure from the world oceans.

Crustal layers	P-wave velocity	Thickness (km)	References
Layer2	5.07±0.63	1.71±0.75	Raitt (1963) (Atlantic, Indian and Pacific Oceans)
Layer3	6.69±0.26	4.86±1.42	
Mantle	8.13±0.24		
	Igneous Crustal Thickness=6.57±1.61 km.		
Layer2	5.19±0.64	1.49±0.98	Shor et al. (1970) (Pacific Ocean)
Layer 3	6.81±0.16	4.62±1.30	
Mantle	8.15±0.30		
	Igneous Crustal Thickness=6.11±1.63 km.		
Layer2	2.5 to 6.6	2.11±0.55	White et al. (1992) (Updated mean oceanic crustal structure from world oceans)
Layer3	6.6 to 7.6	4.97±0.90	
Mantle	> 7.6		
	Igneous Crustal Thickness=7.08±0.78 km. **External bounds: 5 to 8.5 km.**		

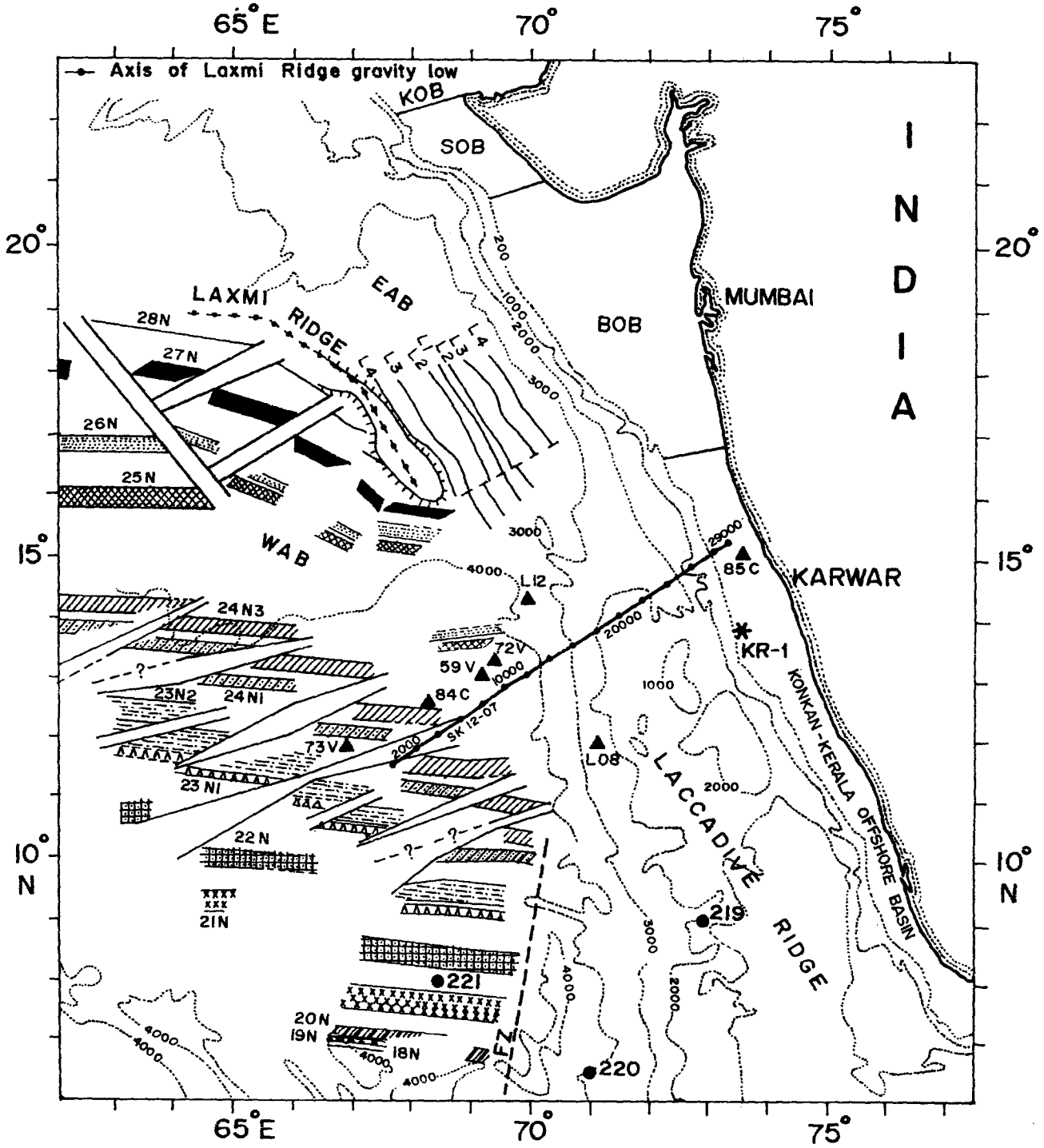

Figure 8.1 Tectonic map of the Eastern Arabian Sea. Magnetic lineations (28N through 18N) are from the present study. Diagonal offsets in the magnetic lineations are interpreted pseudofaults. Dotted lines represent bathymetric contour in meter. Location of DSDP Sites (219-221) are shown as solid circles. Refraction stations (after Francis and Shor, 1966; Naini and Talwani, 1982) are shown as solid triangles. Star denotes drill-well location (KR-1). Multichannel seismic reflection profile (SK12-07) is shown as solid line with dots. EAB=Eastern Arabian Basin; WAB=Western Arabian Basin; L1-L4=Laxmi Basin magnetic lineations. KOB=Kutch Offshore Basin, SOB=Saurashtra Offshore Basin, BOB=Bombay Offshore Basin.

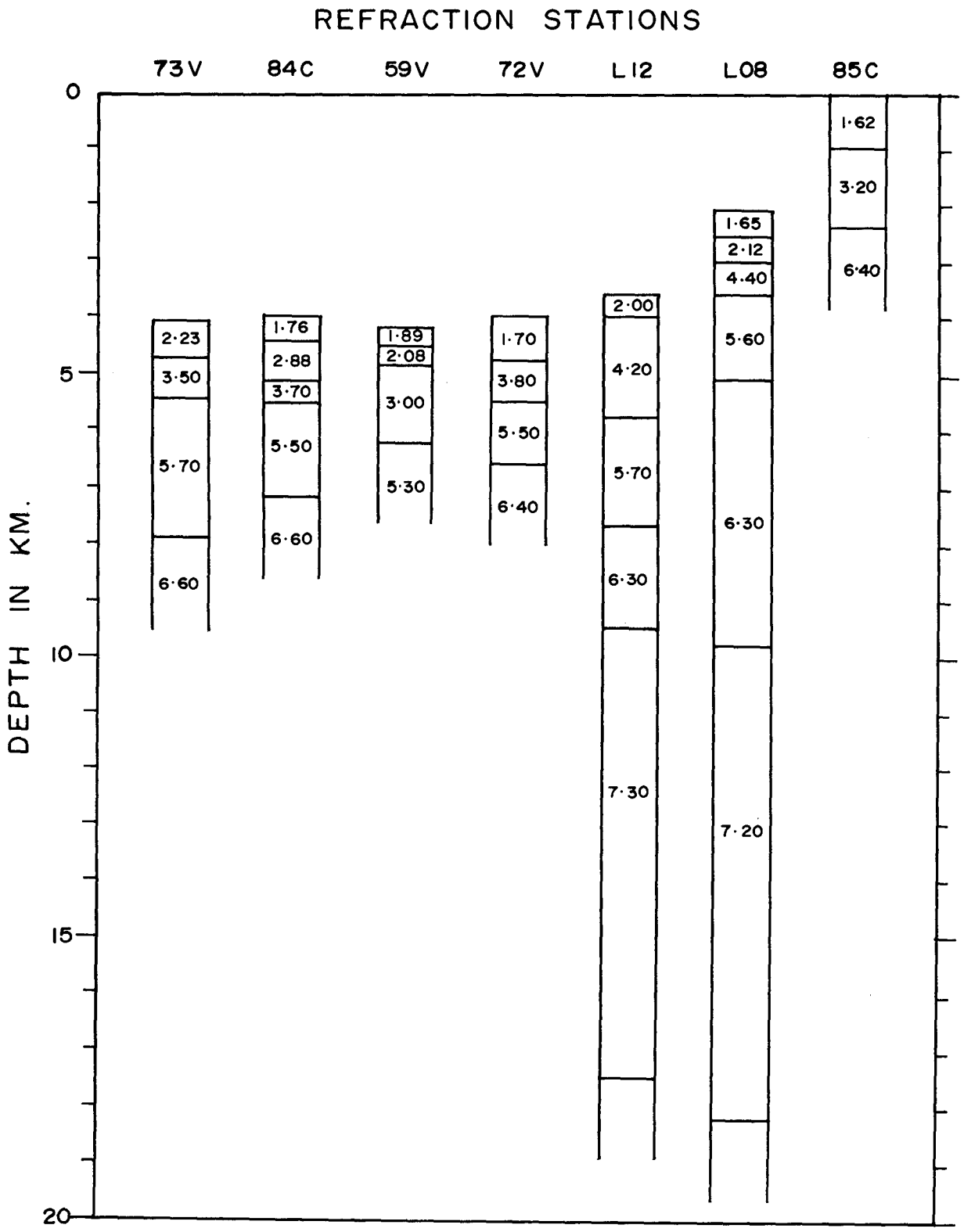

Figure 8.2 Crustal structure depicted as crustal columns at each refraction station. P-wave velocities (km/s) are shown inside the crustal columns. Location of refraction stations are shown in Figure 8.1.

These crustal characteristics and gravity model suggest that the ridge consists of thinned continental crust. However, in the recent past the origin of the Laccadive Ridge is being debated from micro-continent tectonics to a hotspot origin. In the following paragraphs, a detailed discussion is presented to substantiate the interpretation of the present study in light of the published results.

As mentioned earlier, the Chagos-Laccadive Ridge is considered as a mantle plume trace of the Reunion hotspot formed during the northward motion of the Indian plate over this hotspot (Shipboard Scientific Party, 1988; Richards et al., 1989; Duncan, 1990). The Reunion hotspot related volcanism has occurred in a large variety of plate tectonic settings ranging from continental to oceanic lithosphere. In the continental setting magmas erupted through thick and old lithosphere whereas, in oceanic lithospheric setting especially near spreading ridges, high extensional factors allow the mantle plume to generate substantial amount of melt. The total igneous crustal thickness (~17 km) and absence of velocities of typical oceanic Layer 3 over the Laccadive Ridge inferred in this study may point that the ridge is a volcanic buildup created during passage of pre-existing oceanic crust (part of Indian plate) over the Reunion hotspot. Earlier studies have suggested that when an oceanic spreading ridge cuts across a thermal anomaly such as hotspot, greater quantities of melt than normal are generated as mantle material wells up beneath the spreading center (McKenzie and Bickle, 1988; White and McKenzie, 1989). The Ninetyeast Ridge in the northeastern Indian Ocean is a major volcanic feature generated by the Kerguelen hotspot. It is one of the best examples of a linear volcanic feature formed due to plume over the oceanic crust in the Indian Ocean. The seismic refraction and gravity model studies over this ridge indicated ~11 km of igneous crustal thickness (Krishna et al., 1998). Similarly, mantle plumes such as Hawaii, Iceland and the Cape Verdes generated a region of anomalously hot asthenospheric mantle which extends up to 1000 km away from the central plume (Courtney and White, 1986; Watson and McKenzie, 1991). The reported igneous crustal thicknesses from seismic measurements and rare earth element inversion of such regions are 10.3±1.7 km and 10.7±1.6 km respectively where spreading centers

interacts the regions of hotter areas than normal mantle (White et al., 1992). The estimated crustal thickness of ~17 km over the Laccadive Ridge from the present study supported by refraction results is higher than the crustal thickness obtained over plume affected oceanic crust. Therefore, it is unlikely that the Laccadive Ridge is a volcanic buildup due to plume affected oceanic crust.

However, in a tectonic setting where mantle plume lying directly beneath the spreading centers can generate thick igneous crust. The seismic investigations of parts of the aseismic Kergulen and Madagascar Ridges which were formed due to mantle plume lying beneath the spreading center have indicated maximum crustal thickness of 20±1.3 km (Sinha et al., 1981; Recq et al., 1990; White et al., 1992). The volcanic record of the Reunion hotspot and paleo-geographic reconstruction of the western Indian Ocean indicate that the Reunion hotspot was never centered directly below a spreading center at least up to 47 Ma (Duncan, 1990). By the time the hotspot was away from Indian sub-continent and was lying below the Northern Chagos Bank. Thus, the inferred crustal thickness can not be explained in terms of volcanic buildup due to mantle plume lying directly beneath the spreading center. Therefore, it is inferred that the Laccadive Ridge is neither a plume effected oceanic crust nor a volcanic buildup due to mantle plume lying directly beneath spreading center.

The deep seismic sounding (DSS) investigations of the Indian peninsular shield carried out by the National Geophysical Research Institute of India (Figure 8.1) revealed a number of reflection horizons up to the Moho-discontinuity, detailed velocities and crustal structure. The investigations along Kavali-Udipi profile in the south, and Koyna-I and Koyna-II profiles in the north revealed that the P-wave velocities vary between i) 4.7 and 4.9 km/s in Deccan Traps; ii) 5.5 and 5.8 km/s in Cuddapah sediments and Dharwar schists, and iii) 5.8 and 6.2 km/s in granites and granitic gneisses (Kaila et al. 1979; 1981a; 1981b). Further, they interpreted velocities of 5.8-6.2 km/s along Kavali-Udipi profile, and absence of 5.5 and 5.8 km/s velocities below the trap cover along Koyna-I profile. In view of these observations, they inferred that i) the traps overlie the granites and granitic gneisses along the Koyna-I profile, and ii) Cuddapah sediments and

Dharwar schists (velocities 5.5 to 5.8 km/s) may not be extending as far north as Koyna-I profile. The refraction velocities data compiled in the study area comprise of 1.6 - 4.4 km/s, 5.5 - 5.7 km/s, 6.3-6.4 km/s and 7.2-7.3 km/s (Figure 8.2). The rocks with velocities of 5.5-5.7 km/s and 6.3-6.4 km/s overlain by sediments over the Laccadive Ridge are similar to the above velocities of the Dharwar schists/Cuddapah sediments and granitic gneisses respectively. The velocities 7.2-7.3 km/s may represent lower continental crust. It may be noted that the inferred granitic crustal velocities 6.3 to 6.4 km/s are slightly higher compared to that of DSS results. The high velocity may indicate altered granitic layer due to intrusive volcanism during rift related extensional tectonics and/or hotspot magmatism. The 4.7-4.9 km/s velocity layer interpreted as Deccan Traps by Kaila et al. (1981a and 1981b) is absent over the outer continental shelf and the Laccadive Ridge. Moreover, the seismic sequences are correlatable to that of the outer shelf and shelf margin basin. Earlier studies have also indicated that the structural and basement trends of the Laccadive Ridge are parallel and similar to the structural and main tectonic trends of the Indian continent (Eremenko, 1968; Eremenko and Dutta, 1968; Kolla and Coumes, 1990). Reddy et al. (1988) has inferred continental crust of the Laccadive Ridge off Mangalore coast based on crustal thickness.

The Laccadive Ridge axial grabens show block faulted nature on seismic profile SK12-07. Babenko et al. (1981) have also reported block faulting of the ridge from seismic reflection studies. The structural pattern is limited to the Laccadive Ridge and shelf margin basin and do not extend to the west of the Laxmi-Laccadive Ridges (Kolla and Coumes, 1990). In view of these results, it is inferred that the Laccadive Ridge is a thinned continental crust, probably intruded by volcanics during rifting and/or passage of Indian plate over the Reunion hotspot.

The significant crustal features identified from seismic reflection investigations are the Prathap Ridge and the sediment filled half grabens of the shelf margin basin between the continental slope and the Laccadive Ridge. The ridge parallels the shelf edge and divide the western part of the basin into two parts. The half grabens are characterized by fault blocks tilted away and equidistant from the ridge. The sediments

of the eastern part of the basin are comparatively more thick indicating damming of westward flow of the terrigenous sediments. It is possible that continental crust is thinned in the processes of rift emplaced volcanic crust of the Prathap Ridge in the study area. During the emplacement of volcanics, the rifted continental crust blocks are uplifted and tilted away from the ridge. Thus, the inferences reveal that i) the western margin of India has experienced crustal stretching since Late Cretaceous-Early Tertiary followed by linear volcanic construct of the Prathap Ridge of the shelf margin basin carving the present structural configuration of the basin, ii) followed by two different phases of sediment deposition facilitating the carbonate and clastic facies development and iii) the thinned continental crust of the Laccadive Ridge in the area with volcanic intrusives.

The two volcanic features are observed at the seaward edge of the Laccadive Ridge. They are also seen in many unpublished seismic reflection profiles collected by the National Institute of Oceanography, Goa. It is quite likely that they may extend laterally and form linear ridges at the western extremity of the Laccadive Ridge. Such features have also been identified over the ridge off Kerala coast (Gopala Rao et al., 1987). Basement ridges near shelf edges of many rifted margins, e.g. the Gabon-Cango region of west Africa (Belmonte et al., 1965) and Norwegian margins (Talwani and Eldholm, 1972) have been reported. Burk (1968) has identified wide spread existence of basement ridges at the rifted continental margins indicating their common origin, possibly near the site of initial rifting due to volcanic emplacement. Talwani and Eldholm (1973) have opined that a major change in the basement elevation should normally occur at the boundary between oceanic and continental crusts. Almost vertical to steep scarp has been identified at the western end of the Laccadive Ridge where the oceanic crust of the WAB is juxtaposed. Based on the identified volcanic features and steep scarp near the seaward edge of the Laccadive Ridge, it is suggested that the ocean-continent boundary lies close to the western extremity of the Laccadive Ridge.

8.3 EVOLUTION OF THE EASTERN ARABIAN SEA

Based on the results of present study and earlier published results, the revised evolutionary history of the Eastern Arabian Sea can now be proposed under following main sequences of tectonic events:

1) The first major tectonic event affected the western India was the breakup of Madagascar from India (Figure 8.3) ~90 Ma in the Late Cretaceous - a period widely known for the first major plate boundary reorganization in the Indian Ocean (Norton and Sclater, 1979). The breakup appears to have occurred along the ancient Dharwar structural trend (NNW-SSE) which resulted in formation of the Mascarene Basin. The breakup was recorded in a suite of lavas along east coast of Madagascar (Vallier, 1974). Norton and Sclater (1979) have opined that if similar volcanism existed in India its record might have been masked by the later Deccan Traps event. However, few earlier studies do suggest its presence on the western India. Valsangkar et al. (1980) have suggested that St. Mary group of islands on the west coast of India near 13°30'N are volcanic features and formed due to magmatic event ~93 Ma. Radhakrishna et al. (1994) reported the presence of dike swarms within granulite terrain in central Kerala of western India. Their study has suggested that i) NNW-SSE trending leucogabbro dykes are 81±2 m.y. old and are normally magnetized, and ii) most NW-SE trending dolerite dykes are 69±1 m.y. old and are reversely magnetized. Plate reconstructions for the Late Cretaceous place Madagascar over the Marion plume (Storey, 1995). Thus, the magmatic events reported in western India appear to be triggered from Marion thermal plume. Agrawal et al. (1992), based on analysis of geological, geophysical and tectonic signatures of Madagascar and India, suggested that Madagascar is a continental fragment of the paleo-super Dharwar craton of India.

2) The second major tectonic event affected the western India was the separation of Seychelles and Laxmi Ridge from India in north, and the Laccadive Ridge from southern India (Figure 8.4) during reversed magnetic polarity-Chron 29R (~65 Ma). This rifting event was synchronous with the eruption of continental flood basalt in

western India and Seychelles (White and McKenzie, 1989). The rifting event perhaps led to seafloor spreading stage for a limited period of time. This phase of spreading was parallel to the spreading in the Mascarene Basin. For a short period, Seychelles and Laxmi-Laccadive Ridges together remained as a micro-continent. This event marks the beginning of the formation of the Arabian Sea. This phase of rifting created the Eastern Arabian Basin. Seafloor spreading type magnetic lineations (Bhattacharya et al., 1994a; Malod et al., 1997) observed in this basin (north of 16°N) support this reconstruction. The presence of half grabens along profile SK12-07 do indicate short lived spreading south of 16°N in the basin. However, seafloor spreading type magnetic anomalies are yet to be identified in the area.

3) Third episode of tectonic event witnessed by the western India was separation of the Laxmi Ridge from Seychelles in the north and Laccadive Ridge from the adjacent oceanic crust lying west of it in the south at Chron 28N (Figure 8.5). This phase of rifting gave rise to the Carlsberg Ridge. The spreading in the Mascarene and Eastern Arabian Basins was ceased by 28N time. The rifting created two major basins viz. the Western Arabian Basin and its conjugate Eastern Somali Basin by propagating spreading centers under the influence of the Reunion hotspot. The Reunion hotspot started building its trace as the Indian plate migrated northward at a velocity of 13.5 cm/yr (Duncan and Hargraves, 1990) over the hotspot.

4) The first contact (soft collision) of the Indian continent with the southern margin of Eurasia occurred at Chron 23 (~51 Ma). India's rapid northward drift, which started immediately after breakup of Madagascar, slowed down and came to near halt at Chron 18 (~39 Ma) after hard collision between Indian and Eurasian continents (Figure 8.6). By this time, the Reunion hotspot has built most of its trace on the Indian plate. In the Indian Ocean, the second major plate boundary reorganization took place during Chron 19.

5) The spreading of the Carlsberg Ridge (Figure 8.7) resumed just before Chron 11 (~30 Ma) at a very slow rate (half spreading rate ~0.7 cm/yr) after a brief hiatus in spreading. Prior to Chron 11, the Reunion hotspot was centered under a segment of the Central Indian Ridge supplying melts to the Nazareth and Southern Chagos Banks. At Chron 13 (~34 Ma) the spreading ridge system jumped northeast over the Reunion hotspot. As a result, the Reunion hotspot which was initially located on the Indian plate until Chron 13 transferred to African plate. This has resulted in the ending of the development of the Chagos-Laccadive Ridge on the Indian plate.

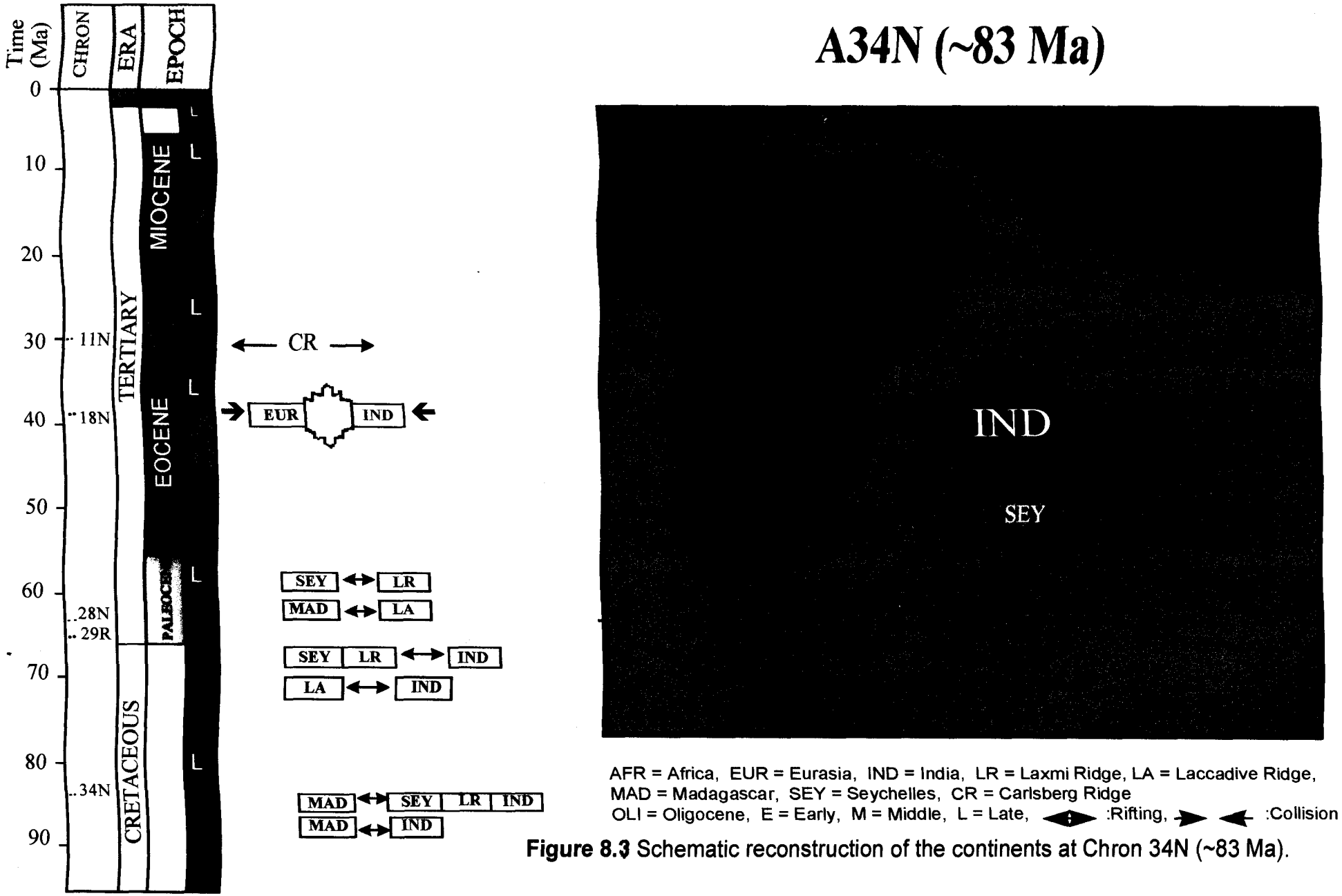

Figure 8.3 Schematic reconstruction of the continents at Chron 34N (~83 Ma).

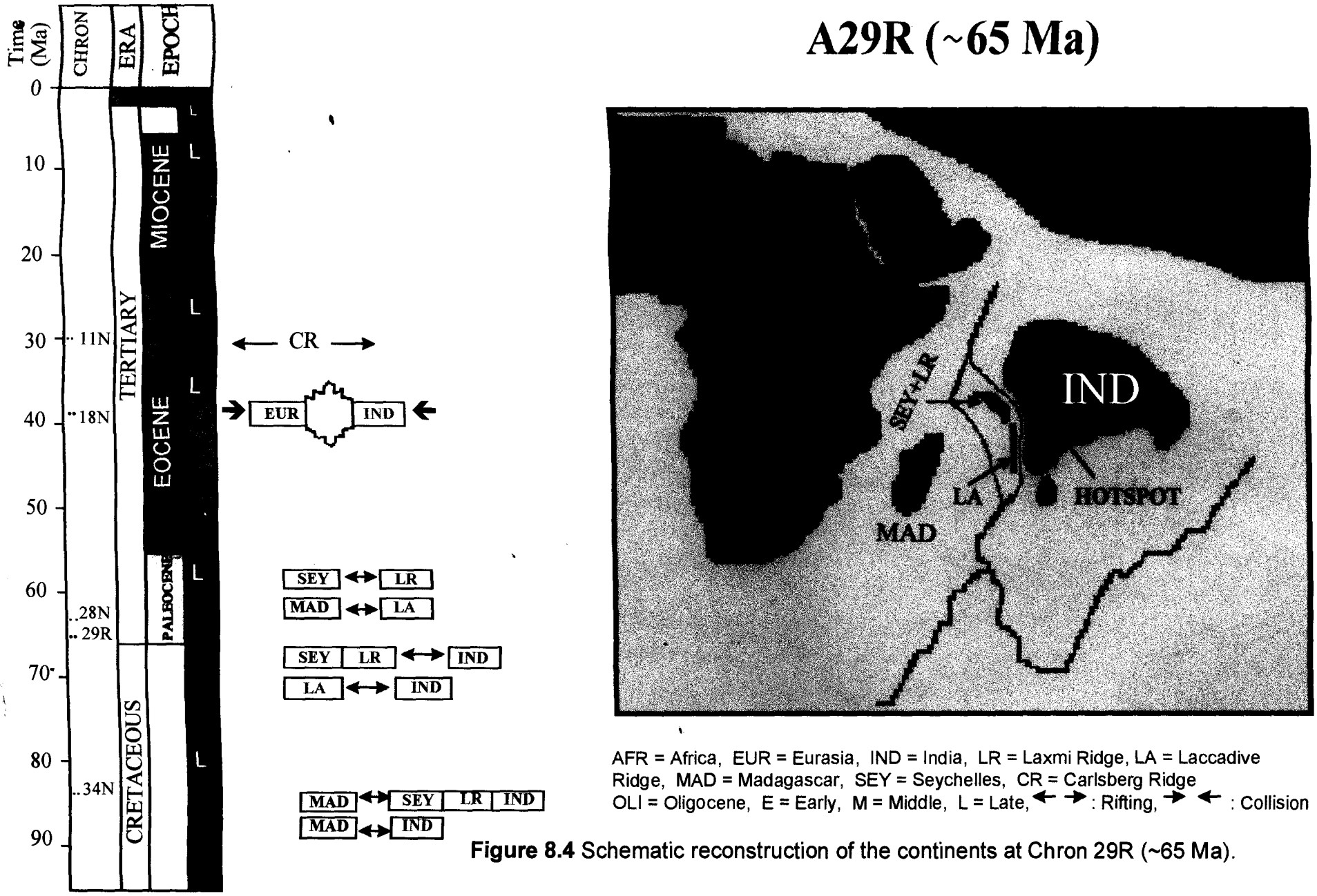

AFR = Africa, EUR = Eurasia, IND = India, LR = Laxmi Ridge, LA = Laccadive Ridge, MAD = Madagascar, SEY = Seychelles, CR = Carlsberg Ridge
OLI = Oligocene, E = Early, M = Middle, L = Late, ← →: Rifting, → ←: Collision

Figure 8.4 Schematic reconstruction of the continents at Chron 29R (~65 Ma).

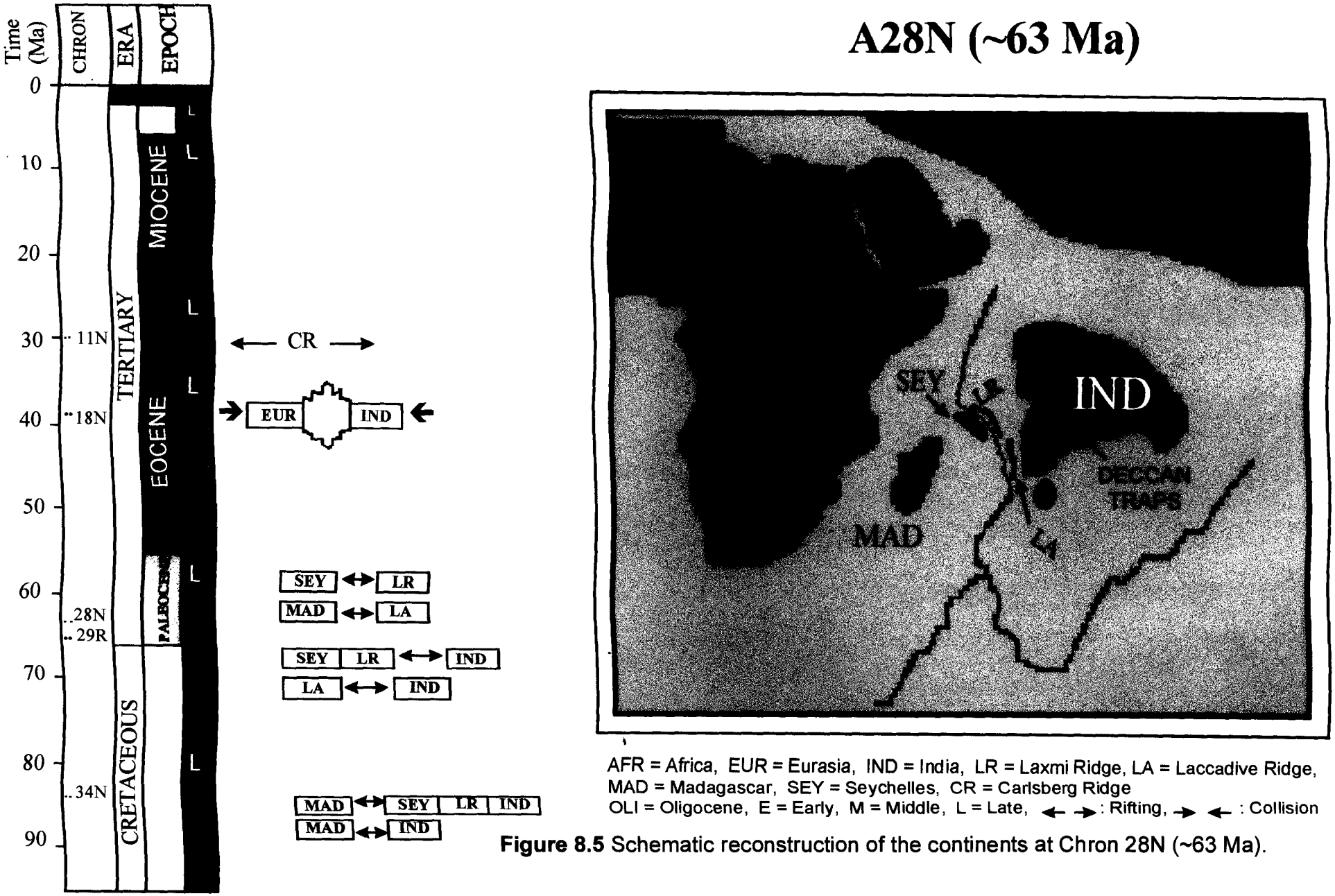

Figure 8.5 Schematic reconstruction of the continents at Chron 28N (~63 Ma).

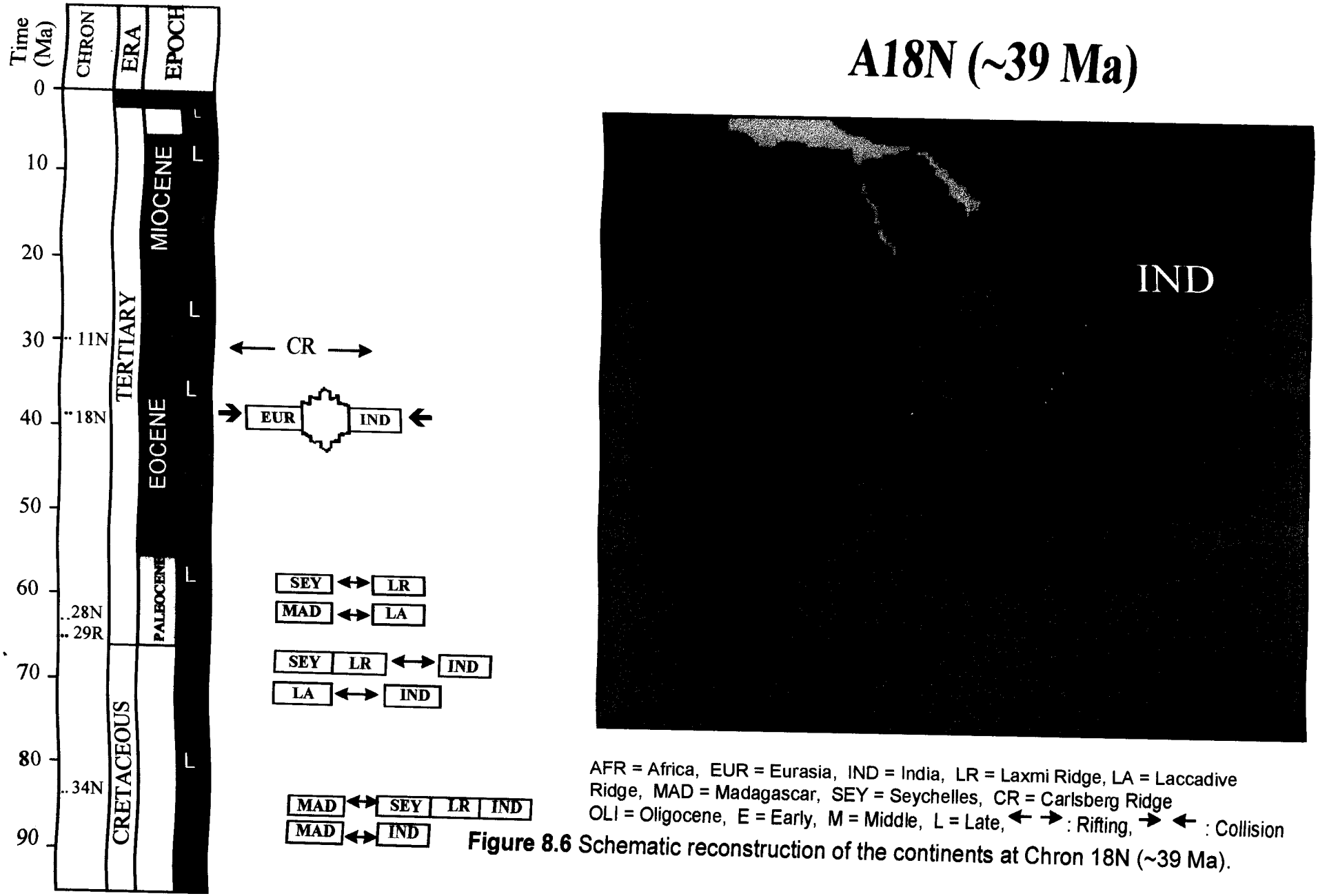

Figure 8.6 Schematic reconstruction of the continents at Chron 18N (~39 Ma).

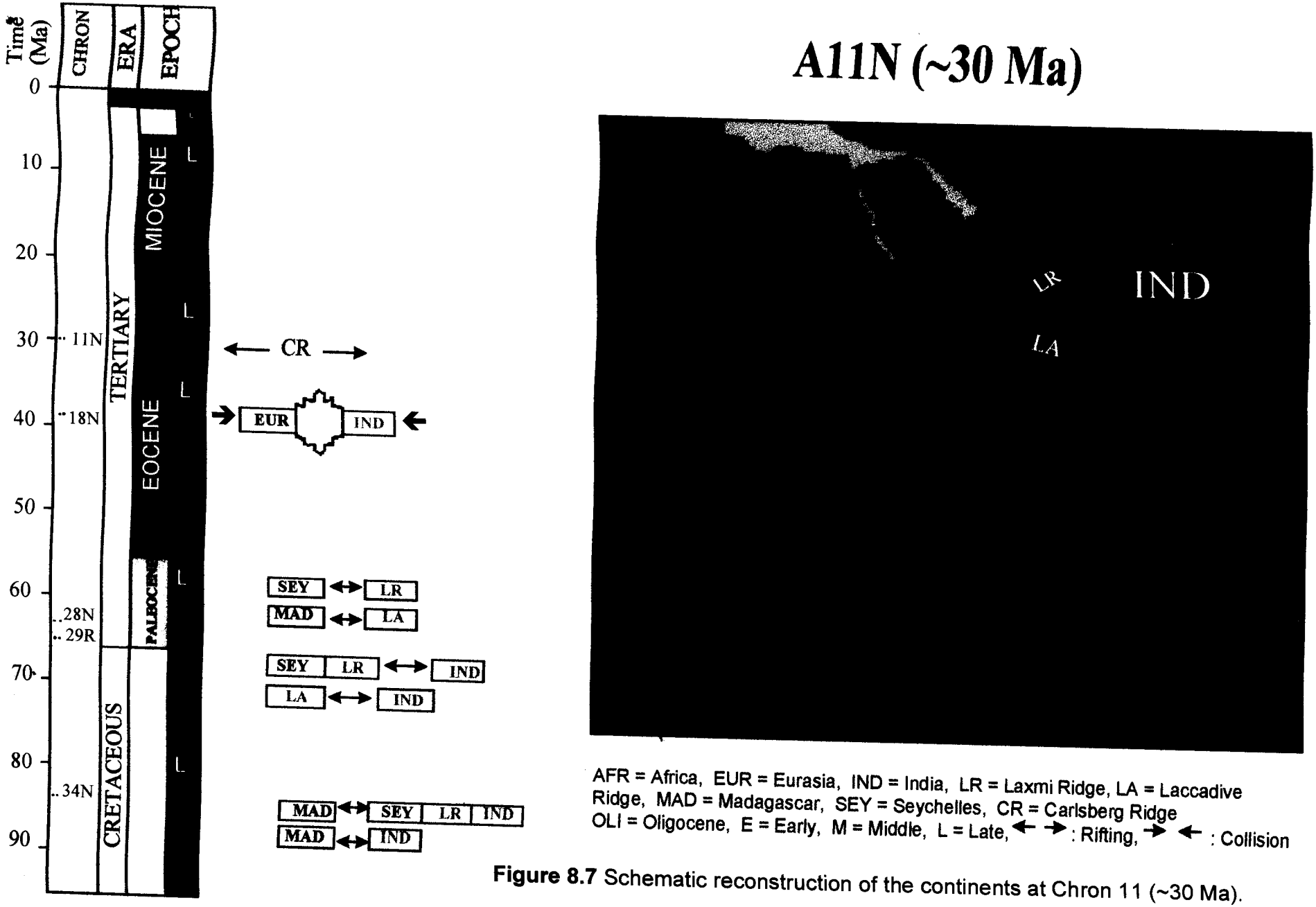

Figure 8.7 Schematic reconstruction of the continents at Chron 11 (~30 Ma).

CHAPTER 9

CHAPTER 9

SUMMARY AND CONCLUSIONS

9.1 SUMMARY

The earlier marine geophysical investigations carried out in the Eastern Arabian Sea have revealed the major structural features and ages of part of the basins which enabled proposing a generalized tectonic framework and a first order evolutionary history of the area. However, detailed analysis of the seafloor spreading magnetic anomalies over large part of the Eastern Arabian Sea remained speculative due to sparse data coverage which did not permit previous workers to propse an elucidative tectonic framework of the area. In view of this, the Eastern Arabian Sea region is considered for detailed studies to provide constraints for better understanding of the evolution of the area. This is of particular importance, because the resulting tectonic framework is related to the kinematics of formation of the western continental margin of India.

The present marine geophysical investigations carried out in the Western Arabian Basin (bounded by the Owen Fracture Zone, aseismic Laxmi-Laccadive Ridges and active Carlsberg Ridge) and adjoining western continental margin of India are aimed to decipher the crustal structure and provide better constraints to understand the evolution of the study area. For this purpose, i) magnetic data in the Western Arabian Basin are analyzed to map the magnetic lineations, their offset pattern and to estimate the rate of spreading of the oceanic crust, ii) bathymetry and magnetic data along two regional profiles extending from the Eastern Arabian Basin to Eastern Somali Basin across the Carlsberg Ridge are analyzed to understand the different phases of spreading in the Arabian Sea, and iii) bathymetry and gravity profiles alongwith one multichannel seismic reflection profile across the southwestern continental margin of India are analyzed to decipher ocean-continent boundary, and crustal structure of the margin.

An updated identification of the early Tertiary linear magnetic anomalies has been proposed in the Western Arabian Basin based on i) inter-profile correlation of anomalies from a dense set of profiles, ii) the fine scale structure of anomalies, and iii) model studies. For the first time the entire magnetic anomaly sequence 28N through 18N is mapped eastwards from 65°E up to about 70°E. The magnetic lineations proposed in this study are validated with the reported age of the crust at DSDP Site 221 and crustal depth compatibility between basement depth derived from cooling plate model and actual crustal depth obtained after sediment load correction. Based on the magnetic anomaly identifications, it is suggested that the age of the oceanic crust of the Western Arabian Basin ranges from 63 to 39 Ma. The oceanic crust is estimated to have evolved with variable half spreading rates ranging from 1.0 to 6.0 cm/yr. The half spreading rates suggest a gradual drop from 5.5 cm/yr at anomaly 23 to 1.0 cm/yr at anomaly 18 in this basin.

Contrary to the earlier studies, the present investigations reveal that the identified magnetic lineations of the Western Arabian Basin are segmented mainly by oblique offsets representing the pseudofaults associated with 11 major paleo-propagating ridges. The pre-anomaly 24N3 period was characterized by ridge reorganization, whereas such a phenomenon was not observed during the post-anomaly 25N period. The ridge propagation events commenced around anomaly 28N (~63 Ma) and continued at least until anomaly 23N1 (~51 Ma) and during the process a large amount of crust was transferred from the African plate to the Indian plate. The major consequence of this systematic ridge propagation has resulted in regional asymmetry in crustal accretion.

All the paleo-propagators except one inferred in the study propagated westward down the regional basement gradient and one propagated eastward up the regional basement gradient. It is inferred that the westward propagation of most of the propagators are due to the close proximity of the then Reunion hotspot with the early Tertiary seafloor spreading regime of the study area. The inference is supported by the commonly outward migration of the propagators from the proximity of the hotspot as

observed in many areas of the world oceans.

The estimated average ridge propagation rate between anomalies 28N and 25N was 3.6 cm/yr and between anomalies 24N3 and 22N was 12.1 cm/yr. This relative increase in propagation rate of the post-anomaly 25N propagators appears to be controlled by the strength and thermal structure of the lithosphere that was rifted by the propagating ridges. The studies further indicate that the paleo-propagating spreading ridge and the nearby the then Reunion hotspot are the major tectonic processes that controlled the accretionary process of the Early Tertiary oceanic crust in the Western Arabian Basin.

Magnetic lineations 11N through 1N trending N50°W are identified across the Carlsberg Ridge on two regional profiles. Variable half spreading rates of 1.2 cm/yr between anomalies 1 and 5C, 1.6 cm/yr between anomalies 5C and 6, 2.3 cm/yr between anomalies 6 and 6A, and 0.7 cm/yr between anomalies 6A and 11 are estimated based on best fit between the synthetic and observed anomalies. A magnetic quiet zone between lineations 18N and 11N is also identified.

Admittance analysis of gravity and bathymetry data over the Laccadive Ridge suggests that i) crustal thickness of the ridge varies between 15 and 20 km with an average value of ~17 km, and ii) local isostatic compensation by the Airy mechanism is an appropriate model for compensation of the topography of the Ridge. Based on the crustal structure and density distribution inferred from the admittance and two-dimensional gravity model studies, seismic reflection and published refraction results, a continental origin for the Laccadive Ridge is suggested. The igneous crustal thickness gradually decreases towards offshore and reaches an average value of ~6 km to the west of the Laccadive Ridge.

The study of a regional multichannel seismic reflection profile across the western continental margin of India revealed six major seismic sequences H1, H2, H3, H4, H5 and H6, H1 being the oldest. The ages of the sequences H1, H2, H3, H4, H5 and H6 are inferred as Paleocene to Late Eocene, Late Eocene to Late Oligocene, Late Oligocene

to Middle Miocene, Middle Miocene to Middle Pliocene, Middle Pliocene to Late Pleistocene and Late Pleistocene to Recent respectively. In the shelf margin basin, the thickness of sediments is up to ~3.55 s TWT. Whereas, it is 0.9 s and 1.2 s TWT over the Laccadive Ridge and the Western Arabian Basin respectively. The seismic section on continental shelf and slope region shows three distinct shelf edges; Late Oligocene, Middle Miocene and Present. The Middle Miocene shelf edge was prograded seaward side by ~8 km to form the present day shelf edge. There is no lateral shift in the location of the Late Oligocene to middle Miocene shelf edges. The Late Oligocene to Middle Miocene sediment deposition of shelf and slope region inferred from the present studies corresponds to an aggradational phase. Whereas, the Middle Miocene to Recent sedimentation is dominated by progradation. The shelf margin basin is characterized by the presence of half-grabens lying between the continental slope and the Laccadive Ridge. The half-grabens inferred as fault blocks tilted away from the Prathap Ridge. This may indicate that the shelf margin basin is a failed rift basin. The ocean-continent boundary is inferred to lie immediate west of Laccadive Ridge based on i) almost vertical to steep contact of the Western Arabian Basin with the Laccadive Ridge, ii) presence of volcanic features on the western end of Ridge, and iii) model studies of free-air gravity anomalies.

Keeping these results in view, a schematic reconstruction is proposed for the evolution of the Eastern Arabian Sea. The model suggests that the western margin of India resulted mainly due to: i) rifting between India and Madagascar at anomaly 34N (~83 ma), and ii) rifting of Seychelles from India and onset of Deccan continental flood basalts at anomaly 29R (~65 Ma). According to the model, the opening of the Arabian Sea started at anomaly 29R (~65 Ma) synchronous with the wide spread volcanism on western India and Seychelles whereas, opening of the Western Arabian Basin started a little later i.e. at anomaly 28N (~63 Ma). The spreading in the Arabian Sea had come to near halt at anomaly 18N (~39 Ma) due to hard collision of India with the southern margin of Eurasia. According to Duncan et al. (1990) the Reunion hotspot which was active on the Indian plate transferred to the African plate due to northeastward ridge jump at anomaly 13 (~33 Ma). Since then, the hotspot is in intraplate position and

presently located 150 km west of the volcanically active island of Reunion. The spreading in the Arabian Sea in its present geometry resumed again slightly before anomaly 11N at slow spread rates and is continuing until now at the half spread rate of 1.2 cm/yr.

9.2 CONCLUSIONS

1. Early Tertiary magnetic lineations 28N through 18N are identified in the Western Arabian Basin. Most of these lineations trend E-W except the central set of lineations 28N-25N which trend NW-SE.

2. Based on the magnetic anomaly identifications, it is suggested that i) opening of the Western Arabian Basin started at anomaly 28N i.e. ~63 Ma, and ii) the age of the oceanic crust of the basin is in the range of 63 to 39 Ma.

3. The oceanic crust is estimated to have been evolved with variable half spreading rates ranging from 1.0 to 6.0 cm/yr. Further, a gradual drop in half spreading rates from 5.5 cm/yr at anomaly 23 to 1.0 cm/yr at anomaly 18 in this basin indicate i) the onset of the soft collision between Indian plate and Eurasian plate at anomaly 23 (~51 Ma), and ii) the hard collision between these plates at anomaly 18N (~39 Ma).

4. The magnetic lineations of the basin are segmented mainly by oblique offsets representing the pseudofaults associated with 11 major paleo-propagating ridges.

5. The ridge propagation events commenced around anomaly 28N (~63 Ma) and continued at least until anomaly 23N (~51 Ma).

6. Almost all the propagating ridges propagated westward down the regional basement gradient to migrate away from the proximity of the then Reunion hotspot.

7. The accretionary process of the early Tertiary oceanic crust in the Western Arabian Basin have been greatly influenced by the propagating ridges and nearby the then

Reunion hotspot and during the process of ridge propagation a large amount of crust was transferred from the African plate to the Indian plate.

8. Marine magnetic lineations 11N through 1N trending N50°W and a new NE-SW trending fracture zone offsetting the entire magnetic anomaly sequences are identified across the Carlsberg Ridge. Variable half spreading rates ranging from 0.7 to 1.2 cm/yr for the last 30 m.y. are estimated.

9. A hiatus in spreading, characterized by a magnetic quiet zone, between lineations 18N and 11N are inferred. This inferred hiatus in spreading was much shorter (~9 m.y.) than previously believed.

10. The spreading in the Arabian Sea resumed in its present geometry slightly before anomaly 11N and is continuing till present.

11. Admittance analysis of gravity and bathymetry data over the Laccadive Ridge suggests that i) crustal thickness of the ridge varies between 15 and 20 km with an average of ~17 km, and ii) local isostatic compensation by the Airy mechanism is an appropriate model for compensation of the topography of the Ridge.

12. The study of a regional multichannel seismic reflection profile across the western continental margin of India revealed six major seismic sequences H1, H2, H3, H4, H5 and H6, H1 being the oldest. The ages of the sequences H1, H2, H3, H4, H5 and H6 are inferred as Paleocene to Late Eocene, Late Eocene to Late Oligocene, Late Oligocene to Middle Miocene, Middle Miocene to Middle Pliocene, Middle Pliocene to Late Pleistocene and Late Pleistocene to Recent respectively.

13. In the shelf margin basin, the sediment is ~3.55 s TWT maximum thick. Whereas, it is 0.9 s and 1.2 s TWT over the Laccadive Ridge and the WAB respectively. The seismic section of continental shelf and slope region shows three distinct shelf edges; Late Oligocene, Middle Miocene and Present. The Middle Miocene shelf edge was prograded seaward side by ~8 km to form the present day shelf edge. There is no

lateral shift in the location of the Late Oligocene to Middle Miocene shelf edges. The Late Oligocene to Middle Miocene sediment deposition of shelf and slope region inferred from the present studies corresponds to an aggradational phase. Whereas, the middle Miocene to Recent sedimentation is dominated by progradation.

14. The shelf margin basin is characterized by the presence of half-grabens lying between the continental slope and the Laccadive Ridge. The half-grabens inferred as fault blocks tilted away from the Prathap Ridge. This may indicate that the shelf margin basin is a failed rift basin.

15. Based on crustal structure and density distribution inferred from the admittance and two-dimensional gravity model studies, published refraction results and results from the multichannel seismic reflection data, a continental origin for the Laccadive Ridge is suggested. The ocean-continent boundary is inferred to lie immediately west of the Laccadive Ridge.

The integrated interpretation of the geophysical data suggests that the seafloor spreading history of the Arabian Sea can be divided into three distinct phases. The first phase (oldest one) of spreading started at anomaly 29R (~65 Ma) when India separated from Seychelles in the north and Laccadive Ridge in the south. This phase of spreading is marked by wide spread volcanism on both western India and Seychelles. The second phase of spreading started at anomaly 28N (~63 Ma) when the spreading center between India and Seychelles together with Laccadive Ridge jumped westward between Laxmi Ridge and Seychelles and west of Laccadive Ridge. The second phase of spreading came to a near halt at anomaly 18N (~39 Ma) after the hard collision between Indian and Eurasian plates. The third phase of spreading (youngest one) resumed in its present geometry slightly before anomaly 11N (~30 Ma) after a brief (~9 m.y.) hiatus in spreading and is continuing till present.

REFERENCES

REFERENCES

Acton, G. and Gordon, R.G., 1989. Limits on the age of the Deccan Traps of India from paleomagnetic and plate reconstruction data and the uncertanities. J. Geophys. Res., 94:17713-17720.

Adams, R.D. and Christoffel, D.A., 1962. Total magnetic field surveys between New Zealand and the Ross Sea. J. Geophys. Res., 67:805-813.

Agrawal, P.K., Pandey, O.P. and Negi, J.G., 1992. Madagascar: A continental fragment of the paleo-super Dharwar craton of India. Geology, 20:543-546.

Airy, G.B., 1855. On the computation of the effect of the attraction of the mountain masses. Phil. Trans. Roy. Soc. London, 145:101-104.

Alvarez, L.W., Alvarez, W., Asaro, F. and Michel, H.V., 1980. Extraterrestrial cause for the Cretaceous-Tertiary Extinction. Science, 208:1095-1108.

Anonymous 1968. Tectonic map of India. Oil and Natural Gas Comission of India, Dehra Dun, India.

Ashalatha, B., Subrahmanyam, C. and Singh, R.N., 1991. Origin and compensation of Chagos-Laccadive ridge, Indian Ocean, from admittance analysis of gravity and bathymetry data. Earth Planet. Sci. Lett., 105:47-54.

Aubert, O. and Droxler, A.W., 1996. Seismic stratigraphy and depositional signatures of the Maldive carbonate system (Indian Ocean). Mar. Petrol. Geol., 13:503-536.

Auzende, J.M., Pelletier, B. and Lafoy, Y., 1994. Twin active spreading ridges in the North Fiji Basin (Southwest Pacific). Geology, 22:63-66.

Avraham, Z.B. and Bunce, E.T., 1977. Geophysical study of the Chagos-Laccadive Ridge, Indian Ocean. J. Geophys. Res., 82:1295-1305.

Ayub, A., 1992. Channel-Levee Systems on the Indus Deep-Sea Fan. Unpublished Ph.D. thesis. University of Wales. pp. 242.

Babenko, K.M., Panaev, V.A., Svistunov, Yu.I. and Shlezinger, A.E., 1981. Tectonics of the eastern margin of the Arabian Sea according to seismic data. Bull. ONGC, 18:37-62.

Baksi, A.K., 1988. Critical evaluation of the age of the Deccan traps, India: Implications for the flood-basalt volcanism and faunal extinction: Reply. Geology, 16:758-759.

Baksi, A.K., 1994. Geochronological studies on whole-rock basalts, Deccan traps, India : Evaluation on the timing of the volcanism relative to the K-T boundary. Earth Planet. Sci. Lett., 121:43-56.

Baksi, A.K. and Farrar, E., 1991. $^{40}Ar/^{39}Ar$ dating of the Siberian Traps, USSR: evaluation of the ages of the two major extinction events relative to episodes of flood-basalt volcanism in the USSR and Deccan Traps, India. Geology, 19:461-464.

Banks, R.J., Parker, R.L. and Huestis, S.P., 1977. Isostatic compensation on a continental scale. Geophys. J. R. Astron. Soc., 51:431-452.

Banks, R.J. and Swain, C.Z., 1978. The isotopic compensation of East Africa. Proc. R. Soc. London, Ser. A, 364:331-352.

Basu, A.R., Renne, P.R., Dasgupta, D.K., Teichmann, F. and Poreda, R.J. 1993. Early and late alkali igneous pulses and high-^{3}He plume origin for the Deccan flood besalts. Science, 261:902-906.

Belmonte, Y., Hirtz, P. and Wenger, R., 1965. The salt basin of the Gabon and Congo (Brazzaville). In: W.Q. Kennedy (Editor), Salt basins around Africa. London Inst. Petroleum, pp. 55-74.

Berggren, W.A., Kent, D.V., Flynn, J.J. and Van Couvering, J.A., 1985. Cenozoic geochronology. Geol. Soc. Am. Bull., 96:1407-1418.

Besse, J. and Courtillot, V., 1988. Paleogeographic maps of the continents bordering the Indian Ocean since the Early Jurassic. J. Geophys. Res., 93:11791-11808.

Bhattacharji, S., Chatterjee, N., Wampler, J.M., Nayak, P.N. and Deshmukh, S.S., 1996. Indian Intraplate and continental margin rifting, lithospheric extension, and mantle upwelling in Deccan flood basalt volcanism near the K/T boundary: Evidence from mafic dike swarms. Geology, 104:379-398.

Bhattacharya, G.C., Chaubey, A.K., Murty, G.P.S., Srinivas, K., Sarma, K.V.L.N.S., Subrahmanyam, V. and Krishna, K.S., 1994a. Evidence for seafloor spreading in the Laxmi Basin, northeastern Arabian Sea. Earth Planet. Sci. Lett., 125:211-220.

Bhattacharya, G.C., Murty, G.P.S., Srinivas, K., Chaubey, A.K., Sudhakar, T. and Nair, R.R., 1994b. Swath bathymetric investigation of the seamounts located in the Laxmi Basin, eastern Arabian Sea. Mar. Geodesy, 17:169-182.

Bhattacharya, G.C. and Subrahmanyam, V. 1986. Extension of the Narmada-Son Lineament on the continental margin off Saurashtra, Western India as obtained from magnetic measurements. Mar. Geophys. Res., 8:329-344.

Biswas, S.K., 1982. Rift basins in western margin of India and their hydrocarbon prospects with special reference to Kutch Basin. Bull. Am. Assoc. Pet. Geol., 66:1497-1513.

Biswas, S.K., 1987. Regional tectonic framework, structure and evolution of the western marginal basins of India. Tectonophysics, 135: 307-327.

Biswas, S.K., 1988. Structure of the western continental margin of India and related igneous activity. Mem. Geol. Soc. Ind., No.10, 371-390.

Biswas, S.K., 1989. Hydrocarbon exploration in western offshore basins of India. Geol. Surv. Ind. Spl. Pub. No 24, 185-194.

Biswas, S.K. and Singh, N.K., 1988. Western continental margin of India and hydrocarbon potential of deep-sea basins. Proc. 7th offshore south east Asia conference, Singapore, pp. 170-181.

Bott, M.H.P., 1967. Solution of the linear inverse problem in magnetic interpretation with application to oceanic magnetic anomalies: Roy. Astron. Soc., Geophys. J., 13:313-323.

Brozena, J.M. and White, R.S., 1990. Ridge jumps and propagations in the South Atlantic Ocean. Nature, 348:149-152.

Brunhes, B., 1906. Recherches sur la direction d'aimentation des roches volcaniques, J. Physique, 5:705-724.

Bull, J. M., 1990. Structural style of intra-plate deformation, Central Indian Ocean Basin: Evidence for the role of fracture zones. Tectonophysics, 184:213-288.

Burk, C.A., 1968. Buried ridges within continental margins. Trans. N.Y., Acad. Sci., 30:397-409.

Cande, S.C. and Kent, D.V., 1992. A new geomagnetic polarity time scale for the Late Cretaceous and Cenozoic. J. Geophys. Res., 97:13917-13951.

Cande, S.C. and Kent, D.V., 1995. Revised calibration of the geomagnetic polarity timescale for the Late Cretaceous and Cenozoic. J. Geophys. Res., 100:6093-6095.

Cann, J.R., and Vine, F.J., 1966. An area on the crest of the Carlsberg Ridge: Petrology and magnetic survey. Phil. Trans. Roy. Soc., A259:198-217.

Carlson, R.L., 1976. Cenozoic plate convergence in the vicinity of the Pacific Northwest: a synthesis and assessment of plate tectonics in the northwestern Pacific. Ph.D. Thesis, University of Washington, 129 pp.

Carter, D.J.T., 1980. Echosounding correction tables. Hydrogr. Dep., Ministry Defence, Taunton, 150 pp.

Christie, D.M. and Sinton, J.M., 1981. Evolution of abyssal lavas along propagating segments of the Galapagos spreading center. Earth Planet. Sci. Lett., 56:321-335.

Closs, H., Bungenstock, H. and Hinz, K., 1969. Results of Seismic refraction measurments in the northern Arabian Sea: A contribution to the International Indian Ocean Expedition. Meteor. Res. Results, 3:1-28.

Cochran, J.R., 1990. Himalayan uplift, sea level, and the record of Bengal Fan sedimentation at the ODP Leg 116 sites. In: J.R. Cochran, D.A.V. Stow, et al. (Editors), Proc. ODP, Sci. Results, 116: College Station, TX(Ocean Drilling Program), 397-414.

Cooley, J.W. and Tukey, J.W., 1965. An algorithm for the machine calculation of complex Fourier Series. Math. Comput., 19:297-301.

Coumes, F. and Kolla, V., 1984. Indus Fan: seismic structure, channel migration and sediment thickness in the upper fan. In: B.U. Haq and J.D. Milliman (Editors), Marine Geology and oceanography of Arabian Sea and coastal Pakistan. New York, Van Nostrand Reinhold, pp. 101-110.

Courtillot, V., Besse, J., Vandamme, D., Montigny, R., Jaeger, J.J. and Cappetta, H., 1986. Deccan flood basalts at the Cretaceous/Tertiary boundary?. Earth Planet. Sci. Lett., 80:361-374.

Courtillot, V., Feraud, G., Maluski, H., Vandamme, D., Moreau, M.G. and Besse, J., 1988. Deccan flood basalts and the Cretaceous/Tertiary boundary. Nature, 333:843-846.

Courtney, R.C. and White, R.S., 1986. Anomalous heat flow and geoid across the Cape Verde Rise: Evidence for dynamic support from a thermal plume in the mantle. Geophys. J. R. Astron. Soc., 87:815-868.

Cox, A., 1959. The remanent magnetization of some Cenozoic rocks, Unpublished Ph.D. thesis, Univ. of California, Berkeley, pp. 193.

Cox, A., 1969. Geomagnetic reversals. Science, 163:237-245.

Cox, A., 1973. Plate tectonics and geomagnetic reversals. W.H. Freeman and Co. USA. pp. 702.

Cox, K.G., 1989. Mantle plumes and continental flood basalts: supporting evidence from drainage patterns. Nature, 342:873-877.

Cox, A., Doell, R.R. and Dalrymple, G.B., 1963a. Geomagnetic polarity epochs and Pliestocene geochronometry. Nature, 198:1049-1051.

Cox, A., Doell, R.R. and Dalrymple, G.B., 1963b. Geomagnetic polarity epochs: Sierra Nevada II. Science, 142:382-385.

Cox, A., Doell, R.R. and Dalrymple, G.B., 1964. Reversals of the earth's magnetic field. Science, 144:1537-1543.

Cox, A., Doell, R.R. and Dalrymple, G.B., 1968. Radiometric time scale for geomagnetic reversals. Geol. Soc. London, Quart. J., 124:53-66.

Crough, S.T., 1983. The correlation for sediment loading on the seafloor. J. Geophys. Res., 88:6449-6454.

Dalloubeix, C., Fleitout, L. and Diament, M., 1988. A new analysis of gravity and topography data over the Mid-Atlantic Ridge: non-compensation of the axial valley. Earth Planet. Sci. Lett., 88:308-320.

Dalrymple, G.B., Izett, G.A., Snee, L.W. and Obradovich, J.D., 1993. 40Ar/39Ar age spectra and total-fusion ages of tektites from Cretaceous-Tertiary boundary sedimentary rocks in the Beloc Formation, Haiti. U.S. Geol. Surv. Bull., 2065:1-20.

Das, S.R. and Ray, A.K. 1976. Fracture pattern, hot springs and lineaments of the west coast. J. Geol. Surv. Ind., 125 Year News Lett., 1-6.

Detrick, R.S., Sclater, J.G. and Thiede, J., 1977. The subsidence of aseismic ridges. Earth Planet. Sci. Lett., 34:185-196.

Dickson, G.O., Pitman III, W.C. and Heirtzler, J.R., 1968. Magnetic anomalies in the South Atlantic and ocean-floor spreading. J. Geophys. Res., 73:2087-2100.

Dietz, R.S., 1961. Continent and ocean basin evolution by spreading of the sea floor. Nature, 190:854-857.

Dietz, R.S. and Holden, J.C., 1970. Reconstruction of Pangaea: Breakup and dispersion of continents, Permian to Present. J. Geophys. Res., 75:4939-4956.

Dorman, L.M. and Lewis, B.T.R., 1970. Experimental isostasy, 1. Theory of the determination of the earths's isostatic response to a concentrated load. J. Geophys. Res., 75:3357-3365.

Driscoll, R.L. and Bender, P.L., 1958. Proton gyromagnetic ratio. Phys. Rev. Let., 1:413.

Driscoll, R.L. and Bender, P.L., 1958a. A free precession determination of the proton gyromagnetic ratio. I.R.E. Trans., 1:176.

Droz, L. and Bellaiche, G., 1987. Morphologie et structure sedimentaire du Cone de l'Indus: premiers resultats de la campagne MD 51/Profindus. C.R. Acad. Sci. Paris, t. 305, Serie II, pp. 109-113.

Duncan, R.A., 1981. Hotspots in the southern oceans: An absolute frame of reference motion of the Gondwana Continents. Tectonophysics, 74:29-42.

Duncan, R.A., 1990. The volcanic record of the Reunion hotspot. In: R.A. Duncan, J. Backman, L.C. Peterson et al. (Editors), Proc. ODP, Sci. Results, 115: College Station, TX (Ocean Drilling Program), 3-10.

Duncan, R.A. and Hargraves, R.B. 1990. ^{40}Ar-^{39}Ar geochronology of basement rocks from the Mascarene Plateau, the Chagos Bank and the Maldives ridge. In: R.A. Duncan, J. Backman, L.C. Peterson et al. (Editors), Proc. ODP, Sci. Results, 115: College Station, TX (Ocean Drilling Program), 43-51.

Duncan, R.A. and Pyle, D.G., 1988. Rapid eruption of the Deccan flood basalts at the Cretaceous/Tertiary boundary. Nature, 333:841-843.

Duncan, R.A., Rea, D.K., Kidd, R.B. von Rad, U. and Weissel, J.K., 1992. Syntheisis of results from scientific drilling in the Indian Ocean. Geophysical Monograph, Vol. 70, American Geophysical Union, Washington, DC, 475 pp.

Duncan, R.A. and Richards, M.A., 1991. Hotspots, mantle plumes, flood basalts, and true polar wander. Rev. Geophys., 29:31-50.

Elvers, D., Srivastava, S.P., Potter, K., Morley, J. and Sdidel, D., 1973. Asymmetric spreading across the Juan de Fuca and Gorda rises as obtained from a detailed magnetic survey, Earth Planet. Sci. Lett., 20:211-219

Eremenko, N.A. 1968. Tectonics and petroleum possibilities of southern part of India. Mem. Geol. Soc. India, 2:371-376.

Eremenko, N.A. and Datta, A.K., 1968. Regional geological framework and evaluation of the petroleum prospects of the Laccadive archipelago and the adjoining offshore territory, southwest India. Bull. ONGC, 5:29-40.

Ewing, M., and Eittreim, S., Truchan, M., and Ewing, J.I., 1969. Sediment distribution in the Indian Ocean. Deep-Sea Res., 16:231-248.

Exon, N.F. and Willcox, J.B., 1978. Geology and petroleum potential of the Exmouth Plateau area off western Australia. Am. Assoc. Pet. Geol. Bull., 62:40-72.

Fairbridge, R.W., 1948. The juvenility of the Indian Ocean. Scope, 1:29-35.

Fairbridge, R.W., 1955. Some bathymetric and geotectonic features of the eastern part of the Indian Ocean. Deep-Sea Res., 2:161-171.

Farrar, E. and Dixon, J.M., 1980. Miocene ridge impingement and the spawning of secondary ridges off Oregon, Washington and British Columbia. Tectonophysics, 69:321-348.

Fisher, R.L., Engel, C.G. and Hilde, T.W.C., 1968. Basalts dredged from Amirante Ridge, Western Indian Ocean. Deep-Sea Res., 15:521-534.

Fisher, R.L., Sclater, J.G. and McKenzie, D.P., 1971. Evolution of the Central Indian Ridge, western Indian Ocean, Geol. Soc. Am. Bull., 82:553-562.

Forsyth, D.W., 1985. Subsurface loading and estimates of the flexural rigidity of continental lithosphere. J. Geophys. Res., 90:12623-12632.

Francis, T.J.G. and Shor, G.G.Jr., 1966. Seismic refraction measurements in the northwest Indian Ocean. J. Geophys. Res., 71:427-449.

Furuta, T., Fujimoto, H. and Toh, H., 1987. Is the oceanic crust over 1 km necessary for the source of marine magnetic anomalies? Phys. Earth Planet. Iner., 49:117-120.

Garland, G.D., 1979. Introduction to Geophysics. Mantle, Core and Crust. W.B. Saunders Co., Toronto, Canada, pp. 494.

Gopala Rao, D., Bhattacharaya, G.C., Subba Raju, L.V., Ramana, M.V., Subrahmanyam, V., Raju, K.A.K., Ram Prasad, T. and Chaubey, A.K., 1987. Regional marine geophysical studies of the south western continental margin of India. Contribution in Marine Sciences, pp. 427-437.

Goapala Rao, D., Krishna, K.S. and Sar, D., 1997. Crustal evolution and sedimentation history of the Bay of Bengal since the Cretaceous. J. Geophys. Res., 102:17747-17768.

Gradstein, F.M. and von Rad, U., 1991. Stratigraphic evolution of Mesozoic continental margin and oceanic sequences: Northwest Australia and northern Himalayas. Mar. Geol., 102:131-173.

Haq, B.U., Hardenbol, J. and Vail, P.R., 1987. Chronology of fluctuating sea levels since the Triassic. Science, 235:1156-1167.

Haq, B.U., Hardenbol, J. and Vail, P.R., 1988. Mesozoic and Cenozoic chronostartigraphy and cycles of sea level changes. Spec. Publ., Soc. Econ. Paleontol. Mineral., 42:71:108.

Harbison, R.N. and Bassinger, B.G., 1973. Marine geophysical study off western India. J. Geophys. Res., 78:432-440.

Harland, W.B., Cox, A.V., Llewellyn, P.G., Pickton, C.A.G., Smith, A.G. and Walters, R., 1982. A geologic time scale. 131 pp, Cambridge University Press, Cambridge, New York.

Hays, D.E., 1988. Age-depth relationships and depth anomalies in the southeast Indian Ocean and south Atlantic Ocean. J. Geophys. Res., 93:2937-2954.

Heezen, B.C. Ewing, M. and Miller, E.T., 1953. Trans-Atlantic profile of total magnetic intensity and topography, Dakar to Barbados, Deep-Sea Res., 1:25-33.

Heezen, B. C., and Tharp, M., 1965. Physiographic diagram of the Indian Ocean (with descriptive sheet). Geol. Soc. Am., New York.

Heirtzler, J.R., 1961. Verma cruise no. 16 magnetic measurements: Colambia University., Lamont. Geol. Observ., Tech Rep. 2, contract CU-3-61 Nonar Geology.

Heirtzler, J.R., Bolli, H.M., Davies, T.A., Saunders, J.B. and Sclater, J.G., 1977. Indian Ocean Geology and biostratigraphy. American Geophys. Union, Washington, D.C., pp. 616.

Heirtzler, J.R., Dickson, G.O., Herron, E.M., Pitman, III, W.C. and Le Pichon, X., 1968. Marine magnetic anomalies, geomagnetic field reversals and motions of the ocean floor and continents. J. Geophys. Res., 73:2119-2136.

Hess, H.H., 1960. Evolution of ocean basins : Report to Office of Naval Research on research supported by ONR contract Nonr 1858, pp.149-150.

Hess, H.H., 1962. History of the Ocean Basins. In: A.E.J. Engel, H.L. James and B.F. Leonard (Editors), Petrologic studies. Geol. Soc. Am., 559-620.

Hey, R., 1977. A new class of "pseudofaults" and their bearing on plate tectonics: A propagating rift model. Earth Planet. Sci. Lett., 37:321-325.

Hey, R., Duennebier, F.K. and Morgan, W.J., 1980. Propagating rifts on the midocean ridges. J. Geophys. Res., 85:3647-3658.

Hey, R. and Vogt, P., 1977. Spreading center jumps and sub-axial asthenosphere flow near the Galapagos hotspot. Tectonophysics, 37:41-52.

Hey, R.N., Kleinrock, M.C., Miller, S.P., Atwater, T.M. and Searle, R.C., 1986. Sea beam/deep-tow investigation of an active oceanic propagating rift system, Galapagos 95.5° W. J. Geophys. Res., 91:3369-3393.

Hey, R.N. and Wilson, D.S., 1982. Propagating rift explanation for the tectonic evolution of the northeast Pacific-the pseudomovie. Earth Planet. Sci. Lett., 58:167-188.

Hey, R.N., Naar, D.F., Kleinrock, M.C., Morgan, P.W.J., Morales, E. and Schilling, J.G., 1985. Microplate tectonics along a superfast seafloor spreading system near Easter Island. Nature, 317:320-325.

Hilgen, F.J., 1991. Extension of the astronomically calibrated (polarity) time scale to the Miocene/Pliocene boundary. Earth Planet. Sci. Lett., 107:349:368.

Hospers, J., 1954. Magnetic correlation in volcanic districts, Geol. Mag., 91:352-360.

IAGA Division V, Working Group 8, 1992. International Geomagnetic Reference Field, 1991 Revision. Geophysics, 57:956-959.

Irving, E., Park, J.K., Haggerty, S.E., Aumento, F. and Loncarevic, B., 1970. Magnetism and opaque mineralogy of basalts from the Mid-Atlantic Ridge at 45°N. Nature, 228:974-976.

Jipa, D. and Kidd, R.B., 1974. Sedimentation of coarser grained interbeds in the Arabian Sea and sedimentation processes of the Indus Cone. In: R.B. Whitmarsh, O.E. Weser, D.A. Ross et al. (Editors), Initial reports of the Deep Sea Drilling Project, Vol. 23, Washington, (U.S. Government. Printing Office), 471-495.

Johnson, H.P., Karsten, J.L., Delaney, J.R., Davis, E.E., Currie, R.G. and Chase, R.L., 1983. A detailed study of the Cobb offset of the Juan de Fuca ridge: Evolution of a propagating rift. J. Geophys. Res., 88:2297-2315.

Kahle, H.G. and Talwani, M., 1973. Gravimetric Indian Ocean Geoid, J. Geophys. (Zeitschrift fur Geophysik), 39: 167.

Kaila, K.L., Murty, P.R.K., Rao, V.K. and Kharetchko, G.E., 1981b. Crustal structure from deep seismic soundings along the Koyna II (Kelsi-Loni) profile in the Deccan Trap area, India. Tectonophysics, 73:365-384.

Kaila, K.L., Reddy, P.R., Dixit, M.M., and Lazarenko, M.A., 1981a. Deep crustal structure at Koyna, Maharashtra, indicated by deep seismic soundings. Geol. Soc. India, 22:1-16.

Kaila, K.L., Reddy, P.R., Krishna, V.G., Roy Chowdhury, K., Tewari, H.C., Murty, P.R.K. and Tripathi, K.M., 1979. Crustal investigations in India from deep seismic soundings. Geophy. Res. Bull., 17:273-292.

Kalyayev, G.I., Karabovich, S.V., Rusakov, O.M. and Starostenkov, V.I., 1983. Deep structure of the Arabian-Indian Ridge and the Owen Fault zone. Geotectonics, 71:32-42

Kamesh Raju, K.A., Ramprasad, T., Bhattacharya, G.C. and Kodagali, V.N., 1986. A system for processing of underway geophysical and geological data (Abstract). XII Annual Convention and Seminar on Exploration Geophysics. AEG souvenier, 54:a24-a25.

Kanaev, V.P., 1967. Relief of the Indian Ocean. In: Relief of the Earth (Morphostructure and Morphosculpture). Nauka, Mascow, pp 276-286.

Karsten, J.L. and Delaney, J.R., 1989. Hotspot - Ridge crest convergence in the northeast Pacific, J. Geophys. Res., 94:700-712.

Keen, M.J., 1963. Magnetic anomalies over the mid-Atlantic ridge. Nature, 197:888-890.

Kent, R. 1991. Lithospheric uplift in eastern Gondwana: evidence for a long-lived mantle plume system? Geology, 19:19-23.

Kent, R.W., Storey, M. and Saunders, A.D., 1992. Large igneous provinces; sites of plume impact or plume initiation. Geology., 20:891-894.

Khramov, A.N., 1957. Paleomagnetism - the basis of a new method of correlation and subdivision of sedimentary strata. Acad. Sci. USSR, Dokl., Earth Sci. Sect., 112:129-132.

Kolla, V. and Coumes, F., 1984. Morpho-acoustic and sedimentologic characteristics of the Indus Fan. Geo-Marine Lett., 3: 133-139.

Kolla, V. and Coumes, F., 1985. Indus Fan, Indian Ocean. In: Submarine Fans and Related Turbidite Systems, A.H. Bouma, W.R. Normark and N.E. Barness, (Editors), Springer-Verlag, 129-136.

Kolla, V. and Coumes, F., 1987. Morphology, internal structure, seismic stratigraphy, and sedimentation of Indus Fan. Am. Assoc. Pet. Geol. Bull., 71:650-677.

Kolla, V. and Coumes, F., 1990. Extension of structural and tectonic trends from the Indian subcontinent into the Eastern Arabian Sea. Mar. Pet. Geol., 7:188-196.

Kolla, V., Ray, P.K. and Kostecki, J.A. 1981. Surficial sediments of the Asian sea. Mar. Geol., 41:183-204.

Krishna, K.S., Gopala Rao, D., Ramana, M.V., Subrahmanyam, V., Sarma, K.V.L.N.S., Pilipenko, A.I., Scherbakov, V.S. and Murthy, I.V.R., 1995. Tectonic model for the evolution of oceanic crust in the northeastern Indian Ocean from the Late Cretaceous to the early Tertiary. J. Geophys. Res., 100:20011-20024.

Krishna, K.S., Murty, G.P.S., Srinivas, K. and Gopala Rao, D., 1992. Magnetic studies over the northern extension of the Prathap Ridge complex, eastern Arabian Sea. Geo-Mar. Lett., 12:7-13.

Krishna, K.S. Neprochnov Yu. P., Gopala Rao, D. and Grinko, B.N., 1998. Crustal structure and tectonics of the Ninetyeast Ridge from seismic reflection and refraction studies. Communicated to J. Geophys. Res.

Krishnan, M.S., 1968. Geology of India and Burma, Higgin-Bothams, Madras. 536 pp.

LaBrecque, J.L., Kent, D.V. and Cande, S.C., 1977. Revised magnetic polarity time scale for Late Cretaceous and Cenozoic time. Geology, 5:330-335.

Langereis, C.G., Van Hoof, A.A.M. and Hilgen, F.J., 1994. Steadying the rates. Nature, 369:615.

Larson, R.L. 1975. Late Jurassic Sea-floor spreading in the eastern Indian Ocean. Geology, 3:69-71.

Laughton, A.S., Matthews, D.H., and Fisher, R.L., 1970a. The structure of the Indian Ocean. In: A.E. Maxwell (Editor), The Sea, Vol. 4, Part II, Wiley-Interscience, New York, 543-586.

Laughton, A.S., Whitmarsh, R.B. and Jones, M.T., 1970b. The evolution of the Gulf of Aden. Phil. Trans. Roy. Soc. London, A267:227-266.

Lawn, B.R. and Wilshaw, T.R., 1975. Fracture of brittle solids. Cambridge University Press, Cambridge, 204 pp.

Le Pichon, X. and Heirtzler, J.R., 1968. Magnetic anomalies in the Indian Ocean and sea-floor spreading. J. Geophys. res., 73:2101-2117.

Lewis, B.T.R. and Dorman, L.M., 1970. Experimental isostasy, 2. An isostatic model for the USA derived from gravity and topographic data. J.Geophys. Res., 86:6961-6984.

Liu, C.S., Curray, J.R. and McDonald, J.M., 1983. New constraints on the tectonic evolution of the eastern Indian Ocean. Earth Planet. Sci. Lett., 65:331-342.

Louden, K.E., 1981. A comparison of the isostatic response of bathymetric features in the north Pacific Ocean and Philippine Sea. Geophys. J. R. Astron. Soc., 64:393-424.

Lowrie, W. and Alvarez, W., 1981. One hundred million years of geomagnetic polarity history. Geology, 9:392-397.

Macdonald, K.C., Haymon, R.M., Miller, S.P., Sempere, J.C. and Fox, P.J., 1988. Deep-tow and sea beam studies of dueling propagating ridges on the East Pacific Rise near 20° 40' S. J. Geophys. Res., 93:2875-2898.

Macdonald, K.C., Sempere, J.C. and Fox, P.J., 1984. East Pacific Rise from Siqueriros to Orozco fracture zones: Along-strike continuity of axial neovolcanic zone and structure and evolution of overlapping spreading centers. J. Geophys. Res., 89:6049-6069.

Malod, J.A., Droz, L., Kemal, B.M. and Patriat, P., 1997. Early spreading and continental to oceanic basement transition beneath the Indus deep-sea fan: northeastern Arabian Sea. Mar. Geol., 141:221-235.

Marshall, M. and Cox, A., 1971. Magnetism of pillow basalts and their petrology. Geol. Soc. Am. Bull., 88:1347-1356.

Mason, R.G., 1958. A magnetic survey off the west-coast of the United States between latitudes 32° and 26°N and longitudes 121° and 128°W. J. Geophys., 320-329.

Mason, R.G. and Raff, A.D., 1961. A magnetic survey off the west coast of north America 33°N to 42°N. Geol. Soc. Am. Bull., 72:1259-1265.

Masson, D.G., 1984. Evolution of the Mascarene basin, western Indian Ocean, and the significance of the Amirante Arc. Mar. Geophys. Res., 6:365-382.

Matthews, D. H., 1963. A major fault scarp under Arabian Sea dispalcing the Carlsberg Ridge near Socotra. Nature, 198:950-952.

Matthews, D.H., 1966. The Owen fracture zone and the northern end of the Carlsberg Ridge, Phil. Trans. Roy. Soc., A259:172-186.

Matthews, D.H., Vine, F.J., and Cann, J.R., 1965. Geology of an area of the Carlsberg Ridge, Indian Ocean. Bull. Geol. Soc. Am., 76:675-682.

Matuyama, M., 1929. On the direction of magnetization of basalt in Japan, Tyosen and Manchuria. Japan Acad. Proc., 5:203-205.

Maxwell, A.E., Von Herzen, R.P., Hsu, K.J., Andrews, J.E., Saito, T., Percival, S.F., Mitlow, E.O. and Boyce, R.E., 1970. Deep-sea drilling in the South Atlantic. Science, 168:1047-1059.

McKenzie, D., 1986. The geometry of propagating rifts. Earth Planet. Sci. Lett., 77:176-186.

McKenzie, D. and Bickle, M.J., 1988. The volume and composition of melt generated by extension of the lithosphere. J. Petrol., 29:625-679.

McKenzie, D. and Bowin, C., 1976. The relationship between bathymetry and gravity in the Atlantic Ocean. J. Geophys. Res., 81:1903-1915.

McKenzie, D. and Sclater, J.G., 1971. The evolution of the Indian Ocean since the Late Cretaceous. Geophys. J. R. Astron. Soc., 25:437-528.

McNutt, M.K., 1979. Compensation of oceanic topography: An application of the response function technique to the Surveyor area. J. Geophys. Res., 84:7589-7598.

McNutt, M.K., 1988. Thermal and mechanical properties of the Cape Verde Rise. J. Geophys. Res., 93:2784-2794.

Mercanton, P.L., 1926. Inversion de l'inclinaison magnetique terrestre aux ages geologiques, J. Geophys. Res., 31:187-190.

Mercuriev, S., Patriat. P. Sochevanova, N., 1995. Evolution de la dorsale de Carlsberg: evidence pour une phase d'expansion tres lente entre 40 et 25 Ma (A18 a A7). Oceanologica Acta, 19:1-13.

Miles, P.R. and Roest, W.R., 1993. Earliest sea-floor spreading magnetic anomalies in the north Arabian Sea and the ocean-continent transition. Geophys. J. Int., 115:1025-1031.

Morgan, J.P. and Parmentier, E.M., 1985. Causes and rate-limiting mechanisms of ridge propagation: A fracture mechanics model. J. Geophys. Res., 90:8603-8612.

Morgan, J.P. and Sandwell, D.T., 1994. Systematics of ridge propagation south of 30°S, Earth Planet. Sci. Lett., 121:245-258.

Morgan, W.J., 1972. Plate motions and deep mantle convection, Geol. Soc. America Mem., 132:7-22.

Morgan, W.J., 1981. Hotspot tracks and the opening of the Atlantic and Indian Oceans. In: C. Emiliani (Editor), The Sea, Vol. 7, Wiley Interscience, New York, pp. 443-487.

Morley, L.W. and Larochelle, A., 1964. Paleomagnetism as a means of dating geological events. R. Soc. Can., Spec. Publ., 8:512-521.

Muller, R.D., J.-Y. Royer and Lawver, L.A., 1993. Revised plate motions relative to the hotspots from combined Atlantic and Indian Ocean hotspot tracks. Geology, 21:275-278.

Naar, D.F. and Hey, R.N., 1986. Fast rift propagation along the East Pacific Rise near Easter Island. J. Geophys. Res., 91:3425-3438.

Naar, D.F. and Hey, R.N., 1991. Tectonic evolution of the Easter microplate. J. Geophys. Res., 96:7961-7993.

Nafe, J.E. and Drake, C.L. 1963. Physical properties of marine sediments. In: Hill, M.N. (Eds.), The Sea 3. Wiley Interscience, New York, 794-815.

Naini, B.R., 1980. A geological and geophysical study of the continental margin of western India, and the adjoining Arabian Sea including the Indus Cone. Unpublished Ph.D. thesis, Columbia University, New-York, pp. 167.

Naini, B.R. and Kolla, V., 1982. Acoustic character and thickness of sediments of the Indus Fan and the continental margin of western India. Marine Geology, 47:181-195.

Naini, B.R. and Talwani, M., 1977. Sediment distribution and structures in the Indus Cone and the western continental margin of India (Arabian Sea), EOS, Trans. Am. Geophys. Union, 58:405.

Naini, B.R. and Talwani, M., 1982. Structural framework and the evolutionary history of the continental margin of western India. In: J.S. Watkins and C.L. Drake (Editors), Studies in Continental Margin Geology. Am. Assoc. Pet. Geol. Mem., 34:167-191.

Nair, K.M., Singh, N.K., Jokhan Ram, Gavarshetty, C.P. and Muraleekrishanan, B., 1992. Stratigraphy and sedimentation of Bombay offshore basin. J. Geol. Soc. India, 40:415-442.

Nairn, A.E.M. and Stehli, F.G. 1982. The ocean basins and margins. Plenum Press, New York, pp.776.

Narain, H., Kaila, K.L. and Verma, R.K., 1968. Continental margins of India. Can. J. Earth. Sci., 5:1051-1065.

Negi, J.G., Agrawal, P.K., Singh, A.P. and Pandey, O.P., 1992. Bombay gravity high and eruption of Deccan flood basalts (India) from a shallow secondary plume. Tectonophysics, 206:341-350.

Neprochnov, Yu.P., 1961. Sediment thickness of the Arabian Sea Basin (in Russian). Dokl. Akad. Nauk., 139: 177-179.

Neprochnov, Yu.P., Gopala Rao, D., Subrahmanyam, C. and Murthy, K.S.R. 1998. Intraplate deformation in the Central Indian Ocean Basin. Geol. Soc. India, Bangalore publication, pp.250.

Ness, G., Levi, S. and Cough, R., 1980. Marine magnetic anomaly timescales for the Cenozoic and Late Cretaceous: A preics, critique and synthesis, Rev. Geophys., 18:735:770.

Nettleton, L.L., 1976. Gravity and magnetics in oil prospecting. McGraw Hill Inc., New York, pp. 464

Norton, I.O. and Sclater, J.G., 1979. A model for the evolution of the Indian Ocean and the breakup of the Gondwanaland. J. Geophys. Res., 84:6803-6830.

Pandey, O.P., Agrawal, P.K. and Negi, J.G., 1995. Lithospheric structure beneath Laxmi Ridge and late Cretaceous geodynamic events. Geo-Marine Lett., 15:85-91.

Pandey, J. and Dave, A., 1998. Stratigraphy of Indian petroliferous basins. XVI Indian colloquium on micropaleontology and stratigraphy. National Institute of Oceanography, Goa, pp. 1-248.

Parsons, B. and Sclater, J.G., 1977. An analysis of the variation of ocean floor bathymetry and heat flow with age. J. Geophys. Res., 82:803-827.

Patriat, P. and Achache, J., 1984. India-Eurasia collision chronology has implications for crustal shortening and driving mechanism of plates. Nature, 311:615-621.

Patriat, P. and Segoufin, J., 1988. Reconstruction of the Central Indian Ocean. Tectonophysics, 155:211-234.

Pollard, A.D. and Aydin, A., 1984. Propagation and linkage of oceanic ridge segments. J. Geophys. Res., 89:10017-10028.

Prell, W.L., Niitsuma, N. et al., 1989. Site 720. In: Initial report of the Ocean Drilling Program Leg 117. College station, Texas, Ocean Drilling Program. 157-195.

Radhakrishna, T., Dallmeyer, R.D. and Joseph, M., 1994. Paleomagnetism and $^{36}Ar/^{40}Ar$ vs. $^{39}Ar/^{40}Ar$ isotope correlation ages of dyke swarms in central Kerala, India: Tectonic implications. Earth Planet. Sci. Lett., 121:213-226.

Raff, A.D. and Mason, R.G. 1961. Magnetic Survey off the West Coast of North America, 40^0 N latitude to 50^0 N latitude. Geo. Soc. Am. Bull., 72:1267-1270.

Raitt, R.W., 1963. The crustal rocks. In: M.N. Hill (Editor), The Sea, Vol. 3, John Wiley-Interscience, New York, pp. 85-102.

Raju, A.T.R., 1979. Basin analysis and petroleum exploration with some examples from Indian sedimentary basins. J. Geol. Soc. India, 20:49-60.

Ramana, M.V. 1986. Regional tectonic trends on the inner continental shelf off Konkan and central west coast of India. Geo-Mar. Lett., 6:1-5.

Ramana, M.V., Ramprasad, T., Kamesh Raju, K.A. and Desa, M., 1993. Geophysical studies over a segment of the Carlsberg Ridge, Indian Ocean. Mar. Geol., 115:21-28.

Ramaswamy, G. and Rao, K.L.N. 1980. Geology of the continental shelf of the west coast of India. Can. Soc. Pet. Geol. Mem., 6:801-821.

Rampino, M.R. and Stothers, R.B., 1988. Flood besalt volcanism during the past 250 million years. Science, 241:663-667.

Rao, R.P. and Srivastava, D.C., 1984. Regional seismic facies analysis of western offshore, India. Bull. Oil Nat. Gas Comm., 21:83-96.

Rao, T.C.S., 1970. Seismic and magnetic surveys over the continental shelf off Konkan coast. Pro. 2nd Symposium on Upper mantle Project, Hyderabad, India, 59-71.

Rea, D.K., 1992. Delivery of Himalayan sediment to the Northern Indian Ocean and its relation to global climate, sea level, uplift and seawater strontium. In: R.A. Duncan et al. (Editors), Synthesis of results from scientific drilling in the Indian Ocean, Geophysical Monograph, American Geophysical Union, 70:387-402.

Recq, M., Brefort, D., Malod, J. and Veinante, J.-L., 1990. The Kerguelen Isles (southern Indian Ocean): New results on deep structure from refraction profiles. Tectonophysics, 182:227-248.

Reddy, S.I., Roychowdhury, K., Drolia, R.K., Ashalata, B., Mittal, G.S., Subrahmanyam, C. and Singh, R.N., 1988. On the structure of the western continental margin off Mangalore coast, India. J. Assoc. Expl. Geophys., 9:181-189.

Richards, M.A., Duncan, R.A. and Courtillot, V.E., 1989. Flood basalts and hot-spot tracks: Plume heads and tails. Science, 246:103-107.

Royer, J.-Y., Peirce, J.W. and Weissel, J.K. 1991. Tectonic constraints on the hot-spot formation of Ninetyeast Ridge, Proc. ODP, Sci. Results, 121:763-776.

Royer, J.-Y., and Sandwell, D.T., 1989. Evolution of the eastern Indian Ocean since the Late Cretaceous : Constraints from Geosa Altimetry. J. Geophys. Res., 94:13755-13782.

Royer, J.-Y., Sclater, J.G., Sandwell, D.T., Cande, S.C., Schlich, R., Munschy, M., Dyment, J., Fisher, R.L., Muller, R.D., Coffin, M.F., Patriat, P. and Bergh, H.W., 1992. Indian Ocean plate reconstructions since the Late Jurassic. In: R.A. Duncan et al. (Editors), Synthesis of results from scientific drilling in the Indian Ocean, Geophysical Monograph, American Geophysical Union, 70:471-475.

Schilling, J.G., Kingsley, R.H. and Devine, J.D. 1982. Galapagoos hotspot-spreading center system; I, Spetial Petrological and Geochemical variations (83^0 W-101^0 W), J. Geophys. Res., 86:5593-5610.

Schilling, J.-G., Sigurdsson, H., Davis, A.N. and Hey, R.N., 1985. Easter microplate evolution. Nature, 317:325-331.

Schlich, R., 1975. Structure et age de l'ocean indien occidental. Mem. Hors-Ser. Soc. Geol. Fr., 6, 103 pp.

Schlich, R., 1982. The Indian Ocean: aseismic ridges, spreading centers, and Oceanic basins. In: A.E.M. Nairn and F.G. Stehli (Editors), The Ocean Basins and Margins, Vol. 6, Plenum, New York, pp. 51-147,

Scotese, C.R., Gahagan, L.M. and Larson, R.L., 1988. Plate tectonic reconstructions of the Cretaceous and Cenozoic ocean basins. In: C.R. Scotese and W.W. Sager (Editor), Mesozoic and Cenozoic plate reconstructions. Tectonophysics, 155:27-48.

Shih, J. and Molnar, P. 1975. Analysis and implications of the sequences of ridge jumps that eliminated the surveyor transform fault. J. Geophys. Res., 80:4815-4822.

Shipboard Scientific Party, 1988. Site 715. In: R.A. Duncan and others (Editors), Proceedings Ocean Drilling Program, pp.917-946.

Shor, G.G.Jr., Menard, H.W. and Raitt, R.S., 1970. Structure of the Pacific basin. In: A.E. Maxwell (Editor), The Sea, Vol. 4, Part II, John Wiley-Interscience, New York, pp. 3-227.

Sigurgeirsson, Th., 1957. Direction of magnetization in Icelandic basalts. Phil. Mag. Suppl., 6:240-246.

Singh, N.K. and Lal, N.K., 1993. Geology and petroleum prospects of Konkan-Kerala basin, In: S.K. Biswas et al. (Editors), Proc. Second Seminar on Petroliferous Basins of India, Vol. 2, Indian Petroleum Publishers, Dehra Dun, India, pp.461-469.

Sinha, M.C., Louden, K.E. and Parsons, B., 1981. The crustal structure of the Madagascar Ridge. Geophys. J. R. Astron. Soc., 66:351-377.

Smith, W.H.F., Staudigel, H., Watts, A.B. and Pringle, M.S., 1989. The Magellan seamounts: Early Cretaceous record of the South Pacific Isotopic and thermal anomaly. J. Geophys. Res., 94:10501-10523.

Stein, C.A. and Cochran, J.R., 1985. The transition between the Sheba Ridge and Owen Basin: rifting of old oceanic lithosphere. Geophys. J. R. Astro. Soc., 81:47-74.

Storey, B.C., 1995. The role of mantle plumes in continental breakup: case histories from Gondwanaland. Nature, 377:301-308.

Stow, D.A.V., Amano, K., Balson, P.S., Brass, G.W., Corrigan, J., Raman, C.V., Tiercelin, J-J., Townsend, M. and Wijayananda, N.P., 1990. Sediment facies and processes on the distal Bengal Fan, In: J.R. Cochran, D.A.V. Stow, et al. (Editors), Proc. ODP, Sci. Results, 116: College Station, TX(Ocean Drilling Program), 377-396.

Subrahmanya, K.R., 1994. Post-Gondwana tectonics of the Indian Peninsula. Curr. Sci., 67:527-530.

Subrahmanyam, V., 1992. Structure and tectonics of part of western continental margin of India between Marmagao and Kasaragod from geophysical investigations. Ph.D. Thesis, Andhra University, Visakhapatnam, 270 pp.

Subrahmanyam, V., Ramana, M.V. and Subba Raju, L.V., 1989. Marine Geophysical studies off Karwar, west coast of India. J. Geol. Soc. India, 34:121-132.

Swisher, C.C., et al., 1992. Coeval $^{40}Ar/^{39}Ar$ ages for 65.0 million years ago from chicxulub crator melt rock and Cretaceous-Tertiary boundary Tektites. Science, 257:954-958.

Swisher, C.C., Dingus, C.L. and Butler, R.F., 1993. $^{40}Ar/^{39}Ar$ dating and magnetostratigraphic correlation of the terrestrial Cretaceous-Paleogene boundary and Puercan Mammal age, Hell Creek-Tullock Formations, eastern Montana. Can. J. Earth Sci., 30:1981-1996.

Talwani, M. and Eldholm, O., 1972. Continental margin off Norway: a geophysical study. Geol. Soc. Am. Bull., 83:3575-3606.

Talwani, M. and Eldholm, O., 1973. Boundary between continental and oceanic crust at the margin of rifted continents. Nature, 241:325-330.

Talwani, M. and Heirtzler, J.R., 1964. Computations of magnetic anomalies caused by two- dimensional structures of arbitrary shape. In : G.A. Parks (Editor), Computers in Mineral Industry, Standford Univ. Pub. Geol. Sci., 9:464-480.

Talwani, M., Windisch, C.C. and Langseth, M.G., 1971. Reykjanes ridge crest: a detailed geophysical study. J. Geophys. Res., 76:473-517.

Talwani, M., Worzel, J.L. and Landisman, M., 1959. Rapid gravity computations for two-dimensional bodies with application to the Mendocino submarine fracture zone. J. Geophys. Res., 64:49-59.

Tamsett, D., 1984. An application of the response function technique to profiles of bathymetry and gravity in the Gulf of Aden. Geophys. J. R. Astr. Soc., 78:349-369.

Udintsev, G.B., 1965. New .data on the bottom topography of the Indian Ocean. Okeanologiya, 5:993-998.

Udintsev, G.B., 1975. Geological-geophysical Atlas of the Indian Ocean. USSR Acad. Sci., Moscow, 151 pp.

Vacquier, V., 1972. Geomagnetism in Marine Geology. Elsevier Publishing Company, Amsterdam, The Netherlands, 185 pp.

Vacquier, V., Raff, A.D. and Warren, R.E., 1961. Horizontal displacements in the floor of the northeastern Pacific Ocean. Geol. Soc. Amer. Bull., 72:1251-1258.

Valdiya, K.S., 1984. Evoluton of the Himalaya. Tectonophysics, 105:229-248.

Vallier, T.L., 1974. Volcanogenic sediments and their relation to landmass volcanism and sea floor-continent movements, Western Indian Ocean. In: E.S.W. Simpson, R. Schlich, et al. (Editors), Initial Reports of the Deep Sea Drilling Project, vol. 25, U.S. Govt. Printing Office, Washington D.C., pp. 515-542.

Valsangkar, A.B., Radhakrishnamurthy, C., Subbarao, K.V. and Beckinsale, R.D., 1981. Paleomagnetism and potassium-argon age studies of acid igneous rocks from St. Mary islands. Geol. Soc. Ind. Mem., 3:265-276.

Vandamme, D., Courtillot, V., Besse, J. and Montigny, R. 1991. Paleomagnetism and age determination of the Deccan Traps (India): Results of a Nagpur-Bombay traverse and review of earlier work: Rev. Geophys, 29:159-190.

Veevers, J.J. 1986. Breakup of Australia and Antarctica estimated as Mid-Creteaceous (95±5 Ma) from magnatic and seismic data at the continental margin. Earth Planet. Sci.Lett., 77:91-99.

Verma, R.K., 1991. Geodynamics of the Indian Peninsula and the Indian plate margin. Oxford and IBH publishing Co., New Delhi. 357 pp.

Vine, F.J., 1966. Spreading of the ocean floor: New evidence. Science, 154:1405-1415.

Vine, F.J., 1968. Magnetic anomalies associated with mid ocean ridges. In: R.A. Phinnet (Editor), The history of the earth's crust, Princeton University press, pp. 73-89.

Vine, F.J. and Matthews, D.H., 1963. Magnetic anomalies over oceanic ridges. Nature. 199:947-949.

Vine, F.J. and Wilson, J.T., 1965. Magnetic anomalies over a young oceanic ridge off Vancouver Island. Science, 150:485-489.

Vink, G.E., 1982. Continental rifting and the implications for plate tectonic reconstructions. J. Geophys. Res., 87:10677-10688.

Vogt, P.R., Cherkis, N.Z. and Morgan, G.N., 1983. Project Investigator, I, Evolution of Austral-Antarctic discordance deduced from a detailed aeromagnetic study. In: R.L. Oliver, P.R.James and J.B. Jago (Editors), Antarctic Earth Sacience, Cambridge University Press, Cambridge.

von der Borch, C.C., 1978. Synthesis of Deep-Sea Drilling Results in the Indian Ocean. Mar. Geol. 26:1-175.

Walcott, R.I., 1976. Lithospheric flexure, analysis of gravity anomalies, and the propagation of seamount chain. In: G.H. Sutton et al. (Editors), The Geophysics of Pacific Ocean Basin and its Margin. Geophys. Mon. 19, Am. Geophys. Union, Washington, D.C., pp. 431-438.

Watson, S. and McKenzie, D., 1991. Melt generation by plumes: A study of Hawaiian volcanism. J. Petrol., 32:501-537.

Watts, A.B., 1978. An analysis of isostasy in the world's oceans 1. Hawaiian-Emperor Seamount chain. J. Geophys. Res., 83:5989-6004.

Weissel, J.K., Anderson, R.N. and Gellar, C.A. 1980. Deformation of the Indo-Australian plate. Nature., 287:284-291.

Weser, O.E., 1974. Sedimentological aspects of strata encountered on Leg 23 in the northern Arabian Sea. In: R.B. Whitmarsh, O.E. Weser, D.A. Ross, et al. (Editors), Initial Reports of the Deep Sea Drilling Project, vol. 23, U.S. Govt. Printing Office, Washington D.C., pp. 503-519.

White, R.S., McKenzie, D. and O'Nions, R.K., 1992. Oceanic crustal thickness from seismic measurements and rare earth element inversions. J. Geophys. Res., 97:19683-19715.

White, R.S. and McKenzie, D.P., 1989. Magmatism at rift zones: The generation of volcanic continental margins and flood basalts. J. Geophys. Res., 94:7685-7729.

Whiting, B.M., Karner, G.D. and Driscoll, N.W., 1994. Flexural and stratigraphic development of the west Indian continental margin. J. Geophys. Res., 99:13791-13811.

Whitmarsh, R.B., 1974. Some aspects of plate tectonics in the Arabian Sea. In: R.B. Whitmarsh, O.E. Weser, D.A. Ross, et al. (Editors), Initial Reports of the Deep Sea Drilling Project, Vol. 23, Washington (U.S. Goverment. Printing Office) pp. 527-535.

Whitmarsh, R.B., Avedik, F. and Saunders, M.R., 1986. The seismic structure of thinned continental crust in the northern Bay of Biscay. Geophys. J. R. Astron. Soc., 86:589-602.

Whitmarsh, R.B., Weser, O.E., Ross, D.A. et al., 1974. Initial Reports of the Deep Sea Drilling Project, Vol. 23, Washington (U.S. Government. Printing Office)., pp. 35-210.

Wiens, D.A., DeMets, C., Gordam, R.G. Stein, S., Argus, D., Engeln, J.F., Lundgren, P., Quible, D., Stein, C., Weinstein, S. and Woods, D.F., 1985. A diffuse plate boundary model for Indian Ocean Tectonics. Geophys. Res. Lett., 12:429-432.

Wilson, D.S., 1988. Tectonic history of the Juan de Fuca ridge over the last 40 million years. J. Geophys. Res., 93:11863-11876.

Wilson, D.S. and Hey, R.N., 1995. History of rift propagation and magnetization intensity for the Cocos-Nazca spreading center. J. Geophys. Res., 100:10041-10056.

Wilson, D.S., Hey, R.N. and Nishimura, C., 1984. Propagation as a mechanism of reorientation of the Juan de Fuca ridge. J. Geophys. Res., 89:9215-9225.

Wilson, J. T., 1965. A new class of faults and their bearing on continental drift. Nature, 207:343-347.

Wiseman, J.D.H. and Seymour-Sewell, 1937. The floor of the Arabian Sea. Geol. Mag., 74:219-230.

Young, R. and Hill, I.A., 1986. An estimate of the effective elastic thickness of the Cape Verde Rise. J. Geophys. Res., 91:4854-4866.

LIST OF PUBLICATIONS OF THE AUTHOR

PUBLICATIONS OF THE AUTHOR

1. Krishna, K.S. and Chaubey, A.K., 1987. Double Off-End configuration in seismic reflection surveys. J. Assoc. Expl. Geophys., 8:35-40.
2. Gopal Rao, D., Bhattacharya, G.C., Subba Raju, L.V., Ramana, M.V., Subrahmanyam, V., Kamesh Raju, K.A., Ramprasad, T. and Chaubey A.K., 1987. Regional marine geophysical studies of the south western continental margin of India. In: T.S.S. Rao et al. (Editors), Contributions in Marine Sciences, National Institute of Oceanography, Dona Pula, Goa, 427-437.
3. Chauhan, O.S. and Chaubey, A.K., 1989. Comparative studies of moment, graphic and phi measures on the sands of the east coast beaches, India. Sedimentary Geol., 65:183-189.
4. Chaubey, A.K., Krishna, K.S., Subba Raju, L.V. and Gopala Rao, D., 1990. Magnetic anomalies across the southern Central Indian Ridge: Evidence for a new transform fault. Deep-Sea Res., 37:647-656.
5. Subba Raju, L.V., Krishna, K.S. and Chaubey, A.K., 1991. Buried Late Pleistocene fluvial channels on the inner continental shelf off Vengurla, west coast of India. J. Coastal Res., 7:509-516.
6. Gopala Rao, D., Chaubey, A. K. and Ramprasad, T., 1992. The Cretaceous-Tertiary sea floor off Dronning Maud Land, Antarctica. Tectonophysics, 205:447-452.
7. Chaubey, A.K., Ramana, M.V., Sarma, K.V.L.N.S., Krishna, K.S., Murty, G.P.S., Subrahmanyam, V., Mittal, G.S. and Drolia, R.K. 1991. Marine geophysical studies over the 85°E Ridge, Bay of Bengal. In: First International seminar & exhibition on "Exploration Geophysics in Nineteen Nineties", AEG Publication, pp 508-515.
8. Bhattacharya, G.C., Chaubey, A.K., Murty, G.P.S., Gopala Rao, D., Scherbakov, V.S., Lygin, V.A., Philipenko, A.I. and Bogomyagkov, A.P., 1992. Marine magnetic anomalies in the northeastern Arabian Sea. In: B.N. Desai (Editor), Oceanography of the Indian Ocean, Oxford-IBH, New Delhi, pp. 503-509.
9. Chauhan, O.S. and Chaubey, A.K., 1992. Submarine physiography off the Lakshadweep Islands, Arabian Sea. In: B.N. Desai (Editor), Oceanography of the Indian Ocean, Oxford-IBH, New Delhi, pp. 487-491.
10. Ramana, M.V., Subrahmanyam, V., Krishna, K.S., Chaubey, A.K., Sarma, K.V.L.N.S., Murty, G.P.S., Mittal, G.S. and Drolia, R.K., 1992. Marine magnetic studies in the northern Bay of Bengal, preliminary results. In: B.N. Desai (Editor), Oceanology of the Indian Ocean, Oxford and IBH, New Delhi, pp. 519-525.
11. Chaubey, A.K., Bhattacharya, G.C., Murty, G.P.S. and Desa, M., 1993. Spreading history of the Arabian Sea: Some new constraints. Marine Geology, 112:343-352.
12. Bhattacharya, G.C., Murty, G.P.S., Srinivas, K., Chaubey, A.K., Sudhakar, T. and Nair, R.R., 1994. Swath bathymetric investigation of the seamounts located in the Laxmi Basin, eastern Arabian Sea. Mar. Geodesy, 17:169-182.

13. Gopala Rao, D., Bhattacharya, G.C., Ramana, M.V., Subrahmanyam, V., Ramprasad, T., Krishna, K.S., Chaubey, A.K., Murty, G.P.S., Srinivas, K., Desa, M., Reddy, S.I., Ashalata, B., Subrahmanyam, C., Mittal, G.S., Drolia, R.K, Rai, S.N., Ghosh, S.K., Singh, R.N. and Majumdar, R., 1994. Analysis of multi-channel seismic reflection and magnetic data along 13°N latitude across the Bay of Bengal. Mar. Geophys. Res., 16:225-236.

14. Ramana, M.V., Subrahmanyam, V., Krishna, K.S., Chaubey, A.K., Sarma, K.V.L.N.S., Murty, G.P.S., Mittal, G.S. and Drolia, R.K., 1994. Magnetic studies in Northern Bay of Bengal. Mar. Geophys. Res., 16:237-242.

15. Sarma, K.V.L.N.S., Ramana, M.V., Murty, G.P.S., Subrahmanyam, V., Krishna, K.S., Chaubey, A.K., Rao, M.M.M. and Narayana, S.L., 1994. Application of Inversion Techniques on marine magnetic data, Andaman shelf. J. Geol. Soc. India, 44:73-75.

16. Bhattacharya, G.C., Chaubey, A.K., Murty, G.P.S., Srinivas, K., Sarma, K.V.L.N.S., Subrahmanyam, V. and Krishna, K.S., 1994. Evidence for Sea-floor spreading in the Laxmi Basin, Northeastern Arabian Basin. Earth Planet. Sci. Lett., 125:211-220.

17. Chaubey, A.K., Bhattacharya, G.C. and Rao, D.G., 1995. Seafloor spreading magnetic anomalies in the southeastern Arabian Sea. Mar. Geol., 128:105-114.

18. Ramana, M.V., Subrahmanyam, V., Chaubey, A.K., Ramprasad, T., Sarma, K.V.L.N.S., Krishna, K.S., Desa, M., Murty, G.P.S. and Subrahmanyam, C., 1997. Structure and origin of the 85°E Ridge. J. Geophys. Res., 102:17995-18012.

19. Chaubey, A.K., Bhattacharya, G.C., Murty, G.P.S., Srinivas, K., Ramprasad, T. and Gopala Rao, D., 1998. Early Tertiary seafloor spreading magnetic anomalies and paleo-propagators in the northern Arabian Sea. Earth Planet. Sci. Lett., 154:41-52.

20. Krishna, K.S., Gopala Rao, D., Subba Raju, L.V., Chaubey, A.K., Scherbakov, V.S., Pilipenko, A.I. and Radhakrishna Murthy, I.V., 1998. Paleocene on-spreading-axis hotspot volcanism: an interaction between the Kerguelen hotspot and the Wharton spreading center. Ind. Acad. Sci. (submitted).

APPENDIX

APPENDIX - 1

LITHOSPHERIC AND TECTONIC ELEMENTS OF THE PROPAGATING RIDGE SYSTEM

The propagating ridge system contains three basic zones of lithosphere with distinct bathymetry and magnetic anomaly patterns. They are: i) normal lithosphere, ii) propagating ridge lithosphere, and iii) transferred lithosphere. These zones are created on or separated by the propagating ridge tectonic elements such as propagating ridge, receding ridge, failing ridge, failed ridge, transform zone, inner and outer pseudofaults. A brief summary of these elements (Hey, 1977; Hey et al., 1980; 1986) are described with respect to Figure 5.3 of Chapter 5 in the following sections.

LITHOSPHERIC ELEMENTS OF THE PROPAGATING RIDGE SYSTEM

i. *NORMAL LITHOSPHERE*

Normal lithosphere is created on the receding ridge axis and is unaffected by ridge propagation. If no ridge propagation occurs, the entire area would consist of normal lithosphere similar to mid-ocean ridge basalt (MORB) type (Christie and Sinton, 1981) and is characterized by normal amplitude magnetic anomalies.

ii. *PROPAGATING RIDGE LITHOSPHERE*

Propagating ridge lithosphere is created at the propagation ridge axis. The V-shaped wedge of young lithosphere is bounded by the pseudofaults and is bathymetrically, magnetically, and petrologically distinct from the normal lithosphere created on the receding ridge axis.

iii. *TRANSFERRED LITHOSPHERE*

The zone of transferred lithosphere consists of lithosphere which has been progressively deformed and transferred from one plate to another plate by the propagation of the ridge tips and migration of the transform zone.

TECTONIC ELEMENTS OF THE PROPAGATING RIDGE SYSTEM

i. *PROPAGATING RIDGE AXIS*

The spreading ridges which propagate forward from their tips and gradually overlapping and overtaking the previously existing spreading center is called propagating ridge axis.

ii. *PROPAGATING RIDGE TIP*

Propagating ridge tip location is represented by intersection of the pseudofaults. Location of the propagator tip is much closer to the place of new extrusive volcanic or the brittle crustal failure produced by the tectonic stresses.

iii. *PSEUDOFAULTS*

Pseudofaults form a V-shaped wake behind the propagating ridge. The V points in the direction of propagation and the angle gives the ratio of propagation to spreading rate (Table 5.1 of chapter 5). If the propagation rate is zero, the pseudofaults become fracture zones. In the magnetic anomaly fabric, the oblique V-shaped traces appear at the first sight to be fault lines along which the anomalies are broken and offset after their formation. In fact, no fractures ever occurred in this direction. There are two types of pseudofaults. They are "inner" and "outer" pseudofaults. The outer pseudofault abuts against older undeformed lithosphere, whereas the inner pseudofault abuts against the deformed zone of transferred lithosphere.

iv. *RECEDING RIDGE*

The receding ridge is the spreading center, which is about to be replaced by the propagating ridge if ridge propagation continues. This is also called as "dying/doomed ridge".

v. *FAILING RIDGE*

Failing ridge is that part of the receding ridge which is currently in the process of being replaced by the propagating ridge but which has not yet completely ceased spreading.

vi. *FAILED RIDGE*

Failed ridge is a former active spreading center, which has ceased tectonic and volcanic activity. In a propagating ridge system, a failed ridge is no longer active part of the receding ridge, which ceased spreading.

vii. *TRANSFORM ZONE*

According to classic plate tectonic theory, a narrow permanent transform fault parallel to the instantaneous relative plate motion connects the offset spreading center segments. Commonly, there are deep narrow troughs and ridges parallel to the fault, and a narrow zone connects the spreading center segments. In this fault zone most earthquakes, strike-slip in the direction of relative plate motion, occur. In contrast, the propagating and failing ridges are connected by a broad zone of anomalously deep bathymetry. This broad zone is called as transform zone.